DEVELOPING A SOLAR–BIO HYBRID ENERGY GENERATION SYSTEM FOR SELF-SUSTAINABLE WASTEWATER TREATMENT

By

Mauricio Jose Bustamante

A DISSERTATION

Submitted to
Michigan State University
in partial fulfillment of the requirements
for the degree of

Biosystems Engineering - Doctor of Philosophy

2016

ABSTRACT

DEVELOPING A SOLAR–BIO HYBRID ENERGY GENERATION SYSTEM FOR SELF-SUSTAINABLE WASTEWATER TREATMENT

By

Mauricio Jose Bustamante

This study delivers a comprehensive analysis of the integration of renewable energy sources for a self-sustaining organic wastewater treatment operation. The increase in human population and the continuous expansion of residential and industrial activities in the last decades has elevated the generation of wastewater that can irreversibly damage the environment. The current technologies to treat wastewater require significant amounts of energy to operate, and most of them use non-renewable energy sources (fossil-based fuels are the main energy sources), which implies that current treatment technologies are not completely sustainable. The goal of this study is to integrate solar energy into the process of wastewater treatment synergistically.

The first stage of this study evaluates the two options to generate electricity (Rankine and Brayton cycles for steam and gas turbines, respectively) using biogas as a sub-product of anaerobic digestion (the first stage in the proposed wastewater treatment) and incorporating solar energy to balance the thermal energy requirements. The results indicate that a steam turbine is the most convenient technology for the integration into a solar–bio concept, although its thermal-to-electrical energy conversion efficiency is lower than that for gas turbines.

The second stage studies the steam turbine energy generation system to provide electricity for the wastewater treatment plant (anaerobic and aerobic digestion), considering two options for solar–bio hybridization: concentrated solar power (CSP) and photovoltaics (PV).

Results show that PV requires a smaller collection area and biomethane volumetric storage capacity to support the electricity needs.

The third stage evaluates the geometrical and operational parameters for a CSP system using refractive Fresnel lenses, as an alternative to parabolic reflectors. The solar concentration ratio and absorber area were the parameters studied to calculate the change in the absorber temperature. The parameters were evaluated using a small bench-scale unit with an accurate solar tracking system using an astronomical algorithm. The results indicate that the absorber area affects the maximum temperature in the solar receiver to a greater degree than the concentration ratio.

The last stage involves the design of two solar thermal receivers for a refractive Fresnel lens. The first design is a single path receiver with a conical absorber; the second is a cavity receiver with a spiral groove for multi-path flows. Both receivers were simulated using computational fluid dynamics, obtaining the fluid outlet temperature under different scenarios. The analysis showed that the cavity receiver exhibited higher efficiencies than the conical receiver, but its application is limited to low concentration ratios.

To my father Manuel, my mother Marta, my sister Laura, and my nieces Gloriana and Mariana, for all the encouragement and support that I have received over the years to fulfill my goals. Thanks.

ACKNOWLEDGMENTS

I would like to express my gratitude to my advisor, Dr. Wei Liao, for his support and mentorship during my PhD study. I have gained plenty of professional experience thanks to his encouragement, guidance, and generous attitude to help his students pursue quality and excellence in their work; I feel truly privileged to have had the opportunity to work with Dr. Liao. I would also like to give thanks to Dr. Dana Kirk for his support on the elaboration of my research and participation in different projects at the Anaerobic Digestion Research and Educational Center (ADREC).

Thanks to my committee members: Drs. Abraham Engeda, Ilson Lee, and Yan Liu for their comments and advice in the development of this study. My gratitude to the faculty and administrative staff in the Department of Biosystems and Agricultural Engineering at Michigan State University and Universidad de Costa Rica, especially Dr. Ajit Srivastava and Mr. José Aguilar Pereira for their support and advice in pursuing the PhD program. To Eilyn Brenes, thanks for her support and company through this time. To my colleagues in the Bioenergy Research Group and my friends, especially Ronald Aguilar, Jocselyn Chacón, Cristina Venegas, Beatriz Mazón, Melissa Rojas, Shikha Singh, Mauricio Losilla, Óscar Quesada, José Daniel Bustamante, , Silvia Guillén, Melissa Hernández, Tony Zhong, Ray Chen, and Yuan Zhong.

I would also like to thank Universidad de Costa Rica for providing financial support to complete my study program.

TABLE OF CONTENTS

LIST OF TABLES

LIST OF FIGURES

KEY TO ABBREVIATIONS

Nomenclature Chapter II

α	Emittance
A_c	Collector area
A_a	Absorber area
CF	Net capacity factor
Cp	Specific heat
DSR	Available solar radiation
ε_{HC}	Burner efficiency
ε_R	Regenerator efficiency
ε_c	Compressor efficiency
ε_{HE}	Heat exchanger thermal efficiency
E_{req}	Thermal energy requirement of anaerobic digester
${E_{th}}^G$	Thermal energy generated
EG	Electricity generation in the power generation system (PGS)
HRT	Hydraulic retention time
G	Direct normal irradiance
h_n	Enthalpy

HG	Heat generation in PGS
h	Convective coefficient
P_i	Steam turbine inlet pressure
P_o	Steam turbine outlet pressure
PGS	Power generation subsystem
r_P	Gas turbine pressure ratio
ρ_{inf}	Influent density
σ	Stefan-Boltzmann constant
${Q_F}^G$	Heat input gas turbine system
Q_F	Energy transferred to the working fluid
Q_H	Heat-extracted steam turbine system
${Q_H}^G$	Heat-extracted gas turbine system
Q_s	Solar heat requirement
Q_{solar}	Solar thermal energy
SC	Solar collector subsystem
S_F	Solar operating factor
T	Temperature
T_{AD}	Anaerobic digestion culture temperature
T_{inf}	Influent temperature

t_c	Solar energy collection time
V_{CH4}	Biomethane requirement
v_ι	Water specific volume
V_{AD}	Digester volume
W_s	Gross power generated
w_P	Pump work
γ	Ratio between air specific heats

Nomenclature Chapter III

AD	Anaerobic digestion
AED	Aerobic digestion
A_{SCA}	Area of solar collector assembly
α	Constant
β_n	Constants
COD	Chemical oxygen demand
C_p	Anaerobic digester (AD) influent specific heat
γ	Constant
ξ_n	Constants
E_{req}	Thermal energy for AD

HCE	Heating collecting element
HRT	Hydraulic retention time
m_{air}	Air mass flow
m_{b_d}	Biogas daily balance
NCF	Net capacity factor
η_e	Turbine thermal-to-electrical efficiency
η_b	Fuel-to-steam efficiency
η_h	Heat exchanger efficiency
η_c	Condenser efficiency
η_{op}	Optical efficiency
η_{comp}	Compressor efficiency
p_0	Atmospheric pressure
p_1	Compressor outlet pressure
P	Electrical power generated in the turbine
P_e	Turbine design power output
P_{e_af}	Hourly electrical demand after solar utilization
P_N	Biogas pressure
P_v	Electricity generated by photovoltaics (PV)
P_{v_b}	Electricity stored in batteries

AD	Anaerobic digestion
P_{comp}	Compressor power
P_{AD}	Biogas standard pressure
ρ_{inf}	AD influent density
Q	Thermal energy extracted in the condenser
Q_i	Heat requirement of turbine
$Q_i{}^{ref}$	Turbine design thermal energy input
Q_o	Thermal energy extracted in the condenser at P_e
Q_{DNI}	Direct normal irradiance
Q_N	Net thermal energy collected in solar collector assembly (SCA)
Q_{HCE_L}	Heat loss in the heating collecting element (HCE)
Q_p	Heat loss in the piping system
$Q_p{}^{ref}$	Reference heat loss in piping system
Q_B	Thermal energy from biogas
Q_{s_th}	Solar thermal energy stored
Q_{s_e}	Electrical energy stored
SCA	Solar collector assembly
SOF	Solar operating factor
T_{AD}	AD culture temperature

T_N	Biogas standard temperature
$\bar{T}_{HTF}$	Average working fluid temperature
T_{inf}	AD influent temperature
$\bar{T}_{amb}$	Average annual ambient temperature
TS	Total solids
TSS	Total soluble solids
TN	Total nitrogen
TS	Total phosphate
V_{AD}	Anaerobic digester volume
V_N	Biogas standard volume
VS	Volatile solids
P_{comp}	Compressor power

Nomenclature Chapter IV

A_a	Absorber area
A_c	Concentration area
A_l	Lens area
CR	Solar concentration ratio
L_h	Horizontal displacement of the lens

L_v	Vertical displacement of the lens
L_{h0}	Horizontal distance from the focal point to the rotational point of the lens
L_{v0}	Vertical distance from the focal point to the rotational point of the lens
L	Distance between the focal point and the rotational point of the lens
α_m	Absorbance of the metallic plate
$\alpha^o{}_1$	Angle of the location of L at its initial position
σ	Stefan-Boltzmann constant
ϵ_m	Emittance of mild steel
S_h	Number of steps for motor 1 for horizontal adjustment
S_v	Number of steps for motor 2 for vertical adjustment
S_θ	Number of steps for motor 3 for zenithal adjustment
S_γ	Number of steps for motor 4 for azimuthal adjustment
θ	Zenith angle
γ	Azimuth angle
θ_o	Zenith initial angle for lens (90°)
γ_o	Azimuth initial angle for lens (0°)
q_o''	Heat inflow at the absorber
T_a	Absorber temperature
T_o	Simulated temperature from FEM model

$\bar{T}$	Average temperature from data collection
T_∞	Ambient temperature
$\dot{Q}_e$	Heat flux emitted by the absorber
$\dot{Q}_{solar}$	Heat flux from solar radiation measured by pyranometer
τ_l	Transmittance of the lens
τ_g	Transmittance of the thermal glass

Nomenclature Chapter V

A	Receiver external area
D	Characteristic length
k	Thermal conductivity
h	Convective coefficient
Nu	Nusselt number
Pr	Prandtl number
σ	Stefan-Boltzmann constant
Re	Reynolds number
Q_c	Heat loss due to convection
Q_R	Heat loss due to radiation
T	Temperature

V	Wind velocity
ν	Viscosity

CHAPTER I. INTRODUCTION

Water is one of the most important natural resources on Earth. It is the essential compound of plants and animals, which means that no life would exist without water. Rapid growth of the world's population, along with rapid industrialization and urbanization, has led to a huge increase in fresh water consumption and wastewater generation. It has been reported that the volume of untreated domestic sewage generated daily per capita is 0.57 m^3 in developed countries and 0.19 m^3 in developing countries (Chapra, 1997). Although many technologies have been studied and developed for sewage treatment, most of these technologies require a significant amount of energy (both heat and electricity) to reduce the organic matter in the sewage and satisfy the discharge standards. Mizuta et al. (Mizuta & Shimada, 2010) reported that the specific power consumptions per m^3 of wastewater ranged from 0.44 to 2.07 kWh for oxidation ditch treatment and from 0.30 to 1.89 kWh for conventional sludge treatment. The high-energy demand and use of non-renewable energy sources (fossil-based fuels are the main energy sources) mean that current wastewater treatment technologies are not completely sustainable and have limited technical and economical flexibility for various scale operations.

In order to replace the fossil energy usage and provide sustainable wastewater treatment (particularly for small- to medium-size operations), renewable energy sources should be synergistically integrated with wastewater treatment. Therefore, the proposed study combines solar and biological technologies to develop a novel self-sustainable solar–bio hybrid energy generation system that satisfies the energy needs for small- to medium-scale wastewater treatment. The solar–bio hybrid energy generation system includes unit operations consisting of solar thermal collection, anaerobic digestion of wastewater, secondary treatment for anaerobic digestion effluent, and solar–bio power generation (Figure I-1).

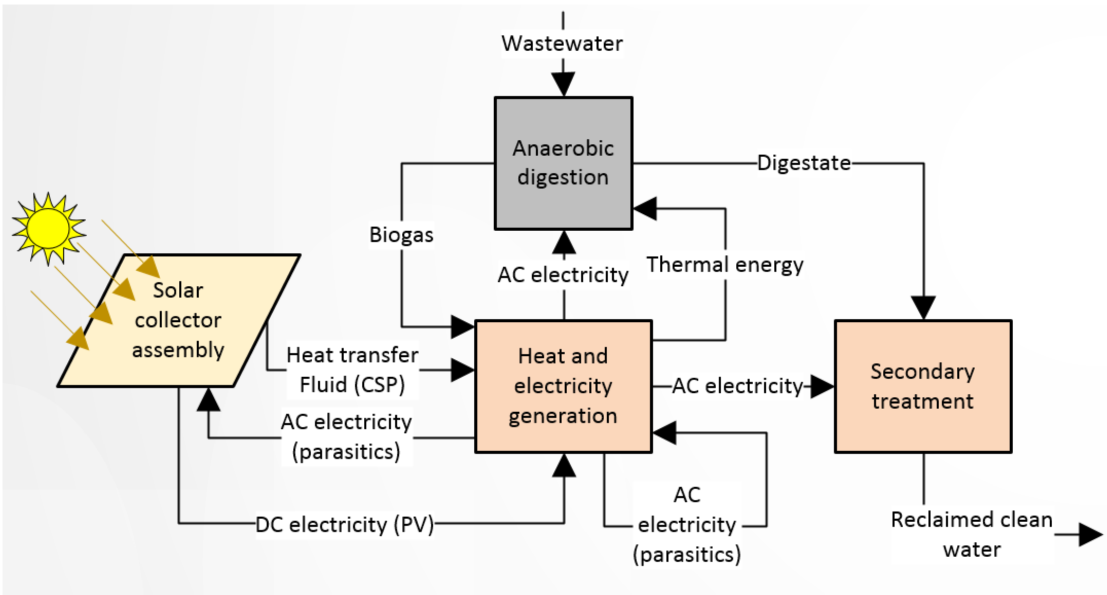

Figure I-1. The key process stages of a solar–bio hybrid energy generation system for wastewater treatment

1. Literature review

1.1. Wastewater treatment process

Human activities generate excessive waste with the potential to damage the environment. Wastewater is one of the most harmful byproducts of industrial and residential activities. Untreated wastewater results in ground water and surface water contamination, leading to serious issues, such as a detrimental impact on wildlife, algae bloom, and pathogen proliferation (EPA, 2004). The identification of all pollutants is complicated due to the complexity of the wastewater components. Biological oxygen demand (BOD) is a method to indicate the polluting capacity, where microorganisms decompose the organic matter in the effluent by consuming the dissolved oxygen. BOD is obtained by measuring the oxygen concentration of the sample before and after a 5-day incubation period (BOD_5), and the difference in concentration is the amount used in the microbial oxidation of organic matter (Chapra, 1997). The organic content in wastewater can also be obtained using chemical procedures, such as chemical oxygen demand (COD). COD is measured using inorganic chemicals to oxidize organic material. The COD measurement consumes less time, but correlates less well with natural conditions (Wang, Pereira, & Hung, 2009).

Biological, physical, and chemical procedures have been studied for wastewater treatment. Among these, biological processes have been widely used and tested to remove organic and inorganic matter, and alleviate the potential environmental issues. Biological wastewater treatment pursues the acceleration of the natural processes to break down the organic compounds, while pollutants such as heavy metals are separated before the discharge of the water into streams. The growth of microbial populations, where the biochemical reactions reduce the organic matter via respiration (oxidative breakdown of organic molecules), is stimulated (Wang et al., 2009).

Anaerobic digestion (AD) and aerobic treatment (AET) are two state-of-art sewage treatment practices. Both technologies possess different target applications, advantages, and disadvantages, depending on the nature of the wastewater.

1.1.1. Fundamentals of anaerobic digestion

AD is an natural and biological conversion process that has been proven effective in converting wet organic wastes into biogas capable of producing clean electricity, while also alleviating many of the environmental concerns associated with the wastes (odor, greenhouse gas emissions, and groundwater contamination) (Caruana & Olsen, 2012). AD is widely used to treat wastewaters of moderate–high strength (> 50 000 mg/L as COD), and can also be used for dilute wastewater (Grady, Daigger, & Lim, 1999). The overall AD chemical process can be described as

$$C_6H_{12}O_6 \rightarrow 3CO_2 + 3CH_4 \qquad \text{(I.1)}$$

where $C_6H_{12}O_6$ represents the organic matter in the wastewater, and CO_2 (carbon dioxide) and CH_4 (methane) are the main products from the AD process. There are four key stages of anaerobic digestion: hydrolysis, fermentation (acidogenesis), acetogenesis, and methanogenesis (Figure I-2, adapted from (R. Chen, 2015)).

Wastewater is usually composed of large organic polymers, such as carbohydrates, fats, and proteins. In order for microbes to carry out the anaerobic digestion and produce biogas, these large polymers must be broken down into smaller constituent monomers. Several of these monomers (i.e. simple sugars, fatty acids, and amino acids) are directly converted into acetate and hydrogen, which are utilized by methanogenic archaea. The remaining monomers need to go through several stages of fermentation to break down the intermediate volatile fatty acids (VFAs) (i.e. propionate, butyrate, succinate, and alcohols) into acetate and hydrogen. Eventually, acetoclastic and hydrogenotrophic methanogenic archaea produce methane, carbon dioxide, and water from the acetate and hydrogen.

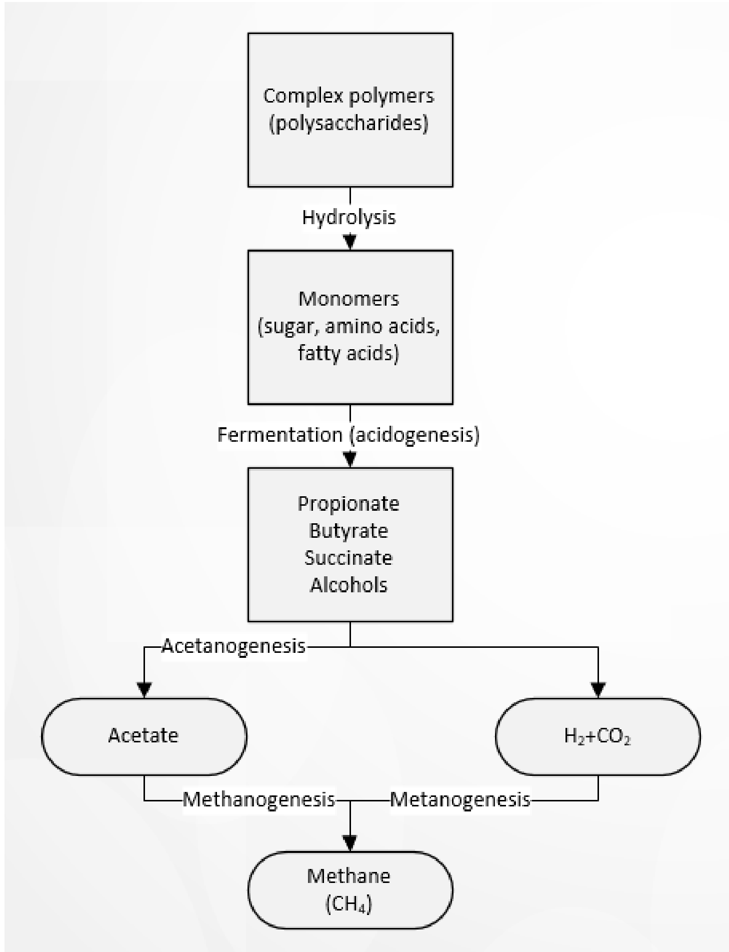

Figure I-2. Stages in the process of anaerobic digestion

The microbial synthesis of AD does not need oxygen, which significantly reduces the energy demand of the process. Moreover, AD helps to alleviate the energy load in the system. AD generates 1.26×10^4 MJ (stored in CH_4) per 100 kg of COD reduced (Speece, 1996). It has been reported that 2,339,339 t of CH_4 per year can be generated from wastewater in the United States (NREL, 2013), which can potentially generate 71×10^9 MJ of thermal energy (with a biogas density of 0.75 kg/m^3, and a biogas lower heating value of 23 MJ/kg (Colmenar-Santos, Bonilla-Gómez, Borge-Diez, & Castro-Gil, 2015; Sun et al., 2015)).

Anaerobic digesters are available in different configurations, and can be classified based on the dry solid content of the feedstock, the number of phases or stages, and the operating temperature (Korres, O'Kiely, & Benzie, 2013). Table I-1 summarizes the general classification of AD systems.

Table I-1. Types of anaerobic digesters

Classification basis	**Digester type**
Feeding	Batch or continuous
Culture temperature	Mesophilic, thermophilic, psychrophilic
Feedstock type	High (20–40%) and low (< 20%) solid concentration
AD Process	Single or multi-stage

Moreover, anaerobic digesters include differences in their geometrical design and operational procedure (PennState Extention, 2016). For instance, a covered lagoon is a large digester with a long hydraulic retention time and high dilution. Covered lagoons are usually installed for flush manure management systems (0.5–2% total solids). Similarly, plug-flow digesters are installed for manure management (without internal agitation) and loaded with thick manure of 11–14% total solids. In addition, a continuous stirred tank reactor (CSTR) is a configuration used for AD where the influent is agitated with a motor driver mixer, a liquid recirculation pump, or biogas mixing for an appropriate contact of the microbial community with the degradable organic matter. Similarly, the up-flow anaerobic sludge blanket (UASB) manages a fast-upward wastewater flow passing through the sludge bed on the bottom of the tank, improving the influent-sludge contact and enhancing the separation of inactive particles from the sludge. Another digester type is the anaerobic fixed-film reactor, which is partially filled with an inert medium (such as plastic pall rings) that provides a large surface area for microbial growth without decreasing the volumetric digester capacity. The influent passes through the media and anaerobic microbes attach themselves to it, stimulating an appropriate biomass concentration for organic matter consumption.

The energy demand varies based on the AD configuration (the different equipment installed, such as pumps, motors, filters). Moreover, typical AD treatment is operated under reaction temperatures ranging from 35–50 °C. Zhong et al. (Zhong et al., 2015) found in their study that for an AD reactor of 10 m^3 with R12 insulation, the thermal energy requirements to maintain the reactor temperature ranged between 0.5–1.1 MJ per m^3 of reactor volume, and 2–5.51 MJ per m^3 of reactor volume to heat the incoming waste stream. The thermal energy to maintain the culture temperature and heat the influent can be obtained from the produced biogas, but the biogas consumption for heating decreases its potential use for electricity generation. Studies have reported on the use of solar energy as a thermal source to maintain the culture temperature and heat the influent (El-Mashad, van Loon, & Zeeman, 2003; El-Mashad, van Loon, Zeeman, Bot, & Lettinga, 2004; Yiannopoulos, Manariotis, & Chrysikopoulos, 2008), which is a potential combination to enhance the global biogas utilization efficiency.

Although there are several advantages of using AD, the energy requirements (heat and electricity) for the digestion operation and incomplete COD/BOD removal are the main drawbacks that limit its extensive application. Moreover, depending on the final use of the effluent or the discharge standards, additional stages are required to reduce the organic load.

1.1.2. Fundamentals of selected secondary wastewater treatments

Owing to the incomplete COD/BOD removal in the primary stage of the wastewater treatment, additional stages are needed to satisfy the EPA discharge standards. Technologies such as aerobic treatment (Caruana & Olsen, 2012), electro-coagulation (EC) (Jiang, Graham, André, Kelsall, & Brandon, 2002), electro-deposition, electro-oxidation (G. Chen, 2004), nano-filtration, and reverse osmosis provide solutions to complete the waste treatment.

Aerobic treatment (AET) is a biochemical process that stabilizes the wastewater sludge via oxidation. This method is capable of handling relatively low-strength wastewater (Wang et al., 2009), and has been tested in a sequence operation with anaerobic digesters (Chan, Chong, Law, & Hassell, 2009; Fricke, Santen, & Wallmann, 2005). Influent concentrations in the range of 50–4,000 mg per liter of COD are effectively treated in the AET processes (Grady et al., 1999). Oxygen or air is supplied by aerators (diffusers) to maintain a dissolved oxygen concentration in the influent in the range of 1–2 mg/L for microbial growth (EPA, 2000). The overall AET process is described as

$$C_5H_7NO_2 + O_2 \rightarrow 5CO_2 + 2H_2O + NH_3 \qquad \text{(I.2)}$$

where $C_5H_7NO_2$ commonly represents the organic matter in the waste stream. AET offers advantages over other treatment processes, such as easy operation (compared with AD), high removal efficiency of volatile solids, odor reduction, production of effluent with low BOD_5/COD content, and short hydraulic retention times. However, AET has certain disadvantages, such as producing a digested sludge with poor dewatering characteristics, requiring a high energy consumption for the aeration process, being influenced by ambient temperature, and carrying out a low level of heavy metal removal.

The AET procedure is used in batch or in continuous operation. For the batch operation, the influent is pumped after the solid stabilization stage, and during the filling operation, the sludge (influent) is continually aerated at a lower rate initially. When the tank or pond is full, aeration continues at a higher rate for a given period to assure the removal of the organic load. The effluent is clarified by decantation to settle the non-soluble solids. For the continuous operation, the treatment works in a similar way to the batch operation, but the aerator functions at a fixed rate, and the liquid overflows into the solid-liquid separator.

In addition to biological treatments, chemical procedures have been applied to remove impurities in wastewater (used in the petroleum, mining, and chemical industries (Mollah, Schennach, Parga, & Cocke, 2001)). Electro-coagulation (EC) is a technology that involves the generation of coagulants by electrically dissolving (consuming DC electricity) either aluminum or iron ions from aluminum or iron electrodes, respectively (G. Chen, 2004). EC has certain advantages, such as short retention times, the efficient removal of fine particles, no additional coagulation-inducing reagents, and a small footprint, representing a convenient process to polish the AD effluent. However, due to the high-energy demand of EC technology, it has not been widely used for wastewater treatment. On the other hand, Liu et al. (Z. G. Liu & Liu, 2016) has studied a case that treats high-strength wastewater from anaerobic digestion for reclaimed water, concluding that the EC process simultaneously coagulates and floats solid particles in the solution, achieving a good removal performance for the wastewater with high organic loading.

1.2. Solar technologies for heat and electricity generation

Solar radiation is the most abundant energy source on the planet. The greatest advantage of solar energy as compared with other forms of energy is that it is clean and can be supplied without negative environmental consequences (Kalogirou, 2009). Solar radiation can be categorized in three forms. First, direct normal irradiance (DNI) is the amount of solar radiation received by a surface held perpendicular to the rays that arrive in a straight line from the direction of the sun (this quantity is of particular interest to concentrating solar thermal installations and installations that track the position of the sun). Second, diffuse horizontal irradiance (DHI) is the amount of radiation received by a surface that does not arrive in a direct path from the sun, but has been dispersed by particles in the atmosphere and comes equally distributed from all directions. Third, global horizontal irradiance (GHI) is the total amount of radiation received from above by a surface horizontal to the ground (GHI is of particular consideration for photovoltaic uses and includes both DNI and DHI).

Depending on the types of energy generation (combined heat and power generation (CHP) or electricity generation only), solar technologies are available as depicted in Figure I-3 (modified from Siva Reddy et al. (Siva Reddy, Kaushik, Ranjan, & Tyagi, 2013)). Moreover, solar thermal technologies for CHP can be classified according to the working fluid temperature (Siva Reddy et al., 2013). Low- and medium-temperature technologies, such as parabolic solar concentrators, collect energy of up to 50 kW (with a fluid temperature of 400 °C and collecting 60–70% of incident solar radiation). High-temperature solar technologies, such as the parabolic dish Stirling engine and central tower receiver, are operated at temperatures higher than 600 °C, and are used in large solar power plants (megawatt or above) to generate electricity and heat.

For low-temperature solar technologies (less than 50 kW), the Fresnel lens (FL) and parabolic trough (PT) are the common configurations (Giostri, Binotti, Silva, Macchi, & Manzolini, 2013). The PT has been widely used in the past decades, presenting an optical efficiency of 75%, higher than the FL (67%). Although the FL has a lower optical efficiency, it still has certain advantages compared to the PT, such as having inexpensive, thin, and lightweight elements. With a lightweight supportive structure, the energy consumption required for the tracking system is lower than that required for systems with massive metallic reflectors.

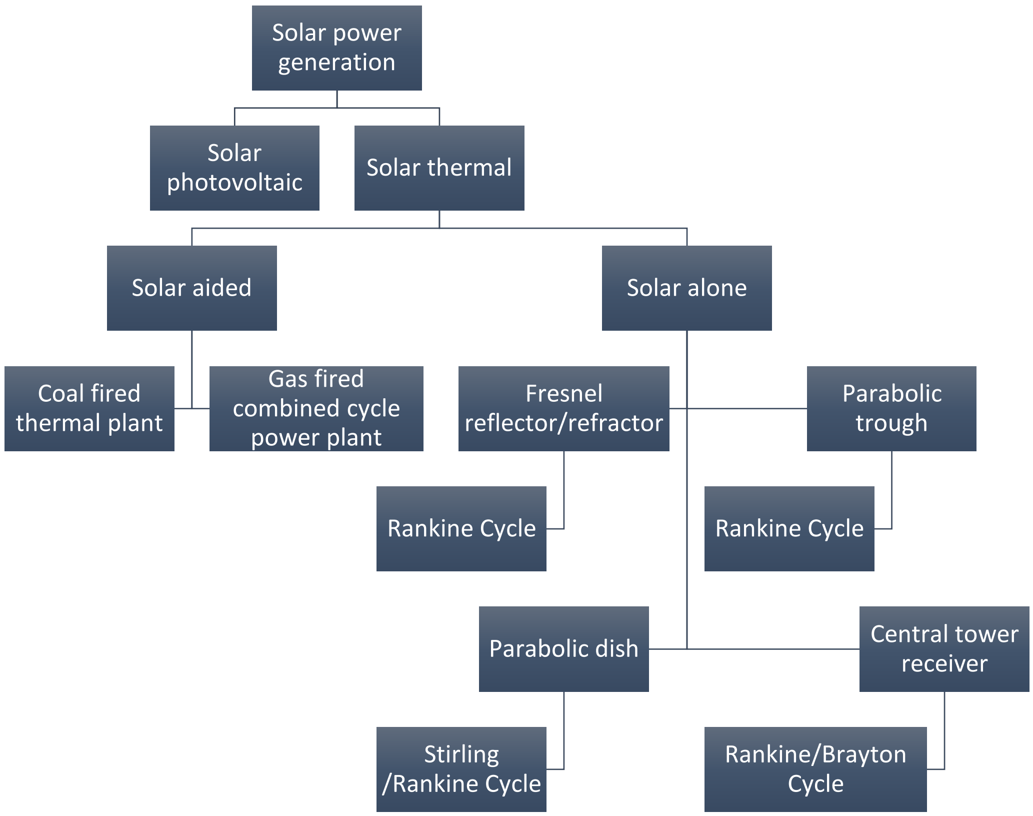

Figure I-3. Schematic diagram of solar power generation methods

The FL applies the same principles as an ordinary lens, but it has a different geometric configuration. The ordinary lens has a thick lens to achieve the focus, which is impractical for lens collector installations. In principle, it is segmented to create several refractive/reflective surfaces, replacing the curved surface of the convectional lens with a series of concentric grooves. These contours perform as individual refracting/reflecting surfaces, bending parallel light rays to a common focal length (Figure I-4 (EdmundOptics, 2016)).

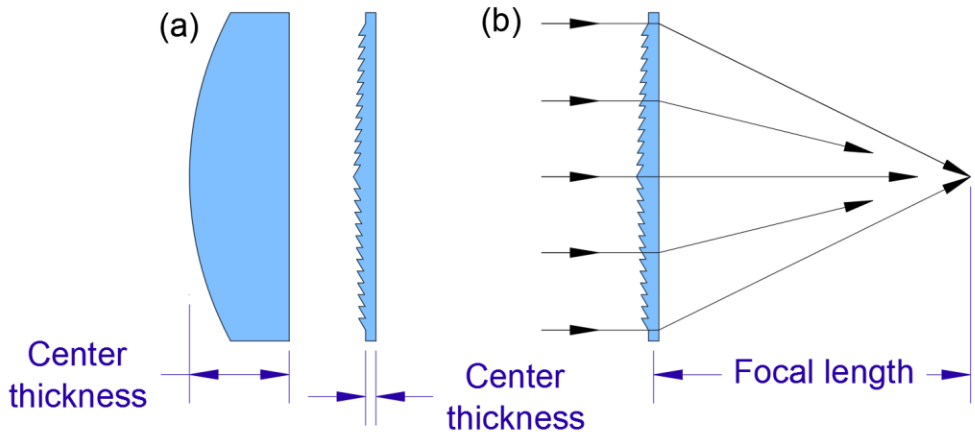

Figure I-4. (a) Ordinary and Fresnel lens profile; (b) refractive Fresnel lens

Fresnel lenses are very useful for solar energy collection (imaging or non-imaging systems) (Xie, Dai, Wang, & Sumathy, 2011), especially in large installations (concentrating light onto a photovoltaic cell or to heat a surface). Linear Fresnel lenses can be used instead of parabolic trough reflectors, as presented by Zhu et al. (G. D. Zhu, Wendelin, Wagner, & Kutscher, 2014) and Zhai et al. (Zhai, Dai, Wu, Wang, & Zhang, 2010). In addition, spherical Fresnel lenses can be used instead of parabolic dish reflectors (Xie, Dai, & Wang, 2013). As the solar collection area increases, the size of the parabolic collectors causes mechanical problems resulting from the increase in weight, such as requiring heavy structures to hold the elements, as well as the high energy consumption of the solar tracking system. In practice, it appears to be uneconomical to build parabolic collectors with aperture areas much larger than 100 m^2 (Böer & SpringerLink, 1986). These problems can be solved by Fresnel lenses.

In the CSP systems, concentrating receivers form an important subsystem that must be analyzed based on the nature of the solar collection (reflected, refracted), and geometry configuration (convex, concave, flat, covered, uncovered) (Duffie & Beckman, 2006). A ratio that is commonly used for the solar receiver design is the concentration ratio (CR):

$$CR = \frac{A_l}{A_a} \tag{I-3}$$

where A_l is the collection area of the reflective or refractive element; and A_a is the absorber area of the solar receiver. In the concentration ratio, the acceptance angle defines the limits of the solar concentration and tracking requirements, and is defined as the angular range over which all or almost all of the incident rays are accepted without moving all or part of the collector (Böer & SpringerLink, 1986). The maximum concentration ratio (CR_{max}) for a given acceptance half-angle (θ_a) and for a two-dimensional (2D) (linear) concentrator is given by

$$CR_{max} = \frac{1}{\sin(\theta_a)} \tag{I-4}$$

For three-dimensional (3D) collectors, the maximum concentration ratio is calculated as

$$CR_{max} = \frac{1}{\sin^2(\theta_a)} \tag{I-5}$$

The angular radius of the sun (θ_a) is approximately 5 mrad (0.25°), and the maximum values of concentration for 2D and 3D concentrators are 200 and 40,000, respectively.

In addition to combined heat and power generation, photovoltaic panels are an option to generate energy by directly converting the sunlight into electricity (the operational process of converting light to electricity is called the PV effect). Traditional solar cells are made from silicon. Second-generation solar cells are called thin-film solar cells (consisting of layers of semiconductor that are a few micrometers thick), and are made from amorphous silicon or non-silicon materials, such as cadmium telluride. Third-generation solar cells are made from a variety of materials besides silicon, including solar inks, solar dyes, and conductive plastics (NREL, 2016a). Furthermore, new solar cells use plastic lenses or mirrors to concentrate solar radiation onto a small area of high efficiency PV material (called concentrated photovoltaics (CPV)).

Mathematical models predict the behavior of PV configurations under different ambient conditions (Bellia, Youcef, & Fatima, 2014). Although a high value of GHI increases the solar energy availability to generate electricity, the increment in the cell temperature decreases the electricity generation (Skoplaki & Palyvos, 2009). The nominal operating cell temperature (NOCT) is one of the methods used to quantify the energy generation under different solar radiation values. Low cell temperature and high GHI value are the optimal parameters to enhance the conversion efficiency, but these factors are not obtained simultaneously without a cooling system.

1.3. Thermodynamics of heat and energy generation

1.3.1. Gas power systems - the air standard Brayton cycle

Gas power systems utilize gas as a heat transfer fluid (HTF) to complete power generation. The energy remains in the gas-phase during the thermodynamic cycle. In the turbine, shaft-work is produced by a rotor while the HTF expands in a controlled volume (Figure I-5 adapted from (Massoud, 2005)). Air is compressed and forced into a combustion chamber for heat addition. Inside the turbine, the air flows through the static blades and rotates the dynamic blades connected to the rotor. A percentage of this work is transferred to the compressor. When the air leaves the turbine, it also carries a portion of its energy to the heat sink (heat exchanger).

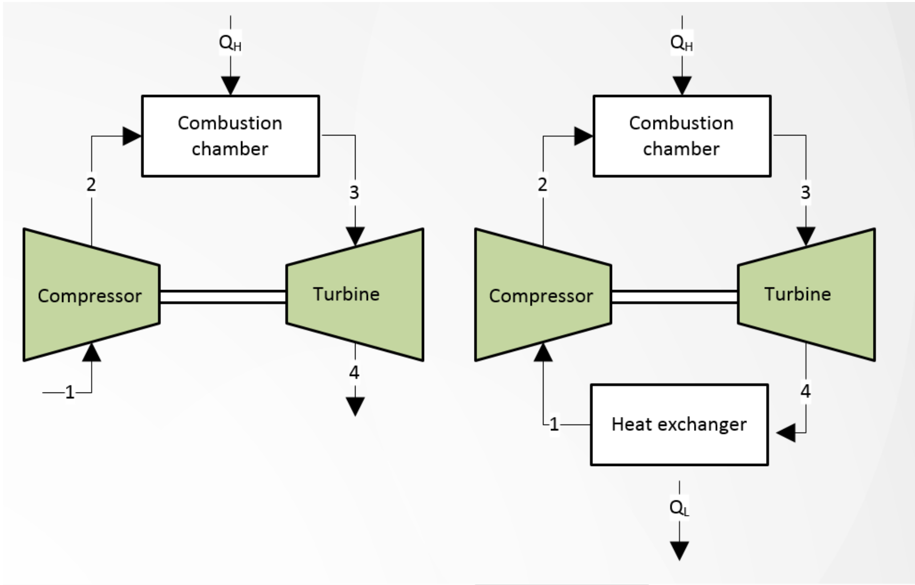

Figure I-5. Schematic of an open- and closed-cycle gas turbine

The following assumptions are often used to simplify the analysis of the air standard cycle: (1) the HTF acts as an ideal gas (this allows the internal energy to be described in terms of temperature and specific heat); (2) the mass flow is fixed for the cycle; and (3) all processes are reversible and the effects of kinetic and potential energies are negligible. The compression and expansion occurs in isentropic processes, and heat addition and rejection in isobaric processes. Three ratios are associated with the energy generation consumption in the cycle: (1) the compression ratio (r_v) is defined as the ratio of the gas volume before compression to the gas volume after compression, $r_v = \frac{v_1}{v_2}$; (2) the pressure ratio or compressor pressure ratio (r_p) is defined as the ratio of gas pressure after compression to gas pressure before compression, $r_p = \frac{p_2}{p_1}$ (for an isentropic compression, $r_p = r_v^{\gamma}$, γ is the ratio between the specific heat at constant pressure and the specific heat at constant volume); and (3) the temperature ratio (r_T) is defined as the ratio of the maximum to the minimum temperature in a cycle, $r_T = \frac{T_3}{T_1}$. The thermal efficiency can be derived from the temperatures in the cycle:

$$n_{ht} = 1 - \frac{\dot{Q}_L}{\dot{Q}_H} = 1 - \frac{\left(\frac{T_4}{T_1} - 1\right) T_1}{\left(\frac{T_3}{T_2}\right) T_2} \tag{I.6}$$

1.3.2. Vapor power systems – the Rankine cycle

The vapor power system is based on the Rankine cycle (Figure I-6, adapted from (Massoud, 2005)). The power is generated based on the phase change of the HTF.

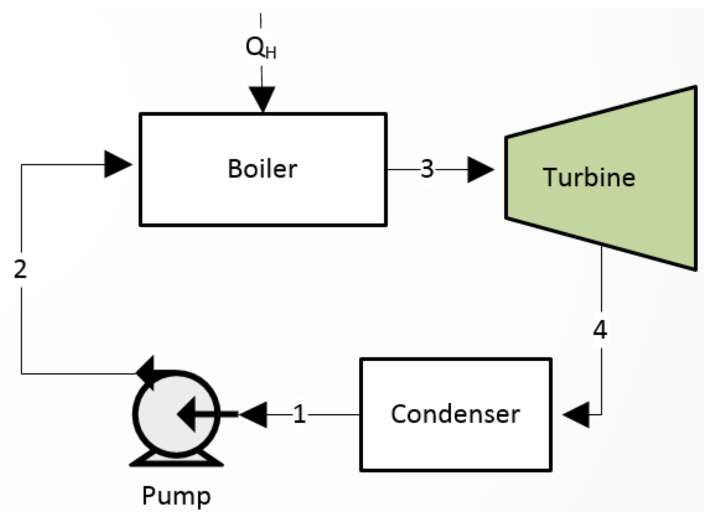

Figure I-6. Rankine cycle for a steam turbine

For steam utilization in the turbine, water is pumped isentropically into the boiler (heat source) that is maintained at constant pressure. Saturated or superheated steam is generated from the boiler, and enters the turbine. The stationary blades direct the flow through the rotary blades fixed on the work shaft. In the Rankine cycle, the expansion occurs isentropically. The steam leaves the turbine and a condenser extracts heat at constant pressure, and then the water is pumped to the heat source for the next cycle. The thermal efficiency of the Rankine cycle is given by the following equation:

$$n_{ht} = \frac{\dot{W}_{net}}{\dot{Q}_H} = \frac{\dot{m}(h_3 - h_4) - \dot{m}(h_2 - h_1)}{\dot{m}(h_3 - h_2)} \qquad \text{(I.7)}$$

where $\dot{W}_{net}$ is the net work of the system; $\dot{Q}_H$ is the heat added; $\dot{m}$ is the mass flow; and h_n is the enthalpy.

1.4. Solar hybrid power generation system

For electricity generation, hybridization has become a strategy incorporating several different energy sources that are collectively used to achieve the benefits of energy stability, electricity flexibility, and efficiency improvement. Several solar-hybrid power generation systems have been studied and implemented (Jamel, Abd Rahman, & Shamsuddin, 2013) (Olivenza-Leon, Medina, & Hernandez, 2015). Popov (Popov, 2014) presents a concept combining gas turbines with solar energy, in which the system uses the solar energy in a chiller to cool down the inlet air in the compressor (point 1 in Figure I-5) (a lower temperature entails a higher mass flow). In addition, Schwarzbozl (Schwarzbözl et al., 2006) uses solar energy to increase the temperature of the compressed air (point 2 in Figure I-5), and consequently reduce the heat demand of the gas burner for the gas turbine system.

Casati et al. (Casati, Galli, & Colonna, 2013) conducted a study of a 100 kW power generation plant using a solar-facilitated Rankine cycle. Solar energy was used to generate the steam (approximately 300 °C) for the thermodynamic cycle (line 2 in Figure I-5). Bao et al. (Bao, Zhao, & Zhang, 2011) studied a concept similar to the solar-facilitated Rankine cycle for power generation except that isopentane/R245fa was used as the HTF.

However, most of these studies focused on large-scale solar-hybrid power generation systems, and only a few were for small-scale micro-power generation. Koai et al. (Koai, Lior, & Yeh, 1984) presented in their study a steam turbine for 22 kW (30 hp) of electrical power. In addition, The Office of Energy Efficiency and Renewable Energy (Energy, 2007) analyzed the case of heat and power gas turbines for 30 kW electricity production. From the results of these studies, it was concluded that the key limitation for small-medium solar-hybrid power plants is low system efficiency.

Additionally, solar hybridization can be implemented by installing photovoltaic panels (Deshmukh & Deshmukh, 2008), which can directly supply the electrical energy generated to cover the power load required. The system can be connected to the national or local electrical grid to supply energy when the PV generation is greater than the demand, and obtain electricity from the grid when the solar radiation is insufficient to cover the power load. For self-sustaining systems, a battery bank can store the excess electrical generation and supply energy during deficit production. Lead acid and lithium ion batteries are used, both differing in their capacity storage, minimum discharge capacity, lifetime, and cost. PV solar–bio hybridization has been integrated with anaerobic digestion treatments (Bhatti, Joshi, Tiwari, & Al-Helal, 2015), which utilizes heat recovered from the PV cell cooling device to maintain the AD culture temperature at 35 °C. Further, Borges et al. (Borges Neto, Carvalho, Carioca, & Canafístula, 2010) present a system that combines biogas from goat manure and PV panels for a small-scale rural community in Brazil. Moreover, for high electricity demand, studies have shown the feasibility of PV hybridization, such as Gazda et al. (Gazda & Stanek, 2016), who presented a bio-hybrid system that provides heat, cooling, and electricity. Gonzáles et al. (González-González, Collares-Pereira, Cuadros, & Fartaria, 2014) studied a feasible bio-PV hybridization for a pig slaughterhouse in

Spain (79 kWe from biogas and 225 kWe from PV installation). Indeed, PV hybridization is an option to cover the energy demand of the wastewater treatment plant.

1.4.1. Biogas utilization for electricity production

Solar–bio hybridization requires biogas to be utilized when solar energy is not available to generate electricity. Biological treatments such as anaerobic and aerobic digestion have a continuous electricity demand for the biological reactions to occur. Solar energy, unless it has massive thermal energy storage, can supply energy for electricity generation for a few hours. At night or during prolonged cloudy days, the reserve in solar energy storage may become unavailable. Long-term biogas storage is an option to continue producing electricity continuously, balancing the thermal energy sources from the hybridization. Biogas from wastewater treatment plants is capable of being stored and upgraded for electrical power generation (Osorio & Torres, 2009). Before storage, it is upgraded into biomethane by removing most of its components, while the heating value is increased, corrosion in the storage tanks is avoided, and undesired components are removed for the biomethane combustion.

Water, hydrogen sulfide (removed during or after digestion), organic silicon, and carbon dioxide are the typical components to remove in the biogas upgrading (Basu, Khan, Cano-Odena, Liu, & Vankelecom, 2010; Ryckebosch, Drouillon, & Vervaeren, 2011). Different processes are available to remove one or more components simultaneously, such as water scrubbing, cryogenic separation, physical or chemical absorption, pressure swing absorption, and membrane separation technology. Whatever the process or processes selected, electricity is required to performed the cleaning and upgrading process (Sun et al., 2015).

Biomethane is not stored easily, as the liquefaction does not occur under ambient pressure and temperature (the critical temperature and pressure required are -82.5 °C and 47.5 bar, respectively) (Kapdi, Vijay, Rajesh, & Prasad, 2005). Most of the processes for biogas upgrading are conducted under high pressure, and the biogas can be stored long-term in commercial gas cylinders. Typical pressures and materials for biogas/biomethane storage are presented in Table I-2 (Kapdi et al., 2005)

Table I-2. Biogas storage options

Pressure	**Storage device**	**Material**
Low (0.138–0.414 bar)	Water sealed gas holder	Steel
Low (0.138–0.414 bar)	Gas bag	Rubber, plastic
Medium (1.05–1.97 bar)	Propane or butane tanks	Steel
High (200 bar)	Commercial gas cylinders	Alloy

2. Goal, scope, and objectives

The goal of the proposed research is to develop a solar–bio hybrid concept for electricity and heat generation that enables the establishment of a self-sustaining small-scale wastewater treatment system. The hypothesis is that a combination of solar energy and biological methane generation could provide stable and sufficient energy to satisfy the requirements of the unit operations of the small-scale treatment system (thermophilic anaerobic digestion, secondary wastewater treatment, water purification, and solar energy collection). Further, this concept could overcome the disadvantages of individual technologies, such as the unsteady energy flow from solar power generation, low conversion efficiency of mesophilic anaerobic digestion, and excessive thermal and electrical energy requirements of the wastewater treatment operations.

The study considers different options to complete the key processes of wastewater treatment (Figure I-7). Solar collection technologies, the characteristics of influent treatment, power generation technologies, and secondary treatments were systematically studied to balance the overall efficiency and overcome potential disadvantages of individual processes.

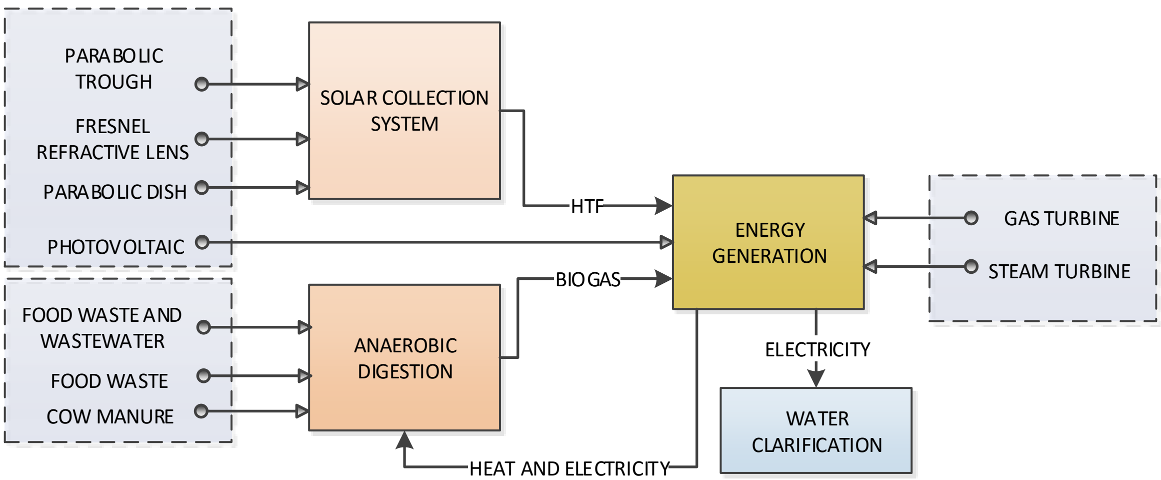

Figure I-7. Different scenarios for the solar–bio hybrid power system and wastewater treatment plant

Four solar collection technologies: Fresnel lenses, parabolic dishes, parabolic troughs, and photovoltaic panels were selected for solar energy collection. Feedstock consisting of food waste, cow manure, and combined food-waste and municipal wastewater were studied for the AD treatment to generate the biomethane. Energy is generated by the combined heat and power (CHP) technologies. Three configurations consisting of CHP with gas turbine, CHP with steam turbine, and CHP with PV electricity and thermal heat were investigated.

The specific objectives of the proposed study were:

(1) To perform a technical analysis of small-scale solar–bio hybrid power generation systems using the Rankine and Brayton cycles to supply the balance in the thermal energy requirements by the anaerobic digestion process (presented in Chapter 2).

(2) To establish an energy and mass balance for the wastewater treatment by a self-sustaining bio-hybrid operation using solar energy (presented in Chapter 3).

(3) To obtain the geometrical and thermal parameters for the design of a solar thermal collector for electricity generation using small refractive Fresnel lenses (presented in Chapter 4).

(4) To design a novel receiver for concentrated solar energy from refractive Fresnel lenses (presented in Chapter 5).

CHAPTER II. SMALL-SCALE SOLAR–BIO HYBRID POWER GENERATION USING BRAYTON AND RANKINE CYCLES

Abstract

This study conducted a detailed technical analysis of small-scale solar–bio hybrid power generation systems using the Rankine (steam turbine) and Brayton (gas turbine) cycles. Thermodynamic models have been developed to characterize the state of the working fluid and select the most suitable solar collection technology for individual power generation systems. The net capacity factor of power generation and utilization efficiencies of solar and biomethane energy were used as parameters to evaluate the energy generation and optimize the system configuration. The analysis elucidated that the global thermal efficiency of the steam turbine system (54.87%) was higher than that of the gas turbine system (41.43%), although the electricity generation efficiency of the steam turbine system (14.69%) was lower than that of the gas turbine system (27.32%). The study also analyzed the effects of different climates on the selection of suitable hybrid systems. Considering global thermal efficiency and system footprint, the steam turbine system was found to be more suitable for both cold and warm climate locations.

Appendices for this chapter:

i. Appendix A: Matlab code for system solar bio-hybrid modeling

ii. Appendix B: Matlab script functions for turbine modeling

iii. Appendix C: Matlab script functions for solar collector modeling

1. Introduction

Hybridization of power generation is a strategy that several different energy sources are collectively used to achieve benefits of energy stability, electricity flexibility, and energy efficiency improvement. Many hybridization studies have focused on combining solar energy with fossil fuels (Pihl, Spelling, & Johnsson, 2014; Zhao, Hong, & Jin, 2014), in which the concentrated solar energy is used as the heat source to raise the temperature of the working fluid prior to the fuel combustion and improve energy generation efficiency (Jamel et al., 2013; Popov, 2014). With increasing attention on utilization of more renewable resources for power generation, combining concentrated solar energy with biomethane becomes a potential alternative to solar-fossil-fuel hybrid power generation (Colmenar-Santos et al., 2015; San Miguel, Miguel, & Corona, 2014). However, current research and development on solar–bio hybridization has focused on large-scale power generation ranging from a few hundred kW to several MW (Immanuel Selwynraj, Iniyan, Polonsky, Suganthi, & Kribus, 2015; Livshits & Kribus, 2012; San Miguel et al., 2014; Schwarzbözl et al., 2006). Only a few studies have been reported on solar–bio hybrid micro-power (less than 100 kW) generation (Buck & Friedmann, 2007; Koai et al., 1984). Considering the end-users of such hybridization power generation technologies, there is a high demand for small-scale distributed renewable systems for farm/food operations and remote villages/towns. Therefore, in-depth studies on small-scale solar–bio hybrid power generation are very much needed to extend the hybridization concept to a wider range of applications.

Anaerobic digestion (AD) is an existing natural and biological conversion process that has been proven effective in converting wet organic wastes into biomethane. It is capable of producing clean electricity, while also alleviating many of the environmental concerns associated with the wastes (odor, greenhouse gas emissions, and groundwater contamination) (Caruana & Olsen, 2012). In addition, contrasting to large-scale power plant operations, AD can be set up in small- or medium-scale biomethane generation plants, such as wastewater treatment plants, food processing plants, and animal farms (e.g., more than 80% of U.S. animal farms have less than 500 heads of animals) (USDA National Agricultural Statistics Service, 2009). Combining the AD operation and solar thermal collection to develop small-scale solar–biomethane hybrid power generation could provide a win-win solution to treat organic wastes and satisfy the energy demands of farm or residential operations.

Solar thermal technologies are classified as low-, medium-, and high-temperature solar thermal collection (Siva Reddy et al., 2013). Due to the temperature requirements of the turbines for power generation, medium- and high-temperature solar thermal collection are the solar thermal technologies that can be used for the hybridization system. Medium-temperature (approximately 400 °C) solar thermal technologies often use parabolic troughs to collect solar energy. Central tower receivers and parabolic dishes are high-temperature (more than 500 °C) solar thermal technologies. Considering the scale of power plants, central tower receivers are mainly used by solar thermal power plants to generate electricity in the magnitude of 100 MW or above. It requires large solar fields, and the operating temperature typically ranges from 600 °C to 1,400 °C (Siva Reddy et al., 2013). However, parabolic dishes and parabolic troughs are solar thermal technologies that could be used for small- and medium-scale power operations and generate electricity in the magnitude of kW.

In order to develop small-scale solar–bio hybrid power generation, 30 kW power generation systems, including three unit operations consisting of AD, solar thermal collector, and engines were comprehensively analyzed in this paper. Biomethane from anaerobic digestion and thermal energy from solar collection were used as the energy sources to power engines to generate electricity and heat. Gas and steam turbines as engine units were compared to determine the most suitable for the studied solar–bio hybrid system. The net capacity factor (the ratio of the energy output to the total energy generation of the system in a given time duration) and solar and biogas utilization factors (the percentage of each energy source used to generate the electrical energy) were used as parameters to evaluate the energy generation and optimize the system configuration.

2. The studied small-scale solar–bio hybrid power generation system

Thermodynamic models were established to analyze the solar–bio hybrid systems consisting of gas and steam turbines (Figure II-1). The biomethane production for the studied systems was based on a biomethane plant using thermophilic anaerobic digestion on a mixture feed of dairy manure and food wastes (90:10 ratio, 5% total solids) (R. Chen et al., 2016). The anaerobic digestion with a culture temperature of 50 °C and a hydraulic retention time (HRT) of 20 days produced 0.38 m^3 methane per m^3 digestion solution per day (the low heating value of methane is 34 MJ/m^3 (Sun et al., 2015)). The steam turbine includes a condenser to recycle the water in a closed-loop circuit (Figure II-1a). The gas turbine uses a regenerator to transfer energy from the exhaust gases into the compressed air in an open-loop air circuit (Figure II-1c). Both systems contain water heat storage to collect energy from the thermodynamic cycle for the heat demand of the anaerobic digester (to maintain the digestion temperature and heat the influent). The solar–bio hybrid power generation systems (which include a secondary heat source of solar energy) have slightly more complicated configurations than the turbine power generation systems. Molten salt is used as the solar thermal storage (Halotechnics, 2013).

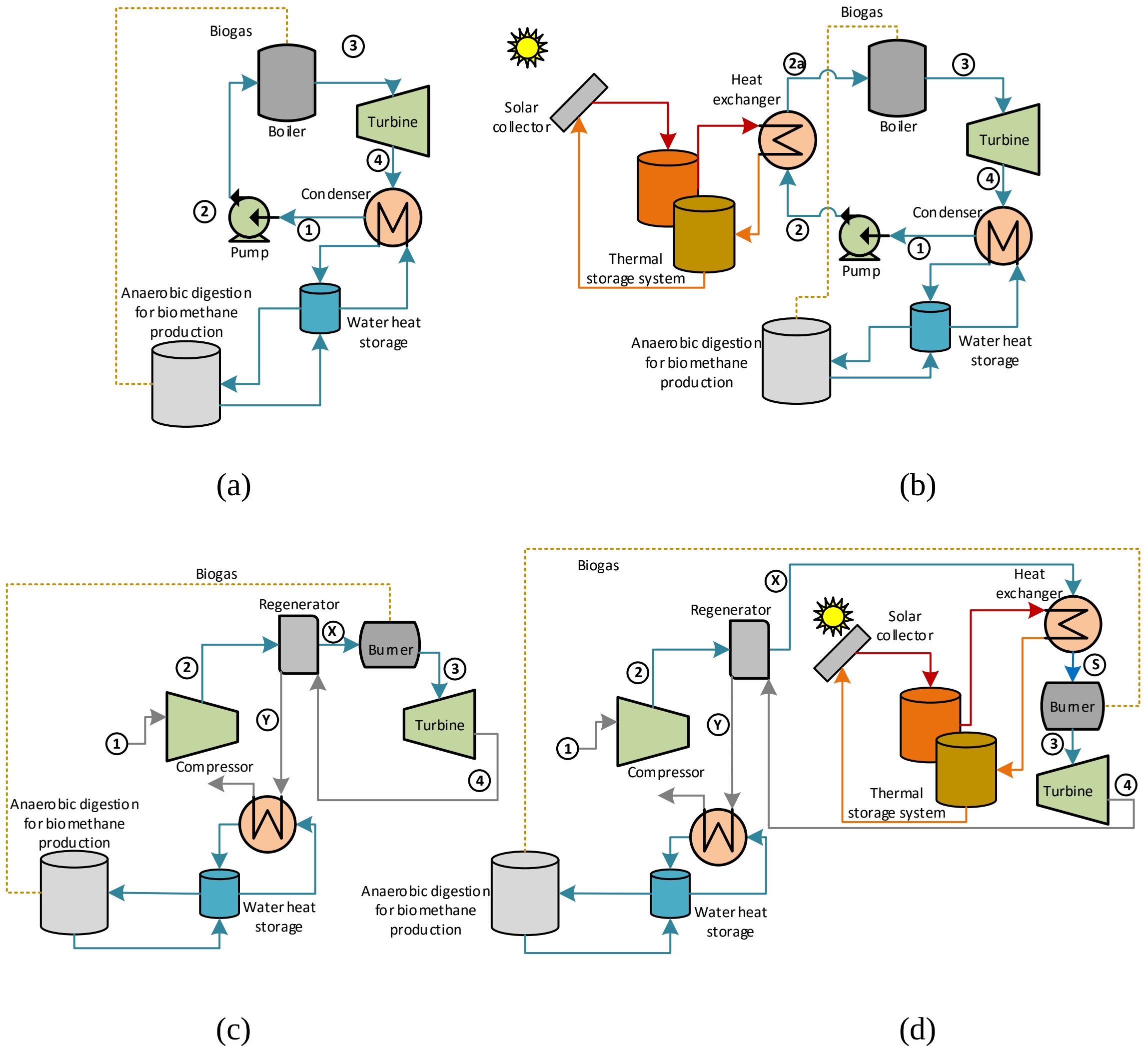

Figure II-1. Schematics of the studied solar–bio hybrid power generation systems*

*: (a) the biomethane steam turbine; (b) the solar–bio hybrid power system with steam turbine; (c) the biomethane gas turbine; (d) the solar–bio hybrid power system with gas turbine.

In the solar–bio hybrid system with steam turbine, a heat exchanger was implemented to use the heat from the solar thermal storage to heat the working fluid prior to entering the biomethane boiler. The boiler further heats the working fluid to generate superheated steam to power the steam turbine (Figure II-1b). The solar–bio hybrid system with gas turbine uses the heat from the solar thermal storage to raise the temperature of the hot air from the regenerator in the heat exchanger. This is done before the air is mixed with biomethane fuel in the burner to generate heat for the gas turbine (Figure II-1d). The analyses were based on a constant electricity generation of 30 kW for all studied systems. The operational parameters of the thermodynamic models are listed in Table II-1.

Table II-1. Operational parameters of 30 kW steam and gas turbines*

System	**Parameter**	**Unit**	**Value**
Steam turbine (30 kW)	Water mass flow	kg/s	0.0807
	Steam inlet pressure (turbine)	bar	10
	Condenser pressure	bar	0.2
	Steam inlet temperature (turbine)	°C	200
Gas turbine (30 kW)	Air mass flow	kg/s	0.31
	Air inlet temperature (turbine)	K	1,113
	Compression ratio	-	3.2
	Air inlet temperature (compressor)	K	300
	Air temperature after expansion	K	912

*: The parameters are from commercial steam and gas engines *(A. Liu & Weng, 2009; NextGrid, 2014).*

The Rankine cycle was used to simulate the performance of the biomethane steam turbine. The working fluid consisting of water is pumped into the boiler that is maintained at constant pressure (Figure II-1a and b). The power consumption of the pump and the enthalpies at points 2 and 4 in Figure II-1a and b are calculated by

$$w_P = v_\iota \cdot (P_i - P_o) \cdot 100/\eta_p \qquad \text{(II-1)}$$

$$h_2 = h_1 + w_P \quad \text{(II-2)}$$

$$h_T = h_3 - \frac{W_s}{\dot{m}_{H_2O}} \quad \text{(II-3)}$$

where w_P is the pump work (kJ/kg_{water}); η_p is the pump efficiency (set at 0.65); v_ι is the specific volume (m^3/kg); P_i and P_o are the inlet and outlet pressures in the turbine; h is the enthalpy at given temperature and pressure conditions (kJ/kg_{water}); W_s is the gross power generated (shaft work (30 kW), pump power ($w_P \cdot \dot{m}_{H_2O}$), and vacuum pump (0.5 kW)); and $\dot{m}_{H_2O}$ is the steam requirement (0.0807 kg/s). The fuel efficiency of the system is calculated based on the fluid properties at the inlets and outlets of the turbine and pump:

$$\eta_F = \frac{(h_3 - h_{4a})}{(h_3 - h_2)} \quad \text{(II-4)}$$

where $(h_3 - h_{4\mathrm{a}})$ is the work performed in the turbine (kJ/kg_{water}). The enthalpy at condenser conditions (h_4) is calculated considering an isentropic turbine efficiency. To satisfy the required temperature and pressure of the feedwater for the selected 30 kW steam engine, the heat input Q_F and the heat extracted Q_H of the system are calculated as follows:

$$Q_F = \frac{\dot{m}_{H_2O} \cdot (h_3 - h_2)}{\eta_b} \quad \text{(II-5)}$$

$$Q_H = \dot{m}_{H_2O} \cdot (h_4 - h_1) \cdot \eta_c \quad \text{(II-6)}$$

where η_b is boiler efficiency (set at 0.85); and η_c is the condenser efficiency (heat sink) (set at 0.85). The simulation results for the steam turbine are presented in Table II-2. The enthalpies at points 1, 2, and 3 (Figure II-1) were 243.03 kJ/kg_{water}, 244.57 kJ/kg_{water}, and 2828.3 kJ/kg_{water}, respectively (Table II-1). The temperatures at points 2 and 4a were 58.23 °C and 103.54 °C, respectively. The corresponding heat input and heat extraction were 245.33 kW and 134.61 kW, respectively. The thermal efficiency calculated for this particular equipment under the working parameters showed that 14.69% of the biomethane fuel was transformed into shaft work for electricity generation, and 54.87% of the biomethane fuel was turned into heat.

Table II-2. Simulation results of a 30 kW steam turbine

Parameter	**Unit**	**Simulation results**
P_o	bar $_{abs}$	0.2
w_P	kJ/kg$_{water}$	1.53
h_1	kJ/kg$_{water}$	243.03
h_2	kJ/kg$_{water}$	244.57
T_1	°C	58.06
T_2	°C	58.23
h_3	kJ/kg$_{water}$	2,828.30
h_4	kJ/kg$_{water}$	2,205.2
T_4	°C	60.06
η_T	-	0.1469
Q_F	kW	245.33
Q_H	kW	134.61

In the solar–bio hybrid steam power system (Figure II-1b), the solar thermal energy reduces the amount of heat required by the boiler, and consequently decreases the biomethane consumption. The solar thermal energy (Q_{solar}) heats the water and generates a mixture of saturated steam and liquid at 99.60 °C. The boiler then converts the rest of the liquid into saturated steam and superheats the steam to satisfy the required temperature and pressure by the turbine (200 °C at 10 bar abs). The enthalpy of the mixture after the solar heating is:

$$h_{2a} = \frac{Q_{solar}}{\dot{m}_{H_2O}} + h_2 \tag{II-7}$$

The heat added in the boiler (only required if Q_{solar} is lower than Q_F) is calculated by

$$Q_{bs} = \frac{\dot{m}_{H_2O} \cdot (h_3 - h_{2a})}{\eta_b} \tag{II-8}$$

where η_b is the boiler efficiency. As for the gas turbine, the Brayton cycle was used to simulate the turbine performance. The temperature (T_2^G) after the compressor (point 2 in Figure II-1c and d) was calculated by

$$T_2^G = T_1^G \cdot \left(1 + \frac{1}{\varepsilon_c} \cdot (r_P^\alpha - 1)\right) \tag{II-9}$$

$$\alpha = \frac{\gamma - 1}{\gamma} \tag{II-10}$$

where r_p is the pressure ratio between the inlet and outlet in the compressor; α is a constant; γ is the ratio between the specific heat at constant pressure and the specific heat at constant volume; and ε_c is the compressor efficiency ($\varepsilon_c = 0.82$). The temperature after the regenerator (Point X in Figure II-1c and d) is given by

$$T_x^G = T_4^G \cdot \varepsilon_R + T_2^G \cdot (1 - \varepsilon_R) \tag{II-11}$$

where ε_R is the regenerator efficiency ($\varepsilon_R = 0.78$). The heat input to the burner (${Q_F}^G$) is calculated by

$${Q_F}^G = \dot{m}_{air} \cdot \frac{Cp_3 \cdot (T_3^G - T_x^G)}{\varepsilon_{HC}} \tag{II-12}$$

where Cp_3 is the specific heat at $\frac{T_3^G + T_x^G}{2}$ [kJ/kg·K]; and ε_{HC} is the burner efficiency ($\varepsilon_{HC} = 0.98$). The temperature of the exhaust gases after the regenerator (Point Y in Figure II-1c and d) is given by

$$T_y^G = T_2^G \cdot \varepsilon_R + T_4^G \cdot (1 - \varepsilon_R) \tag{II-13}$$

The fuel efficiency for the gas turbine is:

$$\eta_F^G = \frac{W_s}{Q_F{}^G} \tag{II-14}$$

The heat extracted from the exhaust gases ($Q_H{}^G$) is calculated by

$$Q_H{}^G = \dot{m}_{air} \cdot Cp_{3a} \cdot \left(T_y^G - T_F^G\right) \cdot \varepsilon_L \tag{II-15}$$

where Cp_{3a} is the specific heat at $\frac{T_y^G + T_1^G}{2}$ [kJ/kg·K]; T_F^G is the temperature of the exhaust gases (assumed as 85 °C); and ε_L is the efficiency of the heat exchanger and set at 0.75.

The simulation results for the gas turbine analysis are listed in Table II-3. For a constant air inlet temperature, the heat input and heat extracted was 109.83 kW and 45.50 kW, respectively. The compression increased the air temperature from 300 K at point 1 to 444.58 K at point 2. The regenerator further increased the air temperature to 806.83 K at point X before the air was mixed with biomethane in the burner. The gas turbine unit uses 27.32% of the biomethane for the shaft work of electricity generation, and 41.43% of the biomethane to generate heat.

Table II-3. Operational parameters of a 30 kW gas turbine

Parameter	**Unit**	**Simulation results**
η_F^G	-	0.273
T_2^G	K	444.5
T_x^G	K	806.83
T_y^G	K	549.75
$Q_F{}^G$	kW	109.83

Table II-3. (cont'd)

${Q_H}^G$	kW	45.50

With the addition of solar thermal energy (Figure II-1d), the heat demand of the biomethane burner is also reduced. The temperature after the solar collector is calculated as follows:

$$T_S^G = T_x^G + \frac{Q_{solar}}{\dot{m}_{air} \cdot Cp_{2a}} \tag{II-16}$$

where Cp_{2a} is the specific heat at $\frac{T_x^G + T_3^G}{2}$ [kJ/kg·K]. In addition, due to seasonal and geographical variation of solar radiation, the location of the studied systems has a great impact on their performance. The direct normal irradiance (DNI) and ambient temperature decrease with an increase in latitude. Therefore, the two locations of Lansing (MI) and Phoenix (AZ) in the United States, which have significant temperature differences and solar radiation, were selected for this study. Figure II-2 represents solar radiation and ambient temperature during a year for both locations (NREL, 2015; U.S.ClimateData, 2015).

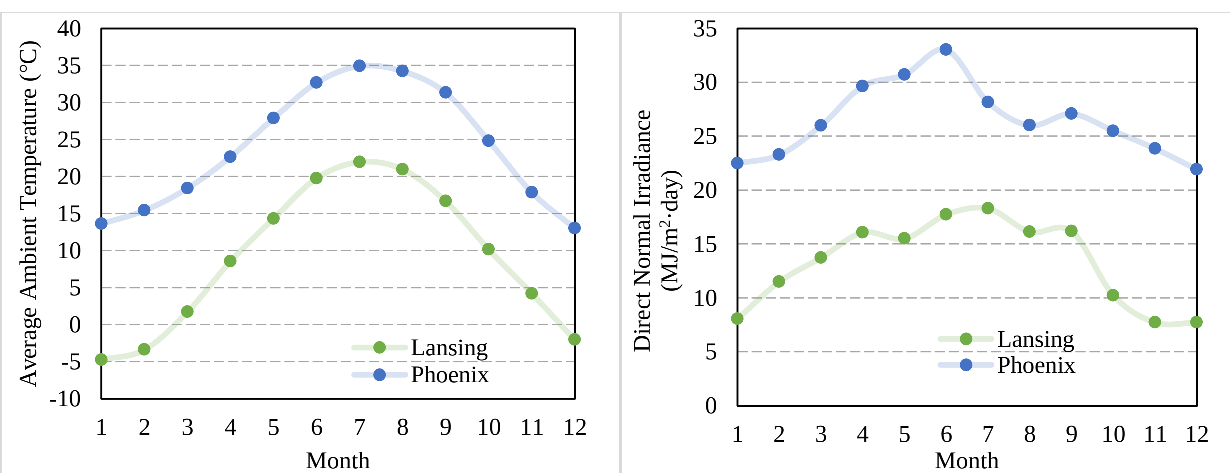

Figure II-2. Monthly average temperature and DNI for Lansing and Phoenix

3. System analysis

3.1. Relationship between solar energy, capacity factor, and ratio of solar energy to biomethane energy

The biomethane consumption of solar–bio hybrid power systems (steam and gas turbines) depends on the usage of solar energy (the heat input from solar energy) and the net capacity factor of the power generation. The effects of capacity factor and solar usage on bioreactor volume and solar energy requirements for solar–bio hybrid steam and gas turbine systems are presented in Figure II-3. With an increase in net capacity factor and solar usage, the solar energy demands of both systems linearly increase. At the same time, the hybrid steam engine system demands more solar energy than the hybrid gas turbine system (Figure II-3a and b). During full utilization of solar energy (100% solar usage and 1 net capacity factor) to power the hybrid systems, the hybrid steam turbine system requires 18,017 MJ/day of solar energy, which is approximately double the demand of the hybrid gas turbine system (9299.4 MJ/day). Meanwhile, the required bioreactor volume to generate biomethane for 30 kW electricity generation increases with an increase in net capacity factor and decrease in solar usage for both systems, and the hybrid steam engine system requires a larger bioreactor volume than the hybrid gas engine system (Figure II-3c and d). At the point of 0% solar usage and a net capacity factor of 1, the hybrid steam engine system requires a bioreactor volume of 1,435.3 m^3, while the hybrid gas turbine only requires a bioreactor volume of 642.53 m^3.

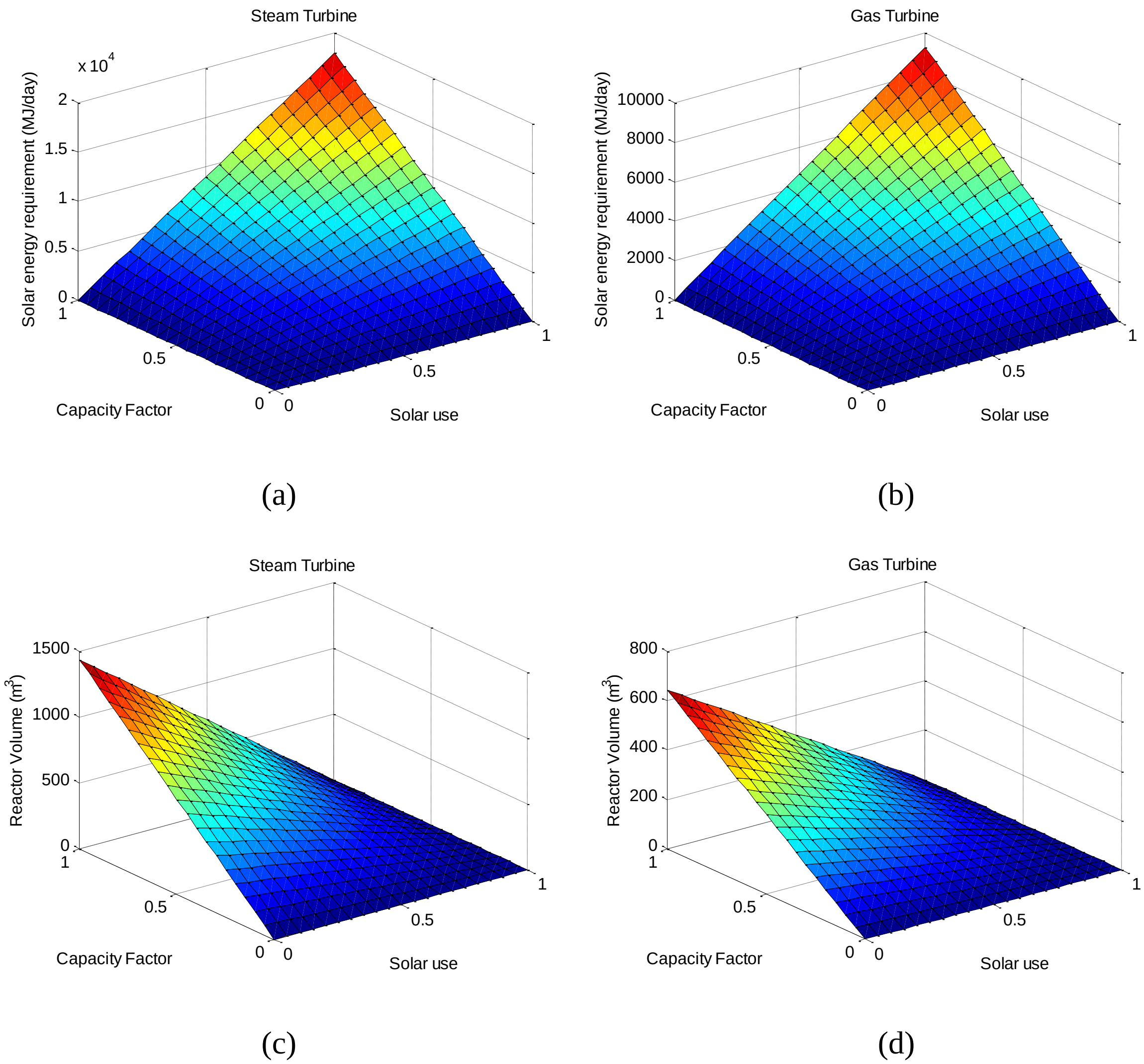

Figure II-3. Effects of net capacity factor and solar usage on bioreactor volume and solar energy requirements for different solar–bio hybrid systems*

*: (a) Solar energy requirements for the solar–bio hybrid steam turbine system; (b) solar energy requirements for the solar–bio hybrid gas turbine system; (c) bioreactor volume for the solar–bio hybrid steam turbine system; (d) bioreactor volume for the solar–bio hybrid gas turbine system.

3.2. Energy requirements for biomethane production

3.2.1. Thermal energy requirements for biomethane production

Thermal energy is needed by the anaerobic digestion of biomethane production to heat the feed and maintain the culture temperature at 50 °C. The energy requirement per day (E_{req} (MJ/day)) is calculated as follows (Yue, MacLellan, Liu, & Liao, 2013):

$$E_{req} = \frac{V_{AD}}{HRT} \cdot \rho_{inf} \cdot C_p \cdot \left(T_{AD} - T_{inf}\right) \cdot (1 + 30\%)/10^6 \qquad \text{(II-17)}$$

where V_{AD} is the digester volume (m^3); HRT is the hydraulic retention time (days); ρ_{inf} is the feed density (1220 kg/m^3); C_p is the feed specific heat (3606 J/kg·°C); T_{AD} is the culture temperature (50 °C); T_{inf} is the feed temperature and assumed to be the same as that for ambient temperature when the ambient temperature is above 4 °C (the feed temperature is set at 4 °C when the ambient temperature is below 4 °C); and 30% is the additional heat that is needed to maintain the thermophilic culture condition of the digester.

The maximum thermal energy demands at Lansing on the coldest winter day under the conditions of a net capacity factor of 1 without solar utilization for steam and gas turbines are 18,880 MJ/day and 8451.9 MJ/day, respectively. The corresponding thermal energy demands at Phoenix for steam and gas turbines are 15,186 MJ/day and 6,798.2 MJ/day, respectively. To satisfy the requirements of year-round power generation, the solar–bio hybrid system should have a positive energy balance on the coldest winter days. Thus, the maximum thermal energy demands at the two locations were used to determine the size of the solar unit and anaerobic bioreactor for 30 kW electricity output.

The solar utilization value was selected based on the balance between thermal energy required by the anaerobic digester and thermal energy generated in the power generation system at a given net capacity factor. The thermal energy generated in the power system (MJ/day) is calculated as follows:

$$E_{th}{}^{G} = \frac{Q_H{}^{*} \cdot CF \cdot (24 \cdot 3600)}{1000} \tag{II-18}$$

where $Q_H{}^{*}$ is the heat generated ($Q_H{}^{G}$ or Q_H) (kW) and CF is the net capacity factor. The energy requirements per day (E_{req} (MJ/day)) given by Equation II-17 can also be expressed as

$$E_{req} = \frac{V_{CH4}}{\eta_{CH4} \cdot HRT} \cdot \rho_{inf} \cdot C_p \cdot \left(T_{AD} - T_{inf}\right) \cdot (1 + 30\%)/10^6 \tag{II-19.a}$$

$$V_{CH4} = \frac{E_{CH4}}{HC} \tag{II-19.b}$$

$$E_{CH4} = \frac{Q^{*} \cdot (1 - SU) \cdot (CF \cdot 24 \cdot 3600)}{1000} \tag{II-19.c}$$

where V_{CH4} is the biomethane requirement (m^3); η_{CH4} is the biomethane productivity ($m^3_{CH4}/m^3_{digester}$); E_{CH4} is the energy provided by the biomethane (MJ/day); HC is the heat of combustion of methane ($HC = 34$ MJ/m^3); Q^{*} is the heat input (Q_F or $Q_F{}^{G}$) (for the turbine) (kW); and SU is the solar utilization factor. Substituting Eq. II-19.b and Eq. II-19.c into Eq. II-19.a, and combining with Eq. II-18, the solar utilization factor can be calculated.

For instances of a given net capacity factor of 0.5, the relationship between solar utilization and the required thermal energy by the AD is shown in Figure II-4. To satisfy the energy demands of heating the influent and maintaining the digestion temperature, the solar utilization required at Lansing for steam and gas turbines is 0.3840 and 0.5349, respectively; and the corresponding values at Phoenix for steam and gas turbines are 0.2341 and 0.4217, respectively. These values at the capacity factor of 0.5 are used as the base numbers to select the anaerobic digester volume and solar collector for each location and power system (Table II-4).

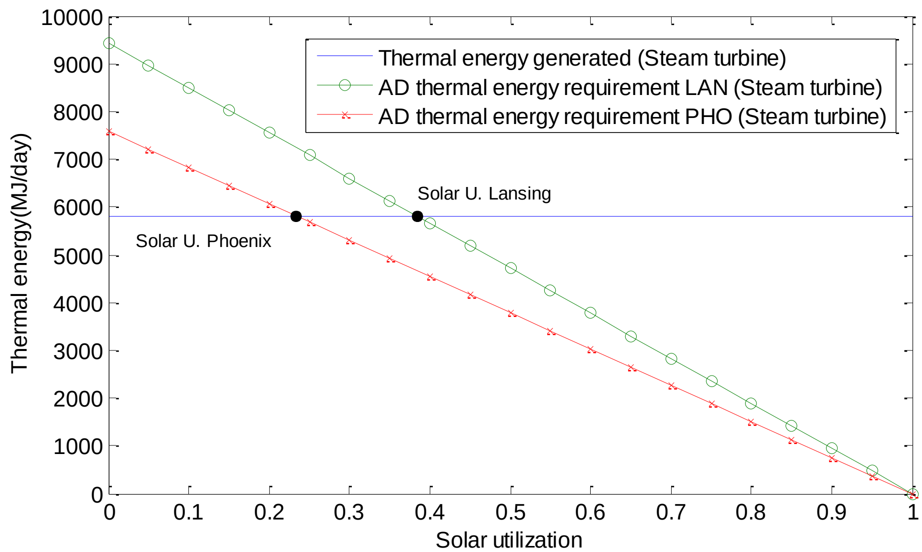

(a)

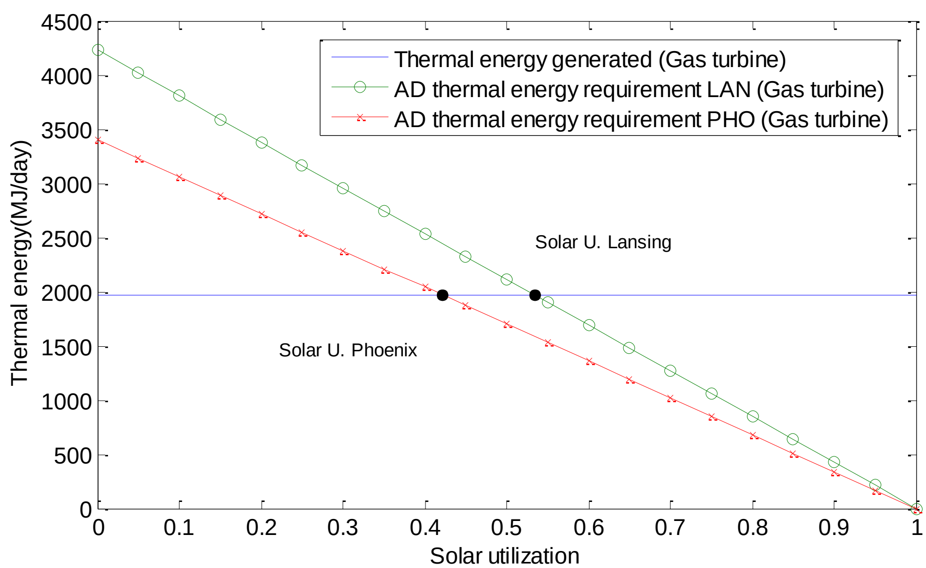

(b)

Figure II-4. Relationship between the solar utilization and thermal energy requirements of the AD for the solar–bio hybridization systems*: a) steam turbine system; (b) gas turbine system.

*: A net capacity factor of 0.5 was used to calculate these numbers.

Table II-4. Bioreactor volume and daily biomethane production for selected solar utilization*

Location	Reactor volume (m^3)		Biomethane production (m^3/day)	
	Steam	**Gas**	**Steam**	**Gas**
Lansing	442.08	149.43	166.34	56.23
Phoenix	549.62	185.78	206.81	69.90

*: The net capacity factor of 0.5 was used to calculate these numbers.

3.2.2. Electricity requirements for biomethane production and upgrading

Besides the thermal energy demand, biomethane production and upgrading also require electricity to power the liquid handling equipment and biomethane upgrading process. It has been reported that the electricity consumption by the liquid handling equipment (pumps, agitators, and screw compressor) is 0.0509 MJ per m^3 digester per hour (Lijó et al., 2014).

Biomethane also has many other compounds, such as carbon dioxide, moisture, hydrogen sulfide (H_2S), siloxanes, hydrocarbons, ammonia, and carbon monoxide. Among these compounds, H_2S and water vapor are the most corrosive compounds. The H_2S can be converted into SO_2 and SO_3 during the biomethane combustion, and consequently damage turbines and other necessary equipment. The water vapor in biomethane reacts with H_2S, NH_3, and CO_2 to form corrosive acids (Ryckebosch et al., 2011). Thus, they must be removed before the biomethane is sent to the boiler or combustion chamber for heat and electricity generation. The typical biomethane upgrading process includes three steps consisting of water scrubbing and regeneration, cryogenic separation, and physical absorption. The electricity demands for the individual cleaning steps are listed in Table II-5 (Sun et al., 2015). Depending on the engine units, they can be configured differently. The Brayton cycle (gas turbine) requires fuel gas and air to be mixed in the burner and directly expanded in the turbine, so that it requires all three steps to clean up the biomethane and protect the turbine. The Rankine cycle (steam turbine) does not require direct contact between the biomethane and turbine, so a single step treatment of water scrubbing and regeneration is a suitable clean-up method for steam turbine application.

Table II-5. Energy consumption for biomethane cleaning

Cleaning technology	**Electricity consumption (kWh/normalized m^3 biomethane)**
Water scrubbing and regeneration	0.275
Cryogenic separation	0.24
Physical absorption	0.25

To calculate the electricity consumption required to treat the amount of biomethane from the studied thermophilic digester (Table II-4), the following conversion equation was used to determine the effect of temperature on normalized biomethane volume from Table II-5.

$$V_N = \frac{P_{AD} \cdot V_{AD}}{T_{AD}} \cdot \frac{T_N}{P_N} \qquad \text{(II-20)}$$

where $P_N = 1\ atm$; $T_N = 288.15\ K$; $P_{AD} = 1.025\ atm$; and $T_{AD} = 323.15\ K$. The calculation data show that the electricity demands for biomethane cleaning for the solar–bio hybrid gas and steam turbine systems were 2.517 MJ/m^3 and 0.9048 MJ/m^3 biogas (containing 58.6% biomethane), respectively.

3.3. Selection of solar thermal collectors for the hybrid systems

The selection of solar thermal collectors for the solar–bio hybrid systems was based on the desired temperature of the heating fluid for the steam and gas turbines. The central tower, parabolic dish, and parabolic trough are the three most popular solar thermal collection technologies (Jamel et al., 2013; Popov, 2014; Siva Reddy et al., 2013). Central tower solar collection can generate extremely high temperatures (above 1,000 °C), but requires a large footprint to accommodate the solar reflectors, which is not suitable for small-scale solar power generation. Parabolic dish solar thermal collection also generates high temperatures (500–900 °C). However, parabolic troughs generate medium temperatures (200–400 °C), so are more suitable for small-scale solar power generation (Siva Reddy et al., 2013). For the small-scale solar–bio hybrid power generation systems, considering the required temperature of the heating fluid for steam (200 °C) and gas turbines (840 °C), parabolic trough collectors were selected to be integrated with the steam turbines and parabolic dish collectors with the gas turbines.

It has been reported that the optical efficiencies for parabolic trough and parabolic dish are approximately 0.76 and 0.93, respectively (Giostri et al., 2013; Siva Reddy et al., 2013). The solar concentration ratio (C_r) is another important parameter for solar thermal collectors, and is expressed as the absorber area (A_a) vs. the collector area (A_c). The numbers of 70 and 750 are used as the concentration ratios for parabolic trough and parabolic dish collectors (Siva Reddy et al., 2013; Skouri, Bouadila, Ben Salah, & Ben Nasrallah, 2013).

Based on the collector type, working fluid temperature, and solar concentration ratio, the solar energy can be calculated by the following equation:

$$Q_s = \eta_o \cdot A_c \cdot G \cdot S_F - [\alpha \cdot \sigma \cdot A_a \cdot (T_{HS}^4 - T_\infty^4) - h \cdot A_a \cdot (T_{HS} - T_\infty)] \cdot \left(\frac{t_c}{1x10^6}\right) \qquad \text{(II-21)}$$

where Q_s is the solar heat required (MJ/day); η_o is the optical efficiency; A_c is the collector area (m^2); G is the direct normal irradiance ($MJ/m^2 \cdot day$); S_F is the solar operating factor (which, for parabolic trough and parabolic dish collectors, is 0.878 and 0.429, respectively, at Lansing and 0.934 and 0.4752, respectively, at Phoenix); α is the absorber emittance (0.27, stainless steel Type 312 (M. F. Modest, 2013)); σ is the Stefan-Boltzmann constant (5.67×10^{-8} W/m^2·K^4); A_a is the absorber area (m^2); T_∞ is the ambient temperature (K); h is the convective coefficient (8 W/m^2·K); t_c is the solar energy collection time (which, for the parabolic dish and parabolic trough collectors is 5.65 and 5.88 h per day, respectively, at Lansing; and 9.66 and 9.69 h per day, respectively, at Phoenix); and T_{HS} is the receiver's absorber temperature (K), which is assumed to be 25% higher than the maximum temperature of the working fluid (water or air) in the system. The solar operating factor (S_F) is defined as the ratio of direct normal irradiance that can be used by the solar collection technology for electricity generation, and is calculated as the ratio of the total thermal power produced and the absorbed thermal energy. The S_F values were obtained using the software System Advisor Model (NREL, 2016b).

In addition, the working fluids (water and air) have a large impact on the thermal efficiency of the heat exchanger (ε_{HE}). The overall heat transfer coefficient (the capability of the heat exchanger to transfer thermal energy) is several orders of magnitude higher for water than for air (Çengel, 1998; Kakaç & Liu, 1998), and the thermal efficiency of air is correspondingly lower than that of water. The ε_{HE} values for air and water were selected as 0.70 and 0.85, respectively, in this study. Therefore, the heat that the working fluid transfers from the absorber to the boiler and burner can be calculated as

$$Q_{FL} = \frac{Q_S}{\varepsilon_{HE}} \tag{II-22}$$

where Q_{FL} is the energy transferred (MJ/day) from the absorber to the working fluid; and ε_{HE} is the thermal efficiency of the heat exchanger.

Under the conditions of the coldest winter day and a net capacity factor of 0.5, the solar collector area required by the solar–bio hybrid systems to generate 30 kW electricity can be calculated using Equations 24 and 25 (Table II-6). Because Phoenix has a much higher ambient temperature and DNI than Lansing year-round, the required solar collector areas at Phoenix for steam and gas turbines were 180.4 m^2 and 330.1 m^2, respectively, much smaller than those in Lansing, which for steam and gas turbines were 1,034.8 m^2 and 1,502.1 m^2, respectively.

Table II-6. Required solar collector areas for steam and gas turbines at Lansing and Phoenix on the coldest winter day for a net capacity factor of 0.5

Location	**Solar collector area (m^2)**	
	Steam	**Gas**
Lansing	1,034.8	1,502.1
Phoenix	180.4	330.1

Based on the selected solar collector area at the coldest time, the monthly net capacity factors were simulated for both systems at Phoenix and Lansing (Figure II-5). Since the coldest time of the year is used as a reference state to select the solar collector area, the solar thermal energy generated during most of the year exceeds the value for the minimum heat requirements. The biomethane is therefore used to extend the operating hours of the power generation system, and the net capacity factor is correspondingly increased. In the warm climate location (Phoenix), during the month of July, which has the highest ambient temperature, the net capacity factors for the steam and gas turbine systems were increased by 13.82% and 24.50%, respectively (Figure II-5b). In the cold climate location (Lansing), the net capacity factors changed more dramatically. During July, the net capacity factors for the steam and gas turbine systems were increased by 70.88% and 95.82%, respectively (Figure II-5a).

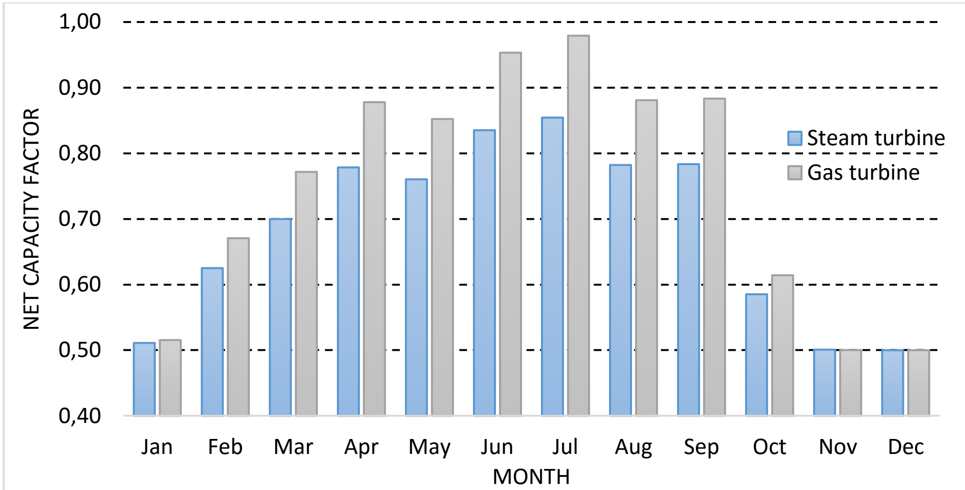

(a)

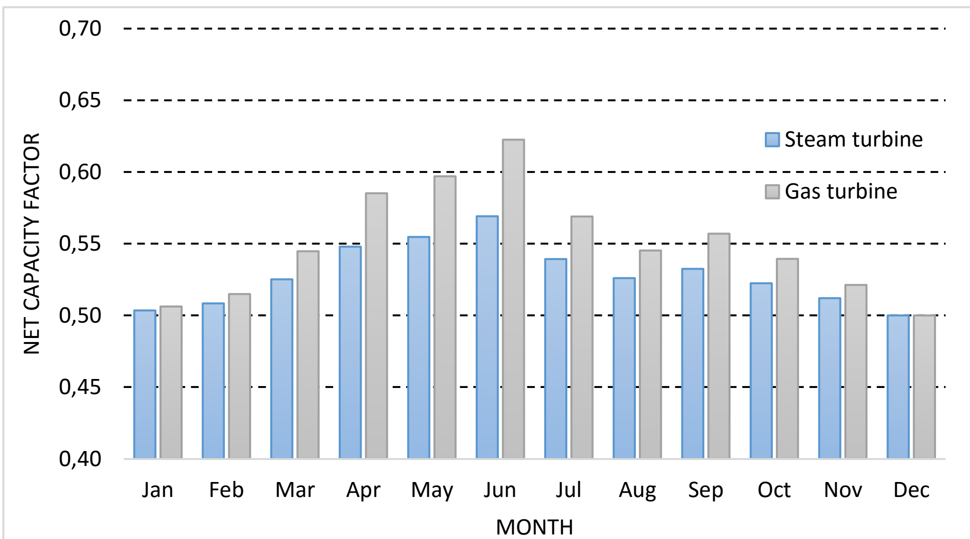

(b)

Figure II-5. Effects of location and month on the net capacity factor of the solar–bio hybrid power generation system: (a) Lansing; (b) Phoenix.

4. Discussions

The system analysis shows the relationship between the net capacity factor, bioreactor volume, solar thermal utilization, and geographic location for both the Brayton and Rankine cycles. According to the system configurations (Figure II-1), the highest temperatures required for individual thermal cycles determine the solar collector technologies that can be integrated into the solar–bio hybrid power generation systems. In the case of the steam turbine (Rankine cycle), the maximum temperature (turbine inlet) is 200 °C (Figure II-1b), which can be achieved by medium-temperature solar thermal technologies, such as the parabolic trough proposed by this study. However, the working fluid in the gas turbine (Brayton cycle) needs to be heated by solar thermal energy from 533 °C at the outlet of the regenerator to 840 °C before entering the burner (Figure II-1d). High-temperature solar thermal technologies, such as the parabolic dish selected by this study, are required to satisfy the need of such a high temperature increase. However, 840 °C is at the higher end of the temperature range that conventional parabolic dishes (with a reflector area ranging from 43 m^2 to 117 m^2) can achieve (Baharoon, Rahman, Omar, & Fadhl, 2015; Mancini et al., 2003). This is a limiting factor for the further increase of solar thermal energy utilization in the gas turbine hybrid system. Although it is theoretically possible to raise the temperature at the absorber of a parabolic dish to above 1,000 °C by extending the reflection area, fabricating such large parabolic dishes may pose certain manufacturing and installation difficulties, as well as economic barriers for small-scale applications.

Since the solar radiation and ambient temperature vary significantly between seasons and locations (Figure II-2), the bioreactor volume must be large enough to produce sufficient methane to satisfy the system energy demands when the solar thermal energy is not able to fulfill the heating requirements (i.e., in the winter months at Lansing). This is the reason that the minimum solar utilization values for the system design were selected by this study based on maintaining the capacity factor of 0.5 on the coldest day of a year. Moreover, due to the thermodynamic difference in fuel efficiency between the gas and steam turbines, the required bioreactor volumes are different for the hybrid systems. The fuel efficiency for the gas turbine (27.32%) is much higher than that for the steam turbine (14.69%). The corresponding bioreactor of the steam turbine hybrid system is approximately 2.95 times larger than that of the gas turbine hybrid system (Table II-4).

In addition, as mentioned previously, the ambient temperature and solar radiation have a strong influence on the configuration of hybrid systems. The simulation results demonstrated that the solar–bio hybrid steam turbine system required a smaller solar collector area (1,034.8 m^2 and 180.4 m^2 for Lansing and Phoenix, respectively) than the gas turbine system (1,502.1 m^2 and 330.1 m^2 for Lansing and Phoenix, respectively) (Table II-6). This is mainly caused by the low value of the solar operating factor for the gas turbine systems. The solar collector area must be over-sized to satisfy the energy demand of the working fluid when the direct normal irradiance is weak during the winter months. Considering the fact that a smaller footprint is desirable for small-scale systems, the solar–bio hybrid steam turbine power generation with a smaller solar collector area is thus preferred

The overall energy balance for the coldest and hottest months at the two locations elucidates the comprehensive energy distribution profiles for both systems (Figure II-6). Because of the low thermal efficiency of the steam turbine, the solar–bio hybrid steam turbine system (245.33 kW) demanded 2.23 times more heat than the hybrid gas turbine system (109.83 kW) to generate 30 kW electricity (Tables II-2 and II-3). The steam turbine hybrid system had a higher ratio of heat generation to total energy input (0.5487) than the gas turbine hybrid system (0.4143); and the corresponding heat generated for the steam and gas turbine hybrid systems was 134.61 kW and 45.50 kW, respectively. During the coldest winter month, the heat was completely used to maintain the culture temperature of the anaerobic digestion for biomethane production and ensure the generation of the target electricity amount.

During the hottest summer month, extra heat was generated from both systems in both locations (Figure II-6a, c, e, and f). In addition, although the fuel efficiency of the gas turbine is higher than that of the steam turbine, the global efficiencies (electricity and heat outputs vs. biomethane and solar energy inputs) of the solar–bio hybrid steam turbine system (47.75% in July and 49.00% in December at Lansing, 58.13% in July and 58.92% in December at Phoenix) were significantly higher than those of the solar–bio hybrid gas turbine system (21.52% in July and 23.64% in December at Lansing, 30.84% in July and 32.69% in December at Phoenix). Moreover, due to the temperature differences between winter and summer for both locations, the larger temperature difference requires larger solar collectors and correspondingly more heat. The hybrid steam and gas turbine systems located at Lansing generate 38.9% and 45.9% more heat, respectively, than those located at Phoenix. As for electricity generation, the solar–bio hybrid steam turbine system requires more biomethane to maintain the net electricity output of 30 kW. The parasitic electricity energy required by the hybrid steam turbine system (279 MJ/day and 347 MJ/day for Lansing and Phoenix, respectively) was higher than that required by the hybrid gas turbine systems (249 MJ/day and 310 MJ/day for Lansing and Phoenix, respectively), although the gas turbine requires more electricity to clean up the biomethane for power generation. In addition, the systems at the location with lower solar thermal utilization (i.e., Phoenix) require more biomethane energy, and correspondingly increase the consumption of parasitic electricity, which leads to a lower net electricity output (Figure II-6).

The analysis in this study is based upon the use of solar thermal energy as a supplemental energy source to facilitate the utilization of the biofuel–biomethane, and indirectly improve the power generation performance of the system. As a matter of the fact, the net capacity factor can be significantly increased if the solar thermal energy can be utilized directly as a single energy source in the thermodynamic cycle for several hours per day (once solar radiation is able to bring the working fluid to the desired temperatures for the gas and steam turbines). Further studies are needed to explore such scenarios.

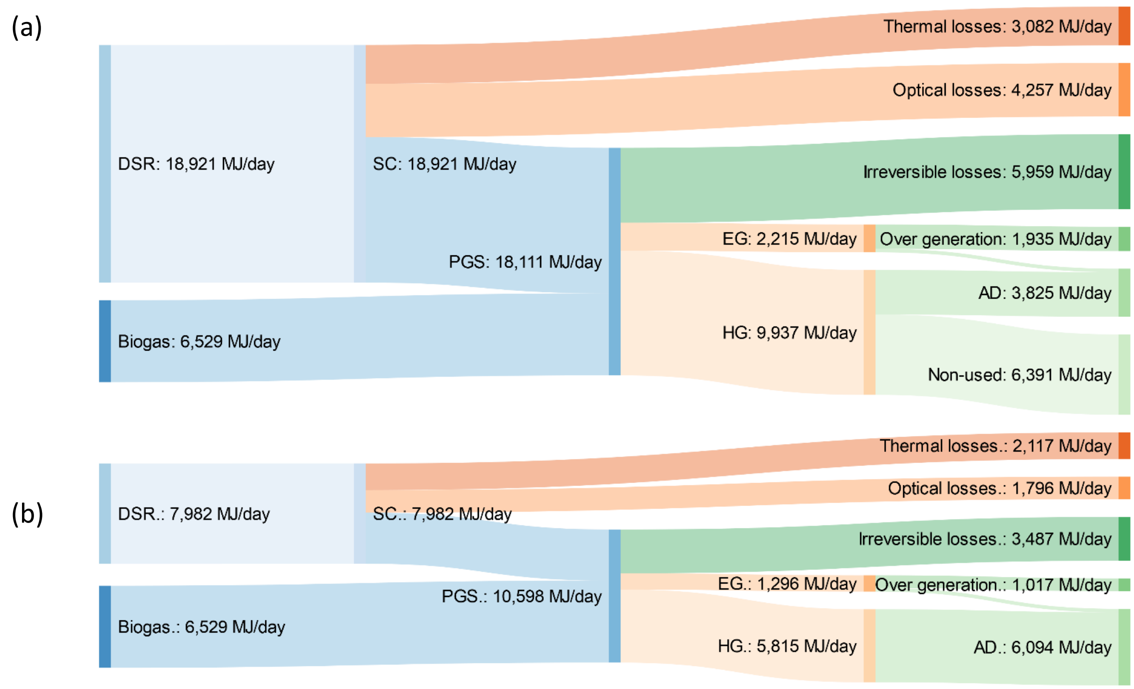

Figure II-6. Energy balance of small-scale solar–bio hybrid power generation systems*

Figure II-6. (cont'd)

(c)

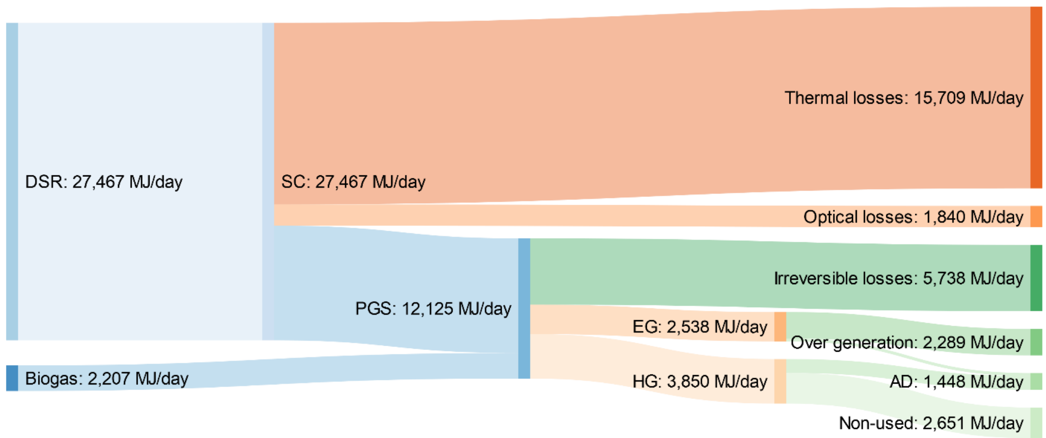

(d)

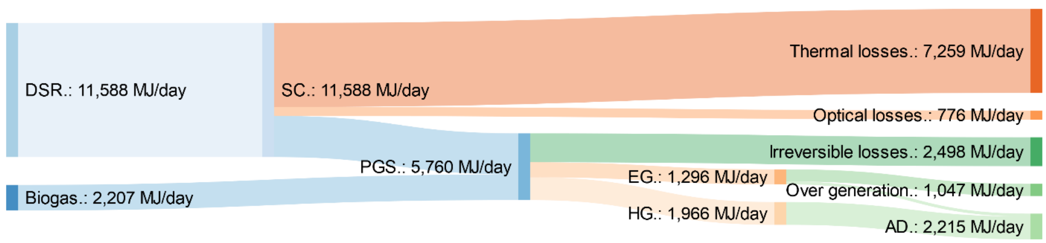

(e)

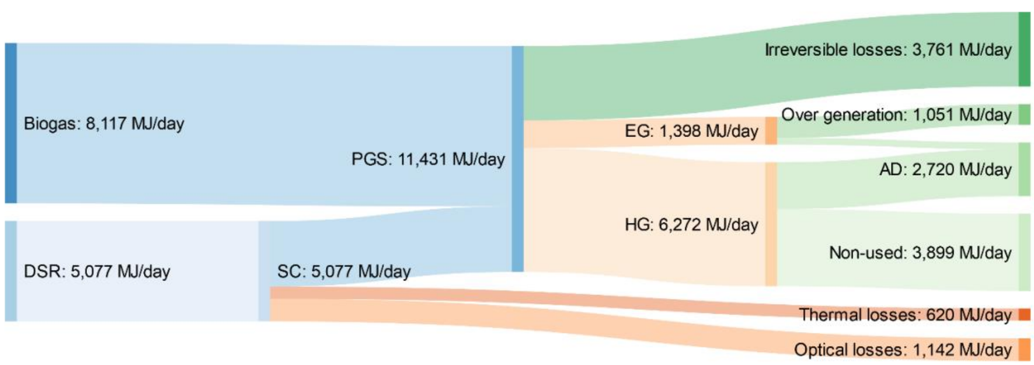

(f)

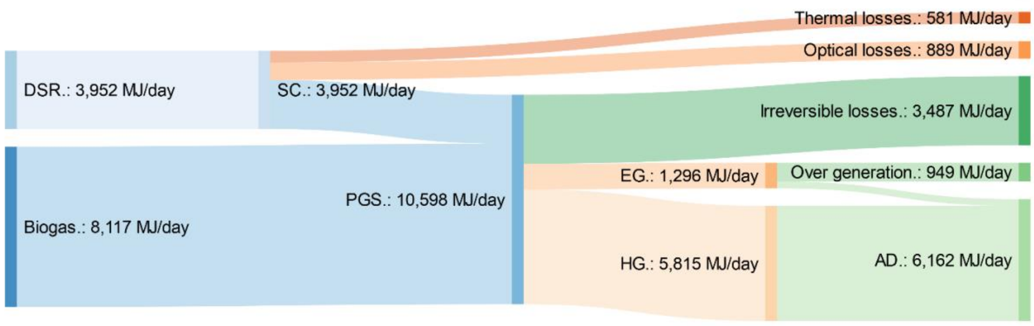

Figure II-6. (cont'd)

(g)

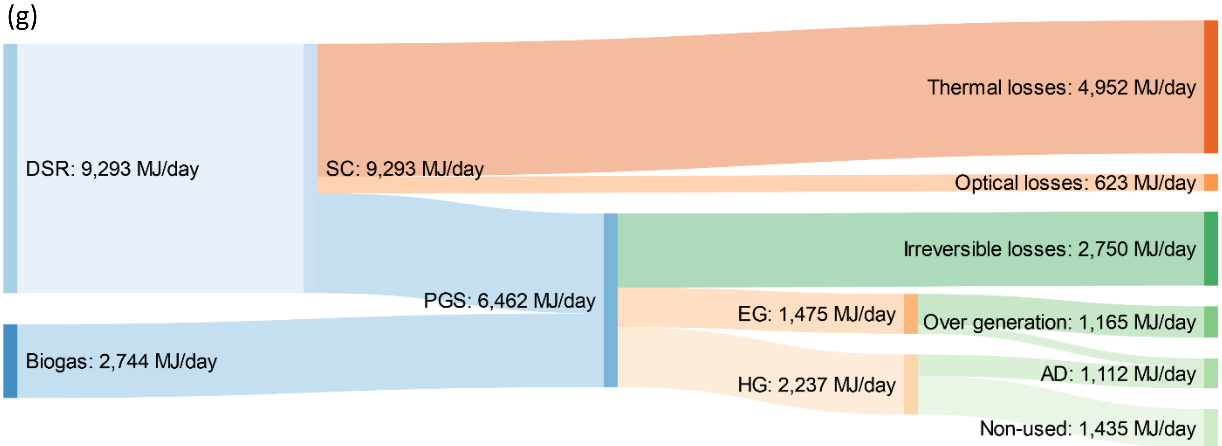

(h)

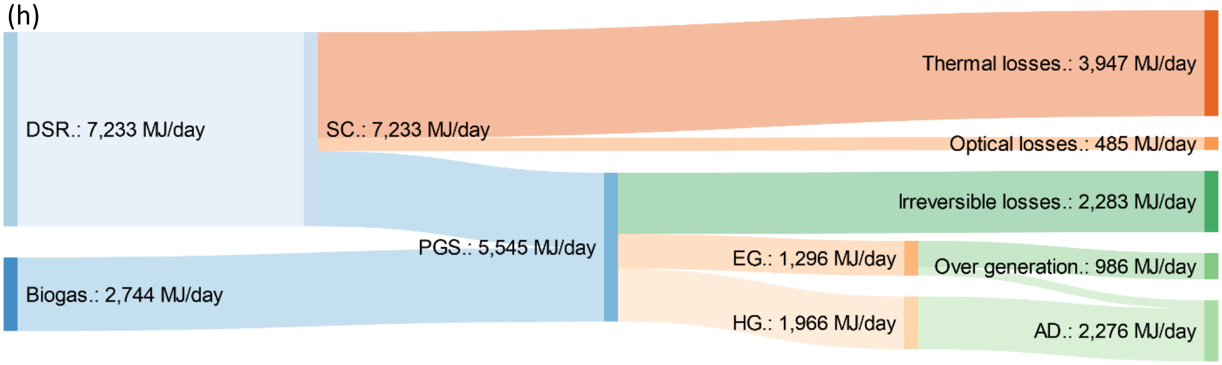

*: (a) Steam power generation system in Lansing in July; (b) steam power generation system in Lansing in December; (c) gas power generation system in Lansing in July; (d) gas power generation system in Lansing in December; (e) steam power generation system in Phoenix in July; (f) steam power generation system in Phoenix in December; (g) gas power generation system in Phoenix in July; (h) gas power generation system in Phoenix in December.

DSR: available direct solar radiation; Biomethane: energy obtained from biomethane combustion; SC: solar collector subsystem; PGS: power generation subsystem; Thermal losses: losses in the solar collector due to radiation, convection, and solar operating factor influence; Optical losses: losses in the solar collector due to absorptivity of the reflector and reflectivity of the absorber; Irreversible losses: energy losses in the heat transfer equipment; EG: electricity generation in the PGS; NEG: net electricity generation; HG: heat generation in the PGS; AD:

electricity required in the anaerobic digestion subsystem; and Extra heat: heat generated in the power generation system not used by the anaerobic digestion process.

5. Conclusions

This study carried out a comprehensive analysis on small-scale solar–bio hybrid power generation (30 kW). The relationship between net capacity factor, solar utilization efficiency, and biomethane utilization efficiency has been determined. The analysis demonstrated that the hybrid steam turbine system had better global thermal efficiency (54.87%) than the hybrid gas turbine system (41.43%), although the electricity generation efficiency of the hybrid steam turbine system (14.69%) was lower than that of the hybrid gas turbine system (27.32%). Moreover, the global efficiencies of the solar–bio hybrid steam turbine system were significantly higher than those of the solar–bio hybrid gas turbine system, regardless of location. It was found from the analysis that, in order to reduce the system footprint, the hybrid steam turbine is preferable to the hybrid gas turbine system.

CHAPTER III. A SELF-SUSTAINING WASTEWATER TREATMENT PLANT INTEGRATING SOLAR TECHNOLOGIES, ANAEROBIC DIGESTION, AND AEROBIC TREATMENT

Abstract

This chapter focuses on system analysis of the self-sustaining wastewater treatment concept combining solar technologies, anaerobic digestion, and aerobic treatment to reclaim clean water. A solar bio-hybrid power generation unit was adopted to power the wastewater treatment (with a volume of 76 m^3 influent per day for the studied case). The results showed that the synergistic integration of biogas and solar energy generation could satisfy the power demands of the wastewater treatment. Concentrated solar power (CSP) and photovoltaics (PV) were compared for the solar–bio hybrid power generation at two locations (Lansing and Phoenix). With short-term solar energy storage (a battery for PV and molten salt for CSP), the PV-bio hybrid power unit requires a smaller solar collection area and biogas storage than the CSP-bio hybrid power unit regardless of location. In addition, using biogas to store the extra energy generated by the solar–bio hybrid unit during the warm months enables the year-round wastewater treatment operation to be completely self-sustainable. It was determined from the energy balance analysis that the PV-bio hybrid power unit is the preferred energy unit to realize the self-sustaining wastewater treatment.

Appendices for this chapter:

i. Appendix D: Matlab code for solar–bio hybridization for anaerobic digestion and aerobic treatment

ii. Appendix E: Matlab sub-functions for solar–bio hybridization for anaerobic digestion and aerobic treatment

1. Introduction

It has been reported by the United Nations Environment Programme (UNEP) that two billion tons of sewage as well as industrial and agricultural wastewater is discharged into the world's waterways every day. An estimated 90% of all wastewater in developing countries is directly discharged untreated into rivers, lakes, and the ocean. The wastewater has affected approximately 245,000 km^2 of marine ecosystems (Corcoran, UNEP, & Arendal, 2010). In addition, methane and nitrous oxide from the degradation of organic matter in the wastewater greatly contribute to global greenhouse gas emissions. On the other hand, the wastewater is rich in organic matter, which represents a good carbon and nutrient (P and N) source for microbes to synthesize energy and chemical products. However, fecal matters and low nutrient concentrates in the wastewater present certain technical challenges to recover the nutrients and utilize them for energy and chemical production. New scientific and engineering solutions seek to address the challenge of transforming the wastewater from a major environmental and health hazard into a clean and environmentally attractive resource through technical and economical means.

Current wastewater treatment technologies mainly rely on aerobic treatment (AET) in which aerobic microbes metabolize the soluble and colloidal organics, which flocculate and settle out so that reclaimed water is achieved (Wang et al., 2009; Water Environment & ebrary, 2008). However, the energy-intensive aeration operations of current aerobic treatment practices (the carbon is not balanced, and additional carbon from the energy sources is consumed to clean up the water) still lead to a relatively large carbon footprint. Therefore, next-generation wastewater treatment technologies must be carbon neutral, robust, and self-sustainable. Compared to conventional aerobic treatment, anaerobic digestion (AD) is another biological means that is able to simultaneously treat wastewater and generate bioenergy, and has the potential to be further developed into a carbon neutral process (Sun et al., 2015). However, due to the microbial community structure and their metabolic pathways, the growth of anaerobic microbes is much slower than aerobic microbes, so that the nutrient removal of AD is not very efficient, and the wastewater cannot be reclaimed completely. It has been demonstrated that integrating anaerobic and aerobic treatments to treat wastewater is an effective approach to take advantage of both systems (i.e., AD's capability of handling high-strength wastewater and its high energy production, and AET's efficient nutrient removal). It can thus be used to completely reclaim water from a wide range of organic wastewater streams (Deshpande, Satyanarayan, & Ramakant, 2012; Martin, Pidou, Soares, Judd, & Jefferson, 2011; Novak, Banjade, & Murthy, 2011; Zhou et al., 2015). Although the AD in the integrated system can provide a certain amount of energy to support the operations, the integrated system, including biogas cleaning and upgrading, maintaining the temperature of AD, and aeration of AET demands more energy than can be provided by the biogas energy of the AD. Therefore, in order to develop a self-sustaining wastewater, additional energy sources are required.

In response to this need for a hybridization treatment system, a second renewable energy source is needed to satisfy the energy demand. A power generation concept using biogas and solar energy is investigated in this study. In the past decades, many solar energy conversion technologies, such as evacuated-tube solar thermal collectors, parabolic trough systems, central tower systems, dish solar systems, Fresnel reflectors, and photovoltaic cells have been developed (Mills, 2004). They are mainly classified into two categories: solar thermal and electrical (PV) conversion. In this study, both types were studied. The parabolic trough collector was selected as the solar thermal conversion technology, due to the fact that its temperature is compatible with the steam generation system (< 400 °C (Siva Reddy et al., 2013)). In addition, PV cells were investigated as the solar electric conversion technology, considering their simplicity for direct electricity generation. One of the key criteria for the hybridization power system is that the energy sources of solar and biogas energy must be balanced for a continuous power supply to satisfy the wastewater operation need. Therefore, the solar collection area (for CSP and PV) must be determined to match the storage needs of biogas for year-round operation. The objectives of this study were to model a solar–bio hybrid wastewater treatment that could self-sustainably reclaim agricultural wastewater, and to understand the effects of the seasonal and temporal variation (direct normal irradiance and global horizontal irradiance) on the energy uses of the solar–bio hybrid wastewater treatment system.

2. The solar–bio hybrid wastewater treatment

2.1. Anaerobic digestion (AD)

The simulation of the AD of animal manure and food waste was based on the data obtained from a commercial anaerobic digester located at Michigan State University (MSU) south campus (42.6988, -84.4880). The animal feed of the dairy farm consisted of alfalfa and corn silage blended according to the Natural Research Council (NRC)'s standard Total Mixed Rations (TMRs) for dairy cattle. The food waste came from dining halls at MSU campus. The digester is a completely stirred tank reactor (CSTR), operated at a temperature of 40 °C and with a retention time of 25 days. The characteristics of the feedstock are listed in Table III-1. The animal manure and food waste were collected in two pits with volumes of 7 m^3 and 12 m^3. The waste in the pits was ground and diluted with the filtrate to reach an average of 8% total solids, and pumped into a mixing tank (with a volume of 27 m^3). The mixed AD influent was then pumped into the digester (with a volume of 1,570 m^3). In order to maintain the culture temperature, a heating loop was installed to circulate the hot water continuously (heated by the power generation system) to the digester. A double high-density polyethylene (HDPE) membrane covers the top of the digester. The AD effluent was separated by a liquid/solid separator to obtain AD fiber and liquid filtrate. A conveyor moved the wet AD fiber to a storage barn, and the liquid filtrate was transferred to a tank for the secondary treatment (Figure III-1).

Table III-1. Feedstocks of the anaerobic digester

Description	**Total solids (%)**	**Volatile solids (%)**	**pH**
Animal manure [A]	9.9 ± 1.3	8.3 ± 1.2	7.13 ± 0.98
Food waste [B]	8.5 ± 2.8	7.7 ± 2.4	4.60 ± 0.82
Mixed AD influent [C]	8.5 ± 2.2	7.2 ± 1.9	6.21 ± 0.93

[A]: Data are the average of 25 samples with standard deviation.
[B]: Data are the average of 24 samples with standard deviation.
[C]: Data are the average of 45 samples with standard deviation.

2.2. Biogas upgrading

The mass balance and energy consumption of the biogas upgrading was based on the literature (Ryckebosch et al., 2011; Sun et al., 2015). The raw biogas was cleaned and upgraded using a two-stage process of water scrubbing and cryogenic separation to remove humidity, CO_2, and other chemical compounds. The upgraded biogas was stored in a metallic heavy-duty tank to be used as the fuel for the power generation.

2.3. Aerobic treatment (AET)

After the solid/liquid separation, the AD effluent (filtrate) was further treated by a conventional AET operation (Figure III-1). The simulation of the AET was based on the laboratory and literature data. The filtrate entered into the aeration chamber, where the dissolved oxygen concentration was maintained between 1–2 mg/L (EPA, 2000; Wang et al., 2009). The daily operation consisted of two batches (12 hours operation time). The AET effluent was pumped into a clarifier tank where solids were settled out and recycled back to the AD. The reclaimed water after the clarification, which satisfied the EPA discharging standard, was then used for other non-potable agricultural applications.

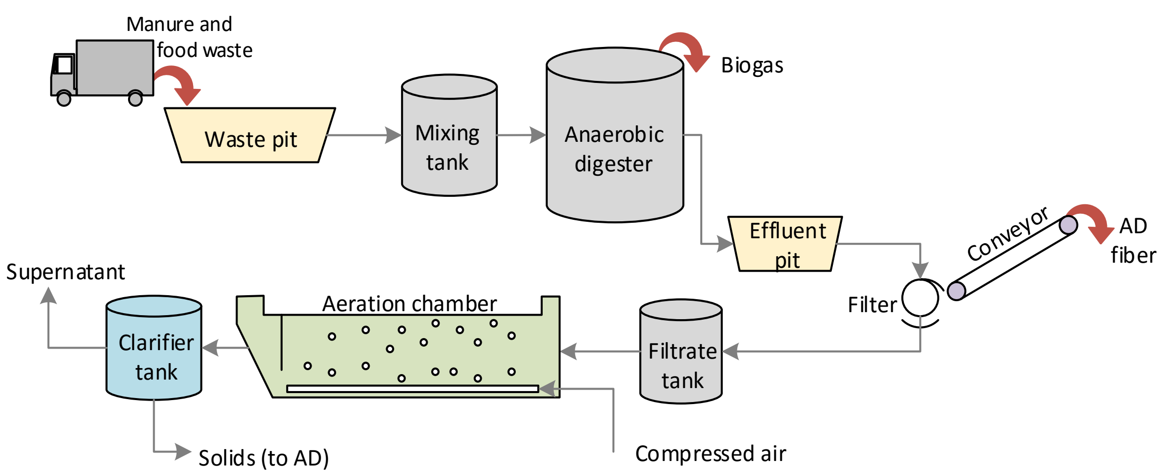

Figure III-1. Flow diagram for a conventional anaerobic/aerobic digestion process

2.4. Analytical method for AD and AET

The methane and carbon dioxide content were quantified using a SRI 8610c gas chromatograph (Torrance, CA). The system was equipped with a thermal conductivity detector. The detector was maintained at 150 °C during the analysis. Hydrogen and helium were carrier gases, and maintained at 21 psi. The biogas sample volume was 100 μL, and the syringe was purged three times before sample injection. The chemical oxygen demand (COD), total phosphate (TP) and total nitrogen (TN) of the animal manure and food waste, AD effluent, and liquid filtrate were measured using Hach methods. The total solids (TS) and volatile solids (VS) were analyzed using the methods developed by the National Renewable Energy Laboratory (NREL).

2.5. Solar–bio hybridization of power generation

2.5.1. Solar–thermal–bio hybridization power generation

The solar–bio hybridization is shown in Figure III-2a. The energy requirements (thermal and electrical) of the wastewater treatment were set to be provided by steam power generation. A concentrated solar collector (CSP) was installed to collect and transfer solar energy into a working fluid to preheat the feedwater. The preheated water was then sent into the boiler to produce superheated steam using the upgraded biogas as the fuel. The steam was then expanded in the turbine, generating shaft work that was used as an electric generator. The expanded steam was cooled and condensed, in order to be returned to the feedwater tank to continue with the cycle. The extracted thermal energy was used to maintain the AD temperature.

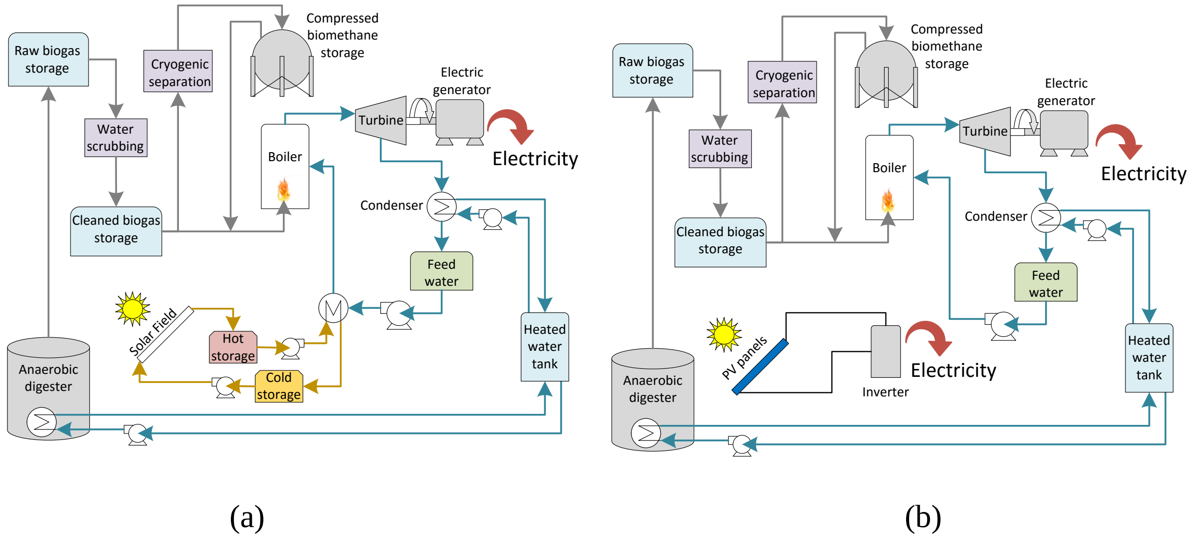

Figure III-2. Components of energy generation combining biomethane and solar concentrated energy: (a) concentrated solar power, (b) photovoltaic panels

The power generator consisted of a 325 kWe steam turbine that was designed to accommodate the use of both biogas and solar energy. The heat input (${Q_i}^{ref}$) required to satisfy the temperature and pressure of the superheated steam, is calculated as

$$ {Q_i}^{ref} = \frac{P_e}{\eta_e \cdot \eta_*} \tag{III-1} $$

where η_e is the turbine efficiency (thermal to electrical energy); and η_* is the heat exchanger (η_h) efficiency (set at 0.85), or the fuel-to-steam efficiency (η_b). The thermal energy extracted in the condenser (Q_o) is defined as follows:

$$ Q_o = \left({Q_i}^{ref} \cdot 0.5\right) \cdot \eta_c \tag{III-2} $$

where η_c is the condenser efficiency. The parasitic energy required by the power generation system was set at 5% of the designed electricity power output (16.25 kWe), which considers the energy consumed by pumps, gas fans, and miscellaneous equipment for the operation. The parameters for the steam turbine are summarized in Table III-2.

Table III-2. Operational parameters of 325 kW steam turbine

Parameter	**Value**	**Unit**
Maximum electricity output	390	kWe
Minimum electricity output	81.25	kWe
Turbine efficiency	0.35	-
Design heat input	928.57	kWt
Maximum heat input	1,111.2	kWt
Minimum heat input	275.62	kWt
Thermal energy extracted	464.2	kWt

The steam was generated by a commercial boiler, model CBEX Elite 125 BHP (Cleaver-Brooks, 2011). For load capacities of 25%, 50%, 75%, and 100%, the fuel-to-steam efficiencies were 84.2%, 84.7%, 84.6%, and 84.4%, respectively. An average fuel-to-steam efficiency of η_b = 84.48% was considered for the thermal energy input calculation (η_b includes convection and radiation losses, combustion efficiency, heat exchanger efficiency, and 15% excess air in the exhaust flue gas for the selected model).

In addition, the relationship between electricity generation and thermal energy input can be expressed by a polynomial equation (NREL, 2016b) as follows:

$$P = \left(\beta_0 + \beta_1 \cdot \left(\frac{Q_i}{Q_i^{ref}}\right) + \beta_2 \cdot \left(\frac{Q_i}{Q_i^{ref}}\right)^2 + \beta_3 \cdot \left(\frac{Q_i}{Q_i^{ref}}\right)^3\right) \cdot P_e \qquad \text{(III-3)}$$

where P is the electrical power generated (kWe); Q_i is the input thermal energy (kWt); β_{0-3} are coefficients for turbine modeling (-0.0572; 1.0041; 0.1255; -0.0724, respectively). The extracted thermal energy in the condenser can also be defined by the polynomial equation:

$$Q = \left(\beta_0 + \beta_1 \cdot \left(\frac{Q_{in}}{Q_i}\right) + \beta_2 \cdot \left(\frac{Q_{in}}{Q_i}\right)^2 + \beta_3 \cdot \left(\frac{Q_{in}}{Q_i}\right)^3\right) \cdot Q_o \qquad \text{(III-4)}$$

Siemens SunField solar collector assembly (SCA) parabolic reflectors (aperture reflecting area 6 m^2, average focal length 1.5 m) were selected as the solar collectors. The heating collection elements (HCE) consisted of model 2008 Schott PTR70 vacuum tubes. The optical factors for the SCA and HCE are listed in Table III-3.

Table III-3. Optical factors for CSP collection

Parameter	**Value**
Tracking error	0.99
Geometric accuracy	0.968
Surface reflectance	0.925
Concentration factor	0.97
Cleanliness factor	0.98
Shadow factor	0.95
Transmissivity	0.96
Absorptivity	0.96

A single-axis tracing system (the trough is placed from east to west) was used to concentrate solar radiation into vacuum tubes, where synthetic oil (working fluid) absorbed and transferred the thermal energy. The heated synthetic oil was then used to preheat the feedwater before the boiler. Two buffer tanks (hot and cold storage) were used to store the thermal energy and heat the feedwater.

2.5.2. Solar–thermal–bio hybridization power generation

The PV-electricity-bio hybridization power unit was also studied to supply extra electricity energy instead of thermal energy to the wastewater treatment system (Figure III-2b). The analysis was performed by modeling the installation of panels, model SolarWorld SW235 mono, 60 cells per module, 30° tilted, degradation of 0.5% per year, and maximum power of 235 W under reference conditions (cell temperature at 25 °C and 1000 W/m^2 of solar radiation). The nominal operating cell temperature (NOCT) was used to quantify the energy generation under different solar radiation values. System losses include losses in the DC and AC energy conversion, such as in the diodes and connections (0.5%), DC wiring (2%), soiling (5%), AC wiring (1%), and transformer (1%).

3. System analysis

3.1. Mass balance of the wastewater treatment

A mass balance was conducted to evaluate the system performance. The operational parameters for the anaerobic digester used for the mass balance analysis are listed in Table III-4. The AD system generated 2,919.9 m^3/day of biogas, 11.41 m^3/day of solid digestate (AD fiber), and 64.66 m^3/day of liquid filtrate under the conditions of 25 days hydraulic retention time (HRT) and a digestion temperature of 40 °C (Figure III-3). The corresponding TS and COD removal were 41% and 62%, respectively. However, there was still a significant quantity of nutrients remaining in the filtrate, particularly TN (4,290 mg/L) and total soluble solids (23,734 mg/L) (Table III-5). Further treatment was needed to reclaim the water for other uses.

Table III-4. Performance of anaerobic digestion

Description	Unit	Value
Operating temperature	°C	40
Hydraulic retention time	day	25
Feed pH [A]	-	6.22 ± 0.93
Feed COD [B]	mg/L	133,250 ± 21,173
Biogas production	m^3/day	2,919.9
Methane composition	-	0.60
Daily waste feeding	m^3/day	76.07
Liquid filtrate	m^3/day	64.66
Solid digestate (AD fiber)	m^3/day	11.41
Average energy demand for the AD operation	kWh/day	1,276

[A]: Data is the average of 45 samples with standard deviation.
[B]: Data is the average of 8 samples with standard deviation.

Table III-5. Characteristics of the AD effluent, AD fiber, and filtrate*

Sample	Parameter	Value	Number of samples
AD effluent	Total solids (%)	5.04 ± 1.51	125
	Total soluble solids (mg/L)	28,553.30 ± 8,896.92	37
	Volatile solids (%)	3.85 ± 1.30	125
	COD (mg/L)	51,183.3 ± 1,874	6
	TP (mg/L)	538 ± 22	2
	TN (mg/L)	3,909 ± 832	16

Table III-5. (cont'd)

AD effluent	pH	7.82 ± 0.22	135
AD fiber	Total solids (%)	25.41 ± 3.60	57
	Volatile solids (%)	22.42 ± 3.24	57
Filtrate	Total solids (%)	3.68 ± 0.75	58
	Total soluble solids (mg/L)	23,734 ± 3,227	7
	COD (mg/L)	47,250 ± 3,106	8
	TP (mg/L)	427 ± 5	2
	TN (mg/L)	4290 ± 788	9
	pH	7.86 ± 0.16	56

*: Data are the average with standard deviation.

The AD filtrate was then treated by the AET process, including an aeration chamber and clarifier tank (Figure III-1). The minimum nutrient removal requirement for secondary treatments is shown in Table III-6 (Federation, 2009), as well as the water quality standard for agricultural use (Lazarova & Bahri, 2005). According to these parameters, the total soluble solids (TSS), COD, TP, and TN in the influent of the AET process must be less than 250 mg/L, 400 mg/L, 15 mg/L, and 20 mg/L, respectively. Because the AD filtrate had much higher concentrations than these values (Table III-5), the AD filtrate needed to be diluted. The COD was used as the critical parameter to perform the dilution. The volume of the aeration chamber needed to treat the diluted AD filtrate (AET influent) was 5,080.98 m^3 (Figure III-3).

Table III-6. Characteristics of liquid effluent for secondary wastewater treatment

Parameter	**Minimum removal requirement (%)**	**Water for agricultural uses (mg/L)**
TSS	90	5–50
COD	75	50–100
TP	75	1–30
TN	80	10–30

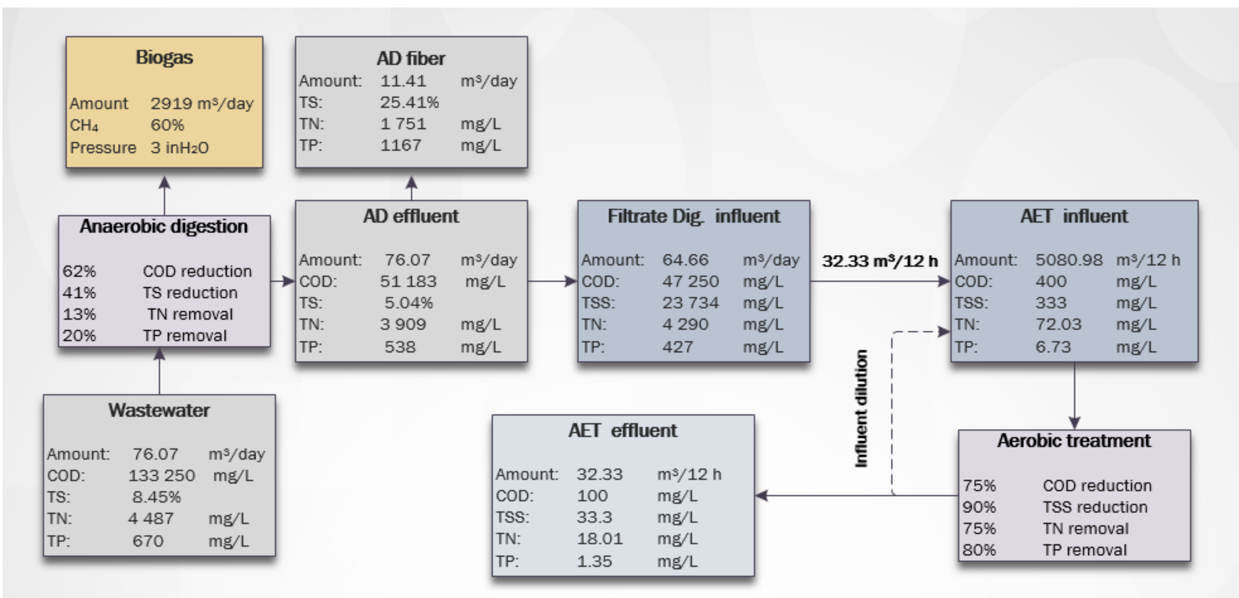

Figure III-3. Mass balance of the integrated anaerobic digestion and aerobic treatment

The AD treatment produced 38.37 m^3 of biogas per m^3 of influent wastewater per day, generating 1,751 m^3 of biomethane and 11.41 m^3 (wet basis) of fiber. After the AET, the system generated 32.33 m^3 of reclaimed water every 12 hours of the quality applicable to agronomic uses.

3.2. Energy balance of the solar–bio hybridization wastewater treatment

3.2.1. Electricity demands of the wastewater treatment

Table III-7 shows the electricity demand by the AD operation. The electricity usage of the different equipment during the AD operation has been arranged to enable a relatively even distribution of the electricity loading throughout a day, which avoids the uncertainty of engine operation and improves the engine efficiency. The average electricity demand for the AD operation was 293 kW (Figure III-4).

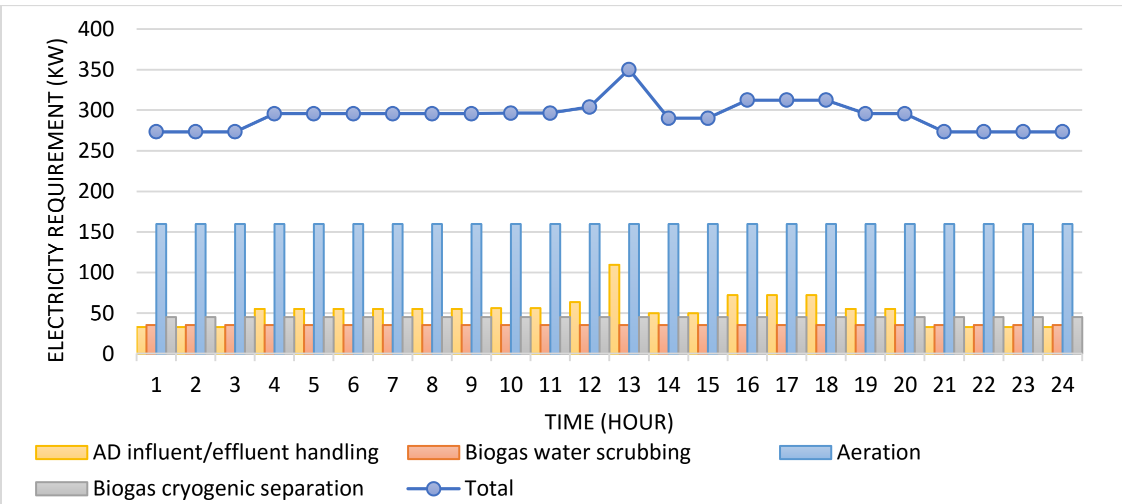

Figure III-4. Daily electricity demands of the wastewater treatment

Table III-7. Electrical energy consumption by the anaerobic digestion system

Location	Equipment	Power (kW)	Operating time (hours/day)
Food waste pit	Pump	13.35	1
	Mixer	22.38	1
Animal manure pit	Pump	29.84	1
	Mixer	11.19	24

Table III-7. (cont'd)

Mixing tank	Grinder	5.60	5
	Pump	11.19	5
	Mixer	2.98	24
Digester	Mixer	22.38	17
	Mixer	22.38	18
	Fan	0.18	24
Heating unit	Pump	7.46	24
Solid/liquid separator	Pump solid separator	14.92	3
	Pump filtrate	7.46	1
	Scrub Motor	7.46	3
	Solids conveyor	0.75	3

The biogas cleaning and upgrading had the highest electricity requirements. It has been reported that the electricity demands of water scrubbing and methane cryogenic separation are 0.275 kWh/Nm^3_{biogas} and 0.35 kWh/Nm^3_{biogas}, respectively (Sun et al., 2015). The effect of temperature on normalized biogas volume is expressed as follows:

$$V_N = \frac{P_{AD} \cdot V_{AD}}{T_{AD}} \cdot \frac{T_N}{P_N} \qquad \text{(III-5)}$$

where $P_N = 1\ atm$; $T_N = 288.15\ K$; $P_{AD} = 1.0074\ atm$; and $T_{AD} = 308.15\ K$. Equation (III-5) was then used to calculate the conversion factor between real biogas and normalized biogas. The electricity demands for water scrubbing and cryogenic separation were 1.068 MJ/m^3_{biogas} and 1.359 MJ/m^3_{biogas}.

As for the AET operation, it has been reported that the aeration ranges from 3.75 to 15 $m^3_{air}/m^3_{influent}$ in order to maintain the dissolved oxygen concentration between 1–2 mg/L (Wang et al., 2009). An intermediate value of 9.375 $m^3_{air}/m^3_{influent}$ was selected by this study to carry out the energy analysis. Since the volume of each AET operation was 5,080 m^3 influent each 12 hours, the aeration rate needed to be 1.103 m^3 air/s (0.013 m^3 air/ m^3 influent per min) to satisfy the required dissolved oxygen concentration. The power for the air compressor can be correspondingly calculated as

$$P_{comp} = \frac{\alpha \cdot m_{air}}{\eta_{comp}} \tag{III-6}$$

$$\alpha = \frac{\gamma}{\gamma-1} \cdot p_0 \cdot \left(\left(\frac{p_1}{p_0} \right)^{\frac{\gamma-1}{\gamma}} - 1 \right) \tag{III-7}$$

where m_{air} is the air flow requirement (m^3_{air}/s); η_{comp} is the compressor efficiency (0.90); γ is the ratio between the specific heat at constant pressure and the specific heat at constant volume (γ = 1.4); p_0 is the atmospheric pressure (101,000 Pa); and p_1 is the outlet air pressure (303,000 Pa). The compressor requires 159.70 kW to provide the air needed for the process. Figure III-4 indicates that aeration is the largest energy consumer among the unit operations of the wastewater treatment.

3.2.2. Thermal energy requirements of the wastewater treatment

Thermal energy is needed by the anaerobic digestion to heat the feed and maintain the culture temperature at 40 °C. The energy requirement per day (E_{req} (MJ/day)) is calculated as follows (Yue et al., 2013):

$$E_{req} = \frac{V_{AD}}{HRT} \cdot \rho_{inf} \cdot C_p \cdot \left(T_{AD} - T_{inf}\right) \cdot (1 + 0.3)/10^6 \tag{III-8}$$

where V_{AD} is the digester volume (m^3); HRT is the hydraulic retention time (days); ρ_{inf} is the feed density (1220 kg/m^3); C_p is the feed specific heat (4,120 J/kg·°C); T_{AD} is the culture temperature (40 °C); T_{inf} is the feed temperature and assumed to be the same as the ambient temperature when the ambient temperature is above 4 °C (the feed temperature is set at 4 °C when the ambient temperature is below 4 °C); and 0.3 is the additional heat that is needed to maintain the mesophilic culture condition of the digester. Due to the lower atmospheric temperature year-round in Lansing, the thermal energy needed to maintain the AD culture was an average of 323,099 MJ for the operation, which was almost double that in Phoenix (153,182 MJ) (Figure III-8).

3.2.3. Energy generation

In the studied systems, the AD, as the first stage of the wastewater treatment, generates energy that is used for the treatment system. However, the generated electricity (5,548.14 kWh/day with the AD on 76 $m^3_{influent}$ per day) is still insufficient to cover the energy demand (7,032 kWhe/day) of the wastewater treatment system, owing to the high electricity demand of the AET operation. Solar energy was then added into the system as the secondary energy source.

Since solar energy collection is largely influenced by the geographical location and season, a year-round and hourly-based analysis was carried out at the two locations (Lansing, MI and Phoenix, AZ) to compare the energy generation of the solar–bio hybrid unit at different seasonal and geographical conditions. Figure III-5 shows the variation of solar radiation (Direct Normal Irradiance (DNI) and Global Horizontal Irradiance (GHI)) and ambient temperature during a year for both locations (NREL, 2015). The DNI is the amount of solar radiation received by a surface held perpendicular to the rays that arrive in a straight line from the direction of the sun; DNI is of particular interest to concentrating solar thermal installations, such as parabolic troughs. GHI is the amount of solar radiation received by a surface horizontal to the ground, and consists of a combination of direct and diffuse solar radiation. GHI is used for static collection systems, such as photovoltaic panels. Phoenix has much higher DNI, GHI, and atmospheric temperature than Lansing. However, the ratios between DNI and GHI are different for the two locations. Lansing has a higher GHI than DNI, while Phoenix has a higher DNI (Figure III-5).

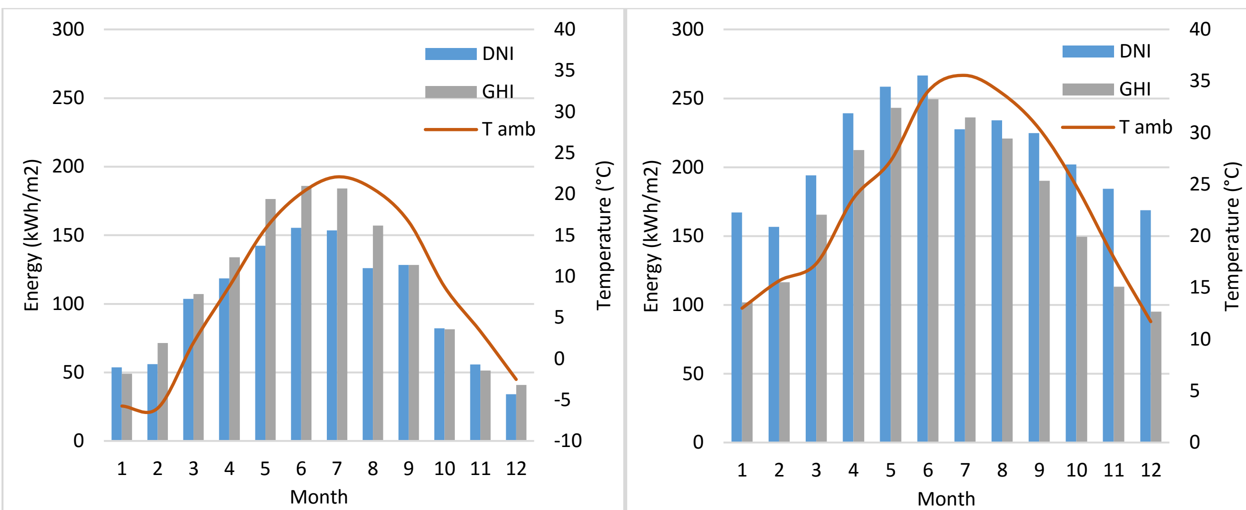

(a) (b)

Figure III-5. Variation of the ambient temperature (T_{amb}), DNI, and GHI for: (a) Lansing; (b) Phoenix

The parabolic trough collectors use SCA and HCE to collect and transfer solar heat via the HTF to support electricity production. The optical efficiency was calculated ($\eta_{op} = 0.74$ from Table III-3), and the energy loss of HTF can be obtained as

$$Q_p = \left(\xi_3 \cdot (\bar{T}_{HTF} - T_{amb})^3 + \xi_2 \cdot (\bar{T}_{HTF} - T_{amb})^2 + \xi_1 \cdot (\bar{T}_{HTF} - T_{amb})\right) \cdot {Q_p}^{ref} \cdot A_{SCA} \quad \text{(III-9)}$$

where Q_p is the heat loss in the piping system (kW); $\xi_{1\ldots3}$ are coefficients (0.001693, -1.68 × 10^{-5}, 6.78 × 10^{-8}); $\bar{T}_{HTF}$ is the average temperature of the working fluid for this study (325 °C); T_{amb} is the ambient temperature (°C); ${Q_p}^{ref}$ is the reference heat loss in the piping system when $\bar{T}_{HTF} = 316.5°C$ (10 W/m^2_{SCA}); and A_{SCA} is the area of the SCA (m^2). Furthermore, heat loss in the HCE has been documented as $Q_{HCE\_L} = 6.609\, W/m^2$ for the selected vacuum tube model (NREL, 2016b). The net thermal energy collected from the SCA ($Q_N\ (kW)$) is then calculated as

$$Q_N = \left(Q_{DNI} \cdot \eta_{op} \cdot A_{SCA}\right) - \left(\frac{Q_{HCE\_L} \cdot A_{SCA}}{1000}\right) - \left(Q_p\right) \qquad \text{(III-10)}$$

where Q_{DNI} is the direct normal irradiance (kW/m^2). The net heat used for steam generation is obtained as $Q_i = Q_N \cdot \eta_h$. Equation (III-3) is used to calculate the electricity generation.

The electricity load of the wastewater treatment (Figure III-4) is compared hourly with the electricity generation from the solar–bio hybrid unit. In the hybrid configuration, if the energy amount collected from the DNI is insufficient to satisfy the superheated steam demand of the turbine for electricity generation, biogas is burned to compensate the energy deficiency and generate extra superheated steam (Colmenar-Santos et al., 2015; Sun et al., 2015). If the energy quality (temperature) collected from the DNI is lower than the requirement for superheated steam generation, the energy collected in the SCA is then used to preheat the feedwater for the boiler and reduce the biogas demand during the superheated steam generation. It is apparent that combining biogas and solar energy can synergistically mitigate the issues of unstable solar energy flow and limited biogas production.

The PV-bio hybrid power unit functions differently from the CSP-bio hybrid unit to provide electricity to the wastewater treatment system (Figure III-2b). Biogas is the thermal energy source of the power unit and is only utilized when the electricity from the PV (after DC to AC conversion, parasitic, and system losses) is insufficient to cover the electricity demands of the system (Figure III-4).

In order to understand the performance of the solar–bio hybrid power unit to satisfy the energy demands of the wastewater treatment, two scenarios of electricity generation with and without short-term solar energy storage were analyzed.

3.2.3.1. Electricity generation without short-term solar energy storage

A solar collection system without solar energy storage means that both thermal heat from CSP and electricity from PV are directly used by the solar–bio hybrid unit for energy generation when DNI and GHI are available.

For the CSP-bio hybrid power unit, the hourly energy required from biogas (Q_B) is calculated as the difference between the hourly thermal energy required to generate the needed electricity ($Q\{P_{e\_af}\}$), and the hourly thermal heat collected from solar radiation ($Q_N \cdot \eta_h$) (Equation III-11.a). However, the biogas energy needed for the PV-bio hybrid unit is the thermal energy required by the turbine to generate the electricity that compensates the insufficient electricity from the PV ($Q\{P_{e\_af} - P_v\}$) (Equation III-11.b).

$$Q_B = \frac{Q\{P_{e\_af}\} - (Q_N \cdot \eta_h)}{\eta_b} \quad \text{(III-11.a)}$$

$$Q_B = \frac{Q\{P_{e\_af} - P_v\}}{\eta_b} \quad \text{(III-11.b)}$$

The solar operation factor (SOF) is a critical parameter to determine whether the solar–bio hybrid unit is a feasible solution to power the integrated AD and AET process. The SOF is defined as the time when CSP or PV units can collect net useful energy (the energy from biogas and solar energy collected after thermal and electricity losses to fulfill the minimum requirements of the solar–bio hybrid unit).

Since the solar–bio hybrid units need to provide a minimum energy input of 324.3 kWt (including η_b, Table III-2) to power the combined AD and AET processes, A_{SCA} was used to calculate the biogas daily balance of the solar–bio hybrid units. A positive biogas daily balance (m_{b_d}, m^3_{biogas}/day, the biogas amount required to generate Q_B) means that extra biogas is produced and can be stored for use at night or on cloudy days. A negative balance indicates that the daily biogas production is insufficient to cover the electricity demands of the wastewater treatment. An iterative approach was then applied to calculate the annual biogas balance. The annual biogas balance was used to evaluate the performance of the solar–bio hybrid power units. The CSP-bio hybrid unit at Phoenix and the PV-bio hybrid units at Lansing and Phoenix all have positive net annual biogas balances, while the CSP-bio hybrid unit at Lansing has a negative net annual biogas balance (Figure III-6). These results indicate that PV-bio hybrid power generation works for both Phoenix and Lansing, while CSP-bio hybrid power generation only works for Phoenix. The low DNI and short daylight time during winter in Lansing are the main reasons that the CSP-bio hybrid unit cannot accumulate sufficient solar radiation to generate the required amount of the energy. It was also determined from the simulation results that in Phoenix, the A_{SCA} of the CSP-bio hybrid and PV-electricity-bio hybrid power units were 21,498 m^2 and 6,128 m^2, respectively, and in Lansing the A_{SCA} of the PV-electricity-bio hybrid unit was 12,030 m^2 (Table III-8). These A_{SCA} values enable the solar–bio hybrid units to store 87,304 m^3_{biogas} for the CSP-bio-hybrid unit in Phoenix, 36,175 m^3_{biogas} for the PV-bio-hybrid unit in Phoenix, and 68,507 m^3_{biogas} for the PV-bio-hybrid unit in Lansing (Table III-8). These are all larger than the corresponding biogas demands, so that self-sustaining wastewater treatment can be realized by

PV-bio hybrid and CSP-bio hybrid power generation in Phoenix, and PV-bio hybrid power generation in Lansing.

However, since there is no short-term solar storage for the solar–bio hybrid power units, a very large area of solar collection is needed to generate energy during the daylight time to save the biogas energy for use at night or when cloudy. The large collection area leads to the generation of excess electricity and thermal energy from solar collection when DNI and GHI are at their maximum values (Figure III-7).

In addition, the thermal energy generated from solar–bio hybrid units is sufficient to support the heat needed by the wastewater treatment for all solar–bio hybrid operations (Figure III-8). In Phoenix, the thermal energy extracted from both CSP-bio hybrid and PV-bio hybrid units is much greater that the wastewater treatment requirements. However, the thermal energy extracted from the PV-bio hybrid unit in Lansing has an improved thermal energy balance compared to that in Phoenix (Figure III-8).

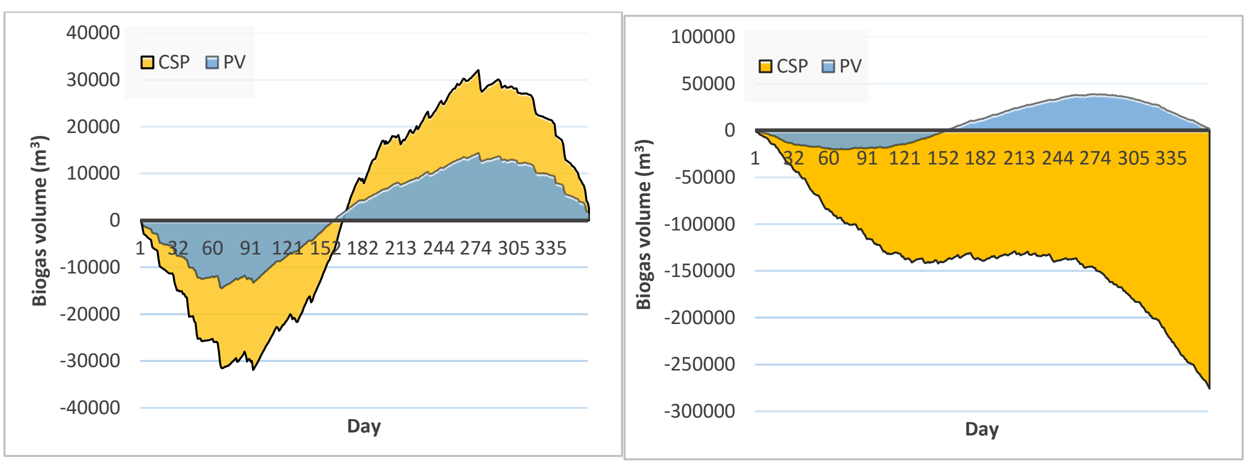

(a) (b)

Figure III-6. Biogas balance without solar energy short-term storage: (a) Phoenix; (b) Lansing*

*: Biogas balance at Lansing using an area of 500,000 m^2 (CSP).

Table III-8. Biogas balance for the electricity generation (without short-term solar energy storage)

Location	Solar collection system	Solar collection Area (m^2)	Biogas deficit (m^3/yr) A	Biogas stored (m^3/yr) B	Biogas stored initial volume (m^3)	Biogas reserved (m^3)	Biogas tank capacity (m^3) C
Phoenix	CSP	21,498	84,647	87,304	31,905	2,656	76.75
	PV	6,128.6	35,175	36,275	14,454	1,100	34.61
Lansing	PV	12,030.5	67,098	68,507	20,073	1,408	68.88

A: Biogas deficit is the total biogas daily requirement that exceeds the daily generation of the AD.
B: Biogas stored is the non-used biogas from the daily generation in the AD.
C: Tank capacity considering a biomethane compression factor of 500.

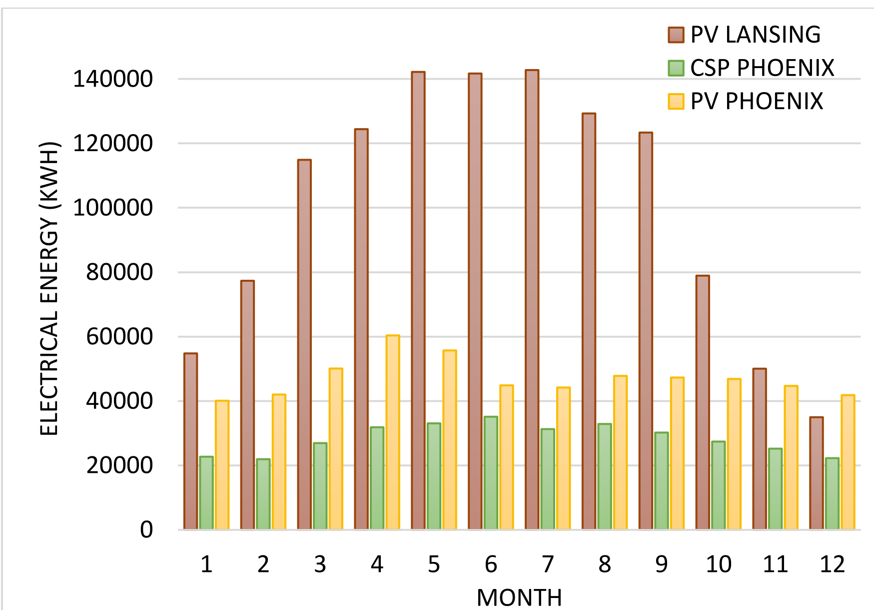

Figure III-7. Surplus electricity from solar–bio hybridization without short-term energy storage

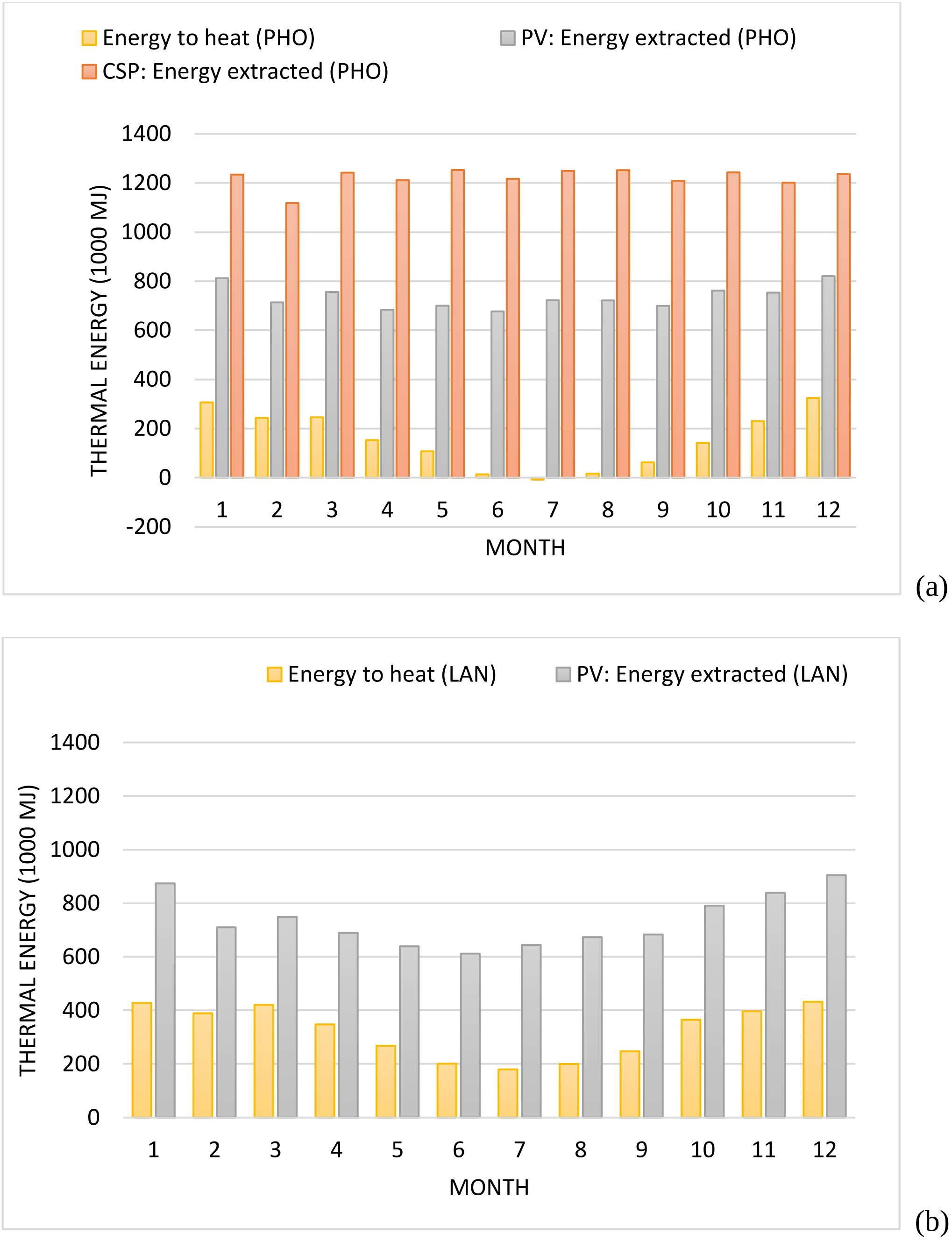

Figure III-8. Required and generated thermal energy for the system without short-term solar energy storage: (a) Phoenix, (b) Lansing

3.2.3.2. Electricity generation with short-term solar energy storage

Considering the large energy surplus from the solar–bio hybrid units without short-term solar energy storage, it is not a technically feasible solution to use the solar–bio hybrid units without short-term solar energy storage to power the wastewater treatment. Short-term solar energy storage needs to be investigated to determine the optimal conditions of solar–bio hybrid power generation, so that Q_B and the solar collection footprint can both be significantly reduced. A thermal reservoir for the CSP-bio hybrid unit and a battery bank for the PV-bio hybrid unit were used to store the extra solar energy when the DNI and GHI were higher than the requirements to fulfill the electricity demands of the wastewater treatment. The stored energy in the short-term storage was then used during the times when the DNI and GHI were not available to power the system and save on biogas usage.

Thermal collection for CSP uses a massive storage tank and saves the extra energy for electricity generation in the form of sensible heat, and the thermal storage selected was one-day sensible heat storage. Electricity storage for the PV consisted of battery storage that was selected as half of the maximum daily electricity production in a year. Equation (III-11) can be modified to include the energy from thermal or electrical storage for the biogas balance.

$$Q_B = \frac{Q\{P_{e\_af}\} - (Q_N \cdot \eta_h + Q_{s\_th})}{\eta_b} \tag{III-12.a}$$

$$Q_B = \frac{Q\{P_{e\_af} - P_v - P_{v\_b}\}}{\eta_b} \tag{III-12.b}$$

where Q_{s_th} is the thermal energy stored; and P_{v_b} is the electrical energy stored. The size for the energy storage was based on the thermal and electrical energy over-generated in the CSP and PV installation. Thermal storage for CSP for Phoenix and Lansing was 8,851 kWht (thermal) and 26,722 kWht, and the battery bank size was 425 kWhe (electrical) and 1,236 kWhe, respectively.

The iteration process calculated the A_{SCA} based on zero biogas balance in a year. It was determined from the calculations with short-term storage that in Phoenix, the required A_{SCA} for CSP- and PV-collection was 3,054 m^2 and 4,032 m^2, respectively; and in Lansing, the required A_{SCA} for CSP- and PV-collection was 6,756 m^2 and 5,821 m^2, respectively. Figure III-9 shows the biogas accumulation for the selected solar collection area in a year. It was found from the annual biogas balance that, in order to maintain a net positive energy balance, in Phoenix the additional biogas amounts for the CSP-bio hybrid and PV-bio hybrid power units were 135,217 m^3 and 45,054 m^3, respectively; and in Lansing, for the CSP-bio hybrid and PV-bio solar units, they were 292,486 m^3 and 113,386 m^3, respectively. In Phoenix, the calculated A_{SCA} allows the CSP-bio hybrid and PV bio-hybrid units to store 137,684 m^3 and 46,002 m^3 biogas, respectively; and in Lansing 298,098 m^3 and 117,301 m^3 biogas, respectively. Since the solar–bio hybrid power units with short-term storage generate slightly more biogas than the requirements of the wastewater treatment, both the CSP-bio hybrid and PV-bio hybrid units are capable of handling the weather variation and support the wastewater treatment in both Phoenix and Lansing (Table III-9).

In addition, the monthly surplus electricity of the solar–bio hybrid units with short-term solar storage is much lower than for units without short-term solar storage (Figures III-7 and III-10). The corresponding A_{SCA} values were much smaller than for units without short-term solar storage, which makes the solar–bio hybrid units more feasible (Table III-8 and III-9).

As for the thermal energy balance, the solar–bio hybrid units with short-term storage have a similar trend to the solar–bio hybrid units without the storage (Figures III-8 and III-11).

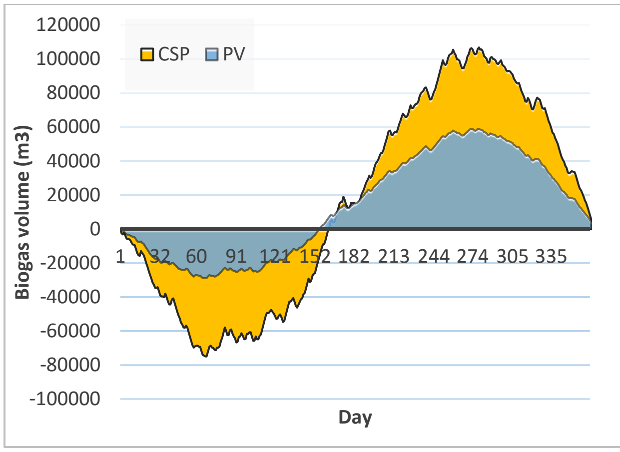

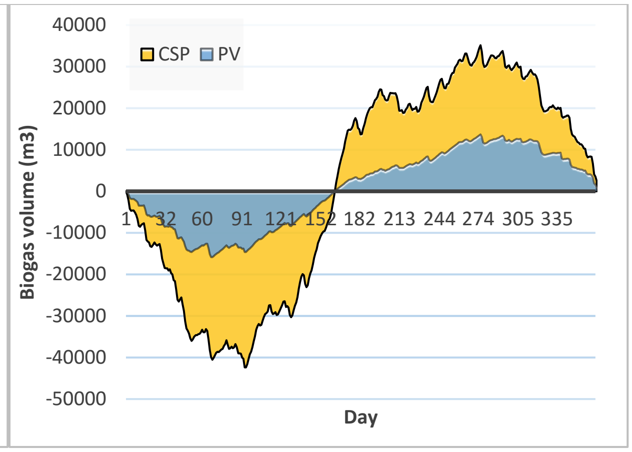

(c) (d)

Figure III-9. Biogas balance with solar energy short-term storage: (a) Phoenix, (b) Lansing

Table III-9. Biogas balance for the electricity generation (with short-term solar energy storage)

Location	**Solar collection system**	**Solar collection Area (m^2)**	**Biogas deficit (m^3/yr) [A]**	**Biogas stored (m^3/yr) [B]**	**Biogas stored initial volume (m^3)**	**Biogas reserved (m^3)**	**Biogas tank capacity (m^3) [C]**
Phoenix	CSP	3,054	135,217	137,684	42,380	2,466	93.05
	PV	4,032	45,054	46,002	15,848	475	35.43
Lansing	CSP	6,756	292,486	298,098	74,920	5,612	218.13
	PV	5,821.2	113,386	117,301	28,864	3,916	105.33

[A]: Biogas deficit is the total biogas daily requirement that exceeds the daily productivity in the AD.
[B]: Biogas stored is the biogas non-used from the daily generation in the AD.
[C]: Tank capacity considering a biomethane compression factor of 500.

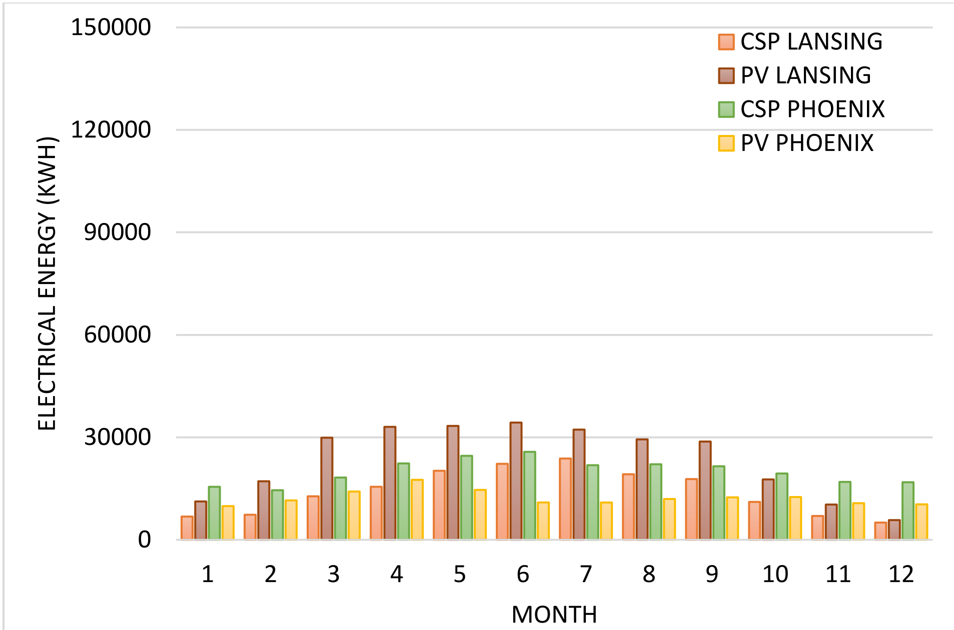

Figure III-10. Surplus electricity from solar–bio hybridization with short-term energy storage

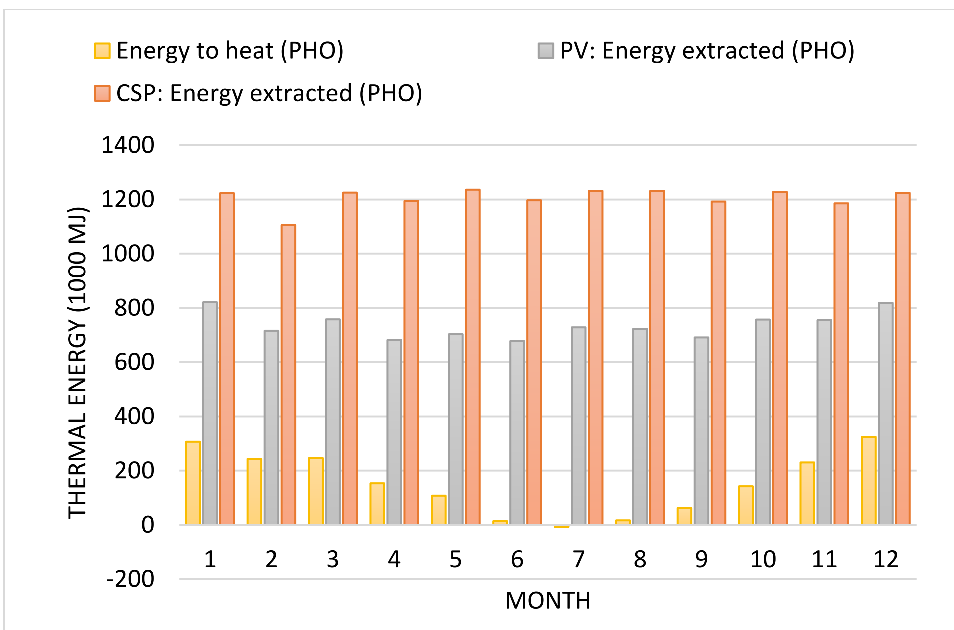

(a)

Figure III-11. Required and generated thermal energy for the system with short-term solar energy storage: (a) Phoenix, (b) Lansing

Figure III-11. (cont'd)

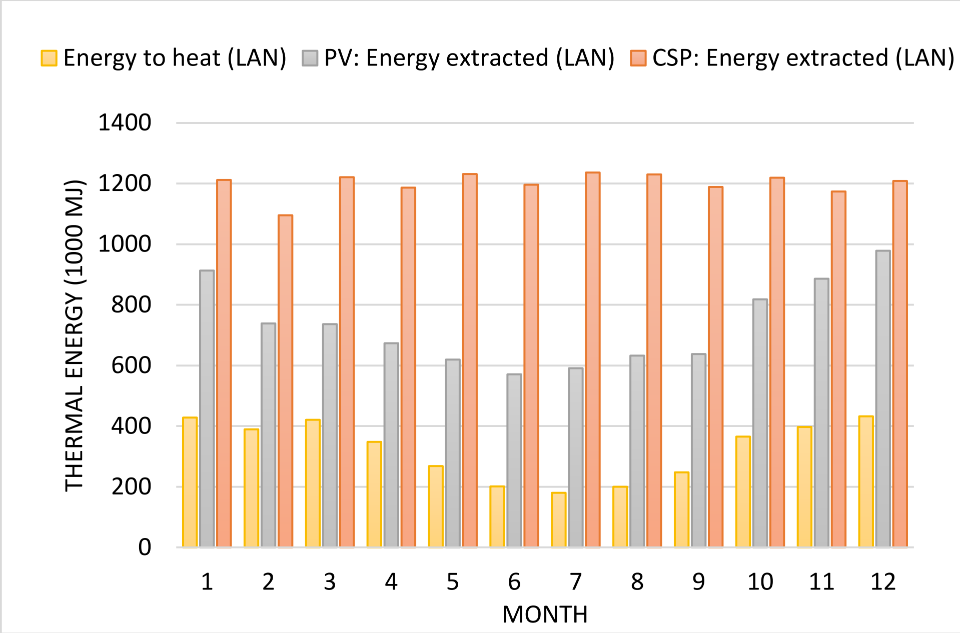

(b)

4. Discussions

This study presents a self-sustaining wastewater treatment concept for agricultural applications. Solar and biogas energy were used to support the treatment process completely, including AD and AET. Based on the geographic location of the treatment system, the effects of ambient temperature, DNI, and GHI on the system configuration and performance has been comprehensively investigated.

The AD unit in the self-sustaining system plays a dual role of reducing the organic matter (mainly carbon) and producing the biogas for electricity generation. The total solids in the AD influent (8.5%) were reduced by 41%, producing an average of 2,919 m^3_{biogas}/day (0.48 m^3_{biogas}/kg $_{volatile\ solids}$ ·day). The biogas from the AD is the major energy component to enable the realization of the self-sustaining nature of the system (of the 7,043.5 kWhe required for the wastewater treatment, biogas can supply 5,548.13 kWhe).

Since AD has limited capability to remove other nutrients, such as P and N, and reclaim the water, AET is needed to post-treat the AD effluent and complete the wastewater treatment. AET requires a considerable amount of electricity (3,832.8 kWhe per day, which is 54.4% of the total electrical consumption) to support the growth of aerobic microbes, leading to a negative energy balance for the wastewater treatment if the biogas is the only energy source for the combined AD and AET processes. Thus, a second energy source, solar energy, needs to be integrated into the system to satisfy the energy demands of the AD and AET. CSP and PV were the two selected solar energy collection methods for the solar–bio hybrid power units. The CSP-bio hybrid unit has the advantages of collecting energy at medium temperatures (< 350 °C) and increasing the solar energy utilization efficiency ($\eta_{op} \cdot \eta_e$). The PV-bio hybrid unit has the advantages of generating electricity from diffuse solar radiation and having a higher SOF.

Energy balance analysis indicates that there is a significant difference in the solar collection area between solar–bio hybrid systems with and without short-term solar energy storage. Without the storage, the SOF must be maximized by increasing A_{SCA} to collect solar energy to obtain sufficient thermal energy for the CSP-bio hybrid unit, or sufficient DC current for the PV-bio hybrid unit to satisfy the energy demands of the wastewater treatment. With the storage, the SOF is significantly reduced for both CSP-bio hybrid and PV-bio hybrid units. Correspondingly, the values of A_{SCA} were also greatly decreased (Tables 8 and 9). In addition, the PV-bio hybrid unit had a lower A_{SCA} and smaller biogas storage tank than the CSP-bio hybrid unit at both locations of Phoenix and Lansing. It is apparent that the PV-bio hybrid unit is the preferred power solution for the studied self-sustaining wastewater treatment.

5. Conclusions

A self-sustaining wastewater treatment concept using solar- and bio-energy to power AD and AET was studied. The results indicate that the combination of AD and AET can effectively reclaim the water from the agricultural wastewater. The solar–bio hybrid power generation addresses the challenge of the high energy demand of the AET. The energy balance analysis demonstrates that biogas storage to store the extra energy generated by the solar–bio hybrid unit during the warm months enables the wastewater treatment operation to be completely self-sustainable year-round. The PV-bio hybrid unit with short-term energy storage requires a smaller solar collection area and smaller biogas storage tank than the CSP-bio hybrid unit at both studied locations. Therefore, synergistically integrating PV-bio hybrid power generation, biogas storage, AD, and AET provides a technically feasible solution of a self-sustaining wastewater treatment.

CHAPTER IV. DESIGN AND EVALUATION OF A TWO-MODULE FRESNEL LENS SOLAR THERMAL COLLECTOR FOR A SCALABLE CONCENTRATED SOLAR POWER GENERATION CONCEPT

Abstract

This study analyzed a two-module Fresnel lens solar thermal collector to facilitate the development of a scalable solar power generation concept. The two-module structure enables the connection of multiple Fresnel lenses, with a view to enhancing the collection of solar thermal energy, and correspondingly addressing the scaling issue facing Fresnel lens solar thermal collectors. A bench-scale two-module collector was developed in this study to evaluate the performance of solar thermal collection. The experimental results indicated that a two-module structure with a high-resolution control system enables accurate solar tracking. Finite element method (FEM) simulated the temperature profile of the absorber under different concentration ratios and demonstrated that the absorber area has a greater impact on the surface temperature of the absorber than the concentration ratio. The relationship between absorber area, surface temperature, and heat loss was determined by combining the incident heat radiation model and FEM simulation. It was found that heat loss reduction could be achieved by increasing the absorber area with a relatively small temperature drop. The two-module Fresnel lens thermal collection unit decouples the thermal collector and receiver, so that a scalable concentrated solar power generation concept can be achieved.

Appendices added for this chapter:

i. Appendix F: Additional figures for a two-module Fresnel lens solar thermal collector

ii. Appendix G: Astronomical algorithm for solar tracking system

iii. Appendix H: Labview screenshots for control in solar tracking system

1. Introduction

Solar energy, the most abundant source of energy on the planet, represents a renewable alternative to fossil fuels. Many solar thermal technologies have been developed in the past decades, such as parabolic reflector concentrators, flat-panel collectors, evacuated tube collectors, central tower systems, and Fresnel lens refractive collectors (Franchini, Perdichizzi, Ravelli, & Barigozzi, 2013; Mills, 2004; Ávila-Marín, 2011). Among these, Fresnel lenses have recently attracted increasing attention as one of the concentrated solar energy technologies because of its advantages of light weight, relatively low cost, and high efficiency in increasing solar energy density (Lv et al., 2015; Xie et al., 2011). However, current research and development of Fresnel lens thermal collectors mainly focuses on the use of single module structures (the lens and thermal receiver are on a fixed structure) to concentrate solar energy (Wu, Eames, Mallick, & Sabry, 2012; Xie et al., 2013; Zhai et al., 2010). The single module design encounters several key technical issues as follows.

1) Due to the fact that Fresnel lenses use multiple refracting surfaces to densify the solar radiation, it is inevitable that using large lenses to obtain a high concentration of solar radiation leads to a significant reflection loss. This is caused by the increasing angles of incidence and emergence as the margin of the large lens is approached, so that the solar thermal efficiency may be greatly reduced.

2) Besides the reflection loss, large single-module collectors also require rigid and heavy structures to withstand high wind velocities and other severe weather conditions, which need large motors and gearboxes to move the units. Therefore, the low-weight advantage of Fresnel lenses is neutralized by the heavy supportive structure and thermal receiving units (Lovegrove & Stein, 2012; G. D. Zhu et al., 2014).

These issues significantly limit the use of Fresnel lens thermal collectors. A two-module Fresnel lens collector could be an effective approach to address the issues and establish a scalable concentrated solar power generation (Figure IV-1).

The two-module structure splits the solar collection system into two separate unit operations of moving the Fresnel lens solar collector and the light reflector or static thermal receiver. The two-module solar collection system only moves the Fresnel lenses, which significantly reduces the energy demand related with rotating and braking the Fresnel lens module. Fresnel lens modules with small- or medium-sized lenses track the sun and concentrate the solar radiation. The light reflector and thermal receiver modules at the focal point are fixed on the ground to transfer and collect the solar radiation (a similar concept to heliostat array concentrated solar power generation). Since the reflector and receiver modules are static (instead of hanging up and moving in the air), it is feasible to use the reflectors to transfer the concentrated solar radiation to a centrally located thermal receiver to generate a relatively large amount of heat. This could provide flexibility to accommodate a variety of thermal applications, such as heat exchangers, engines, and boilers. Correspondingly, a scalable concentrated solar power generation concept based on a two-module Fresnel lens solar energy collector can be realized (Figure IV-1).

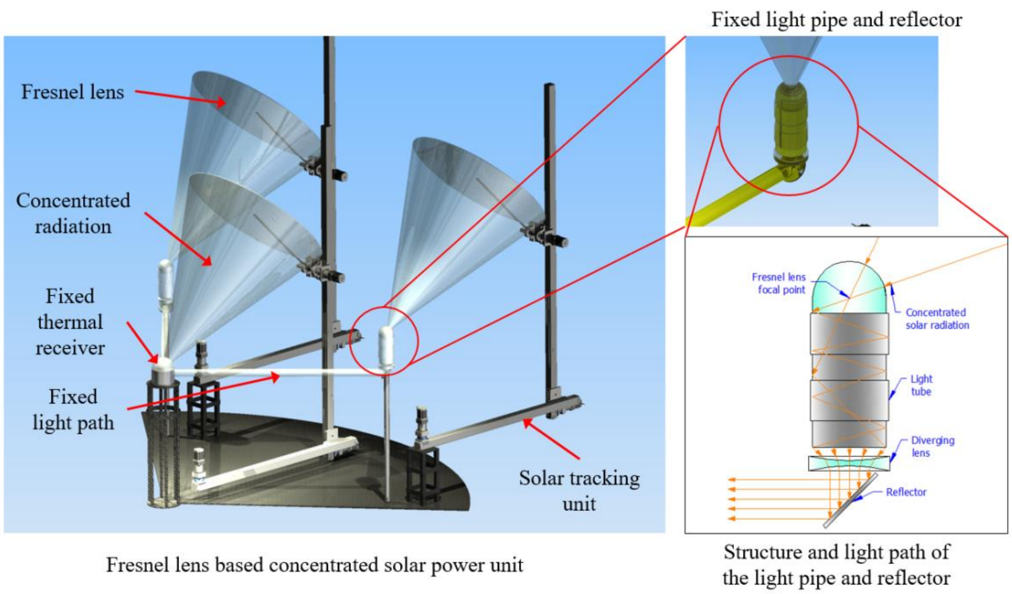

Figure IV-1. A scalable Fresnel lens solar thermal power generation concept

This study focused on developing a two-module Fresnel lens thermal collector (the Fresnel lens and fixed thermal receiver) to elucidate the feasibility of the scalable concentrated solar power generation concept. Since the two-module Fresnel lens collector requires different control mechanisms to track and concentrate the solar radiation on the receiver, a high-resolution tracking system has to be developed to realize the solar tracking. In addition, the receiver temperature and heat absorber area are critical to maximize the efficiency of solar energy collection. The relationship between absorber surface temperature, absorber area, and heat loss needs to be determined for the two-module solar collector. Therefore, the specific objectives of this study were to: 1) design a bench-scale Fresnel solar thermal collector unit; 2) evaluate the solar tracking for the two-module Fresnel lens thermal collector; and 3) investigate the relationship between heat loss, absorber temperature, and absorber area.

2. Design of a bench-scale two-module Fresnel solar thermal collector

2.1. Two-module thermal collector structure

A bench-scale two-module Fresnel solar thermal collector was designed and fabricated to carry out the study (Figure IV-2). A supportive platform was fixed on the bench (⑨ in Figure IV-2a) to support the Fresnel lens, which was slowly moved according to the topocentric azimuth angle (measured from the north vector, clockwise). Two mechanical actuators (model TB055 PBC Linear Co. Roscoe, IL) were used to move the lens, which were horizontally and vertically positioned on the platform (⑤ and ⑥ in Figure IV-2a). During the operation of the solar thermal collection (Figure IV-2a and b), a Fresnel lens (50 grooves per in, diameter of 18.25 in, focal length of 24 in, index of refraction of 1.49, transmittance of 0.92) was placed in the carriage of the vertical actuator (⑥ in Figure IV-2a). The lens rotated according to the zenith angle (measured from the vertical direction opposite to the apparent gravitational force). The receiver was fixed on the supportive platform.

In order to align the lens toward the sun and maintain a fixed focal distance between the Fresnel lens and fixed receiver, two automatic movements were required: 1) the lens rotated according to the zenith angle; and 2) the platform rotated according to the azimuth angle. These movements were achieved by actuators and gearboxes. The actuators used for the solar collector unit had a position accuracy of lower than 0.05 mm between repeated movements. The gearboxes with a 15:1 ratio (23VL015 NEMA 23 Planetary Gearhead) were used to adjust the horizontal and vertical displacement movements. The gearboxes with a 70:1 ratio (23VL070 NEMA 23 Planetary Gearhead) were used for the lens rotation and platform rotation. The resolutions were 0.00885 mm/step and 0.025°/step for linear displacement and rotation, respectively. In this particular study, steel plates were used as the thermal absorbers. The parts for the bench-scale unit presented in Figure IV-2 are: ① stepper motor for vertical adjustment of the lens (gearbox 15:1); ② stepper motor for horizontal adjustment of the lens (gearbox 15:1); ③ stepper motor for zenith angle adjustment (gearbox 70:1); ④ stepper motor for azimuth angle adjustment (gearbox 70:1); ⑤ horizontal linear actuator (700 mm stroke); ⑥ foldable vertical linear actuator (1,280 mm stroke); ⑦ Fresnel lens (24 in focal length); ⑧ receiver for solar radiation; and ⑨ supportive platform.

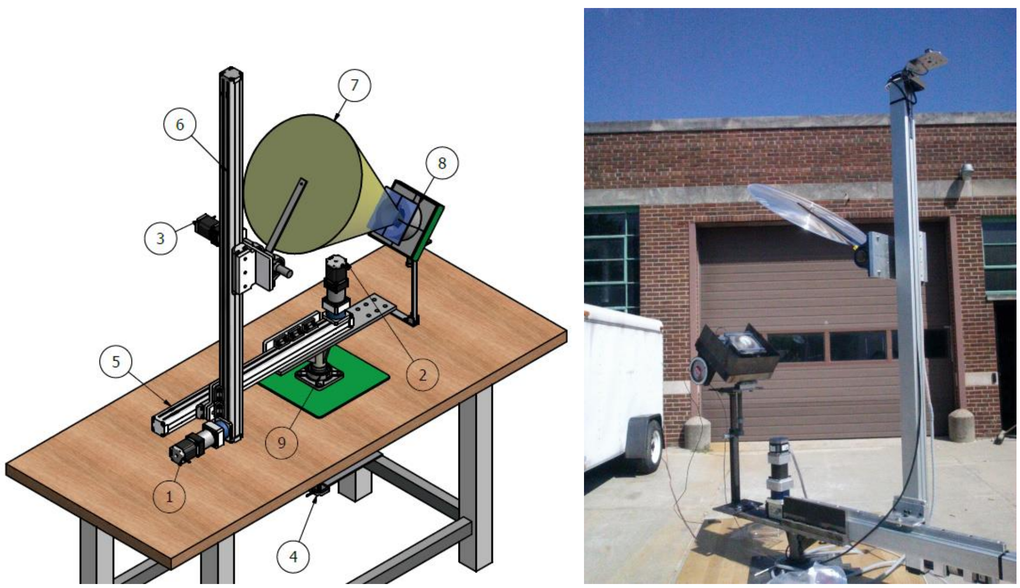

(a) (b)

Figure IV-2. Bench-scale two-module foldable Fresnel solar thermal collector*

Figure IV-2. (cont'd)

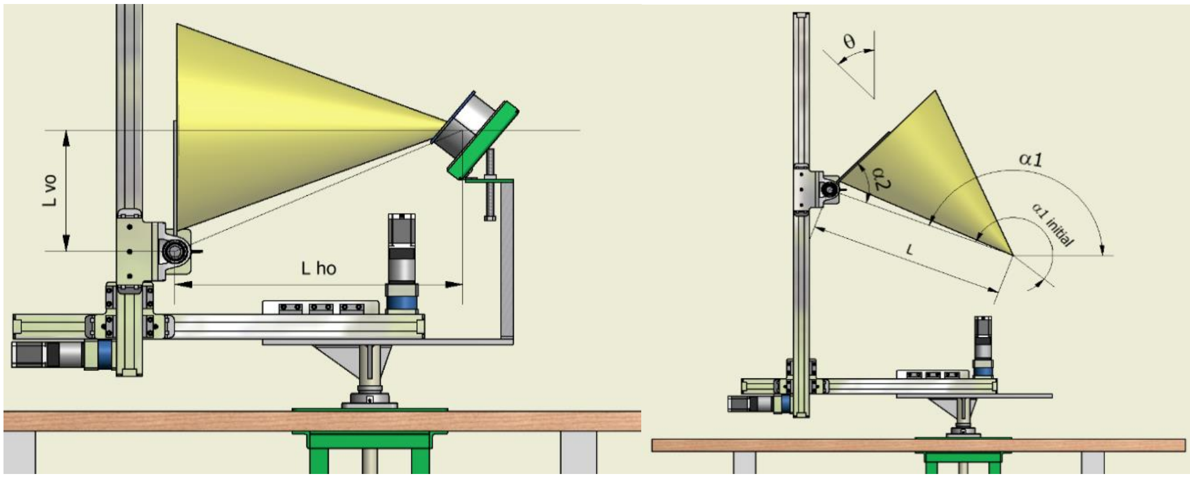

(c) (d)

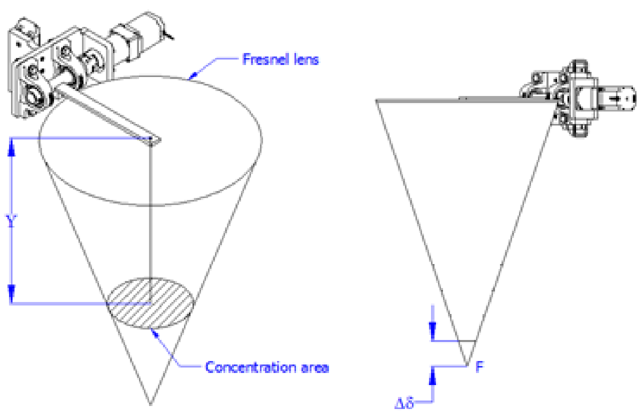

(e)

*(a) CAD drawing of the solar thermal collector in working mode; (b) the bench-scale solar thermal collector; (c) initial position of the solar thermal collector; (d) zenith angle and lens adjustment at mid-position; (e) concentration ratio for temperature measurement.

2.2. Thermal absorbers for temperature profile at focal area

In order to determine the temperature profile at the focal area of the collector unit, a thermal receiver was specially designed to collect solar radiation for this study (Figure IV- 3).

The receiver includes a metallic cylindrical column (with a height of 65 mm and a diameter of 92 mm), a square thermal glass (with a size of 158 ×158 mm, a thickness of 6.35 mm, and a transmittance of 0.9) covering the top of the column (Figure IV-3a). Three layers (10 mm each) of Pyrogel XT (an insulation material with the thermal conductivity of 90 $mW \cdot m^{-1} \cdot K^{-1}$ at 650 °C) were placed at the bottom of the column. The absorbers were fixed on the top of the Pyrogel XT layers. The absorbers consisted of mild steel plates of different sizes (4,032 mm^2; 2,580 mm^2; and 1,451 mm^2) (Figure IV-3c). In addition, two layers of Pyrogel XT were used to cover the sides of the metallic column to prevent excess heat loss.

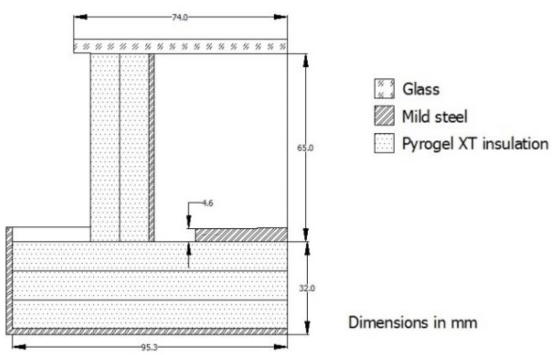

(a)

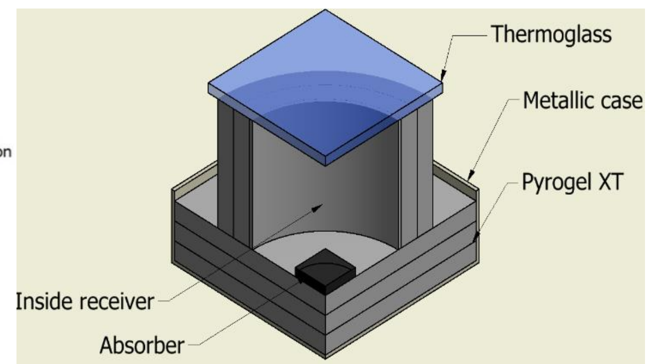

(b)

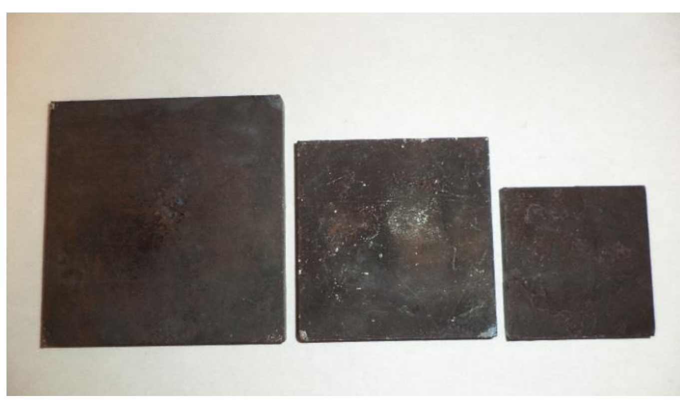

(c)

Figure IV-3. The receiver and metallic absorbers*

Figure IV-3. (cont'd)

*: (a) Dimensions of the receiver (one-quarter size); (b) geometric model of the receiver (one-quarter size); (c) metallic absorbers of three different sizes (4,032 mm^2; 2,580 mm^2; and 1,451 mm^2).

2.3. Instruments for solar tracking

Four stepper motors (NEMA 23, 20,000 steps per revolution in increments of 100 steps, 24 V DC) were used to control the linear displacement and rotation of the Fresnel lens collector. The stepper motors were powered by four power supplies (model PS150A24, input 120 V AC, output 24 V DC, 150 W) via the drives (model ST5-Si-NN) that were programmed using the software Si Programmer™ (Figure IV-4). The stepper motors were connected to the drives using bipolar parallel connection (Appendix F). A hub (model SiNet-Hub 444) transmitted the control signals to the drives via a RJ 11 connection. A RJ11-RS232 connector was used to connect the control hub to a computer.

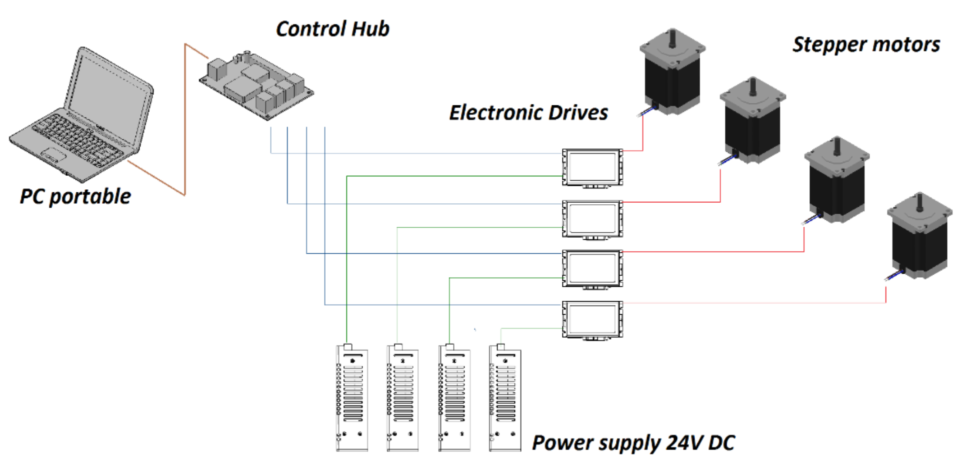

Figure IV-4. The control system of the solar tracking

3. Solar tracking model and control mechanism

An astronomical algorithm (Reda & Andreas, 2008) was programmed in Matlab 2011a (MathWorks, Natick, MA) (Appendix G) to calculate the position of the sun. The software program LabVIEW 2011 (National Instruments Co, Austin, TX) was used to run the Matlab function to track the position of the sun, and control the stepper motors to move the Fresnel lens solar thermal collector (Figure IV-5) (Appendix H). A virtual clock provided time parameters to the algorithm (processes 1 and 2 in Figure IV-5).

The displacement of the linear actuators was calculated based on the following equations in the Matlab® function.

$$L_h = L_{h0} - L \cdot \cos\left(\alpha^{o}{}_{1} - \frac{\pi}{2} + \theta\right) \quad \text{(IV-1)}$$

$$L_v = L_{v0} - L \cdot \sin\left(\alpha^{o}{}_{1} - \frac{\pi}{2} + \theta\right) \quad \text{(IV-2)}$$

where L_h and L_v are the horizontal and vertical displacements of the lens (mm), respectively; L_{h0} and L_{v0} are the horizontal and vertical distances from the focal point to the rotational point of the lens in the initial position (mm), respectively; L *i*s the distance between the focal point and the rotational point of the lens; $\alpha^{o}{}_{1}$ is the angle of the position of L at its initial position (rad); and θ is the topocentric zenith angle of the sun's position (rad) (Figures IV-2c and IV-2d).

The displacement and rotation of the lens were then converted to steps by LabVIEW using the following equations to control the movement of the stepper motors 1–2 and 3–4 (the corresponding gearboxes had ratios of 1:15 and 1:70, respectively) (Figure IV-5).

$$S_h = L_h \cdot \frac{1}{R} \cdot \frac{15}{1} \cdot \frac{20\,000}{1} \quad \text{(IV-3a)}$$

$$S_v = L_v \cdot \frac{1}{R} \cdot \frac{15}{1} \cdot \frac{20\,000}{1} \quad \text{(IV-3b)}$$

$$S_\theta = (\theta - \theta_o) \cdot \frac{1}{360} \cdot \frac{70}{1} \cdot \frac{20\,000}{1} \quad \text{(IV-4a)}$$

$$S_\gamma = (\gamma - \gamma_o) \cdot \frac{1}{360} \cdot \frac{70}{1} \cdot \frac{20\,000}{1} \quad \text{(IV-4b)}$$

where S_h and S_v are the number of steps for the motors 1 and 2 (for the horizontal and vertical adjustments, respectively); R is the linear displacement per actuator-shaft revolution (0.04 rev/mm); S_θ and S_γ are the number of steps for motors 3 and 4 (for the zenith and azimuth adjustments, respectively); θ_o and γ_o are topocentric angles for the initial position ($\theta_o = 90°$, $\gamma_o = 0°$); θ and γ are the zenith and azimuth angles for the position of the sun.

The speed of the stepper motors was set at 5 rev/s. According to the sun's position in East Lansing, MI, a filter code was included to limit the range of movement of the step motors 3 and 4, so that the movements of the azimuth and zenith angles were 90–270° and 0–90°, respectively (process 4 in Figure IV-5).

During the operation, the sequence of actions was set up as azimuth angle rotation, horizontal displacement, vertical displacement, zenith angle rotation, and receiver inclination adjustment. Structured Control Language (SCL) was used to send commands to the motors. The acceleration and deceleration of the movements were set at 25 rev·s^{-2}. A delay of 1.5 s between the motor movement commands was included to avoid data saturation in the control hub. The continuous loop (Figure IV-5) was repeated every 30 s.

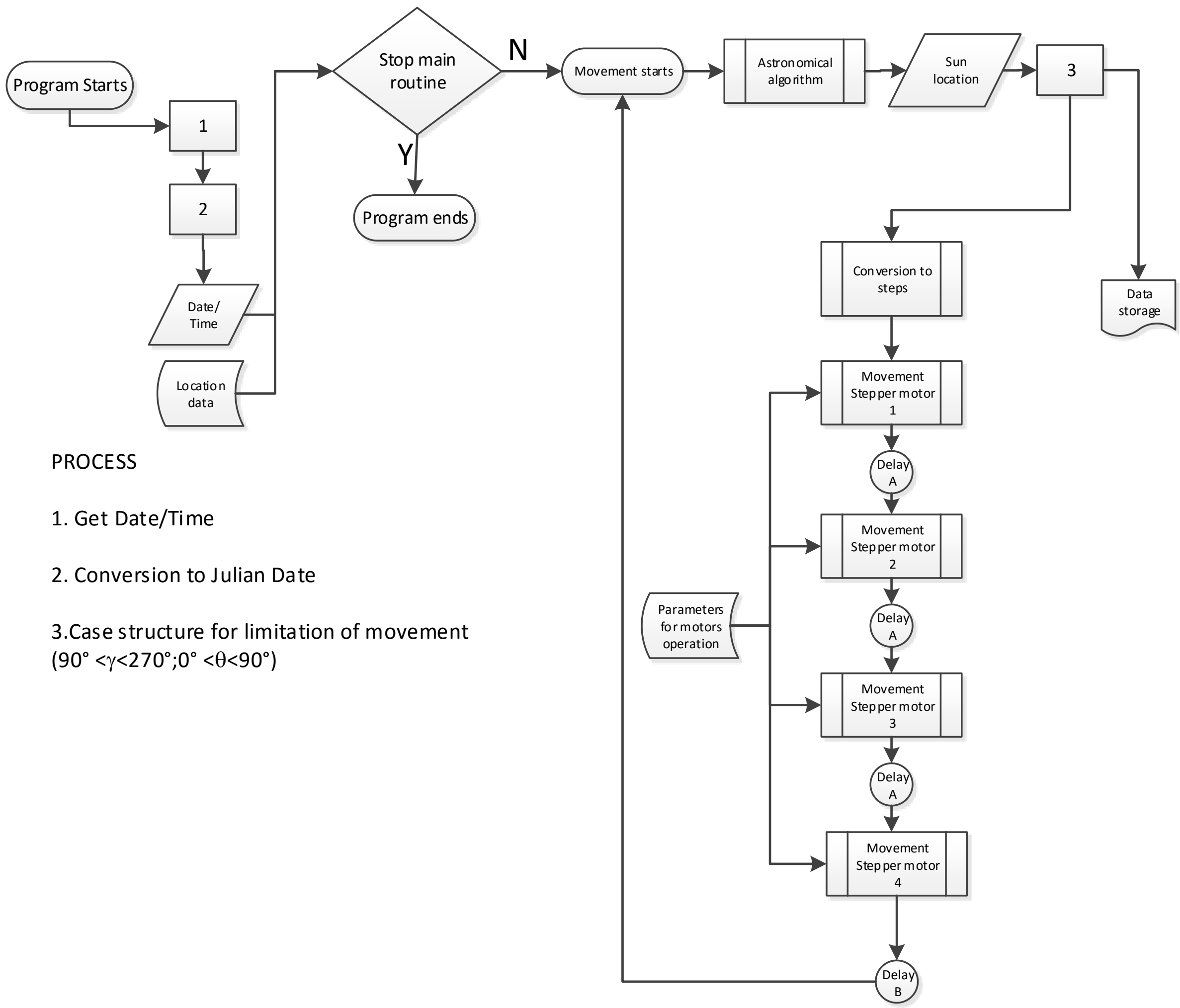

Figure IV-5. The tracking logic diagram of the LabVIEW program

4. FEM simulation of temperature profiles of the receiver

The temperature profiles of the absorbers under different concentration ratios (CR) and absorber areas were simulated using finite element methods (FEM). ANSYS 14.5 (ANSYS, Inc. Canonsburg, PA) was used to perform the analysis. The energy input for the FEM model was the solar radiation values collected at East Lansing, MI. The geometric model of the receiver and absorbers for the FEM model is presented in Figures IV-3b and c. The temperature inside the receiver was measured and used for the simulation. The heat inflow received by the absorber is described as

$$q_o'' = \dot{Q}_{solar} \cdot \tau_l \cdot \tau_g \cdot \alpha_m \cdot A_l \tag{IV-5}$$

where $\dot{Q}_{solar}$ is the heat flux from the solar radiation measured by the pyranometer; τ_l and τ_g are the transmittance of the lens and the thermal glass, respectively; α_m is the absorbance of the metallic plate; and A_l is the area of the lens. The transmittances were obtained from the technical specifications of the metallic absorber manufacturer ($\tau_l = 0.92$ and $\tau_g = 0.90$). The absorbance was assumed to be equal to the emittance (ϵ_m) of mild steel. It has been reported that ϵ_m ranges from 0.3 for clean and polished surfaces to 0.8 for oxidized surfaces (M. F. Modest, 2013). For this study, since the absorber surface was neither polished nor totally oxidized (Figure IV-3c), ϵ_m was set at 0.5. Other parameters for the FEM simulation are listed in Table IV-1. For the model, $\dot{Q}_{solar}$ was assumed to be completely absorbed by the metallic plate. Additionally, it was assumed that the absorber total emissive power was constantly emitted in all directions, and calculated as $\dot{Q}_e = \sigma \cdot A_a \cdot \epsilon_m \cdot (T_a^4 - T_\infty^4)$, where T_a is the absorber temperature, and T_∞ is the ambient temperature.

Table IV-1. Parameters used in FEM simulation*

Concentration ratio (CR)	**256**			**576**			**1,000**		
Absorber area (mm^2)	1,451	2,580	4,032	1,451	2,580	4,032	1,451	2,580	4,032
$\dot{Q}$ Heat flow (W)	11.06	11.78	11.87	10.87	11.63	11.36	10.77	11.65	11.71

*: Ambient temperature: 20 °C; external convection: 8 W/m^2·°C; and internal convection: 10 W/m^2·°C.

5. Data Collection

The distance $\Delta\delta$ between the lens and the absorber was adjusted ($\Delta\delta = 1.5, 1, \text{and } 0.75\ in$) to achieve different concentration ratios ($CR = 256, 576, \text{and } 1000$) (Figure IV-2e). The temperature at the center of the absorber was measured by a type K thermocouple that was connected to a CR800 Data Acquisition System (DAQ) (Campbell Scientific, Inc. Logan, UT). The solar radiation was measured using a LI 200 pyranometer (LI-COR, Lincoln, NE) that was also connected to the DAQ. The absorber temperature and solar radiation were recorded every 30 s. The temperature inside the receiver (Figure IV-3) was measured using a type K thermocouple connected to a multimeter MN35 (Extech Instruments), which was read manually every 10 min. The LabVIEW recorded the movement of the collector every 60 s.

6. Statistical analysis

The one-sample t-test was used to compare the measured temperature and simulated temperature from the FEM model. The confidence interval of the mean was set at 90%, and the corresponding p-value was 0.1. The t-value was determined by the following equation.

$$t = \left| \frac{\overline{T} - T_0}{\frac{s}{\sqrt{n}}} \right| \tag{IV-6}$$

where t is the t-value; T_0 is the simulated temperature; $\overline{T}$ is the average temperature from multiple measurements; s is the sample standard deviation of the temperature measurements; and n is the number of measurements.

7. Experimental results and discussion

7.1. Solar tracking of the two-module collection unit

The Fresnel lens solar thermal collector was operated and tested in East Lansing, Michigan (elevation 262 m, latitude 42°43'27.8" N, longitude 84°28'38.6" W) from July 2013 to October 2013. As demonstrated in Figure IV-2, the accuracy of the solar tracking was mainly dependent on the movement of Fresnel lens (stepper motors and linear actuators). The calculated decimal position data from the astronomical algorithm were converted into integer numbers (step numbers of the stepper motors) before being transferred to the step motors. Large step numbers should be used to achieve a high position resolution, which is the reason that the stepper motors with 20,000 steps per revolution were selected to move the Fresnel lens collector. In addition, high and low integer step numbers generated by the round function in LabVIEW were able to compensate each other during the operation, which also facilitated reducing the position errors. The comparison between the theoretical position (astronomical algorithm) and the position obtained from the solar tracker verified that the control system enabled the two-module unit to realize the solar tracking accurately (Figure IV-6). During the tracking test, differences in azimuth and zenith angles between the lens and actual sun positions were 0.221° ± 0.238° and 0.025° ± 0.019°, respectively, which were very small and had no significant influence on solar thermal collection.

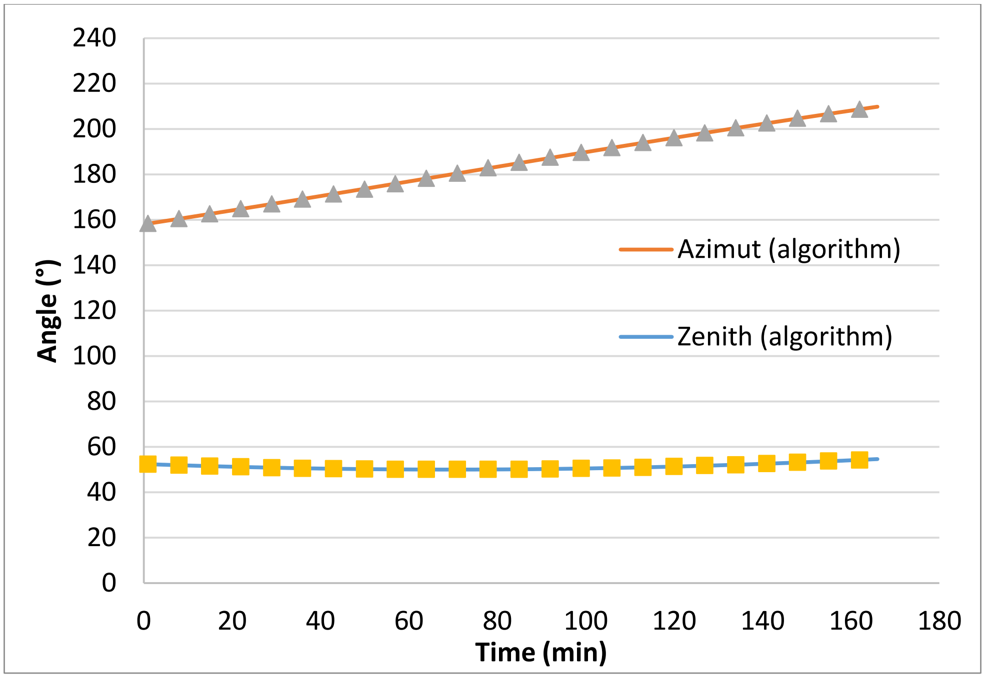

(a)

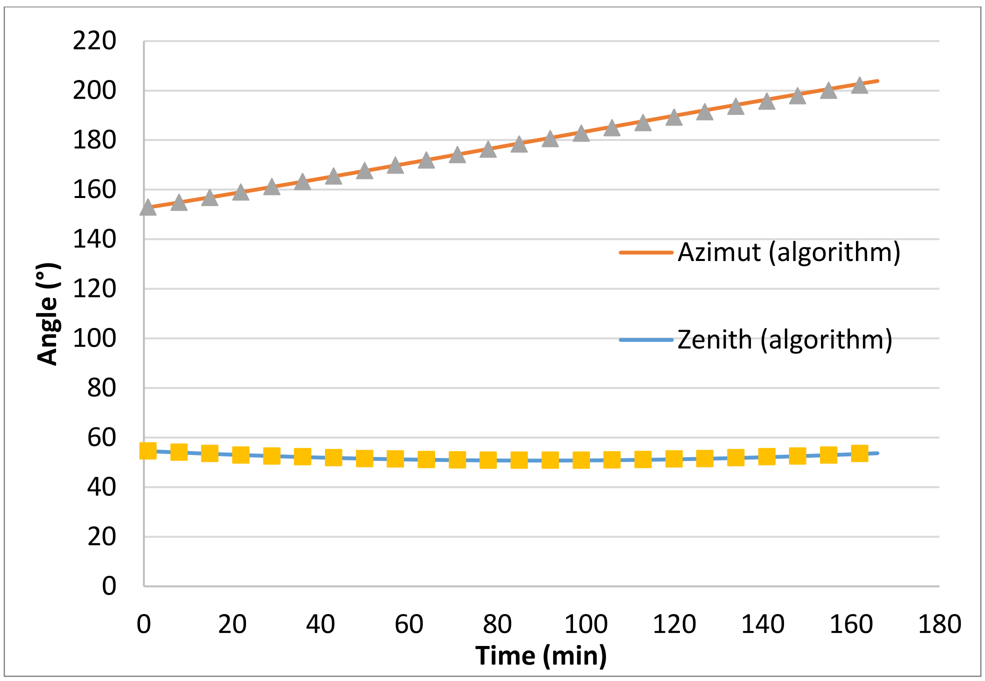

(b)

Figure IV-6. Topocentric azimut and zenith angles of the Fresnel lens position during the solar tracking test on: (a) October 11, 2013; (b) October 13, 2013

7.2. FEM simulation and verification of temperature profile of thermal absorbers

The solar radiation and receiver column temperature (inside the receiver) were measured and used for the FEM simulation (Table IV-2). The FEM simulation results are presented in Table IV-3 and Figure IV-7 (see Figure VII-2 Appendix F for all results). The data demonstrate that, under the same operational conditions (ambient temperature and solar radiation), the larger the CR, the higher the temperatures at the center of the absorber. However, the increase of temperature was not proportional to the increase of CR or decrease of absorber area. For instance, when the CR was increased from 256 to 1,000, the temperatures were only increased by 3.49%, 4.85%, and 6.28% for absorber areas of 1,451 mm^2, 2,580 mm^2, and 4,032 mm^2, respectively. However, compared to the temperature response to the CR changes, the absorber temperatures changed more dramatically according to the change in size of the absorbers. When the absorber area was decreased from 4,032 mm^2 to 1,451 mm^2, the temperatures at the center of absorber increased by 36.75%, 37.00%, and 33.16% for concentration ratios of 256, 576, and 1000, respectively.

Table IV-2. Solar radiation and receiver column temperature for the FEM model

CR	**Area A_a (mm^2)**	**Solar radiation (W/m^2)**	**Number of measurements^{*A}**	**Inside receiver temperature (°C)**	**Number of measurements^{*B}**
256	1,451	633.17 ± 18.66	163	204.36 ± 36.35	11
	2,580	674.16 ± 5.19	106	217.00 ± 21.33	9
	4,032	679.54 ± 5.22	107	181.67 ± 31.40	9
576	1,451	622.48 ± 15.13	85	256.80 ± 9.20	5

Table IV-2. (cont'd)

576	2,580	665.78 ± 7.11	69	274.20 ± 15.80	5
	4,032	650.63 ± 14.32	94	209.40 ± 14.72	5
1,000	1,451	616.72 ± 23.53	86	301.80 ± 7.98	5
	2,580	666.82 ± 4.49	81	278.60 ± 15.97	5
	4,032	670.64 ± 4.37	73	241.75 ± 24.51	4

*A: Data were collected every 1 min; *B: Data were collected every 10 min.

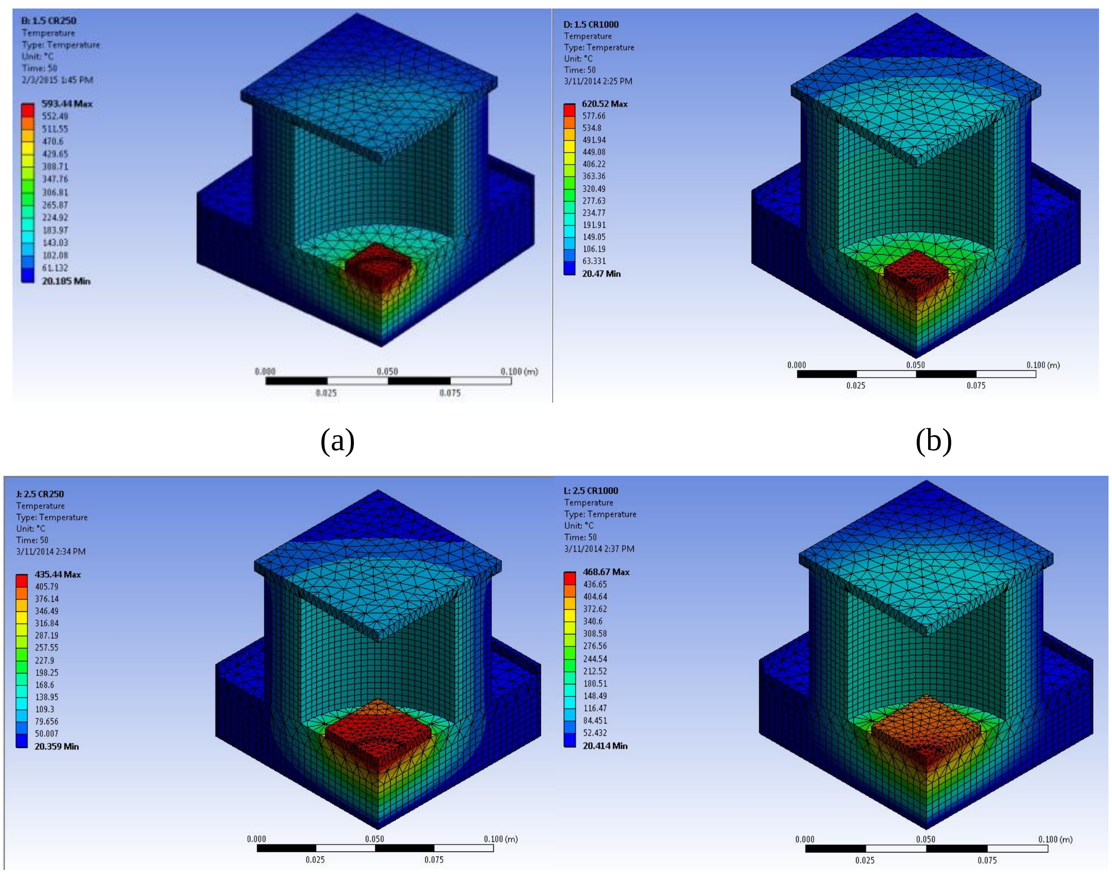

(a) (b)

(c) (d)

Figure IV-7. Temperature profiles obtained using FEM simulation*

Figure IV-7. (cont'd)

*(a) 1,451 mm^2 absorber area and 256 CR; (b) 1,451 mm^2 absorber area and 1,000 CR; (c) 4,032 mm^2 absorber area and 256 CR; (d) 4,032 mm^2 absorber area and 1000 CR.

The simulation results were verified by measuring the temperatures of the absorbers for the two concentration ratios of 256 and 576 (Table IV-3). A one-sample t-test found that all measurements were in the 90% confidence interval of the model results (Table IV-3).

Table IV-3. Temperature at the center of the absorbers and statistical comparison

CR	**Area A_a (mm^2)**	**Temperature from the FEM model (°C)**	**Measured temperature (°C)**	**Number of measurements *1**	**One-sample t-test**	
					t-value	**p-value**
256	1,451	592.94	564.49 ± 38.75	163	4.643	> 0.1
	2,580	508.76	531.79 ± 51.67	106	2.819	> 0.1
	4,032	433.58	410.79 ± 31.36	107	4.596	> 0.1
576	1,451	603.83	633.28 ± 13.17	85	14.143	> 0.1
	2,580	525.70	533.94 ± 24.17	69	1.983	> 0.1
	4,032	440.74	418.66 ± 24.20	125	5.771	> 0.1
1000	1,451	613.65	-	-	-	-
	2,580	533.44	-	-	-	-
	4,032	460.83	-	-	-	-

*1: Data were collected every 1 min.

As for the temperature distribution of the absorber, a homogenous temperature profile requires that the ratio of concentration area (A_c) to absorber area (A_a) should be close to 1. However, high A_c/A_a ratios require extreme accuracy of movement, which is difficult to achieve for most reflective and refractive solar thermal collectors. Therefore, the A_c/A_a ratios of the studied two-module collector were varied between 0.042 and 0.454 (Table IV-4). The simulation results indicate that a temperature gradient occurred for all combinations of CR and absorber area (Figure IV-7). The temperature difference between the center and corners of the absorbers increased with an increase in A_c/A_a ratio (Tables IV-3 and IV-5). For a CR of 256, for the three absorbers with sizes of 1,451 mm^2, 2,580 mm^2, and 4,032 mm^2, the percentage temperature differences were 3.19%, 4.63%, and 5.54%, respectively. For a CR of 576, the corresponding percentage temperature differences for the absorbers were 5.16%, 6.87%, and 8.07 %, respectively; and for a CR of 1,000, they were 7.27%, 9.13%, 10.48%, respectively. The smallest difference of 3.19% was obtained for the 1,451 mm^2 absorber with a CR of 256 and an A_c/A_a ratio of 0.454; and the largest difference of 10.48% was obtained for the 4,032 mm^2 absorber and the CR of 1,000 with an A_c/A_a ratio of 0.042.

Table IV-4. A_c/A_a ratios for different CRs and absorber areas

CR	**Area A_a (mm^2)**		
	1,451	**2,580**	**4,032**
256	0.454	0.255	0.163
576	0.202	0.114	0.073
1,000	0.116	0.065	0.042

Table IV-5. Simulated central temperature of absorbers (°C)

Absorber (mm^2)	**Concentration ratio (CR)**		
	256	**576**	**1,000**
1,451	574.00	575.90	579.68
2,580	482.51	489.56	490.39
4,032	402.06	400.50	412.54

8. Relationship between concentration area and surface temperature

Solar thermal collectors are intended to transfer as much solar energy as possible via a receiver to various heat applications. It is apparent that the surface temperature and absorber area are two key factors that determine the quality and quantity of the heat transfer of solar radiation. However, these two factors are oppositely related for a given lens area (fixed solar radiation). According to the discussion in the previous sections, the increase of the surface temperature can only be achieved by reducing the absorber area. In addition, heat losses (i.e., radiation and convection heat losses) of the absorber are associated with the absorber area and surface temperature, which further influences the net heat flux of the absorber. Therefore, the relationship between surface temperature, absorber area, and heat loss should be evaluated to facilitate the selection and design of the receiver to transfer solar thermal energy efficiently.

Integrating the results from both the incident heat radiation model and FEM analysis shows the relationship between heat loss, surface temperature, and absorber area (Figure IV-8). The heat loss and absorber temperature both decreased with an increase in absorber area, although the decrease in the heat loss was much greater than the decrease in absorber temperature. This means that the heat loss is more sensitive to the change of absorber area than the absorber temperature. When the absorber area (A_a) was increased from 1,451 mm^2 to 4,032 mm^2 under the fixed lens area (0.17 m^2), the heat loss decreased by 60% from 30 kW/m^2 absorber to 12 kW/m^2 absorber, although the corresponding decrease in the absorber temperature was only 26%, dropping from 603 °C to 445 °C (Figure IV-8). Therefore, within the targeted temperature range of the absorber, sacrificing the temperature to achieve low heat loss could be an effective approach to enhance the thermal efficiency of the Fresnel solar thermal collector. Considering the configuration of a scalable concentrated solar power generation system (Figure IV-1), the heat loss during solar radiation transfer needs to be reduced by as much as possible. Increasing the absorber (or reflector in Figure IV-1) area could be an effective way to enhance the thermal performance of the solar power generation.

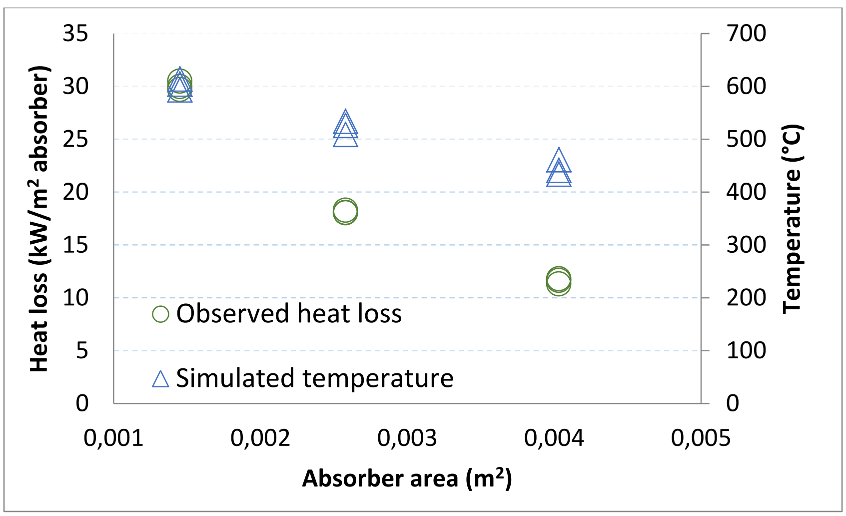

Figure IV-8. Temperature and heat loss of the absorber (A_a)*

*: The lens area was fixed at 0.17 m^2.

9. Conclusions

The study demonstrates that the two-module structure can be used to develop Fresnel lens thermal collectors for a scalable concentrated solar power generation system. With high-resolution stepper motors, the bench-scale solar collector can accurately realize the solar tracking. The FEM simulation of the thermal absorber indicates that the absorber area has a greater impact on the surface temperature of the absorber than the concentration ratio. The relationship between absorber area, absorber heat loss, and absorber temperature was determined from the combination of incident heat radiation model and FEM simulation. Heat loss reduction can be achieved by increasing the absorber area with a relatively small temperature drop. Due to the decoupling of the solar thermal collector and receiver, a scalable Fresnel-lens-based concentrated solar power generation concept can be achieved by combining multiple two-module Fresnel lens collectors with a centralized thermal receiver.

CHAPTER V. DESIGN OF NEW SMALL-SCALE SOLAR RECEIVER FOR CONCENTRATED SOLAR THERMAL COLLECTOR

Abstract

Two solar–thermal receiver designs for concentrated solar thermal collection are presented in this study. The first design applies a cavity absorber with multiple flow paths for the working fluid. The second design uses a conical absorber with single flow path to heat the working fluid. Computational fluid dynamics (CFD) was used to determine the heating fluid temperature profiles of both receivers under different oil mass flows, direct normal irradiance (DNI), and wind velocities. The results elucidate that the cavity receiver has an uneven surface temperature distribution although it has a good overall thermal transfer efficiency. However, the conical receiver with single flow path overcomes the issue of surface temperature distribution, and can be used for applications with high solar concentration ratios (CR).

1. Introduction

Solar thermal power generation technologies have been intensively studied over the past several decades (Michael F. Modest, 2013; Siva Reddy et al., 2013). According to the temperature of the working fluid, solar thermal power generation technologies can be classified into three categories of low-, medium-, and high-temperature technologies. For low- and medium-temperature technologies, such as parabolic trough and Fresnel lens thermal collection, the working fluid temperature is often less than 400 °C and the efficiency of incident solar radiation collection is approximately 60–70% (Siva Reddy et al., 2013). High-temperature technologies, such as the parabolic dish and central tower receiver, operate at temperatures higher than 600 °C.

In spite of the differences in solar thermal power generation technologies, all require a thermal receiver to transfer solar radiation to the working fluid (heat transfer fluid) efficiently for power generation. Water, air, molten salt, mineral and synthetic oil are the typical working fluids (Behar, Khellaf, & Mohammedi, 2013) (Ávila-Marín, 2011). Different types of solar receivers have been designed and used with parabolic trough, parabolic dish, and heliocentric solar thermal collection systems. For instance, Zhu et al. (J. Zhu et al., 2015) designed a coiled tube for a parabolic dish receiver (with an aperture area of 56.8 m^2). A small-particle heat exchanger has also been modified as the receiver to enhance the thermal absorption using air as the working fluid (Fernández & Miller, 2015).

However, the majority of these receivers are designed for large collection areas and high power generation. Solar receivers for small-scale solar thermal power generation technologies have not been widely reported. Therefore, the objective of this study was to design a receiver for a small-scale generation system (in kW), and overcome the issue of small heat transfer area (high heat loss during solar thermal collection) that small- and medium-size solar collection units encounter.

2. Design concept

Two new receiver designs consisting of cavity and conical solar thermal absorbers were designed for small-scale solar thermal collection (Figure V-1). Transferring thermal energy in small-scale systems is always accompanied by the issue of how to use a small heat transfer area to heat a relatively large amount of working fluid to the targeted temperature. In addition, energy loss to the ambient environment is another problem that significantly reduces the thermal efficiency of such receiver units. In order to address these issues, the objective is to increase the contact time of the working fluid with the heat source to overcome the disadvantage of the small heat transfer area, and to apply a vacuum to reduce heat losses significantly, so that the thermal efficiency of small solar receivers can be significantly improved.

Based on this idea, the new receivers were housed in a vacuum chamber with a quartz thermal-glass (Novatec 825F, with a thickness of 9.525 mm (0.375 in)) at the top, a heat exchanger sitting in the vacuum chamber, and thermal insulation (Pyrogel XT) to cover the entire chamber. The vacuum chamber was sealed with O-rings (Parker S455-70) to maintain the inner pressure at -0.84 bar abs (25 inHg).

In order to address the issue of a small transfer area, the contact time of the working fluid with the absorber of the receiver needs to be extended. The conical absorber has a single fluid path so that the working fluid enters the absorber from its bottom and leaves from its top (Figure V-2a). Since the conical shape of the absorber provides an effective heat transfer area, the heat transfer area is significantly increased. The cavity absorber has a spiral cave in the receiver. The working fluid pumping through the cavity absorber has multiple flow paths. The residence time of the working fluid is also increased. In the spiral cavity, the working fluid enters the absorber from the bottom of the chamber, reaches the center of the heating area, rotates in the spiral shape, and exits at one side of the receiver. During the process, the working fluid needs to travel along several parallel paths to extend the residence time and improve the efficiency.

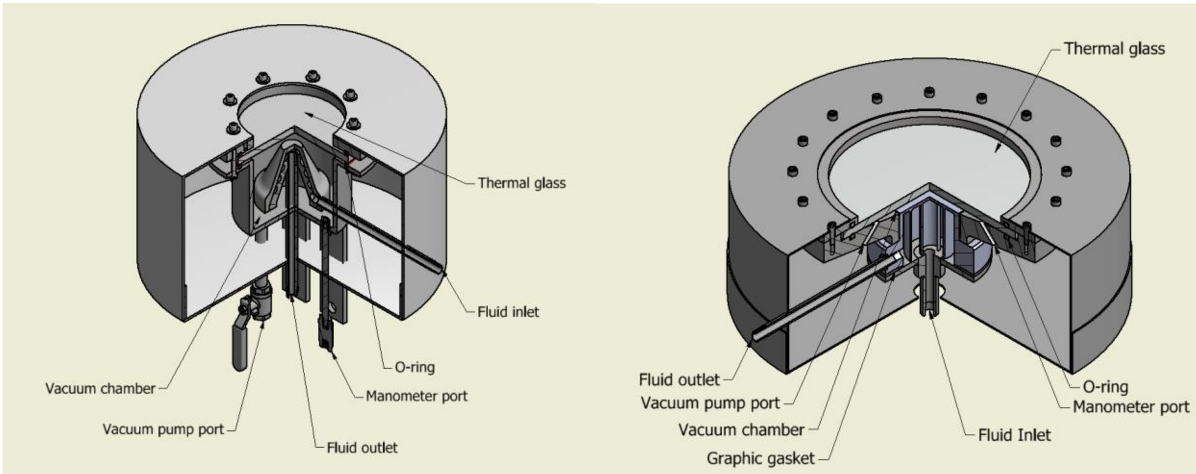

(a) (b)

Figure V-1. Solar receivers: (a) with conical absorber; (b) with cavity absorber

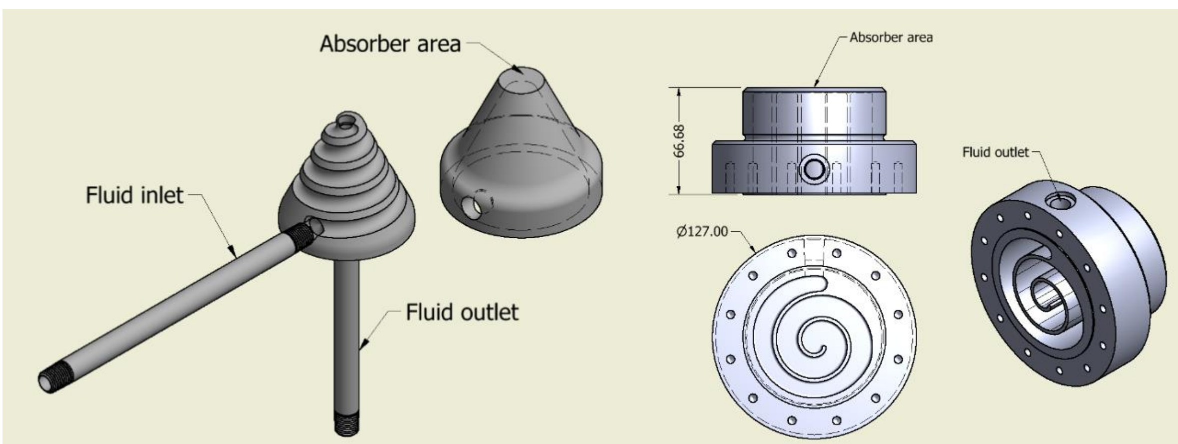

(a) (b)

Figure V-2. Heat absorbers: (a) conical absorber; (b) cavity absorber

The geometric characteristics of both absorbers are listed in Table V-1. The inner volumes of the conical and cavity absorbers (single flow path and multiple flow paths) were 16,527 mm^3 and 229,645 mm^3, respectively. For volumetric flows of 11,507 mm^3/s and 5,753 mm^3/s, the residence times for the conical absorber were 1.44 s and 2.88 s, respectively; while those for the cavity absorber were 19.96 s and 39.92 s, respectively. The dimensions of the two receivers are shown in Figure V-3. The receiver size was selected based on a solar collection area of 1 m^2. A refractive Fresnel lens was used as the solar thermal concentrator for this study.

Table V-1. Design parameters for the absorbers

Receiver type	Fluid contact area (mm^2)	Volume (mm^3)	Fluid volumetric flow (mm^3/s)	Residence time (s)
Conical absorber	11,426	16,527	11,507	1.44
			5,753	2.88
Cavity absorber	59,001	229,645	11,507	19.96
			5,753	39.92

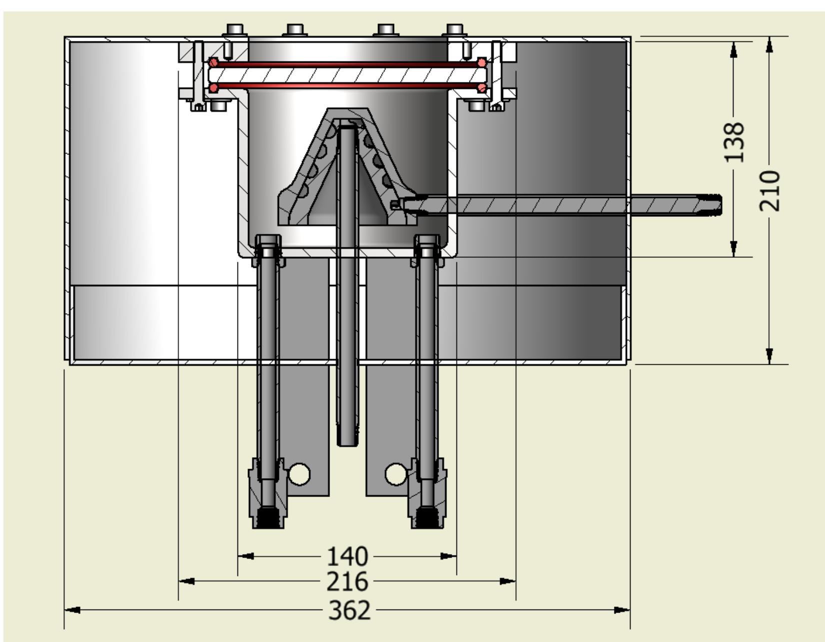

(a)

Figure V-3. Dimensions of the solar receivers (in mm): (a) with conical absorber; (b) with cavity absorber

Figure V-3. (cont'd)

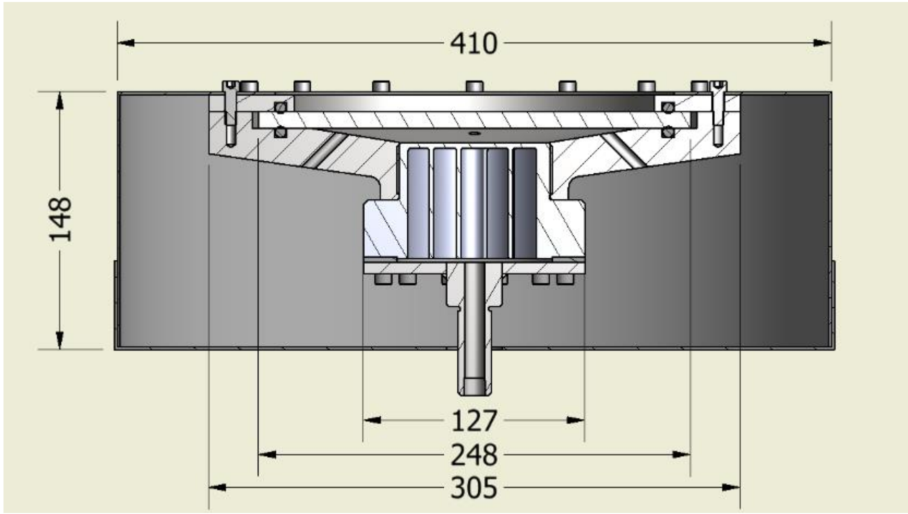

(b)

3. Modeling solar receivers (computational fluid dynamics)

Synthetic oil (Dowtherm A) was selected as the working fluid. Energy from solar radiation was transferred to the oil used for steam generation. A micro-turbine of 1.4 kW (NextGrid, 2014) was selected as the power generation unit. The operational parameters of the micro-turbine were used to carry out the calculation and receiver modeling. This particular turbine needs superheated steam at 180–220 °C and 8–10 bar. The temperature of the feeding water was 45 °C. In the model, the temperature change of the synthetic oil due to the solar radiation was set in the range of 220–250 °C. The ambient conditions (average direct normal irradiance (DNI) (Figure V-4)) in Lansing were used as the environmental parameters to run the simulation, and average wind velocities were used to calculate the convection heat loss.

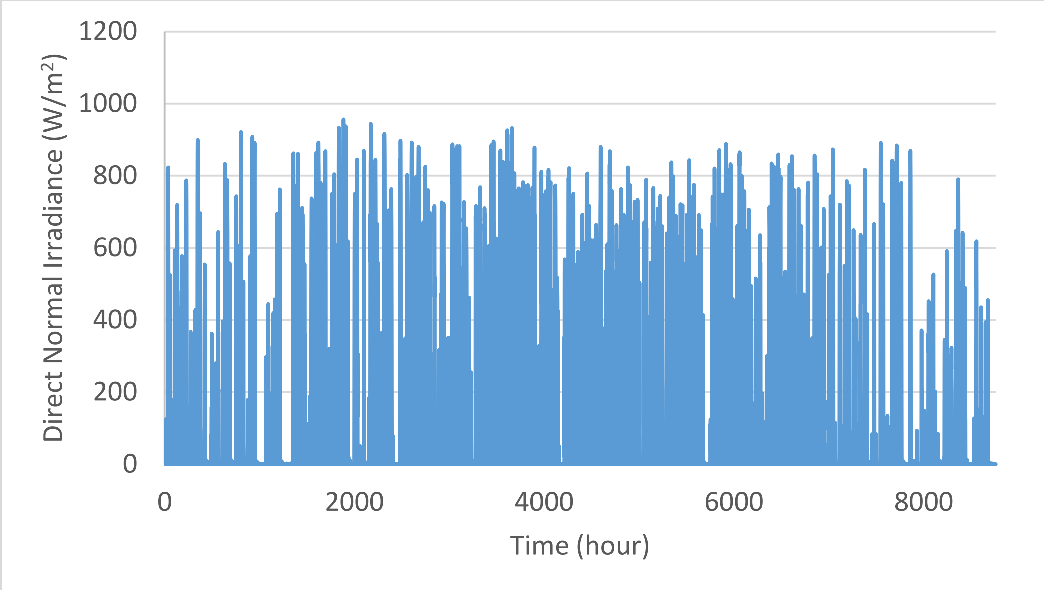

Figure V-4. DNI during a year at Lansing, MI

Simulation CFD software (Autodesk, 2015) was used to carry out the analysis. Both receivers were discretized, and the mesh size was tested using a heat input value (with no heat losses). The heat input must be completely transferred to the fluid, and the corresponding fluid outlet temperature can be calculated. Using the correlation $Q = \dot{m} \cdot C_p \cdot \Delta T$, where mass flow, heat capacity, and temperature difference are known, the absorbed heat was calculated and compared with the heat input. The difference between the heat input and the absorbed heat was set at less than 1%. The analysis used the K-epsilon to model turbulent flow. The outlet working fluid temperature and heat transfer efficiency under steady-state receiver operation for two oil mass flows (5 g/s and 10 g/s) and three DNI values (750 W/m^2, 940 W/m^2, and 1125 W/m^2) were then determined.

Since Fresnel lenses were the targeted solar thermal collection technology, optical efficiencies for the lens and the thermal glass were considered for the total heat flux receiver in the absorber area. The transmittances for the Fresnel lens and thermal glass reported by the manufacturers were 0.92 and 0.90, respectively. The DNI was then adjusted to the losses in the transmittance for the glass and the lens. Moreover, heat losses due to convection and radiation were taken into account for the external receiver surfaces. The calculation of the heat loss due to forced convection included the wind velocity (4.69 m/s (annual average at Lansing) and 2 m/s (the wind velocity reduced by a screen installation to cover the refractive collector sides)). The heat loss due to convection was calculated according to the Newton's law of cooling:

$$Q_c = h \cdot A \cdot (T_s - T_\infty) \tag{V-1}$$

where Q_c is the heat loss due to convection (W); h is the convective coefficient (W/m^2·°C); A is the surface in contact with the external air (m^2); T_s is the surface temperature (°C); and T_∞ is the ambient temperature (20 °C). Furthermore, the convective coefficient was calculated as

$$h = \frac{Nu \cdot k}{D} \tag{V-2}$$

where Nu is the Nusselt number; k is the ambient air thermal conductivity (W/m·°C); and D is the characteristic length for the receiver geometry (m) (outside diameter). The dimensionless Nusselt number was calculated using the empirical correction for cylinders (Çengel, 1998):

$$Nu = 0.027 \cdot Re^{0.805} \cdot \mathrm{Pr}^{1/3} \tag{V-3}$$

$$Re = \frac{V \cdot D}{\nu} \tag{V-4}$$

where Re is the Reynolds number; Pr is the Prandtl number; V is the wind velocity (m/s); and ν is the ambient air viscosity (m^2/s). Table V-2 summarizes the calculation of the convective heat transfer coefficient.

Table V-2. Convective coefficient for heat loss

Parameter	**Cavity absorber**	**Conical absorber**
Diameter (mm)	409.58	361.95
Height (mm)	122.56	206.38
Wind speed (m/s)	2 4.69	2 4.69
T_∞ (°C)	20	20
T_s assumed (°C)	45	45
ν (m^2/s) @ T_s	1.75×10^{-5}	1.75×10^{-5}
Re	4.68×10^{4} 1.10×10^{5}	4.14×10^{4} 9.70×10^{4}
Pr @ T_∞	0.7323	0.7323
Nu	227.0 468.4	204.4 421.8
k (W/m·°C) @ T_∞	0.02476	0.02476
h (W/m^2·°C)	13.723 28.319	13.98 28.856

In addition to the convective heat loss, the energy losses of solar receivers due to radiation can be calculated as

$$Q_R = \varepsilon \cdot \sigma \cdot A \cdot \left({T_s}^4 - {T_\infty}^4\right) \tag{V-5}$$

where ε is the material emmisivity; σ is the Stefan-Boltzmann constant ($W/m^2 \cdot K^4$); A is the surface area (m^2); and T_s and T_∞ are the surface and ambient temperature, respectively. The conical receiver material consisted of aluminum, with an emissivity of 0.18, and the cavity receiver had a emissivity of 0.27 (that of stainless steel) (M. F. Modest, 2013)

Both receiver designs allowed the refractive Fresnel lens to concentrate 750 times solar radiation into the absorber area (1,333.33 mm^2). A homogenous distribution of input heat in the absorber area is assumed as the boundary condition in the CFD analysis.

4. Results and discussion

The fluid temperature at the outlet of the receivers was significantly influenced by different values of DNI, working fluid mass flows, and wind velocities. When the wind velocity changed from 2 m/s to 4.69 m/s, the convective factor increased from 13 $W/m^2 \cdot °C$ to 28 $W/m^2 \cdot °C$ (Table V-2). In addition, the CFD results show that, for a mass flow of 5 g/s, when the wind velocity changed from 2 m/s to 4.69 m/s, the heat transfer efficiencies for cavity absorbers decreased from 57.92% to 48.11%, respectively; while that for conical absorbers decreased from 61.09% to 51.92%, respectively (Table V-3). For a high mass flow of 10 g/s, when the wind velocity changed from 2 m/s to 4.69 m/s, the heat transfer efficiencies for cavity absorbers decreased from 51.91% to 45.37%, respectively, and for conical absorbers from 53.74% to 46.88%, respectively (Table V-3). Although the heat transfer efficiencies for a high mass flow were significantly lower than those for a low mass flow, the changes in the heat transfer efficiencies corresponding to the increase in convective factor were smaller than those for the low mass flow. For the high mass flow, the changes in the heat transfer efficiencies for the cavity and conical absorbers were 6.54% and 6.86%, respectively, while the corresponding changes for the low mass flow were 9.81% and 9.17%, respectively. In addition, there were no significant differences in the final working fluid temperature between the two absorbers for the same wind velocity and mass flow (Table V-3).

Table V-3. Heat transfer efficiency for wind velocity variation

Receiver	**Cavity absorber**				**Conical absorber**			
Wind velocity (m/s)	4.69	2	4.69	2	4.69	2	4.69	2
Mass flow (g/s)	5	5	10	10	5	5	10	10
T initial (°C)	220	220	220	220	220	220	220	220
T final (°C)	248	253.71	235.11	237.78	246.41	250.21	233.64	235.64
Q absorbed (W)	298.76	359.65	322.4	379.36	281.76	322.38	291.12	333.74
Transfer efficiency	48.1%	57.9%	51.9%	61.0%	45.4%	51.9%	46.9%	53.7%

The DNI is the most critical parameter that has an effect on the thermal transfer efficiency and working fluid temperature. An increase in the net DNI can significantly improve the solar thermal collection for both receivers. When the net DNI increased from 621 W to 931 W, the thermal transfer efficiency of the cavity receiver increased from 58% to 68% for a mass flow of 5 g/s, and from 61% to 72% for a mass flow of 10 g/s. The corresponding increase for the conical absorber was from 52% to 66% for a mass flow of 5 g/s, and from 54% to 68% for a mass flow of 10 g/s (Figure V-5). Comparing the impact of change of net DNI on heat collection efficiencies, those of the conical receiver (single path) were affected more than those of the cavity receiver (multiple paths).

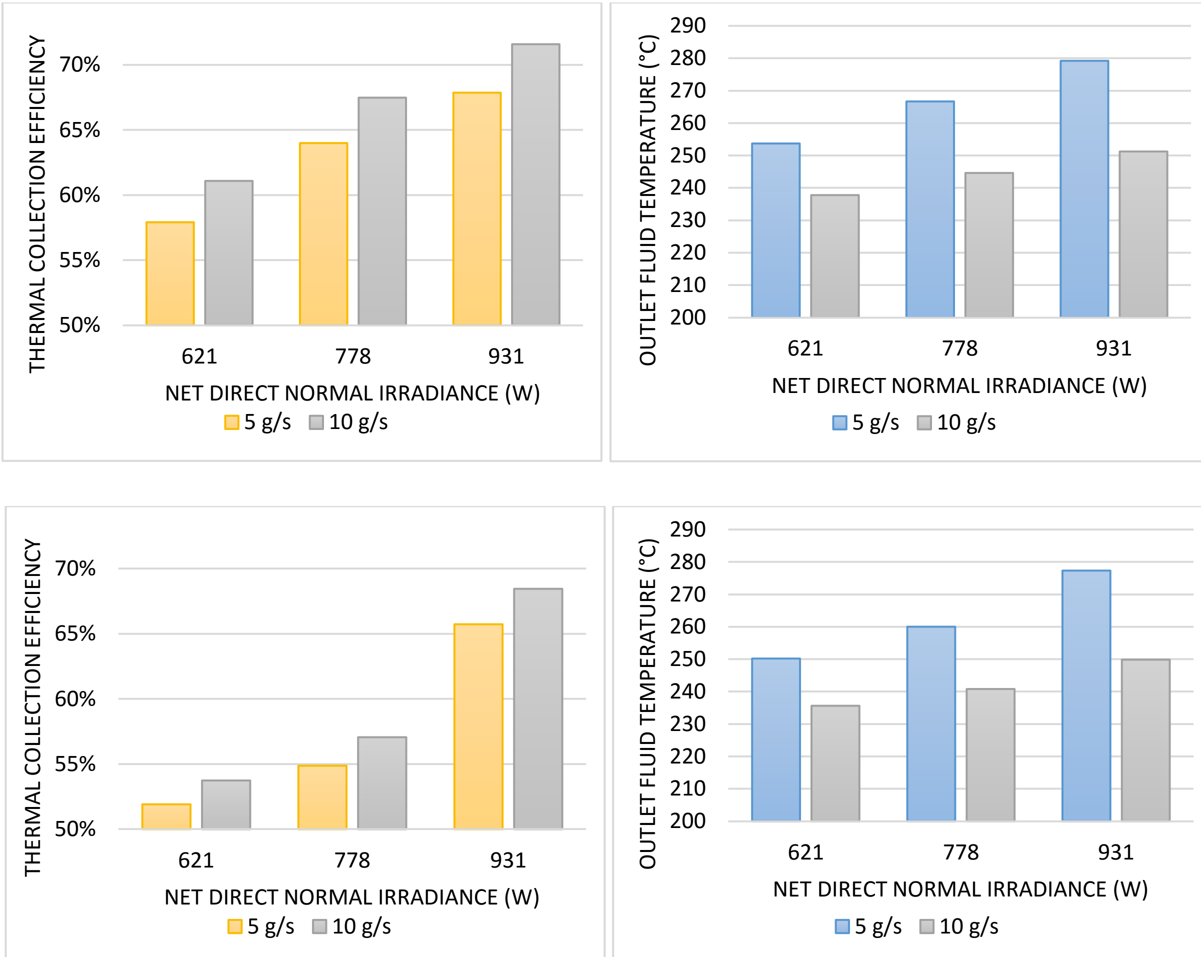

(a)

(b)

Figure V-5. Thermal collection efficiency and fluid output temperature of the receivers for two fluid mass flows: (a) cavity absorber; (b) conical absorber

Tables V-4 and V-5 summarize the results from the CFD analysis for both cavity and conical receivers, and Figure V-6 shows the fluid temperature profile for selected scenarios. For the conditions of a net DNI of 931 W and the lower mass flow of 5 g/s, the maximum temperatures of the working fluid were 582.31 °C and 399.19 °C for the cavity and conical receivers, respectively.

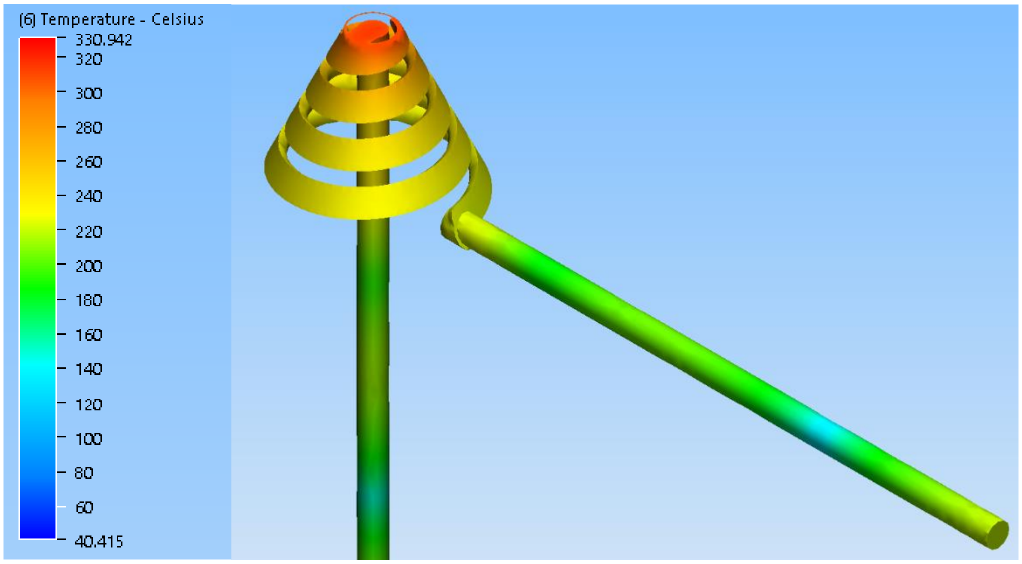

(a)

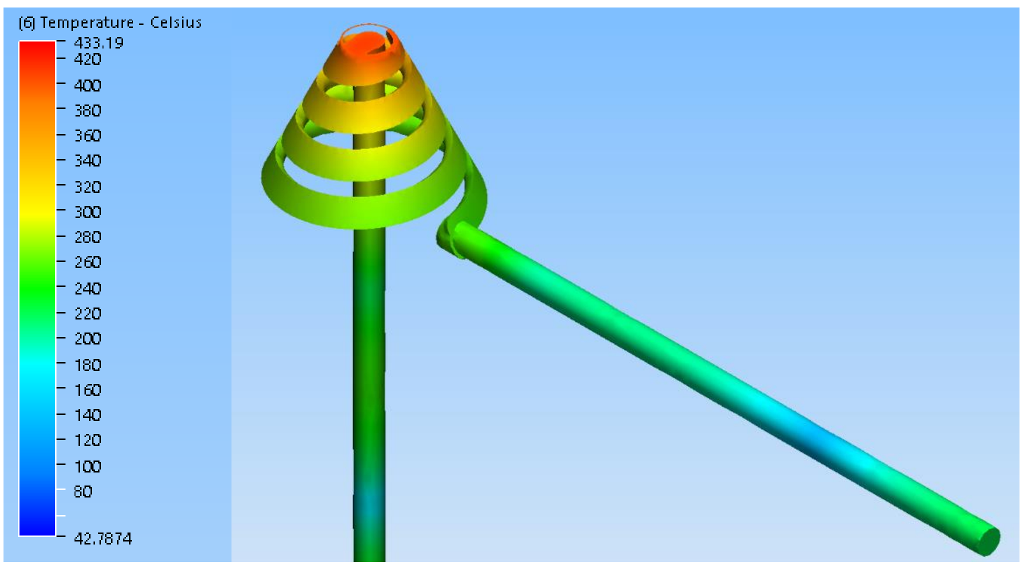

(b)

Figure V-6. Fluid temperature distribution in the studied receivers for selected scenarios. conical receiver*

*(a) 621 W at 10 g/s, (b) 931 W at 5 g/s; cavity receiver: (c) 621 W at 10 g/s, (d) 931 W at 5 g/s

Figure V-6. (cont'd)

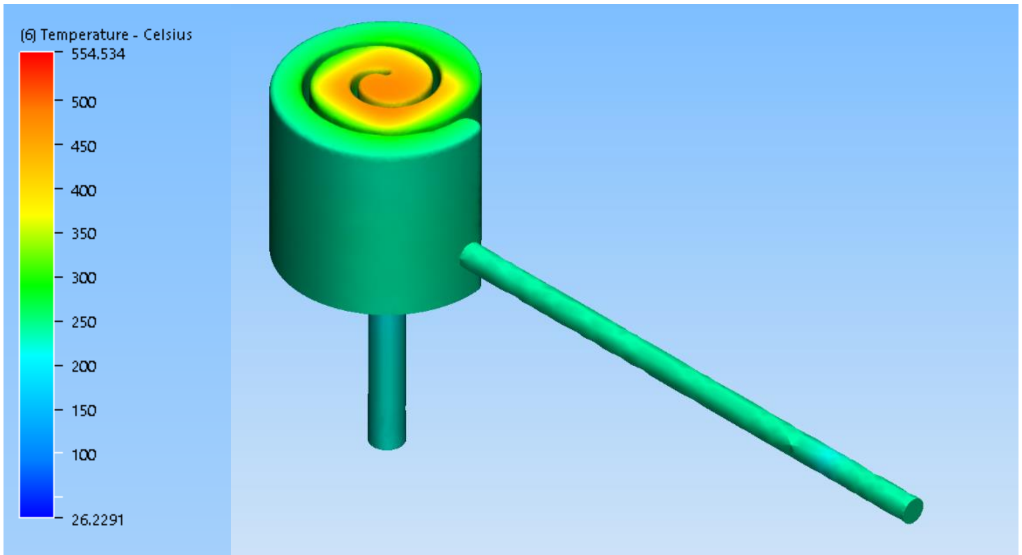

(c)

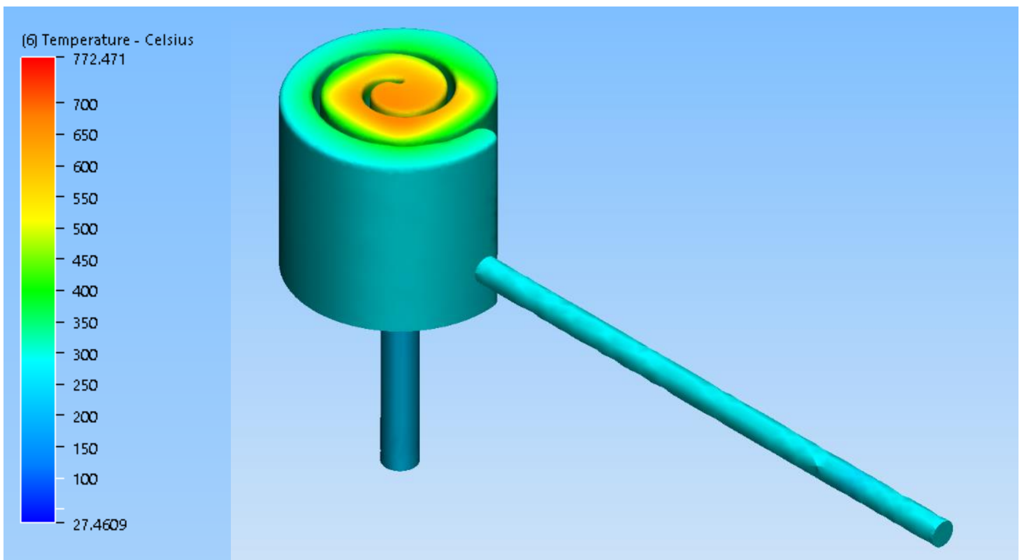

(d)

Since the synthetic oil (Dowtherm A) used by this paper has a maximum operating temperature of 400 °C, the maximum temperature for the cavity receiver exceeds the limit of the synthetic oil. Due to the multiple paths in the spiral hole, the fluid molecules around the heating surface have a longer residence time, increasing their temperature much higher than the average, hich could cause a dangerous degradation of the synthetic oil. Reduction of the concentration ratio (CR) and increase of the mass flow of the working fluid can be used to limit the maximum temperature that the fluid reaches. By reducing the CR by half (to CR = 375), the surface absorber temperature decreases from 772.72 °C to 516.70 °C, which limits the maximum working fluid temperature to 474.70 °C, still exceeding the recommendation for the synthetic oil. However, since the cavity absorber has multiple paths for the working fluid, the temperature profile is not evenly distributed on the surface. The cavity absorber has zones with low velocities near the heating surfaces (hot spots), which lead to an uneven heating and a high working fluid temperature at these spots (exceeding the temperature limit of the synthetic oil) even at the low CR. As mentioned previously, a low CR and high fluid mass can reduce the thermal transfer efficiency. Therefore, the conical (single path) absorber, which has a relatively homogenous temperature distribution in the working fluid, represents a preferable design for the solar thermal receiver.

Table V-4. The effects of DNI on the conical absorber

Parameter	**Value**					
Direct normal Irradiance (W)	621	621	778.3	778.3	931	931
Wind velocity (m/s)	2	2	2	2	2	2
Mass flow (g/s)	5	10	5	10	5	10
T initial (°C)	220	220	220	220	220	220
T final (°C)	250.2	235.6	260.0	240.8	277.4	249.9
Cp (J/kg·°C)	2,134	2,134	2,134	2,134	2,134	2,134
Q absorbed (W)	322.4	333.7	427.1	444.1	612.0	637.3
Transfer efficiency	51.9%	53.7%	54.9%	57.1%	65.7%	68.5%

Table V-5. Effects of DNI on the cavity absorber

Parameter	**Value**					
Direct normal Irradiance (W)	621	621	778.3	778.3	931	931
Wind velocity (m/s)	2	2	2	2	2	2
Mass flow (g/s)	5	10	5	10	5	10
T initial (°C)	220	220	220	220	220	220
T final (°C)	253.7	237.8	266.7	244.6	279.2	251.2
Cp (J/kg·°C)	2,134	2,134	2,134	2,134	2,134	2,134
Q absorbed (W)	359.7	379.4	498.1	525.2	631.8	666.5
Transfer efficiency	57.9%	61.1%	64.0%	67.5%	67.9%	71.6%

5. Conclusions

Two solar thermal receiver designs have been presented. The receiver with the cavity absorber, which has multiple paths and provides a longer residence time of the working fluid, presents a higher thermal transfer efficiency than the receiver with conical absorber, which has a single path and provides a short residence time of the working fluid. However, the cavity absorber has hot spots, where the high working fluid temperature at the spots exceeds the temperature limit of the synthetic oil. Reducing the concentration ratio and increasing the mass flow can solve the issue, although the fluid outlet temperature is reduced correspondingly. The receiver with the conical absorber demonstrates similar thermal efficiencies to the cavity receiver and avoids the adverse effects of low local velocities that the cavity receiver encounters. Therefore, the conical absorber represents a preferable design to collect solar thermal energy considering the currently available synthetic oil.

CHAPTER VI. STUDY SUMMARY AND FUTURE WORK

1. Summary

Solar–bio hybridization for power generation offers an alternative to provide electricity for a self-sustaining wastewater treatment plant using anaerobic digestion as the main process for organic load reduction. Chapter II of this dissertation presented a comprehensive analysis of two turbo-machines (steam and gas turbines), which are both feasible systems combining biogas and solar energy. The analysis demonstrated that the steam turbine has a higher global efficiency (heat and electricity) than the gas turbine, although the electrical generation efficiency of the gas turbine is higher than that of the steam turbine. In addition, due to the complexity of collecting solar energy at elevated temperatures and high concentration ratios for the gas turbine system, the steam turbine presents favorable conditions for its use in the solar hybridization, both in medium-temperature solar collection systems and in its global efficiency.

Thus, it is necessary to determine proper mechanisms combining biogas and solar energy to enable the self-sustainable operation of the power plant. Chapter III of this dissertation presented a model to set up a self-sustaining wastewater treatment plant by balancing the biogas produced and the solar energy collected for their incorporation in the hybrid power generation. The storage capacity for upgraded biogas and the solar collection area were the parameters that could be balanced to provide stable and continuous electrical energy. In addition, a comparison between photovoltaic panels (PV) and a parabolic trough collector (PT) was conducted, showing that PV collectors require a smaller collection area and biogas storage capacity than a PT, but implying a complex operating and control mechanism in the PV-bio hybrid power generation.

Moreover, in Chapter IV, solar collection using a refractive Fresnel lens was presented. The bench-scale unit constructed showed that a two-module system, with high-resolution stepper motors, can achieve an accurate movement for the dual-solar tracking. This enables the possibility to expand the use of small Fresnel lenses for medium-scale solar field collectors by decoupling the refractor and the solar receiver. Additionally, the analysis of the solar energy absorber using finite element methods showed that the absorber area has a greater impact on the average surface temperature of the receiver than the solar concentration ratio, which is an important parameter in the solar receiver design to avoid local hot points.

In Chapter V, two solar receiver designs for refractive Fresnel lens collectors were presented. The receiver with a longer working fluid residence time (cavity receiver) exhibited higher thermal transfer efficiency than the receiver with a lower residence time (conical receiver). The computational fluid dynamics model showed that the cavity receiver presented a zone with low velocities near the heating surface, creating local hot points. A low concentration ratio and higher mass flow can solve the issue of local hot points without modifying the receiver geometry.

2. Future work

The analysis performed in the previous chapters has provided the design parameters to establish a self-sustaining small-scale pilot plant for wastewater treatment, where the energy required by the processes is generated from biogas and solar radiation.

The studied technologies to treat wastewater can provide water that satisfies the EPA discharge standards. However, the secondary treatment of AET requires a large area for the aeration, which is not feasible for small-scale systems. In order to overcome this disadvantage, it is necessary to research and develop alternatives for water clarification.

As presented in Section 1.1.2, electro-chemical reactions can be used as a secondary treatment for water reclamation. The processes of electro-coagulation (EC), centrifuge, and filtration (reverse osmosis and carbon filters) can complete the secondary treatment for a high-strength organic wastewater, such as the AD effluent. Moreover, a pilot-scale solar–bio hybrid power generation system for the wastewater treatment plant has been implemented and will be tested (Figure VI-1). Anaerobic digesters will produce biogas for the solar–bio hybridization and stabilize solid residues, while an EC unit, centrifuge, and filter unit will carry out the water reclamation process. Photovoltaic panels and CSP collectors (refractive Fresnel lenses) will provide energy to complement the biogas energy for electricity and heat generation.

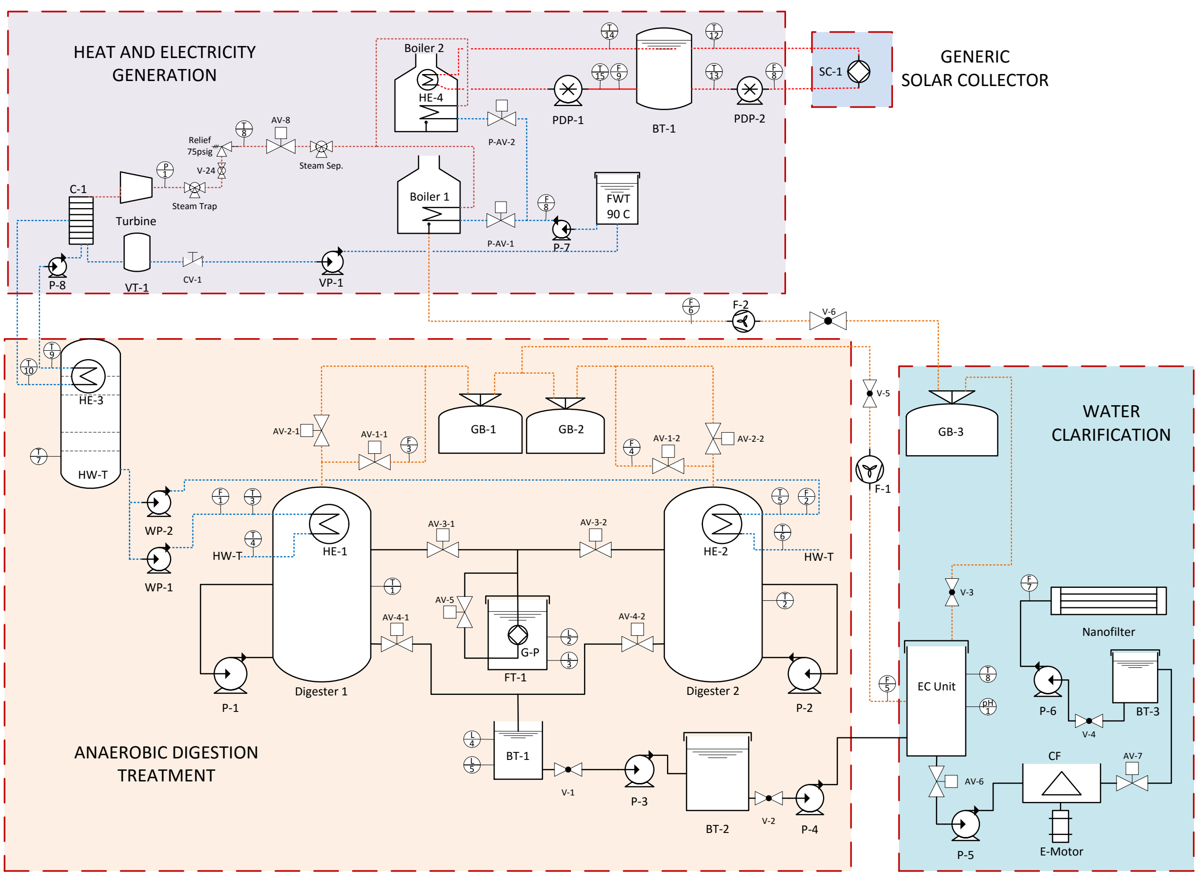

Figure VI-1. Flowchart of the solar–bio hybrid energy generation system to treat wastewater

A biogas storage bag serves as the fuel storage for engine use to compensate unsteady solar radiation. The boiler uses both solar and biogas energy to produce steam. The steam is then used by the turbine to generate power. During the daytime, when solar radiation is available, the concentrated solar power (CSP) unit collects heat via the heat-transfer fluid (synthetic oil) and stores it the buffer tank. The heat from solar radiation is used to generate steam, and the steam is superheated in the biogas boiler. The superheated steam then drives the turbine for power generation. The electricity generated from the solar–bio hybrid unit is used in the self-sustaining system to power the pumps, centrifuge, DC power supply, and control panel to satisfy operational requirements. The residual heat from the turbine is used to maintain the anaerobic digester at thermophilic conditions (50 °C) to enhance solid reduction, eliminate pathogens, and improve biogas production. The extra electricity and heat from the combined treatment system is used for other on-site applications. The wastewater treatment plant and solar collection system will be installed in a shipping container, and tested at the MSU Anaerobic Digestion Research and Educational Center (ADREC). Figures VI-2 and VI-3 show the configuration of the treatment processes and the equipment distribution in the container.

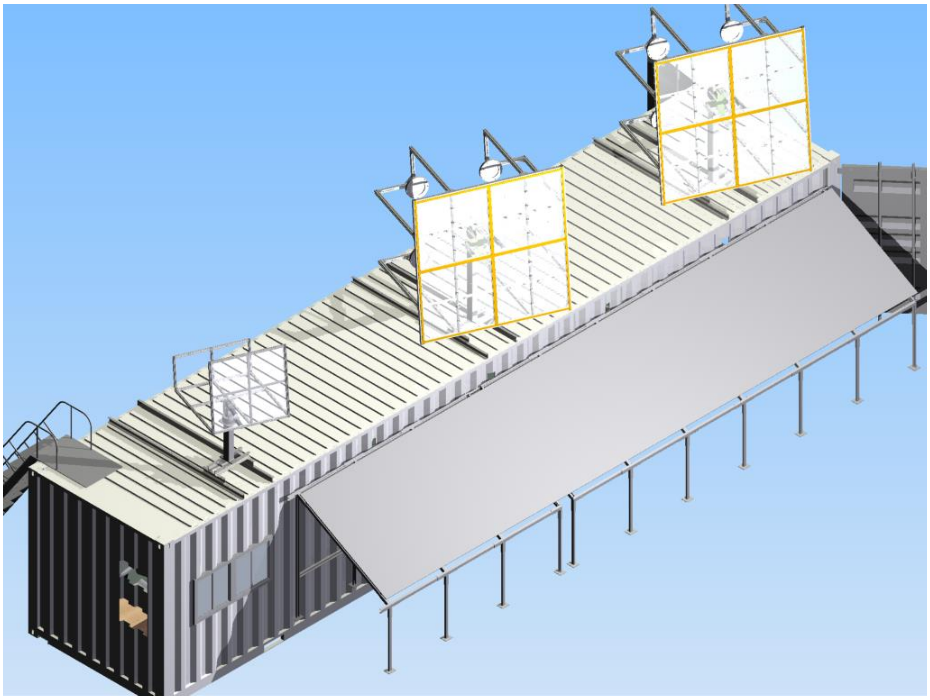

(a)

(b)

Figure VI-2. (a) CSP using refractive Fresnel lenses and PV collectors for solar thermal energy collection; (b) PV panels in the solar–bio hybridization concept

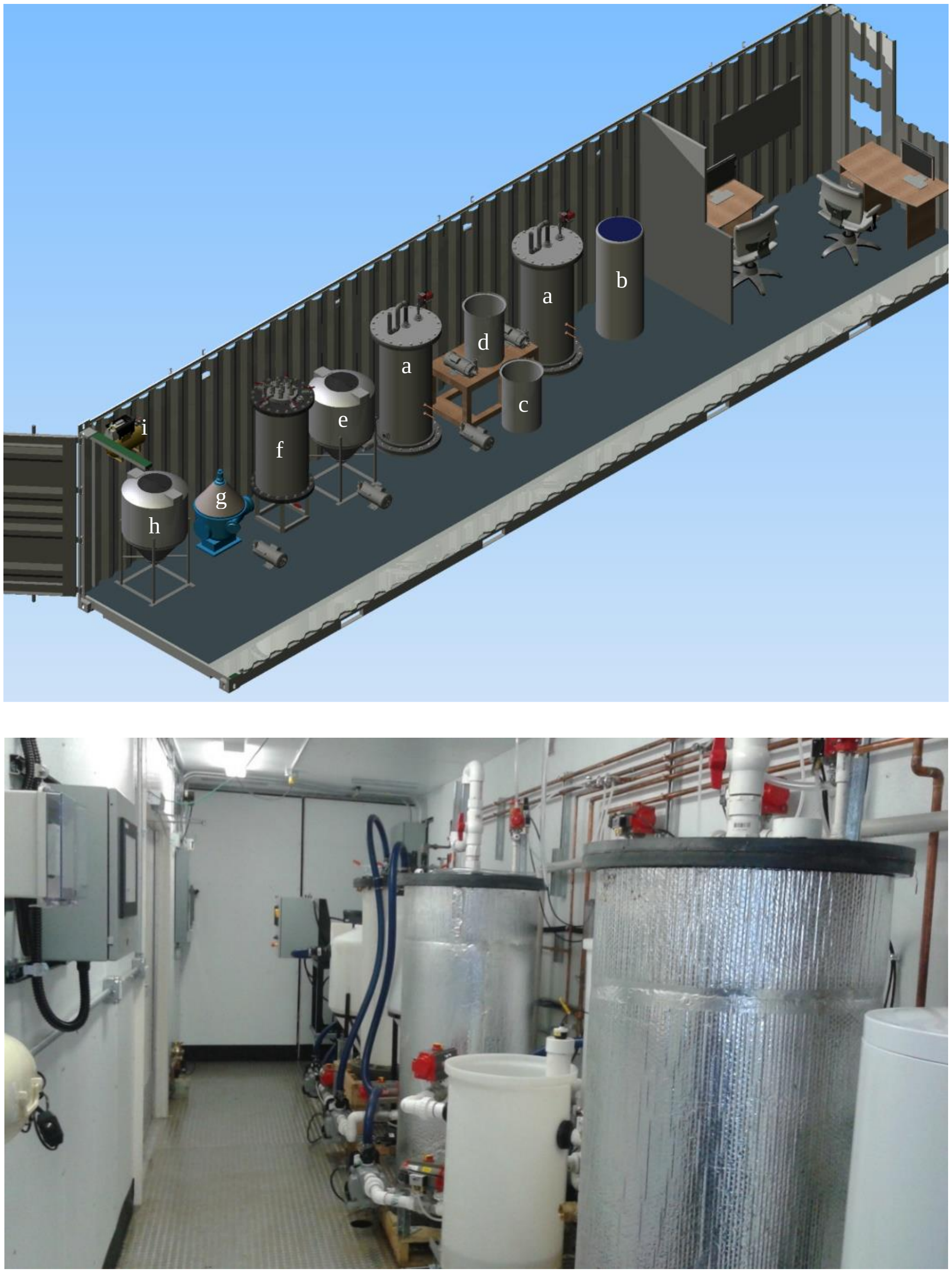

Figure VI-3. Equipment and reactor distribution of the wastewater treatment plant*

*: a) fixed-film AD digesters; b) water heater; c) AD effluent tank; d) AD influent tank; e) long-term storage AD effluent; f) electro-coagulation reactor; g) centrifuge; h) clarified water tank before filtration (not shown); i) air compressor for automatic valves.

A high-efficiency thermophilic fixed-film anaerobic digester (0.4 m^3) has been designed for the small-scale wastewater treatment (Figure VI-4). This configuration significantly enhances the accumulation of microbial biomass (using Pall rings between Screens #1 and #2 to retain the biomass), and consequently improves the performance of the digestion. A copper coil is installed inside the reactor to transfer heat from the hot water in order to maintain the thermophilic culture temperature.

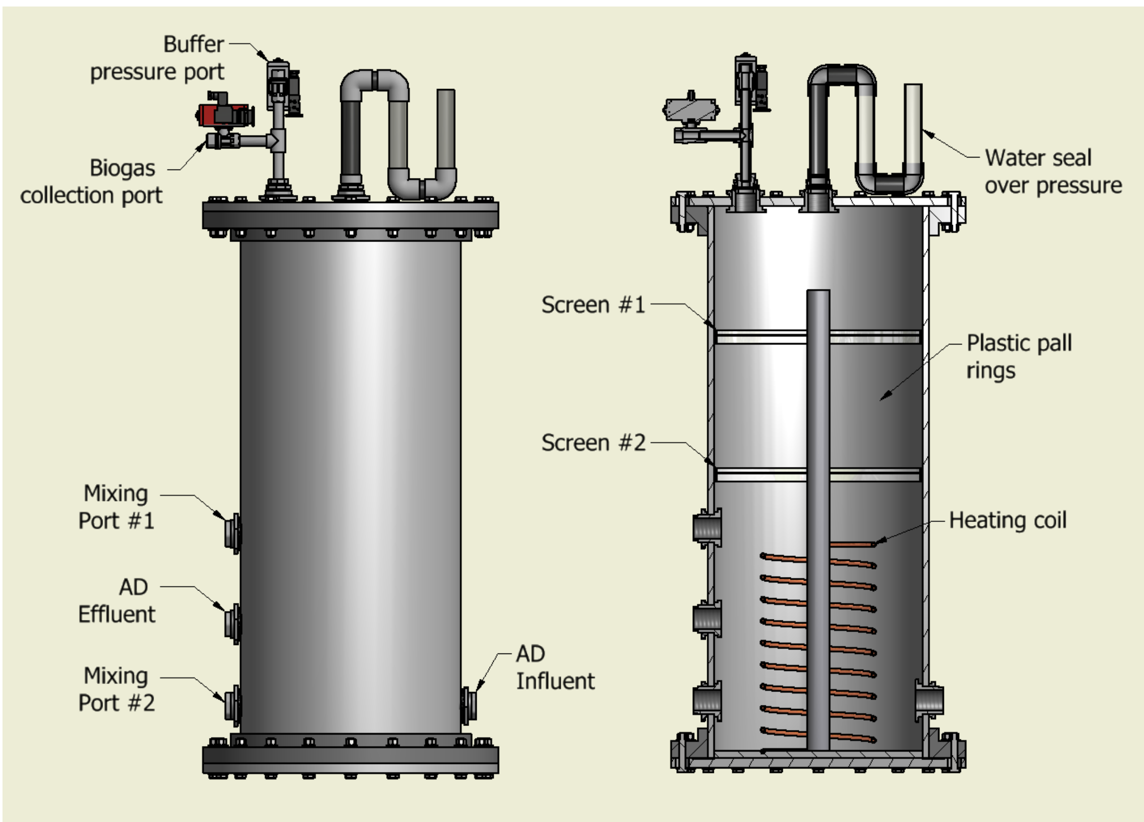

Figure VI-4. Fixed-film anaerobic digester

Electro-coagulation is the secondary treatment to further reclaim the water from the AD effluent (Figure VI-5) The equipment consists of six metallic pipes (mild steel anodes) to provide the ions, and a cylindrical metallic sheet (with a thickness of 3 mm) completes the DC circuit for the electrochemical reaction. On the lid, a port is installed for further biogas cleaning.

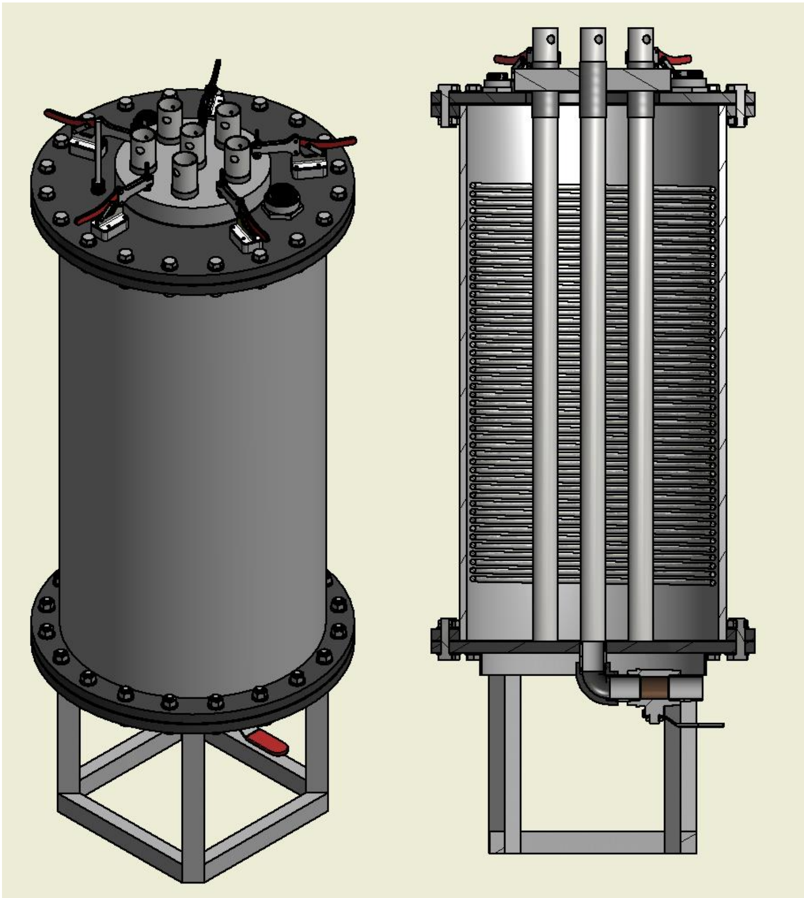

Figure VI-5. Electro-coagulation reactor for water clarification

In addition, the solar–bio hybrid power generation includes both solar technologies of photovoltaics and concentrated solar power. The photovoltaic unit has been designed to generate 4 kW under reference conditions (a cell temperature of 25 °C and a power of 1000 W/m^2); to achieve this, 14 SolarWorld SW235 mono PV panels have been installed (Figure IV-2). In addition, a battery bank is used to store the electricity, consisting of 16 batteries (170 Ah) to store the energy from the PV and supply power to the inverter (Radian 4048 4kW) for AC conversion.

The concentrated solar power consists of two modules of four refractive Fresnel lenses (with an area of 1 m^2 each) to collect energy and transfer it to a solar receiver (Figures VI-2 and VI-6) using synthetic oil (Dowtherm A) as the transfer media. The solar receiver is installed on the aluminum frame, moved by a gearbox connected to brushless motors. The tracking system consists of a control module, with the NREL solar position algorithm, a power supply, two drivers, and magnetic limit switches to control the positions of the lenses.


(a)

(b)

Figure VI-6. Fresnel lens assembly: (a) collector module; (b) single-collector test unit

The integration of the processes for the self-sustaining small-scale wastewater treatment plant will be tested in the near future to treat a mixture of black water and food waste.

APPENDICES

Appendix A: Matlab code for system solar bio-hybrid modeling

```
clear
close all
clc
%Directories to read libraries
addpath('C:\Users\Mauricio\Desktop\Projects MSU\PUBLICATIONS\SOLAR HYBRID POWER SYSTEM\EVERYTHING
NEW VACUUM PUMP\Gas an steam turbine analysis\MATLAB water properties')
addpath('C:\Users\Mauricio\Desktop\Projects MSU\PUBLICATIONS\SOLAR HYBRID POWER SYSTEM\EVERYTHING
NEW VACUUM PUMP\Gas an steam turbine analysis\MATLAB air properties')
addpath('E:\WORKING PROJECTS\Gas an steam turbine analysis\MATLAB water properties')
addpath('E:\WORKING PROJECTS\Gas an steam turbine analysis\MATLAB air properties')
```

GLOBAL VARIABLES

```
global Percent_solar Biogas_p HC_biogas T_AD HRT rho_inf n_b e_HC CpInfluent Perc_methane Elec_AD
Percent_solar=0:0.05:1;                                   %[]                         Solar
utilization
Biogas_p=0.6421;                                          %[m3biogas/m3reactor·day]   Daily
biogas production
HC_biogas=23;                                             %[MJ/m3]
Biogas heat of combustion
T_AD=50;                                                  %[°C]
Culture temperature AD
HRT=20;                                                   %[days]
Hydraulic retention time
rho_inf=1220;                                             %[kg/m3]
Density influent
n_b=0.85;                                                 %[]
Efficiency boiler
e_HC=0.98;                                                %[]
Combustion chamber efficiency
CpInfluent=3606;                                          %[J/kg·°C]
Specific heat influent
Perc_methane=0.586;                                       %[]
Percentage methane in biogas

global e_o_parabolic e_o_dish ems c_SB Cr_Parabolic Cr_Dish UL E_r1 E_r2 THS_1 THS_2 T_Fin
Biogas_CU_steam_N Biogas_CU_gas_N Biogas_CU_steam Biogas_CU_gas
global t_collection_Steam_LAN t_collection_Gas_LAN t_collection_Steam_PHO t_collection_Gas_PHO
global percent_Solar_useful_steam_LAN percent_Solar_useful_gas_LAN percent_Solar_useful_steam_PHO
percent_Solar_useful_gas_PHO
e_o_parabolic=0.775;                                      %[]            Optical
efficiency
e_o_dish=0.933;                                           %[]            Optical
efficiency
ems=0.27;                                                 %[]            Emisivity steel
c_SB=5.670373*10^-8;                                      %[W/m^2·K^4]   Stefan-Boltzman
constant
Cr_Parabolic=70;                                          %[]            Concentration
ratio
Cr_Dish=750;                                              %[]            Concentration
```

```
ratio
UL=8;                                                           %[W/m^2·K]      Convection
coeficient
E_r1=0.85;                                                      %[]             Efficiency heat
exchanger Steam-Molten Salt
E_r2=0.70;                                                      %[]             Efficiency heat
exchanger Gas-Molten Salt
THS_1=(200+273)*1.25;                                           %[K]            Temperature
absorber for steam system
THS_2=800+273.15;                                               %[K]            Temperature
absorber for gas system
T_Fin=700+273.15;                                               %[K]            Temperature after
solar energy addition in the gas cycle
%COLLECTION TIMES AND SOLAR UTILIZATION FACTORS (obtanined from a simulation using SAM)
t_collection_Steam_LAN=5.88*3600;                               %[s]             time for solar
energy collection Parabolic trough
t_collection_Gas_LAN=5.65*3600;                                 %[s]             time for solar
energy collection Parabolic dish
t_collection_Steam_PHO=9.69*3600;                               %[s]             time for solar
energy collection Parabolic trough
t_collection_Gas_PHO=9.66*3600;                                 %[s]             time for solar
energy collection Parabolic dish
percent_Solar_useful_steam_LAN=0.8778;
percent_Solar_useful_gas_LAN=0.429;
percent_Solar_useful_steam_PHO=0.9337;
percent_Solar_useful_gas_PHO=0.4752;

% Electricity for biogas cleaning and upgrading
Biogas_CU_steam_N=0.275;
%[kWh/Nm3biogas] From reference
Biogas_CU_gas_N=0.765;
%[kWh/Nm3biogas] From reference
Biogas_CU_steam=(Biogas_CU_steam_N/(((T_AD+273.15)/288.15)*(1/1.025)))*(3.6/1);
%[MJ/m3biogas] corrected
Biogas_CU_gas=(Biogas_CU_gas_N/(((T_AD+273.15)/288.15)*(1/1.025)))*(3.6/1);
%[MJ/m3biogas] corrected
t_biogas_cleaning=1*3600;                                                           %[s]
Operating time for biogas cleaning and upgrading

% Electricity for influent handling
Elec_AD=0.0509;                                                         %[MJ/h·m3digester] From
reference. Electricity for influent handling (digester), except for biogas improvement stages
```

POWER SYSTEMS

```
%STEAM  SYSTEMS************************************************************
%WITHOUT SOLAR
[Qboiler_n,Qsink,n_turb_steam] = Steam_30kW( );
%SOLAR HYBRID
[DATA_table_STEAM] = Steam_30kW_solar(Percent_solar,Qboiler_n,0);
%[Perc_solar] [T1] [T2] [T3] [T4] [Qb_n] [Qsink] [Qsolar] [M_biogas];

% GAS SYSTEMS**************************************************************
%WITHOUT SOLAR
```

```
[Qh_n_burner,Q_gen,n_th] = Gas_30kW(  );
%SOLAR GAS HYBRID SYSTEM (after regenerator)
[A_II] = Gas_30kW_II(Percent_solar, Qh_n_burner,0);
%[Perc_solar] [T1] [T2] [Tx1] [Tx] [T3] [T4] [Ty] [Qh_n_burner] [Qsolar] [Q_gen] [M_biogas]

%For manuscript
fprintf('\nElectricity and Thermal efficiencies steam\n')
n_turb_steam
Qsink/Qboiler_n
fprintf('\nTElectricity and Thermal efficiencies gas\n')
n_th
Q_gen/Qh_n_burner

% Plots
figure
plot(Percent_solar,A_II(9,:),'*',Percent_solar,DATA_table_STEAM(6,:),'*','LineWidth',1)
set(gca,'fontsize',12)
xlabel('Solar utilization')
ylabel('Fuel consumption (kW)')
legend('Gas turbine II', 'Steam turbine','Location','Best')
figure
set(gca,'fontsize',12)
plot(Percent_solar,A_II(11,:),'*',Percent_solar,DATA_table_STEAM(7,:),'*','LineWidth',1)
xlabel('Solar utilization')
ylabel('Heat generated(kW)')
legend('Gas turbine II', 'Steam turbine','Location','Best')
```

NET CAPACITY FACTOR

```
CF=0:0.05:1;                                                                          %[]         Capacity
Factor
t_d=((24*3600).*CF);                                                                  %[s/day]        Time
of operation per day
n=size(CF);
n=n(1,2);
%solar use ----->
for i=1:n
    Er_STEAM_BIOGAS(i,:)=t_d(i).*DATA_table_STEAM(6,:)./1000;              %[MJ/day]       BIOGAS
Energy requirement for the specified net capacity factor  (21x21)  solar use ->
    Er_GAS_II_BIOGAS(i,:)=t_d(i).*A_II(9,:)./1000;                         %[MJ/day]       BIOGAS
Energy requirement for the specified net capacity factor  (21x21)
end
for i=1:n
    Er_STEAM_SOLAR(i,:)=t_d(i).*DATA_table_STEAM(8,:)./1000;               %[MJ/day]       SOLAR
Energy requirement for the specified net capacity factor  (21x21)
    Er_GAS_II_SOLAR(i,:)=t_d(i).*A_II(10,:)./1000;                         %[MJ/day]       SOLAR
Energy requirement for the specified net capacity factor  (21x21)
end

for i=1:n
    HEAT_STEAM_SOLAR(i,:)=t_d(i).*DATA_table_STEAM(7,:)./1000;             %[MJ/day]       Heat
generation for the specified net capacity factor  (21x21)
    HEAT_GAS_II_SOLAR(i,:)=t_d(i).*A_II(11,:)./1000;                       %[MJ/day]       Heat
generation for the specified net capacity factor  (21x21)
```

```
end
[X,Y]=meshgrid(CF);

figure
surf(X,Y,Er_STEAM_BIOGAS)
set(gca,'fontsize',12)
xlabel('Solar use')
ylabel('Capacity Factor')
zlabel('Fuel energy requirement (MJ/day)')
title('Steam Turbine')
figure
surf(X,Y,Er_GAS_II_BIOGAS)
set(gca,'fontsize',12)
xlabel('Solar use')
ylabel('Capacity Factor')
zlabel('Fuel energy requirement (MJ/day)')
title('Gas Turbine')
figure
surf(X,Y,Er_STEAM_SOLAR)
set(gca,'fontsize',12)
xlabel('Solar use')
ylabel('Capacity Factor')
zlabel('Solar energy requirement (MJ/day)')
title('Steam Turbine')
figure
surf(X,Y,Er_GAS_II_SOLAR)
set(gca,'fontsize',12)
xlabel('Solar use')
ylabel('Capacity Factor')
zlabel('Solar energy requirement (MJ/day)')
title('Gas Turbine')
%For manuscript
fprintf('\nfull utilization of solar energy, solar energy requirement \n')
max(max(Er_STEAM_SOLAR))
max(max(Er_GAS_II_SOLAR))


figure
surf(X,Y,HEAT_STEAM_SOLAR)
set(gca,'fontsize',12)
xlabel('Solar use')
ylabel('Capacity Factor')
zlabel('Heat generation (MJ/day)')
title('Steam Turbine')
figure
surf(X,Y,HEAT_GAS_II_SOLAR)
set(gca,'fontsize',12)
xlabel('Solar use')
ylabel('Capacity Factor')
zlabel('Heat generation (MJ/day)')
title('Gas Turbine')
```

BIOGAS REQUIREMENT

```
V_biomethane_STEAM=Er_STEAM_BIOGAS.*(1/HC_biogas);                    %[m3]          biogas
volume requirement per day Steam turbine
V_biomethane_GAS_II=Er_GAS_II_BIOGAS.*(1/HC_biogas);                  %[m3]          biogas
volume requirement per day Gas turbine II

V_reactor_STEAM=V_biomethane_STEAM.*(1/Biogas_p);                     %[m3]          Digester
volume Steam turbine
V_reactor_GAS_II=V_biomethane_GAS_II.*(1/Biogas_p);                   %[m3]          Digester
volume Gas turbine II

figure
surf(X,Y,V_reactor_STEAM)
set(gca,'fontsize',12)
xlabel('Solar use')
ylabel('Capacity Factor')
zlabel('Reactor Volume (m3)')
title('Steam Turbine')
figure
surf(X,Y,V_reactor_GAS_II)
set(gca,'fontsize',12)
xlabel('Solar use')
ylabel('Capacity Factor')
zlabel('Reactor Volume (m3)')
title('Gas Turbine')

%For manuscript
fprintf('\nMax digester volumes \n')
max(max(V_reactor_STEAM))
max(max(V_reactor_GAS_II))
```

SOLAR COLLECTORS ANALYSIS

```
Lansing=[1, 2238.095
2, 3190.476
3, 3809.524
4, 4460.317
5, 4301.587
6, 4920.635
7, 5079.365
8, 4476.19
9, 4492.063
10, 2841.27
11, 2142.857
12, 2142.857].*0.0036;                    %[MJ/m2·day] <- [Wh/m2·day]    Solar energy
per month

Phoenix=[1, 6243.09
2, 6461.265
3, 7212.79
4, 8230.948
5, 8527.565
6, 9169.261
7, 7818.869
8, 7221.375
```

```
9, 7517.964
10, 7077.358
11, 6621.037
12, 6086.287].*0.0036;                                   %[MJ/m2·day] <- [Wh/m2·day]    Solar energy
per month
Tamb_Lansing=[-4.75
-3.4
1.7
8.55
14.3
19.75
21.95
20.95
16.65
10.15
4.2
-2.05];                                                  %[C] Average ambient temperature
Tamb_Phoenix=[13.6
15.4
18.4
22.65
27.85
32.65
34.9
34.2
31.3
24.8
17.85
13];                                                   %[C] Average ambient temperature
T_min_LAN=min(Tamb_Lansing);
T_min_PHO=min(Tamb_Phoenix);
figure
plot(1:12,Lansing(:,2),1:12,Phoenix(:,2),'LineWidth',2)
xlabel('Month')
ylabel('Direct Solar Radiation (MJ/m2·day)')
legend('Lansing','Phoenix','Location','Best')
figure
plot(1:12,Tamb_Lansing,1:12,Tamb_Phoenix,'LineWidth',2)
xlabel('Month')
ylabel('Average ambient temperature (°C)')
legend('Lansing','Phoenix','Location','Best')

%Minimum solar energy in a year per location
min_Lansing=min(Lansing(:,2));           %[MJ/m2·day]
min_Phoenix=min(Phoenix(:,2));           %[MJ/m2·day]
```

ENERGY REQUIREMENT FOR HEATING CRITICAL CASE (min temp)

```
Tmanure_LAN=4;                                                             %[C]        Minimum
influent temperature
Tmanure_PHO=13;                                                            %[C]        Minimum
influent temperature
                                                                           %[J/kg·C]   Heat
capacity of the influent
```

```
m1=(V_reactor_STEAM./HRT).*rho_inf;                                       %[kg]       Mass of
influent per day
m2=(V_reactor_GAS_II./HRT).*rho_inf;                                      %[kg]       Mass of
influent per day
%------------------------->SOLAR USE -----> this direction on the matrix
Heat_req_STEAM_LAN=m1.*CpInfluent.*(T_AD-Tmanure_LAN).*(1+0.3)./1e6;         %[MJ/day]   (21x21)
ENERGY requirement for AD culture
Heat_req_GAS_II_LAN=m2.*CpInfluent.*(T_AD-Tmanure_LAN).*(1+0.3)./1e6;        %[MJ/day]   (21x21)
ENERGY requirement for AD culture

Heat_req_STEAM_PHO=m1.*CpInfluent.*(T_AD-Tmanure_PHO).*(1+0.3)./1e6;         %[MJ/day]   (21x21)
ENERGY requirement for AD culture
Heat_req_GAS_II_PHO=m2.*CpInfluent.*(T_AD-Tmanure_PHO).*(1+0.3)./1e6;        %[MJ/day]   (21x21)
ENERGY requirement for AD culture

%For manuscript
fprintf('\nMAX thermal energy required by AD \n')
max(max(Heat_req_STEAM_LAN))
max(max(Heat_req_GAS_II_LAN))
max(max(Heat_req_STEAM_PHO))
max(max(Heat_req_GAS_II_PHO))
```

SELECTION OF PLANT CAPACITY FACTOR AND SOLAR USE (For CF=0.5 and SU=0.5)

```
CF_s=0.5;                                      %[]             Selected Net Capacity Factor
t_d_s=(24*3600).*CF_s;                         %[s/day]        Time
n2=(1/0.05)*CF_s+1;                            %[]             Index location for the CF
E_gen_Steam_CF=HEAT_STEAM_SOLAR(n2,n2);        %[MJ/day]       (1x1) Heat generation steam
system for CF_s
E_gen_Gas_CF=HEAT_GAS_II_SOLAR(n2,n2);         %[MJ/day]       (1x1) Heat generation gas system
for CF_s

%SOLAR USE Lansing
y1=Heat_req_STEAM_LAN(n2,:);
P = polyfit(Percent_solar,y1,1);
SU_LAN_STEAM=(E_gen_Steam_CF-P(2))/P(1);       %[]             Solar use Lansing steam system
BU_LAN_STEAM=(1-SU_LAN_STEAM);                 %[]             Biogas use use Lansing steam
system

y1=Heat_req_GAS_II_LAN(n2,:);
P = polyfit(Percent_solar,y1,1);
SU_LAN_GAS=(E_gen_Gas_CF-P(2))/P(1);           %[]             Solar use Lansing gas system
BU_LAN_GAS=(1-SU_LAN_GAS);                     %[]             Biogas use Lansing gas system

%SOLAR USE Phoenix
y1=Heat_req_STEAM_PHO(n2,:);
P = polyfit(Percent_solar,y1,1);
SU_PHO_STEAM=(E_gen_Steam_CF-P(2))/P(1);       %[]             Solar use Phoenix steam system
BU_PHO_STEAM=(1-SU_PHO_STEAM);                 %[]             Biogas use Phoenix steam system

y1=Heat_req_GAS_II_PHO(n2,:);
P = polyfit(Percent_solar,y1,1);
SU_PHO_GAS=(E_gen_Gas_CF-P(2))/P(1);           %[]             Solar use Phoenix gas system
BU_PHO_GAS=(1-SU_PHO_GAS);                     %[]             Biogas use Phoenix gas system
```

```
%For manuscript
fprintf('\n Solar Use \n')
SOLAR_USE_CITIES=[SU_LAN_STEAM SU_LAN_GAS
SU_PHO_STEAM SU_PHO_GAS]


figure
plot(Percent_solar,HEAT_STEAM_SOLAR(n2,:),Percent_solar,Heat_req_STEAM_LAN(n2,:),'-
o',Percent_solar,Heat_req_STEAM_PHO(n2,:),'-x')
set(gca,'fontsize',12)
xlabel('Solar utilization')
ylabel('Thermal energy(MJ/day)')
legend('Thermal energy generated (Steam turbine)','AD thermal energy requirement LAN (Steam
turbine)','AD thermal energy requirement PHO (Steam turbine)','Location','Best')
xeq(1) =SOLAR_USE_CITIES(1,1);
yeq(1) =HEAT_STEAM_SOLAR(n2,1);
xeq(2) =SOLAR_USE_CITIES(2,1);
yeq(2) =HEAT_STEAM_SOLAR(n2,1);
hold
plot(xeq, yeq, 'o', 'MarkerFaceColor', 'k', 'MarkerEdgeColor','k','LineWidth', 1.5, 'MarkerSize',
5)
text(xeq(1),yeq(1)+500, 'Solar U. Lansing', 'Color', 'k')
text(xeq(2)-0.2,yeq(2)-500, 'Solar U. Phoenix', 'Color', 'k')
figure
plot(Percent_solar,HEAT_GAS_II_SOLAR(n2,:),Percent_solar,Heat_req_GAS_II_LAN(n2,:),'-
o',Percent_solar,Heat_req_GAS_II_PHO(n2,:),'-x')
set(gca,'fontsize',12)
xlabel('Solar utilization')
ylabel('Thermal energy(MJ/day)')
legend('Thermal energy generated (Gas turbine)','AD thermal energy requirement LAN (Gas
turbine)','AD thermal energy requirement PHO (Gas turbine)','Location','Best')
xeq(1) =SOLAR_USE_CITIES(1,2);
yeq(1) =HEAT_GAS_II_SOLAR(n2,1);
xeq(2) =SOLAR_USE_CITIES(2,2);
yeq(2) =HEAT_GAS_II_SOLAR(n2,1);
hold
plot(xeq, yeq, 'o', 'MarkerFaceColor', 'k', 'MarkerEdgeColor','k','LineWidth', 1.5, 'MarkerSize',
5)
text(xeq(1),yeq(1)+500, 'Solar U. Lansing', 'Color', 'k')
text(xeq(2)-0.2,yeq(2)-500, 'Solar U. Phoenix', 'Color', 'k')


for i=1:12                                     %[°C] Manure temperature
    Tmanure_LAN(i)=Tamb_Lansing(i);
    Tmanure_PHO(i)=Tamb_Phoenix(i);
    if Tmanure_LAN(i)<4
        Tmanure_LAN(i)=4;
    end
    if Tmanure_PHO(i)<4
        Tmanure_PHO(i)=4;
    end
end
```

LANSING

```
%CRITICAL SELECTION USING CF=0.5
T_amb_LAN=-2.05; %[°C]
% STEAM ____________________________________________________________________
vq1=V_reactor_STEAM(n2,:);
AD_volumen_steam=interp1(Percent_solar',vq1',SU_LAN_STEAM);
%[m3]           AD reactor volume for the specified net capacity factor
m1=(AD_volumen_steam/HRT)*rho_inf;
%[kg]           Mass of influent per day
Heat_req_STEAM_LAN=m1.*CpInfluent.*(T_AD-Tmanure_LAN).*(1+0.3)./1e6;
%[MJ/day]       (1x12)Heat requirement for AD culture
STEAM_Biogas=interp1(DATA_table_STEAM(1,:),DATA_table_STEAM(6,:),SU_LAN_STEAM,'linear')*t_d_s/100
0;    %[MJ/day]       BIOGAS Energy requirement for the specified net capacity factor
STEAM_Solar=interp1(DATA_table_STEAM(1,:),DATA_table_STEAM(8,:),SU_LAN_STEAM,'linear')*t_d_s/1000
;     %[MJ/day]       SOLAR Energy requirement for the specified net capacity factor
STEAM_Solar=STEAM_Solar/E_r1;
%[MJ/day]       Solar energy requirement considering heat exchanger efficiency (Steam)
A1=(STEAM_Solar)/((e_o_parabolic*min_Lansing.*percent_Solar_useful_steam_LAN)-
(t_collection_Steam_LAN./1e6).*((ems*c_SB/Cr_Parabolic)*(THS_1^4-
(T_amb_LAN+273.15)^4)+(UL/Cr_Parabolic)*(THS_1-(T_amb_LAN+273.15))));     %[m2]    Solar
collector area steam system considering heat losses in the solar collector (radiation and
convection)
% GAS ______________________________________________________________________
vq1=V_reactor_GAS_II(n2,:);
AD_volumen_gas_II=interp1(Percent_solar',vq1',SU_LAN_GAS);
%[m3]           AD reactor volume for the specified net capacity factor
m3=(AD_volumen_gas_II/HRT)*rho_inf;
%[kg]           Mass of influent per day
Heat_req_GAS_II_LAN=m3.*CpInfluent.*(T_AD-Tmanure_LAN).*(1+0.3)./1e6;
%[MJ/day]       (1x12)Heat requirement for AD culture
GAS_II_Biogas=interp1(A_II(1,:),A_II(9,:),SU_LAN_GAS,'linear')*t_d_s/1000;
%[MJ/day]       BIOGAS Energy requirement for the specified net capacity factor
GAS_II_Solar=interp1(A_II(1,:),A_II(10,:),SU_LAN_GAS,'linear')*t_d_s/1000;
%[MJ/day]       SOLAR Energy requirement for the specified net capacity factor
GAS_II_Solar=GAS_II_Solar/E_r2;
%[MJ/day]       Solar energy requirement considering heat exchanger efficiency (Gas)
A2=(GAS_II_Solar)/((e_o_dish*min_Lansing.*percent_Solar_useful_gas_LAN)-
(t_collection_Gas_LAN./1e6).*((ems*c_SB/Cr_Dish)*(THS_2^4-
(T_amb_LAN+273.15)^4)+(UL/Cr_Dish)*(THS_2-(T_amb_LAN+273.15))));     %[m2]    Solar collector
area steam system considering heat losses in the solar collector (radiation and convection)
% Sumary for critical situation ___________________________________________

%For manuscript
fprintf('\n SOLAR AREA LANSING \n')
SOLAR_Area_LAN=[A1
    A2]
fprintf('\n Digester VOLUME LANSING \n')
DIGESTER_volume_LAN=[AD_volumen_steam
    AD_volumen_gas_II]
fprintf('\n Biogas productivity LANSING \n')
Biogas_volume_LAN=DIGESTER_volume_LAN.*Biogas_p
%[m3biogas/day] Biogas daily productivity
```

```
% Solar energy collection
[DRS_S1,DSR_G1,DRS_S_opt1,DSR_G_opt1,DRS_S_ther1,DRS_G_ther1,Potential_solar1] =
Solar_collector(Lansing,SOLAR_Area_LAN,Tamb_Lansing,1);

% Operating time_____________________________________________________________
%Steam turbine total/total
T_time_S_LAN_BIOGAS=((STEAM_Biogas*n_b).*1000)./(Qboiler_n*n_b);              %[s]
T_time_S_LAN_SOLAR=((Potential_solar1(:,1)*E_r1).*1000)./(Qboiler_n*n_b);     %[s]
T_time_S_LAN=T_time_S_LAN_BIOGAS+T_time_S_LAN_SOLAR;                          %[s]
%Gas turbine total/total
SOLAR_EXTRA=Potential_solar1(:,2)-GAS_II_Solar;                               %[MJ/day]
T_time_G_LAN_BIOGAS=((GAS_II_Biogas*e_HC).*1000)./(Qh_n_burner*e_HC);         %[s]
T_time_G_LAN_SOLAR=((GAS_II_Solar*E_r2).*1000)./(Qh_n_burner*e_HC);           %[s]
T_time_G_LAN_SOLAR_E=((SOLAR_EXTRA*E_r2).*1000)./(Qh_n_burner*e_HC);          %[s]
T_time_G_LAN=T_time_G_LAN_BIOGAS+T_time_G_LAN_SOLAR+T_time_G_LAN_SOLAR_E;     %[s]

%NET CAPACITY FACTORS
NCF_1_LAN=(T_time_S_LAN)./(24*3600);
NCF_2_LAN=(T_time_G_LAN)./(24*3600);


% SANKEY DIAGRAM STEAM__________________________________________________________
LAN_S_1=zeros(12,1)+STEAM_Biogas;
%[MJ/day] Energy from biogas
LAN_S_2=DRS_S1;
%[MJ/day] Direct solar radiation
LAN_S_3=Potential_solar1(:,1);
%[MJ/day] Energy collected in solar field
LAN_S_4=Heat_req_STEAM_LAN';
%[MJ/day] Thermal energy required by AD
LAN_S_5=(T_time_S_LAN.*Qsink)./1000;
%[MJ/day] Thermal energy generated by power block
LAN_S_6=(LAN_S_5-LAN_S_4);
%[MJ/day] Thermal energy non used
LAN_S_7=(T_time_S_LAN.*30)./1000;
%[MJ/day] Electrical energy generated
LAN_S_8=(1-e_o_parabolic).*LAN_S_2;
%[MJ/day] Energy loss by optical efficiency
LAN_S_9=LAN_S_2-(LAN_S_8+LAN_S_3);
%[MJ/day] Solar energy non used  (THERMAL LOSSES)
LAN_S_10=(LAN_S_1+LAN_S_3)-(LAN_S_7+LAN_S_5);
%[MJ/day] Irreversible losses
LAN_S_11=zeros(12,1)+(Biogas_CU_steam*Biogas_volume_LAN(1))+Elec_AD.*AD_volumen_steam.*(1);
%[MJ/day] Electrical energy required by AD (one hour for influent handling)
LAN_S_12=LAN_S_7-LAN_S_11;
%[MJ/day] Electrical energy non used
SANKEY_1_LAN=[LAN_S_1 LAN_S_2 LAN_S_3 LAN_S_4 LAN_S_5 LAN_S_6 LAN_S_7 LAN_S_8 LAN_S_9 LAN_S_10
LAN_S_11 LAN_S_12];

% SANKEY DIAGRAM GAS_____________________________________________________
LAN_G_1=zeros(12,1)+GAS_II_Biogas;
%[MJ/day] Energy from biogas
LAN_G_2=DSR_G1;
%[MJ/day] Direct solar radiation
```

```
LAN_G_3=Potential_solar1(:,2);
%[MJ/day] Energy collected in solar field
LAN_G_4=Heat_req_GAS_II_LAN';
%[MJ/day] Thermal energy required by AD
LAN_G_5=(T_time_G_LAN.*A_II(11,1))./1000;
%[MJ/day] Thermal energy generated by power block
LAN_G_6=(LAN_G_5-LAN_G_4);
%[MJ/day] Thermal energy non used
LAN_G_7=(T_time_G_LAN.*30)./1000;
%[MJ/day] Electrical energy generated
LAN_G_8=(1-e_o_dish).*LAN_G_2;
%[MJ/day] Energy loss by optical efficiency
LAN_G_9=LAN_G_2-(LAN_G_8+LAN_G_3);
%[MJ/day] Solar energy non used (THERMAL LOSSES)
LAN_G_10=(LAN_G_1+LAN_G_3)-(LAN_G_7+LAN_G_5);
%[MJ/day] Irreversible losses
LAN_G_11=zeros(12,1)+(Biogas_CU_gas*Biogas_volume_LAN(2))+Elec_AD.*AD_volumen_gas_II.*(1);
%[MJ/day] Electrical energy required by AD (one hour for influent handling)
LAN_G_12=LAN_G_7-LAN_G_11;
%[MJ/day] Electrical energy non used
SANKEY_2_LAN=[LAN_G_1 LAN_G_2 LAN_G_3 LAN_G_4 LAN_G_5 LAN_G_6 LAN_G_7 LAN_G_8 LAN_G_9 LAN_G_10
LAN_G_11 LAN_G_12];

MNT_LAN=7;      %[] Month for SANKEY diagram
MNT_LAN2=12;    %[] Month for SANKEY diagram
fprintf('\n')
fprintf('http://sankeymatic.com/\n')
fprintf('\n')
fprintf('\n')
fprintf('Lansing_steam_hot*****\n')
formatSpec = 'Biogas [%.0f] PGS\n'; fprintf(formatSpec,SANKEY_1_LAN(MNT_LAN,1))
formatSpec = 'DSR [%.0f] SC \n'; fprintf(formatSpec,SANKEY_1_LAN(MNT_LAN,2))
formatSpec = 'SC  [%.0f] PGS\n'; fprintf(formatSpec,SANKEY_1_LAN(MNT_LAN,3))
formatSpec = 'SC  [%.0f] Thermal losses\n'; fprintf(formatSpec,SANKEY_1_LAN(MNT_LAN,9))
formatSpec = 'SC  [%.0f] Optical losses\n'; fprintf(formatSpec,SANKEY_1_LAN(MNT_LAN,8))
formatSpec = 'PGS [%.0f] EG\n'; fprintf(formatSpec,SANKEY_1_LAN(MNT_LAN,7))
formatSpec = 'PGS [%.0f] HG\n'; fprintf(formatSpec,SANKEY_1_LAN(MNT_LAN,5))
formatSpec = 'PGS [%.0f] Irreversible losses\n'; fprintf(formatSpec,SANKEY_1_LAN(MNT_LAN,10))
formatSpec = 'EG [%.0f] Over generation\n'; fprintf(formatSpec,SANKEY_1_LAN(MNT_LAN,12))
formatSpec = 'EG [%.0f] AD\n'; fprintf(formatSpec,SANKEY_1_LAN(MNT_LAN,11))
formatSpec = 'HG [%.0f] AD\n'; fprintf(formatSpec,SANKEY_1_LAN(MNT_LAN,4))
formatSpec = 'HG [%.0f] Non-used\n'; fprintf(formatSpec,SANKEY_1_LAN(MNT_LAN,6))
fprintf('Lansing_steam_cold*****\n')
formatSpec = 'Biogas. [%.0f] PGS.\n'; fprintf(formatSpec,SANKEY_1_LAN(MNT_LAN2,1))
formatSpec = 'DSR. [%.0f] SC. \n'; fprintf(formatSpec,SANKEY_1_LAN(MNT_LAN2,2))
formatSpec = 'SC.  [%.0f] PGS.\n'; fprintf(formatSpec,SANKEY_1_LAN(MNT_LAN2,3))
formatSpec = 'SC.  [%.0f] Thermal losses.\n'; fprintf(formatSpec,SANKEY_1_LAN(MNT_LAN2,9))
formatSpec = 'SC.  [%.0f] Optical losses.\n'; fprintf(formatSpec,SANKEY_1_LAN(MNT_LAN2,8))
formatSpec = 'PGS. [%.0f] EG.\n'; fprintf(formatSpec,SANKEY_1_LAN(MNT_LAN2,7))
formatSpec = 'PGS. [%.0f] HG.\n'; fprintf(formatSpec,SANKEY_1_LAN(MNT_LAN2,5))
formatSpec = 'PGS. [%.0f] Irreversible losses.\n'; fprintf(formatSpec,SANKEY_1_LAN(MNT_LAN2,10))
formatSpec = 'EG. [%.0f] Over generation.\n'; fprintf(formatSpec,SANKEY_1_LAN(MNT_LAN2,12))
formatSpec = 'EG. [%.0f] AD.\n'; fprintf(formatSpec,SANKEY_1_LAN(MNT_LAN2,11))
formatSpec = 'HG. [%.0f] AD.\n'; fprintf(formatSpec,SANKEY_1_LAN(MNT_LAN2,4))
```

```
formatSpec = 'HG. [%.0f] Non-used.\n'; fprintf(formatSpec,SANKEY_1_LAN(MNT_LAN2,6))
fprintf('\n')
fprintf('\n')
fprintf('GLOBAL EFFICIENCIES\n')
100*(SANKEY_1_LAN(MNT_LAN,7)+SANKEY_1_LAN(MNT_LAN,5))/(SANKEY_1_LAN(MNT_LAN,1)+SANKEY_1_LAN(MNT_L
AN,2))
fprintf('\n')
100*(SANKEY_1_LAN(MNT_LAN2,7)+SANKEY_1_LAN(MNT_LAN2,5))/(SANKEY_1_LAN(MNT_LAN2,1)+SANKEY_1_LAN(MN
T_LAN2,2))
fprintf('\n')
fprintf('\n')
fprintf('Lansing_Gas_Hot_I*****\n')
formatSpec = 'Biogas [%.0f] PGS\n'; fprintf(formatSpec,SANKEY_2_LAN(MNT_LAN,1))
formatSpec = 'DSR [%.0f] SC\n'; fprintf(formatSpec,SANKEY_2_LAN(MNT_LAN,2))
formatSpec = 'SC [%.0f] PGS\n'; fprintf(formatSpec,SANKEY_2_LAN(MNT_LAN,3))
formatSpec = 'SC [%.0f] Thermal losses\n'; fprintf(formatSpec,SANKEY_2_LAN(MNT_LAN,9))
formatSpec = 'SC [%.0f] Optical losses\n'; fprintf(formatSpec,SANKEY_2_LAN(MNT_LAN,8))
formatSpec = 'PGS [%.0f] EG\n'; fprintf(formatSpec,SANKEY_2_LAN(MNT_LAN,7))
formatSpec = 'PGS [%.0f] HG\n'; fprintf(formatSpec,SANKEY_2_LAN(MNT_LAN,5))
formatSpec = 'PGS [%.0f] Irreversible losses\n'; fprintf(formatSpec,SANKEY_2_LAN(MNT_LAN,10))
formatSpec = 'EG [%.0f] Over generation\n'; fprintf(formatSpec,SANKEY_2_LAN(MNT_LAN,12))
formatSpec = 'EG [%.0f] AD\n'; fprintf(formatSpec,SANKEY_2_LAN(MNT_LAN,11))
formatSpec = 'HG [%.0f] AD\n'; fprintf(formatSpec,SANKEY_2_LAN(MNT_LAN,4))
formatSpec = 'HG [%.0f] Non-used\n'; fprintf(formatSpec,SANKEY_2_LAN(MNT_LAN,6))
fprintf('Lansing_Gas_Cold_*****\n')
formatSpec = 'Biogas. [%.0f] PGS.\n'; fprintf(formatSpec,SANKEY_2_LAN(MNT_LAN2,1))
formatSpec = 'DSR. [%.0f] SC.\n'; fprintf(formatSpec,SANKEY_2_LAN(MNT_LAN2,2))
formatSpec = 'SC. [%.0f] PGS.\n'; fprintf(formatSpec,SANKEY_2_LAN(MNT_LAN2,3))
formatSpec = 'SC. [%.0f] Thermal losses.\n'; fprintf(formatSpec,SANKEY_2_LAN(MNT_LAN2,9))
formatSpec = 'SC. [%.0f] Optical losses.\n'; fprintf(formatSpec,SANKEY_2_LAN(MNT_LAN2,8))
formatSpec = 'PGS. [%.0f] EG.\n'; fprintf(formatSpec,SANKEY_2_LAN(MNT_LAN2,7))
formatSpec = 'PGS. [%.0f] HG.\n'; fprintf(formatSpec,SANKEY_2_LAN(MNT_LAN2,5))
formatSpec = 'PGS. [%.0f] Irreversible losses.\n'; fprintf(formatSpec,SANKEY_2_LAN(MNT_LAN2,10))
formatSpec = 'EG. [%.0f] Over generation.\n'; fprintf(formatSpec,SANKEY_2_LAN(MNT_LAN2,12))
formatSpec = 'EG. [%.0f] AD.\n'; fprintf(formatSpec,SANKEY_2_LAN(MNT_LAN2,11))
formatSpec = 'HG. [%.0f] AD.\n'; fprintf(formatSpec,SANKEY_2_LAN(MNT_LAN2,4))
formatSpec = 'HG. [%.0f] Non-used.\n'; fprintf(formatSpec,SANKEY_2_LAN(MNT_LAN2,6))
fprintf('\n')
fprintf('\n')
fprintf('GLOBAL EFFICIENCIES\n')
100*(SANKEY_2_LAN(MNT_LAN,7)+SANKEY_2_LAN(MNT_LAN,5))/(SANKEY_2_LAN(MNT_LAN,1)+SANKEY_2_LAN(MNT_L
AN,2))
fprintf('\n')
100*(SANKEY_2_LAN(MNT_LAN2,7)+SANKEY_2_LAN(MNT_LAN2,5))/(SANKEY_2_LAN(MNT_LAN2,1)+SANKEY_2_LAN(MN
T_LAN2,2))
fprintf('\n')
fprintf('\n')
```

Phoenix

```
%CRITICAL SELECTION USING CF=0.5
T_amb_PHO=13; %[°C]
% STEAM ______________________________________________________________________
vq1=V_reactor_STEAM(n2,:);
```

```
AD_volumen_steam=interp1(Percent_solar',vq1',SU_PHO_STEAM);
%[m3]           AD reactor volume for the specified net capacity factor
m1=(AD_volumen_steam/HRT)*rho_inf;
%[kg]           Mass of influent per day
Heat_req_STEAM_PHO=m1.*CpInfluent.*(T_AD-Tmanure_PHO).*(1+0.3)./1e6;
%[MJ/day]       (1x12)Heat requirement for AD culture
STEAM_Biogas=interp1(DATA_table_STEAM(1,:),DATA_table_STEAM(6,:),SU_PHO_STEAM,'linear')*t_d_s/100
0;    %[MJ/day]       BIOGAS Energy requirement for the specified net capacity factor
STEAM_Solar=interp1(DATA_table_STEAM(1,:),DATA_table_STEAM(8,:),SU_PHO_STEAM,'linear')*t_d_s/1000
;     %[MJ/day]       SOLAR Energy requirement for the specified net capacity factor
STEAM_Solar=STEAM_Solar/E_r1;
%[MJ/day]       Solar energy requirement considering heat exchanger efficiency (Steam)
A1=(STEAM_Solar)/((e_o_parabolic*min_Phoenix.*percent_Solar_useful_steam_PHO)-
(t_collection_Steam_PHO./1e6).*((ems*c_SB/Cr_Parabolic)*(THS_1^4-
(T_amb_PHO+273.15)^4)+(UL/Cr_Parabolic)*(THS_1-(T_amb_PHO+273.15))));     %[m2]     Solar
collector area steam system considering heat losses in the solar collector (radiation and
convection)
% GAS _____________________________________________________________________
vq1=V_reactor_GAS_II(n2,:);
AD_volumen_gas_II=interp1(Percent_solar',vq1',SU_PHO_GAS);
%[m3]           AD reactor volume for the specified net capacity factor
m3=(AD_volumen_gas_II/HRT)*rho_inf;
%[kg]           Mass of influent per day
Heat_req_GAS_II_PHO=m3.*CpInfluent.*(T_AD-Tmanure_PHO).*(1+0.3)./1e6;
%[MJ/day]       (1x12)Heat requirement for AD culture
GAS_II_Biogas=interp1(A_II(1,:),A_II(9,:),SU_PHO_GAS,'linear')*t_d_s/1000;
%[MJ/day]       BIOGAS Energy requirement for the specified net capacity factor
GAS_II_Solar=interp1(A_II(1,:),A_II(10,:),SU_PHO_GAS,'linear')*t_d_s/1000;
%[MJ/day]       SOLAR Energy requirement for the specified net capacity factor
GAS_II_Solar=GAS_II_Solar/E_r2;
%[MJ/day]       Solar energy requirement considering heat exchanger efficiency (Gas)
A2=(GAS_II_Solar)/((e_o_dish*min_Phoenix.*percent_Solar_useful_gas_PHO)-
(t_collection_Gas_PHO./1e6).*((ems*c_SB/Cr_Dish)*(THS_2^4-
(T_amb_PHO+273.15)^4)+(UL/Cr_Dish)*(THS_2-(T_amb_PHO+273.15))));     %[m2]     Solar collector
area steam system considering heat losses in the solar collector (radiation and convection)
% Sumary for critical situation ___________________________________________
fprintf('\n SOLAR AREA PHOENIX \n')
SOLAR_Area_PHO=[A1
            A2]
fprintf('\n Digester VOLUME PHOENIX \n')
DIGESTER_volume_PHO=[AD_volumen_steam
            AD_volumen_gas_II]
fprintf('\n Biogas productivity PHOENIX \n')
Biogas_volume_PHO=DIGESTER_volume_PHO.*Biogas_p
%[m3biogas/day] Biogas daily productivity

% Solar energy collection
[DRS_S3,DSR_G3,DRS_S_opt3,DSR_G_opt3,DRS_S_ther3,DRS_G_ther3,Potential_solar3] =
Solar_collector(Phoenix,SOLAR_Area_PHO,Tamb_Phoenix,2);

% Operating time___________________________________________________________
%Steam turbine total/total
T_time_S_PHO_BIOGAS=((STEAM_Biogas*n_b).*1000)./(Qboiler_n*n_b);                    %[s]
T_time_S_PHO_SOLAR=((Potential_solar3(:,1)*E_r1).*1000)./(Qboiler_n*n_b);           %[s]
```

```
T_time_S_PHO=T_time_S_PHO_BIOGAS+T_time_S_PHO_SOLAR;                              %[s]
%Gas turbine total/total
SOLAR_EXTRA=Potential_solar3(:,2)-GAS_II_Solar;                                   %[MJ/day]
T_time_G_PHO_BIOGAS=((GAS_II_Biogas*e_HC).*1000)./(Qh_n_burner*e_HC);             %[s]
T_time_G_PHO_SOLAR=((GAS_II_Solar*E_r2).*1000)./(Qh_n_burner*e_HC);               %[s]
T_time_G_PHO_SOLAR_E=((SOLAR_EXTRA*E_r2).*1000)./(Qh_n_burner*e_HC);              %[s]
T_time_G_PHO=T_time_G_PHO_BIOGAS+T_time_G_PHO_SOLAR+T_time_G_PHO_SOLAR_E;         %[s]

%NET CAPACITY FACTORS
NCF_1_PHO=(T_time_S_PHO)./(24*3600);
NCF_2_PHO=(T_time_G_PHO)./(24*3600);

% SANKEY DIAGRAM STEAM______________________________________________________________
PHO_S_1=zeros(12,1)+STEAM_Biogas;
%[MJ/day] Energy from biogas
PHO_S_2=DRS_S3;
%[MJ/day] Direct solar radiation
PHO_S_3=Potential_solar3(:,1);
%[MJ/day] Energy collected in solar field
PHO_S_4=Heat_req_STEAM_PHO';
%[MJ/day] Thermal energy required by AD
PHO_S_5=(T_time_S_PHO.*Qsink)./1000;
%[MJ/day] Thermal energy generated by power block
PHO_S_6=(PHO_S_5-PHO_S_4);
%[MJ/day] Thermal energy non used
PHO_S_7=(T_time_S_PHO.*30)./1000;
%[MJ/day] Electrical energy generated
PHO_S_8=(1-e_o_parabolic).*PHO_S_2;
%[MJ/day] Energy loss by optical efficiency
PHO_S_9=PHO_S_2-(PHO_S_8+PHO_S_3);
%[MJ/day] Solar energy non used  (THERMAL LOSSES)
PHO_S_10=(PHO_S_1+PHO_S_3)-(PHO_S_7+PHO_S_5);
%[MJ/day] Irreversible losses
PHO_S_11=zeros(12,1)+(Biogas_CU_steam*Biogas_volume_PHO(1))+Elec_AD.*AD_volumen_steam.*(1);
%[MJ/day] Electrical energy required by AD (one hour for influent handling)
PHO_S_12=PHO_S_7-PHO_S_11;
%[MJ/day] Electrical energy non used
SANKEY_1_PHO=[PHO_S_1 PHO_S_2 PHO_S_3 PHO_S_4 PHO_S_5 PHO_S_6 PHO_S_7 PHO_S_8 PHO_S_9 PHO_S_10
PHO_S_11 PHO_S_12];

% SANKEY DIAGRAM GAS______________________________________________________________
PHO_G_1=zeros(12,1)+GAS_II_Biogas;
%[MJ/day] Energy from biogas
PHO_G_2=DSR_G3;
%[MJ/day] Direct solar radiation
PHO_G_3=Potential_solar3(:,2);
%[MJ/day] Energy collected in solar field
PHO_G_4=Heat_req_GAS_II_PHO';
%[MJ/day] Thermal energy required by AD
PHO_G_5=(T_time_G_PHO.*A_II(11,1))./1000;
%[MJ/day] Thermal energy generated by power block
PHO_G_6=(PHO_G_5-PHO_G_4);
%[MJ/day] Thermal energy non used
PHO_G_7=(T_time_G_PHO.*30)./1000;
```

```
%[MJ/day] Electrical energy generated
PHO_G_8=(1-e_o_dish).*PHO_G_2;
%[MJ/day] Energy loss by optical efficiency
PHO_G_9=PHO_G_2-(PHO_G_8+PHO_G_3);
%[MJ/day] Solar energy non used  (THERMAL LOSSES)
PHO_G_10=(PHO_G_1+PHO_G_3)-(PHO_G_7+PHO_G_5);
%[MJ/day] Irreversible losses
PHO_G_11=zeros(12,1)+(Biogas_CU_gas*Biogas_volume_PHO(2))+Elec_AD.*AD_volumen_gas_II.*(1);
%[MJ/day] Electrical energy required by AD (one hour for influent handling)
PHO_G_12=PHO_G_7-PHO_G_11;
%[MJ/day] Electrical energy non used
SANKEY_2_PHO=[PHO_G_1 PHO_G_2 PHO_G_3 PHO_G_4 PHO_G_5 PHO_G_6 PHO_G_7 PHO_G_8 PHO_G_9 PHO_G_10
PHO_G_11 PHO_G_12];

MNT_PHO=7;      %[] Month for SANKEY diagram
MNT_PHO2=12;    %[] Month for SANKEY diagram
fprintf('\n')
fprintf('\n')
fprintf('\n')
fprintf('\n')
fprintf('Phoenix_steam_hot*****\n')
formatSpec = 'Biogas [%.0f] PGS\n'; fprintf(formatSpec,SANKEY_1_PHO(MNT_PHO,1))
formatSpec = 'DSR [%.0f] SC \n'; fprintf(formatSpec,SANKEY_1_PHO(MNT_PHO,2))
formatSpec = 'SC  [%.0f] PGS\n'; fprintf(formatSpec,SANKEY_1_PHO(MNT_PHO,3))
formatSpec = 'SC  [%.0f] Thermal losses\n'; fprintf(formatSpec,SANKEY_1_PHO(MNT_PHO,9))
formatSpec = 'SC  [%.0f] Optical losses\n'; fprintf(formatSpec,SANKEY_1_PHO(MNT_PHO,8))
formatSpec = 'PGS [%.0f] EG\n'; fprintf(formatSpec,SANKEY_1_PHO(MNT_PHO,7))
formatSpec = 'PGS [%.0f] HG\n'; fprintf(formatSpec,SANKEY_1_PHO(MNT_PHO,5))
formatSpec = 'PGS [%.0f] Irreversible losses\n'; fprintf(formatSpec,SANKEY_1_PHO(MNT_PHO,10))
formatSpec = 'EG [%.0f] Over generation\n'; fprintf(formatSpec,SANKEY_1_PHO(MNT_PHO,12))
formatSpec = 'EG [%.0f] AD\n'; fprintf(formatSpec,SANKEY_1_PHO(MNT_PHO,11))
formatSpec = 'HG [%.0f] AD\n'; fprintf(formatSpec,SANKEY_1_PHO(MNT_PHO,4))
formatSpec = 'HG [%.0f] Non-used\n'; fprintf(formatSpec,SANKEY_1_PHO(MNT_PHO,6))
fprintf('Phoenix_steam_cold*****\n')
formatSpec = 'Biogas. [%.0f] PGS.\n'; fprintf(formatSpec,SANKEY_1_PHO(MNT_PHO2,1))
formatSpec = 'DSR. [%.0f] SC. \n'; fprintf(formatSpec,SANKEY_1_PHO(MNT_PHO2,2))
formatSpec = 'SC.  [%.0f] PGS.\n'; fprintf(formatSpec,SANKEY_1_PHO(MNT_PHO2,3))
formatSpec = 'SC.  [%.0f] Thermal losses.\n'; fprintf(formatSpec,SANKEY_1_PHO(MNT_PHO2,9))
formatSpec = 'SC.  [%.0f] Optical losses.\n'; fprintf(formatSpec,SANKEY_1_PHO(MNT_PHO2,8))
formatSpec = 'PGS. [%.0f] EG.\n'; fprintf(formatSpec,SANKEY_1_PHO(MNT_PHO2,7))
formatSpec = 'PGS. [%.0f] HG.\n'; fprintf(formatSpec,SANKEY_1_PHO(MNT_PHO2,5))
formatSpec = 'PGS. [%.0f] Irreversible losses.\n'; fprintf(formatSpec,SANKEY_1_PHO(MNT_PHO2,10))
formatSpec = 'EG. [%.0f] Over generation.\n'; fprintf(formatSpec,SANKEY_1_PHO(MNT_PHO2,12))
formatSpec = 'EG. [%.0f] AD.\n'; fprintf(formatSpec,SANKEY_1_PHO(MNT_PHO2,11))
formatSpec = 'HG. [%.0f] AD.\n'; fprintf(formatSpec,SANKEY_1_PHO(MNT_PHO2,4))
formatSpec = 'HG. [%.0f] Non-used.\n'; fprintf(formatSpec,SANKEY_1_PHO(MNT_PHO2,6))
fprintf('\n')
fprintf('\n')
fprintf('GLOBAL EFFICIENCIES\n')
100*(SANKEY_1_PHO(MNT_PHO,7)+SANKEY_1_PHO(MNT_PHO,5))/(SANKEY_1_PHO(MNT_PHO,1)+SANKEY_1_PHO(MNT_P
HO,2))
fprintf('\n')
100*(SANKEY_1_PHO(MNT_PHO2,7)+SANKEY_1_PHO(MNT_PHO2,5))/(SANKEY_1_PHO(MNT_PHO2,1)+SANKEY_1_PHO(MN
T_PHO2,2))
```

```
fprintf('\n')
fprintf('\n')
fprintf('Phoenix_Gas_Hot_I*****\n')
formatSpec = 'Biogas [%.0f] PGS\n'; fprintf(formatSpec,SANKEY_2_PHO(MNT_PHO,1))
formatSpec = 'DSR [%.0f] SC\n'; fprintf(formatSpec,SANKEY_2_PHO(MNT_PHO,2))
formatSpec = 'SC [%.0f] PGS\n'; fprintf(formatSpec,SANKEY_2_PHO(MNT_PHO,3))
formatSpec = 'SC [%.0f] Thermal losses\n'; fprintf(formatSpec,SANKEY_2_PHO(MNT_PHO,9))
formatSpec = 'SC [%.0f] Optical losses\n'; fprintf(formatSpec,SANKEY_2_PHO(MNT_PHO,8))
formatSpec = 'PGS [%.0f] EG\n'; fprintf(formatSpec,SANKEY_2_PHO(MNT_PHO,7))
formatSpec = 'PGS [%.0f] HG\n'; fprintf(formatSpec,SANKEY_2_PHO(MNT_PHO,5))
formatSpec = 'PGS [%.0f] Irreversible losses\n'; fprintf(formatSpec,SANKEY_2_PHO(MNT_PHO,10))
formatSpec = 'EG [%.0f] Over generation\n'; fprintf(formatSpec,SANKEY_2_PHO(MNT_PHO,12))
formatSpec = 'EG [%.0f] AD\n'; fprintf(formatSpec,SANKEY_2_PHO(MNT_PHO,11))
formatSpec = 'HG [%.0f] AD\n'; fprintf(formatSpec,SANKEY_2_PHO(MNT_PHO,4))
formatSpec = 'HG [%.0f] Non-used\n'; fprintf(formatSpec,SANKEY_2_PHO(MNT_PHO,6))
fprintf('Phoenix_Gas_Cold_I*****\n')
formatSpec = 'Biogas. [%.0f] PGS.\n'; fprintf(formatSpec,SANKEY_2_PHO(MNT_PHO2,1))
formatSpec = 'DSR. [%.0f] SC.\n'; fprintf(formatSpec,SANKEY_2_PHO(MNT_PHO2,2))
formatSpec = 'SC. [%.0f] PGS.\n'; fprintf(formatSpec,SANKEY_2_PHO(MNT_PHO2,3))
formatSpec = 'SC. [%.0f] Thermal losses.\n'; fprintf(formatSpec,SANKEY_2_PHO(MNT_PHO2,9))
formatSpec = 'SC. [%.0f] Optical losses.\n'; fprintf(formatSpec,SANKEY_2_PHO(MNT_PHO2,8))
formatSpec = 'PGS. [%.0f] EG.\n'; fprintf(formatSpec,SANKEY_2_PHO(MNT_PHO2,7))
formatSpec = 'PGS. [%.0f] HG.\n'; fprintf(formatSpec,SANKEY_2_PHO(MNT_PHO2,5))
formatSpec = 'PGS. [%.0f] Irreversible losses.\n'; fprintf(formatSpec,SANKEY_2_PHO(MNT_PHO2,10))
formatSpec = 'EG. [%.0f] Over generation.\n'; fprintf(formatSpec,SANKEY_2_PHO(MNT_PHO2,12))
formatSpec = 'EG. [%.0f] AD.\n'; fprintf(formatSpec,SANKEY_2_PHO(MNT_PHO2,11))
formatSpec = 'HG. [%.0f] AD.\n'; fprintf(formatSpec,SANKEY_2_PHO(MNT_PHO2,4))
formatSpec = 'HG. [%.0f] Non-used.\n'; fprintf(formatSpec,SANKEY_2_PHO(MNT_PHO2,6))
fprintf('\n')
fprintf('\n')
fprintf('GLOBAL EFFICIENCIES\n')
100*(SANKEY_2_PHO(MNT_PHO,7)+SANKEY_2_PHO(MNT_PHO,5))/(SANKEY_2_PHO(MNT_PHO,1)+SANKEY_2_PHO(MNT_P
HO,2))
fprintf('\n')
100*(SANKEY_2_PHO(MNT_PHO2,7)+SANKEY_2_PHO(MNT_PHO2,5))/(SANKEY_2_PHO(MNT_PHO2,1)+SANKEY_2_PHO(MN
T_PHO2,2))
fprintf('\n')
fprintf('\n')
```

Appendix B: Matlab script functions for turbine modeling

FUNCTION Steam_30kW( )

```
function [Qboiler_n,Qsink,n_turb_steam] = Steam_30kW( )
m=0.08071;                              %[kg/s]     Water mass flow 640 lb/hr
Pin=10;                                 %[Bar]      Turbine pressure in
Pout=0.2;                               %[Bar]      Turbine pressure out
T1=XSteam('Tsat_p',Pout)-2;             %[˚C]       Temperature inlet pump (2˚C safety
factor)
h1=XSteam('hL_T',T1);                   %[kJ/kg]    Enthalpy @ point 1
vf=XSteam('vL_T',T1);                   %[m3/kg]    Specific volume saturated water
Wp=vf*(Pin-Pout)*100/0.65;              %[kJ/kg]    Condensate Pump work (0.65 is the pump
efficiency)
P_vp=0.500;                             %[kW]       Power vacuum pump
P=30+Wp*m+P_vp;                         %[kW]       Power Output
h2=h1+Wp;                               %[kJ/kg]    Enthalpy @ point 2
T2=XSteam('T_ph',Pin,h2);               %[˚C]       Temperature point 2
T3=200;                                 %[˚C]       Temperature inlet turbine
s3=XSteam('s_pT',Pin,T3);               %[kJ/kg·K]  Entropy @ point 3, 10 bar at 200C
h3=XSteam('h_pT',Pin,T3);               %[kJ/kg]    Enthalpy @ point 3, 10 bar at 200C
hTout=h3-P/m;                           %[kJ/kg]    Enthalpy @ inmediatly turbine exit
T_Tout=XSteam('T_hs',hTout,s3);         %[˚C]       Temperature inmediatly turbine exit
h4=XSteam('h_ps',Pout,s3);              %[kJ/kg]    Enthalpy @ condenser pressure
T4=XSteam('Tsat_p',Pout);               %[˚C]       Temperature @ condenser condition
Qboiler=m*(h3-h2);                      %[kW]       Thermal energy added in the cycle
n_b=0.85;                               %[]         Efficiency boiler
Qboiler_n=Qboiler/n_b;                  %[kW]       Net Power boiler
n_turb_steam=(((h3-hTout))/((h3-h2)));  %[]         Thermal efficiency
n_cond=0.85;                            %[]         Efficiency boiler
Qsink=m*(h4-h1)*n_cond;                 %[kW]       Heat generated
end
```

FUNCTION Steam_30kW_solar( )

```
function [ Vect ] = Steam_30kW_solar(varargin)
```

INPUTS

```
Perc_solar=varargin{1};                %[]        Percent_solar
Qboiler_n=varargin{2};                 %[kW]      Qboiler_n
Solar_energy=varargin{3};              %[kW]      Qsolar
```

FUNCTION

```
n_b=0.85;                                  %[]        Efficiency boiler
Pin=10;                                    %[Bar]     Turbine pressure in
Pout=0.2;                                  %[Bar]     Turbine pressure out
T1=XSteam('Tsat_p',Pout)-2;                %[˚C]      Temperature inlet pump (2˚C safety
factor)
h1=XSteam('hL_T',T1);                      %[kJ/kg]   Enthalpy @ point 1
vf=XSteam('vL_T',T1);                      %[m3/kg]   Specific volume saturated water
Wp=vf*(Pin-Pout)*100/0.65;                 %[kJ/kg]   Condensate Pump work (0.65 is the pump
efficiency)
Qboiler=Qboiler_n*n_b;                     %[]        Heat boiler
m=0.08071;                                 %[kg/s]    Water mass flow 640 lb/hr
P_vp=0.500;                                %[kW]      Power vacuum pump
P=30+Wp*m+P_vp;                            %[kW]      Power Output

if Solar_energy == 0 % if solar_energy is zero, the fuction runs the analysis for a vector of
solar utilization from 0 to 100 (solar use precentage)
    n=size(Perc_solar);
    n1=n(1,2);
    n2=n(1,1);
    if n1>n2
        n=n1;
    else
        n=n2;
    end
    Solar=Qboiler.*Perc_solar;          %[kW]           Power from solar radiation
else
    Solar=Solar_energy;
    n=1;
end

Vect=zeros(10,n);
for i=1:n
    Qsolar=Solar(1,i);                         %[kW]      Power required solar for phase change
    h2=h1+Wp;                                  %[kJ/kg]   Enthalpy @ point 2
    T2=XSteam('T_ph',Pin,h2);                  %[˚C]      Temperature point 2
    T3=200;                                    %[˚C]      Temperature inlet turbine
    s3=XSteam('s_pT',Pin,T3);                  %[kJ/kg·K] Entropy @ point 3, 10 bar at 200C
    h3=XSteam('h_pT',Pin,T3);                  %[kJ/kg]   Enthalpy @ point 3, 10 bar at 200C

    if Qsolar>Qboiler
        Qboiler_n=0;                                       %[kW]
        Qb_n=0;                                            %[kW]      Net Power boiler
```

```
        Qsolar_no_used=Qsolar-Qboiler;                          %[kW]       Solar power no used
    else
        Qboiler_n=m*(h3-h2)-Qsolar;                             %[kW]       Thermal energy added
in the cycle
        Qb_n=Qboiler_n/n_b;                                     %[kW]       Net Power boiler
        Qsolar_no_used=0;                                       %[kW]       Solar power no used
    end

    hTout=h3-P/m;                               %[kJ/kg]    Enthalpy @ inmediatly turbine exit
    T_Tout=XSteam('T_hs',hTout,s3);             %[°C]       Temperature inmediatly turbine exit
    h4=XSteam('h_ps',Pout,s3);                  %[kJ/kg]    Enthalpy @ condenser pressure
    T4=XSteam('Tsat_p',Pout);                   %[°C]       Temperature @ condenser condition
    n_turb_steam=(((h3-hTout))/((h3-h2)));   %[]         Thermal efficiency
    n_cond=0.85;                                %[]         Efficiency boiler
    Qsink=m*(h4-h1)*n_cond;                     %[kW]       Heat generated


    Vect(1,i)=Perc_solar(1,i);
    Vect(2,i)=T1;
    Vect(3,i)=T2;
    Vect(4,i)=T3;
    Vect(5,i)=T4;
    Vect(6,i)=Qb_n;
    Vect(7,i)=Qsink;
    Vect(8,i)=Qsolar;
    Vect(10,i)=Qsolar_no_used;
end

end
```

FUNCTION Gas_30kW( )

```
function [Qh_n_burner,Q_gen,n_th] = Gas_30kW(  )
Qsolar=0;                                           %[kW]           Heat from solar collectors
m=0.31;                                             %[kg/s]         Air mass flow
rp=3.2;                                             %[]             Compression ratio
gamma=1.4;                                          %[]             Cp/Cv
e_L=0.75;                                           %[]             Heat exchanger efficiency
e_C=0.818;                                          %[]             Compressor efficiency
e_HC=0.98;                                          %[]             Combustion chamber efficiency
e_T=0.8164;                                         %[]             Turbine efficiency
e_R=0.775;                                          %[]             Regenerator efficiency
ac=rp^((gamma-1)/gamma);                            %[]             Parameter related to pressure
ratio of the compressor
T1=27+273;                                          %[K]            Temperature Inlet compressor
T2=T1*(1+(1/e_C)*(ac-1));                           %[K]            Temperature Outlet compressor
T3=1113;                                            %[K]            Temperature Inlet turbine
T4=912;                                             %[K]            Temperature Outlet turbine
Tx=e_R*T4+T2*(1-e_R);                               %[K]            Temperature after regenerator

Ty=e_R*T2+T4*(1-e_R);                               %[K]            Temperature exhaust after
```

```
regenerator
Cp1=airProp2((Tx+T3)/2,'cp')/1000;                    %[kJ/kg·K]      Specific heat at contant
pressure
Tx1=Tx+(Qsolar)/(m*Cp1);                               %[K]            Temperature after the solar
receiver
Cp2=airProp2((Tx+T3)/2, 'cp')/1000;                   %[kJ/kg·K]      Specific heat at contant
pressure
Qh=m*Cp2*(T3-Tx1);                                     %[kW]           Heat addition in the burner
Qh_n_burner=Qh/e_HC;                                   %[kW]           Heat addition in the burner
w/ efficiency

T_final=85+273.15;                                     %[K]            Temperature of exhaust gases
after giving heat for digester
Cp4a=airProp2((Ty+T_final)/2, 'cp')/1000;              %[kJ/kg·K]      Specific heat at contant
pressure
Q_gen=e_L*m*Cp4a*(Ty-T_final);                         %[kW]           Heat extracted

n_th=30/Qh_n_burner;                                   %[]             Thermal efficiency
end
```

FUNCTION Gas_30kW_II( )

```
function [A] = Gas_30kW_II(varargin)
```

INPUTS

```
Perc_solar=varargin{1};                                                        %[]
Percent_solar
Qh_n_burner=varargin{2};                                                       %[kW]
Qh_n_burner
Solar_energy=varargin{3};                                                      %[kW]
Qsolar
```

CONSTANTS

```
global e_HC T_Fin
```

FUNCTION

```
BASE_energy =Qh_n_burner*e_HC;                                             %[kW]           Heat
without efficiency
if Solar_energy == 0
    n=size(Perc_solar);
    n1=n(1,2);
    n2=n(1,1);
    if n1>n2
        n=n1;
    else
        n=n2;
    end
    Solar=BASE_energy.*Perc_solar;                                         %[kW]           Power
from solar radiation
else
```

```
    Solar=Solar_energy;
    n=1;
end
m=0.31;                                                         %[kg/s]         Air mass
flow
rp=3.2;                                                         %[]
Compression ratio
gamma=1.4;                                                      %[]             Cp/Cv
n_th=1-1/(rp^((gamma-1)/gamma));                                %[]             Thermal
efficiency
e_L=0.75;                                                       %[]             Heat
exchanger efficiency Water-GAS
e_C=0.818;                                                      %[]
Compressor efficiency
e_T=0.8164;                                                     %[]             Turbine
efficiency
e_R=0.775;                                                      %[]
Regenerator efficiency
ac=rp^((gamma-1)/gamma);                                        %[]             Parameter
related to pressure ratio of the compressor
T1=27+273;                                                      %[K]
Temperature Inlet compressor
T2=T1*(1+(1/e_C)*(ac-1));                                       %[K]
Temperature Outlet compressor
T3=1113;                                                        %[K]
Temperature Inlet turbine
T4=912;                                                         %[K]
Temperature Outlet turbine
Tx=e_R*T4+T2*(1-e_R);                                           %[K]
Temperature after regenerator

A=zeros(13,n);
for i=1:n
    Qsolar=Solar(1,i);                                          %[kW]
    Cp1=airProp2((Tx+T3)/2,'cp')/1000;                          %[kJ/kg·K]      Specific
heat at contant pressure
    Tx1=Tx+(Qsolar)/(m*Cp1);                                    %[K]
Temperature after the solar receiver %change this based on heat
    if Tx1>T3
        Qh_n_burner=0;                                          %[kW]           Burner
capacity
        Tx1=T3;
    else
        Cp2=airProp2((Tx+T3)/2, 'cp')/1000;                     %[kJ/kg·K]      Specific
heat at contant pressure
        Qh=m*Cp2*(T3-Tx1);                                      %[kJ/kg]        Heat
addition in the burner
        Qh_n_burner=Qh/e_HC;                                    %[kW]           Heat
addition in the burner w/ efficiency
    end
    %Solar radiation no-used
    if Qsolar>Qh_n_burner
        QSolar_no_used=Qsolar-Qh_n_burner;
    else
```

```
        QSolar_no_used=0;                                                  %[kW]           Burner
capacity
    end
    Ty=e_R*T2+T4*(1-e_R);                                                  %[K]
Temperature exhaust after regenerator


    T_final=85+273.15;                                                     %[K]
Temperature of exhaust gases after giving heat for digester
    Cp4a=airProp2((Ty+T_final)/2, 'cp')/1000;                              %[kJ/kg·K]      Specific
heat at contant pressure
    Q_gen=e_L*m*Cp4a*(Ty-T_final);                                     %[kW]           Heat
extracted

    %for analysis partial heating using solar up to T_Fin
    T_ini=Tx;                                                              %[K]
Temperature before solar energy addition
    Q_ad_solar=m.*Cp1.*(T_Fin-T_ini);                                      %[kW]           Heat
added in the solar part for partial heating
    Q_ad_biogas=((BASE_energy)-Q_ad_solar)./e_HC;                          %[kW]           Heat
added in the gas burner for final heating

    %Function output
    A(1,i)=Perc_solar(1,i);
    A(2,i)=T1;
    A(3,i)=T2;
    A(4,i)=Tx1;
    A(5,i)=Tx;
    A(6,i)=T3;
    A(7,i)=T4;
    A(8,i)=Ty;
    A(9,i)=Qh_n_burner;
    A(10,i)=Qsolar;
    A(11,i)=Q_gen;
    A(12,i)=QSolar_no_used;
    A(13,i)=Q_ad_solar;
    A(14,i)=Q_ad_biogas;
end

end
```

Appendix C: Matlab script function for solar collector modeling

```
function [DRS_S,DSR_G,DRS_S_opt,DSR_G_opt,DRS_S_ther,DRS_G_ther,Potential_solar] =
Solar_collector(Location,SOLAR_Area,T_ambient,nnnn)
```

CONSTANTS

```
global e_o_parabolic e_o_dish ems c_SB Cr_Parabolic Cr_Dish UL E_r1 E_r2 THS_1 THS_2 T_Fin
Biogas_CU_steam_N Biogas_CU_gas_N Biogas_CU_steam Biogas_CU_gas
global t_collection_Steam_LAN t_collection_Gas_LAN t_collection_Steam_PHO t_collection_Gas_PHO
global percent_Solar_useful_steam_LAN percent_Solar_useful_gas_LAN percent_Solar_useful_steam_PHO
percent_Solar_useful_gas_PHO

if nnnn==1
    percent_Solar_useful_steam=percent_Solar_useful_steam_LAN;
    percent_Solar_useful_gas=percent_Solar_useful_gas_LAN;
    t_collection_Steam=t_collection_Steam_LAN;
    t_collection_Gas=t_collection_Gas_LAN;
else
    percent_Solar_useful_steam=percent_Solar_useful_steam_PHO;
    percent_Solar_useful_gas=percent_Solar_useful_gas_PHO;
    t_collection_Steam=t_collection_Steam_PHO;
    t_collection_Gas=t_collection_Gas_PHO;
end

% DRS_S1        DSR_G1             DIRECT SOLAR RADIATION
% DRS_S_opt1    DSR_G_opt1         OPTICAL LOSSES
% DRS_S_ther1   DRS_G_ther1        THERMAL LOSSES
% Potential_solar1                 ENERGY TRANSFERED TO MOLTEN SALT
```

FUNCTION

```
%DIRECT SOLAR RADIATION
DRS_S=Location(:,2).*SOLAR_Area(1);                                  %[MJ/day]       Direct solar
radiation Steam
DSR_G=Location(:,2).*SOLAR_Area(2);                                  %[MJ/day]       Direct solar
radiation Gas
%OPTICAL LOSSES
DRS_S_opt=(1-e_o_parabolic).*DRS_S;
DSR_G_opt=(1-e_o_dish).*DSR_G;
%ENERGY COLLECTED IN MOLTEN SALT
Potential_solar(:,1)=SOLAR_Area(1).*((e_o_parabolic.*Location(:,2).*percent_Solar_useful_steam)-
(t_collection_Steam./1e6).*((ems.*c_SB/Cr_Parabolic).*(THS_1.^4-
(T_ambient+273.15).^4)+(UL./Cr_Parabolic).*(THS_1-(T_ambient+273.15))));  %[MJ/day]
Potential_solar(:,2)=SOLAR_Area(2).*((e_o_dish.*Location(:,2).*percent_Solar_useful_gas)-
(t_collection_Gas./1e6).*((ems.*c_SB/Cr_Dish).*(THS_2.^4-
(T_ambient+273.15).^4)+(UL/Cr_Dish).*(THS_2-(T_ambient+273.15))));                %[MJ/day]
%THERMAL LOSSES
DRS_S_ther=  DRS_S -(Potential_solar(:,1)+DRS_S_opt);     %[MJ/day]
DRS_G_ther= DSR_G -(Potential_solar(:,2)+DSR_G_opt);      %[MJ/day]

end
```

Appendix D: Matlab code for solar–bio hybridization for anaerobic digestion and aerobic treatment

```
clear
clc
close all

num = xlsread('LOCATION DATA','Lansing');
num2 = xlsread('LOCATION DATA','PV_Lansing');.

% OR

%num = xlsread('LOCATION DATA _PHO','Phoenix');
%num2 = xlsread('LOCATION DATA _PHO','PV_Phoenix');

% 1 Hour
% 2 Month
% 3 Day
% 4 Direct Solar radiation
% 5 Ambient temperature
% 6 GHI
% 7 DHI
n=size(num);
n=n(1);

% % Calculation of the Solar Operating Factor
% mbj=1;      %counter
% mbj_PV=1;   %counter
% for i=1:n
%     if num(i,4)>0
%         SOF_CSP(mbj,1)=num(i,4);
%         mbj=mbj+1;
%     end
%     if num2(i,2)>0
%         SOF_PV(mbj_PV,1)=num(i,4);
%         mbj_PV=mbj_PV+1;
%     end
% end

global HC_N TURBINE_P PER_METHANE E_heatexchanger E_condenser E_boiler
TURBINE_P=325;              %[kWe]      Turbine electrical power output (design conditions)
HC_N=23;                    %[MJ/Nm3]   Biogas heating value
PER_METHANE=0.60;           %[]         Percentage methane in biogas
E_heatexchanger=0.90;       %[]         Efficiency steam generator using solar energy
E_condenser=0.85;           %[]         Efficiency thermal energy extraction in the condenser
E_boiler=0.8448;                                 %[] Boiler efficiency

DWF=76.34;                                              %[m3/day]                 Daily
influent flow
[E_biogas,V_biogas]=AnaerobicDigester();                %[MJ/day]                 Thermal
energy from biogas combustion
E_biogas=E_biogas*(1/3.6);                              %[kWh per day]            Thermal
energy from biogas combustion
```

```
Start_hourAE=0;
Finish_hourAE=23;
Aerobic_influent=10161.95/2;                          %[m3/day]              Aerobic
influent
Air_flow_ref_1=9.375;                                 %[m3air/m3influent]    Biological
treatment processes PAG 226
Aerobic_time_op=12;                                   %[h]                   Operating
time for aerobic digestion
Air_flow_ref=Air_flow_ref_1/(Aerobic_time_op*60);     %[m3air/min·m3influent]   Aeration rate
recommended to maintain Dissolved oxygen at 2 mg/L
Air_flow=Air_flow_ref*Aerobic_influent/60;            %[m3air/s]
Inlet_P=101000;                                       %[Pa]                  Compressor
inlet pressure
Outlet_P=303000;                                      %[Pa]                  Compressor
outlet pressure
alpha=(1.4/(1.4-1))*Inlet_P*((Outlet_P/Inlet_P)^((1.4-1)/1.4)-1); %[]        constant
Compr_eff=0.90;                                       %[]                    Compressor
efficiency
Power_AeD_aeration=((alpha*Air_flow)/1000)/Compr_eff;   %[kW]                Electrical
power required for air compression
Power_AeD=Power_AeD_aeration;                         %[kW]                  Electrical
power required for aeration

%Biogas scrubbing
Start_hourBS=0;
Finish_hourBS=23;
E_BS_v=0.275;                             %[kWh/Nm3biogas]
E_BS_v=E_BS_v*(3.6/1);                    %[MJ/Nm3biogas]
T_biogas=273.15+40;                       %[K] Biogas temperature
E_BS_v=E_BS_v/((1.0074/1)*(288.15/T_biogas));%[MJ/m3biogas]
E_BS=E_BS_v*V_biogas;                     %[MJ]
E_BS=E_BS*1000;                           %[kJ]

%Cryogenic separation
Start_hourCS=0;
Finish_hourCS=23;
E_CS_v=0.35;                             %[kWh/Nm3biogas]
E_CS_v=E_CS_v*(3.6/1);                    %[MJ/Nm3biogas]
E_CS_v=E_CS_v/((1.0074/1)*(288.15/T_biogas));%[MJ/m3biogas]
E_CS=E_CS_v*V_biogas;                     %[MJ]
E_CS=E_CS*1000;                           %[kJ]

t_BS=(Finish_hourBS-Start_hourBS)*3600;     %[s]
Power_BS=E_BS/t_BS+E_CS/t_BS;                       %[kW] including cryogenic

%Influent handling
Start_hourIH=0;
Finish_hourIH=23;
Power_IH=[33
33
33
55
55
55
```

```
55
55
55
56
56
64
110
50
50
72
72
72
55
55
33
33
33
33];

Elec=Power_IH+Power_BS+Power_AeD;
Elec_load=zeros(n,1);                       %[kW] Electrical load required
for i=1:n
    if num(i,1)==0
        Elec_load(i:i+23,1)=Elec;
    end
end

Area=500000; %[m2] Collection area  (6757 with storage)
Area_SCA=6;                                             %[m2] Area of the solar collector
assembly
Area=round(Area/6)*6;                                   %[m2] Collection area considering the
area of inividual parabolic trough collectors
% Area1=0;                                              %[m2] Collection area for iteration
% Area2=40000;                                           %[m2] Collection area for iteration
% ZZ=1000;
% ZZZZZ=ZZ+1;
% nnnn=0;
% while ZZZZZ>ZZ || ZZZZZ<0
% nnnn=nnnn+1                                           %[]   iteration counter

QfromBiogas=zeros(n,1);                                 %[kW] Power from biogas

%----------FIRST, THE ELECTRICITY GENERATED USING JUST SOLAR ENERGY
for i=1:n
    [W,X,Y,Z,QdesignB]=turbine(num(i,4)/1000,Area,num(i,5));
    QSolarCollected(i,1)=W;                             %[kW] Heat collected
    Eelectrical(i,1)=X;                                 %[kW] Electrical energy generated
    Qstored(i,1)=Y;                                     %[kW] Thermal energy stored from solar
    E_thermal_Condenser(i,1)=Z;                         %[kW] Thermal energy extracted from
condenser
    if QSolarCollected(i,1)<0
        QSolarCollected(i,1)=0;
    end
```

```
end

% Calculation of the Solar Operating Factor
mbj=1;      %counter
for i=1:n
    if Eelectrical(i,1)>0
        SOF_CSP(mbj,1)=Eelectrical(i,1);
        mbj=mbj+1;
    end
end

%Daily thermal energy stored
ii=1;
for i=1:n
    if num(i,1)==0
        Qstored_THERMAL_TANK(ii,1)= sum(Qstored(i:i+23,1));                    %[kWh]
        ii=ii+1;
    end
end

QstoredDaily=Qstored_THERMAL_TANK.*0; % Multiply by 0 to run analysis without thermal storage


%----------SECOND, THE ELECTRICITY GENERATED USING HEAT STORED, THEN USING BIOGAS
for i=1:n
    if Eelectrical(i,1)<Elec_load(i,1)
        %+++++_____++++%                                        This lines calculates how much
thermal energy is required to generate the electricity (tempo2)
        [Z1,Z2,Pmin,Pmax] = turbine_biogas(Elec_load(i,1),2);
        Eelectrical(i,1)=Z1;                                    %[kW] TOTAL Electrical energy
generated
        tempo2=Z2(1);                                           %[kW] Thermal energy required to
generate the power load (No efficiencies included on this number)
        E_thermal_Condenser(i,1)=Z2(2);                         %[kW] Thermal energy extracted
from condenser
        %+++++_____++++%

        DAY_number=ceil(i/24);                                  %[]   Day number corresponding to
studied hour
        if DAY_number==1                                        %Conditional just for January 1
            DAY_number=366;
        end


        if QstoredDaily(DAY_number-1,1)>(tempo2-QSolarCollected(i,1)*E_heatexchanger)
% Compares the energy stored the day before, with the requirement in the specified hour
            QstoredDaily(DAY_number-1,1)=QstoredDaily(DAY_number-1,1)-(tempo2-
QSolarCollected(i,1)*E_heatexchanger);    % Takes from the energy storage the energy use, for the
next iteration
            QfromBiogas(i,1)=0;
        else
            QfromBiogas(i,1)=(tempo2-
(QSolarCollected(i,1)*E_heatexchanger)+QstoredDaily(DAY_number-1,1))/E_boiler;      %[kW] Thermal
energy required to generate the power load from biogas
```

```
            QstoredDaily(DAY_number-1,1)=0;
% Takes from the energy storage the energy use, for the next iteration
        end
    end

    % Conditional to calculate electricity over generated
    if Elec_load(i,1)<Eelectrical(i,1)
        Over_Generation(i,1)=Eelectrical(i,1)-Elec_load(i,1);               %[kW] Extra
electrical energy generated
    else
        Over_Generation(i,1)=0;
    end
end

% Daily analysis
ii=1;
for i=1:n
    if num(i,1)==0
     QfromBiogasDaily(ii,1)= sum(QfromBiogas(i:i+23,1));                    %[kWh]
     E_thermal_CondenserDaily(ii,1)= sum(E_thermal_Condenser(i:i+23,1));    %[kWh]
     Over_Generation_Daily(ii,1)=sum(Over_Generation(i:i+23,1));            %[kWh]
     DNI_Daily(ii,1)= sum(num(i:i+23,4))/1000;                              %[kWh/m2]
     DNI_Daily_standard_dev(ii,1)= std(num(i:i+23,4))/1000;                 %[kWh/m2]
     GHI_Daily(ii,1)= sum(num(i:i+23,6))/1000;                              %[kWh/m2]
     Tamb_Daily(ii,1)= mean(num(i:i+23,5));                                 %[°C]
     ii=ii+1;
    end
end

% Heat requirement
E_thermal_CondenserDaily=E_thermal_CondenserDaily.*(3.6); %[MJ]
HRT=20;                         %[days]Hydraulic Retention Time
V_reactor=DWF*HRT;              %[m3]Reactor volumen
TAD=40;                         %[°C]AD culture temperature
rho_inf=1100;                   %[kg/m3]
Cp_influent=4120;               %[J/kg·°C]
for i=1:365
    if Tamb_Daily(i,1)<4
        Tamb=4;
    else
        Tamb=Tamb_Daily(i,1);
    end
    E_heating_Daily(i,1)=((V_reactor/HRT)*rho_inf*Cp_influent*(TAD-Tamb)*(1+0.30))/(1e6);
%[MJ/day]
end

% Monthly data
DNI_Monthly=daily_monthly(DNI_Daily,1);                                     %[kWh/m2] Direct
Normal Irradiance
GHI_Monthly=daily_monthly(GHI_Daily,1);                                     %[kWh/m2] Global
Tamb_Monthly=daily_monthly(Tamb_Daily,2);                                   %[°C] Ambient
temperature
E_heating_Monthly=daily_monthly(E_heating_Daily,1);                         %[MJ] Thermal energy
required for heating
```

```
E_thermal_CondenserMonthly=daily_monthly(E_thermal_CondenserDaily,1);       %[MJ] Thermal energy
extracted in the condenser for heating
Over_Generation_Monthly=daily_monthly(Over_Generation_Daily,1);             %[kWh] Electrical
energy generated non used

% Biogas balance
BIOGAS_balance=E_biogas-QfromBiogasDaily;              %[kWh] Energy requirement from biogas
HC=HC_N*(1/3.6);                                       %[kWh/m3] Heat of combustion
BIOGAS_balance_VOL=BIOGAS_balance./HC;                 %[m3] Biogas volume requirement

%Split Biogas balance into negative and positive
for i=1:365
   if BIOGAS_balance_VOL(i,1)<0
       Negative_volumeBiogasGROSS(i,1)=BIOGAS_balance_VOL(i,1);               %[m3]
       Positive_volumeBiogasGROSS(i,1)=0;
   else
       Negative_volumeBiogasGROSS(i,1)=0;
       Positive_volumeBiogasGROSS(i,1)=BIOGAS_balance_VOL(i,1);               %[m3]
   end
end

Accumulative_biogas=zeros(366,1);
Accumulative_biogas(1,1)=0;
for i=1:365
   Accumulative_biogas(i+1,1)=Accumulative_biogas(i,1)+BIOGAS_balance_VOL(i,1);    %[m3]
end

%Biogas compression initial volume Jan 1// Verify the last term
[BiogasVolumeCompression_initial,Day_min]=min(Accumulative_biogas);
if Accumulative_biogas(end)<0
    BiogasVolumeCompression_initial=BiogasVolumeCompression_initial+Accumulative_biogas(end);
%[m3] TOTAL VOLUME OF COMPRESSED BIOGAS
end

%Tank storage analysis
Tank_Volume=zeros(366,1);
Tank_Volume(1,1)=abs(BiogasVolumeCompression_initial);
for i=1:365
   Tank_Volume(i+1,1)=Tank_Volume(i,1)+BIOGAS_balance_VOL(i,1);    %[m3]
end

% %Cryogenic upgrading stage
% V_compresed=(abs(sum(Negative_volumeBiogasGROSS))*PER_METHANE);                      %[m3]
Biomethane volume to compress
% Flow_comp_ref=450;                                                                   %[Nm3/h]
Compressor flow at normal conditions FIND REFERENCE!!!!!!!!!!!!!!!!!
% P_digester=1.025;                                                                    %[atm]
Digester pressure
% P_ref=1;                                                                             %[atm]
reference pressure
% T_biogas=4+273.15;                                                                   %[K] Biogas
temperature
% T_ref=288.15;                                                                        %[K]
reference temperature
```

```
% Flow_comp=Flow_comp_ref*(T_biogas/T_ref)*(P_ref/P_digester);                    %[m3/h]
Cryogenic Compressor flow
% t_CS=V_compresed/Flow_comp;                                                      %[h]
Operating time
% t_CS=t_CS*3600;                                                                  %[s]
Operating time
% %Biogas cryogenic separation
% E_CS_v=0.45;
%[kWh/Nm3biogas] From reference
% E_CS_v=E_CS_v*(3.6/1);
%[MJ/Nm3biogas]
% T_biogas=(4+273.15);                                                             %[K]
% E_CS_v=E_CS_v/((1.025/1)*(288.15/T_biogas));
%[MJ/m3biogas]
% E_CS=E_CS_v*V_compresed;                                                         %[MJe]
Electrical energy required to cryogenically treat biogas
% E_CS=E_CS*1000;                                                                  %[kJe]
Energy required to compress
% Pcompr=0*E_CS/t_CS;                                                                %[kW]
Cryogenic separation electrical power
% [Eelectricalcomp,E_thermalcomp,PminComp,PmaxComp] = turbine_biogas(Pcompr,2);    %[] Use of
steam turbine to power compressor
% ThermalEneg_biogas_compression=E_thermalcomp(1);                                 %[kWt]
Thermal Power required by the compressor including boiler eff
% Energy_biogas_compression=ThermalEneg_biogas_compression*t_CS*(1/1000);          %[MJ]
Thermal Energy required from biogas
% Biogas_vol_compression=Energy_biogas_compression/HC_N;                           %[m3]
Biogas volume required to compress biogas
% ZZZZZ=abs(sum(Positive_volumeBiogasGROSS))-abs(sum(Negative_volumeBiogasGROSS))-
Biogas_vol_compression; %[m3] Rest biogas after compression, must be equal or greater than zero

ZZZZZ=abs(sum(Positive_volumeBiogasGROSS))-abs(sum(Negative_volumeBiogasGROSS));     %[m3]
Rest biogas after compression, must be equal or greater than zero

TANK_SIZE_STORAGE=max(Tank_Volume)*PER_METHANE; %[m3]
%Conditionals to break iteration
% if ZZZZZ >ZZ
%     Area2=Area;
%     Area=(Area+Area1)/2;
%     Area1=Area1;
% end
% if ZZZZZ <0
%     Area1=Area;
%     Area=(Area+Area2)/2;
%     Area2=Area2;
% end
% if ZZZZZ>0 && ZZZZZ<ZZ
%     break
% end
% ZZZZZ
% end
(ZZZZZ/TANK_SIZE_STORAGE)*100

figure
```

```
plot(1:n,Eelectrical)
xlabel('Hour')
ylabel('Electricity generated (kW)')
title('ELECTRICITY GENERATED')
figure
plot(1:365,E_thermal_CondenserDaily,1:365,E_heating_Daily)
xlabel('Day')
ylabel('Energy (kWh)')
legend('Thermal energy generated','Thermal energy required')
title('Thermal ENERGY')
figure
plot(1:365,BIOGAS_balance)
xlabel('Day')
ylabel('Energy (kWh)')
title('BIOGAS BALANCE')
figure
plot(1:365,BIOGAS_balance_VOL)
xlabel('Day')
ylabel('Energy (m3)')
title('BIOGAS BALANCE')
figure
plot(1:366,Accumulative_biogas)
xlabel('Day')
ylabel('Volume (m3)')
title('ACUMMULATIVE BIOGAS VOLUME')
figure
plot(1:366,Tank_Volume)
xlabel('Day')
ylabel('Volume (m3)')
title('BIOGAS TANK VOLUME')

PfromBiogasPV=zeros(n,1);                                    %[kWe] Power from
biogas
EelectricalPV=zeros(n,1);
E_thermal_biogas=zeros(n,1);


%----------FIRST, THE ELECTRICITY GENERATED USING JUST SOLAR ENERGY
for i=1:n
    EelectricalPV(i,1)=num2(i,2);                            %[kWe] TOTAL
Electrical energy generated
    E_thermal2_Condenser(i,1)=0;                             %[kW] Thermal energy
extracted in the condenser
    if EelectricalPV(i,1)>Elec_load(i,1)
        Qstored_Batteries(i,1)=EelectricalPV(i,1)-Elec_load(i,1); %[kWe] Potential energy that
can be save in baterries, or electricity over generated from PV
    else
        Qstored_Batteries(i,1)=0;
    end
end

%Daily electrical energy stored
ii=1;
for i=1:n
```

```
    if num(i,1)==0
        Qstored_ELEC_BATTERY(ii,1)= sum(Qstored_Batteries(i:i+23,1));                    %[kWh]
        ii=ii+1;
    end
end
QstoredDailyPV=Qstored_ELEC_BATTERY; % Multiply by 0 to run analysis without battery storage


%For storage: max(Qstored_Batteries)/2=234.9591 from the simulation
Batt_max=max(QstoredDailyPV)/2; %[kWhe] Battery bank capacity

for i=1:365  % this conditional limits the amount of energy that can be stored
    if QstoredDailyPV(i,1)>Batt_max
        QstoredDailyPV(i,1)=Batt_max;
    end
end

%----------SECOND, THE ELECTRICITY GENERATED USING batteries, THEN USING BIOGAS
for i=1:n
    if EelectricalPV(i,1)<Elec_load(i,1)
        DAY_number=ceil(i/24);                                  %[]   Day number corresponding to
studied hour
        if DAY_number==1                                        %Conditional just for January 1
            DAY_number=366;
        end
        %***************
        tempo2=Elec_load(i,1)-EelectricalPV(i,1); % short of electricyty for the specified hour
        if QstoredDailyPV(DAY_number-1,1)>(tempo2)                                 % Compares
the energy stored the day before, with the requirement in the specified hour
            QstoredDailyPV(DAY_number-1,1)=QstoredDailyPV(DAY_number-1,1)-(tempo2);    % Takes
from the energy storage the energy use, for the next iteration
            QfromBiogas(i,1)=0;
            EelectricalPV(i,1)=Elec_load(i,1);
        else
            if tempo2<Pmin                                      % If the electrical power is
lower than the minimum, the turbine doesnt work, so, the power is set as Pmin
                tempo2=Pmin;
            end
            [XX,Z,Pmin,Pmax] = turbine_biogas(tempo2,2);
            EelectricalPV(i,1)=XX+EelectricalPV(i,1);
%[kWe] TOTAL Electrical energy generated
            E_thermal_biogas(i,1)=Z(1);                                        %[kW] Thermal
energy required from biogas to generated X
            E_thermal2_Condenser(i,1)=Z(2);                                    %[kW] Thermal
energy extracted in the condenser
        end
    end
    % Conditional to calculate electricity over generated
    if Elec_load(i,1)<EelectricalPV(i,1)
        Over_GenerationPV(i,1)=EelectricalPV(i,1)-Elec_load(i,1);                  %[kW] Extra
electrical energy generated
    else
        Over_GenerationPV(i,1)=0;
    end
```

```
end

%Daily biogas consumption requirement
ii=1;
for i=1:n
    if num(i,1)==0
     QfromBiogasDailyPV(ii,1)= sum(E_thermal_biogas(i:i+23,1));                 %[kWh] Thermal
energy required from biogas to generated X
     Over_Generation_DailyPV(ii,1)=sum(Over_GenerationPV(i:i+23,1));            %[kWh] Extra
electrical energy generated
     E_thermal_Condenser_DailyPV(ii,1)=sum(E_thermal2_Condenser(i:i+23,1));     %[kWh] Thermal
energy extracted in the condenser
     ii=ii+1;
    end
end

% Heat requirement
E_thermal_Condenser_DailyPV=E_thermal_Condenser_DailyPV.*(3.6);                 %[MJ] Thermal
energy extracted in the condenser

% Monthly data
E_thermal_Condenser_MonthlyPV=daily_monthly(E_thermal_Condenser_DailyPV,1);     %[MJ] Thermal
energy extracted in the condenser
Over_Generation_MonthlyPV=daily_monthly(Over_Generation_DailyPV,1);             %[kWh] Extra
electrical energy generated


% Biogas balance
BIOGAS_balancePV=E_biogas-QfromBiogasDailyPV;                                   %[kWh] Energy
requirement from biogas


HC=HC_N*(1/3.6);                                                                %[kWh/m3] Heat of
combustion
BIOGAS_balance_VOL_PV=BIOGAS_balancePV./HC;                                     %[m3] Biogas
volume requirement


%Split Negative and positive
for i=1:365
   if BIOGAS_balance_VOL_PV(i,1)<0
       Negative_volumeBiogasGROSSPV(i,1)=BIOGAS_balance_VOL_PV(i,1);            %[m3]
       Positive_volumeBiogasGROSSPV(i,1)=0;
   else
       Negative_volumeBiogasGROSSPV(i,1)=0;
       Positive_volumeBiogasGROSSPV(i,1)=BIOGAS_balance_VOL_PV(i,1);            %[m3]
   end
end

Accumulative_biogasPV=zeros(366,1);
Accumulative_biogasPV(1,1)=0;
for i=1:365
    Accumulative_biogasPV(i+1,1)=Accumulative_biogasPV(i,1)+BIOGAS_balance_VOL_PV(i,1); %[m3]
end
```

```
%Biogas compression initial volume Jan 1// Verify the last term
[BiogasVolumeCompression_initial_PV,Day_min_PV]=min(Accumulative_biogasPV);
if Accumulative_biogasPV(end)<0

BiogasVolumeCompression_initial_PV=BiogasVolumeCompression_initial_PV+Accumulative_biogasPV(end);
%[m3] TOTAL VOLUME OF COMPRESSED BIOGAS
end

%Tank storage analysis
Tank_VolumePV=zeros(366,1);
Tank_VolumePV(1,1)=abs(BiogasVolumeCompression_initial_PV);
for i=1:365
   Tank_VolumePV(i+1,1)=Tank_VolumePV(i,1)+BIOGAS_balance_VOL_PV(i,1);    %[m3]
end


% %Cryogenic upgrading stage
% %Same as CSP
% V_compresed_PV=(abs(sum(Negative_volumeBiogasGROSSPV))*PER_METHANE);
% t_CS_PV=V_compresed_PV/Flow_comp;                                                            %[h]
Operating time
% t_CS_PV=t_CS_PV*3600;
% %Biogas cryogenic separation
% %Same as CSP
% Energy_biogas_compressionPV=ThermalEneg_biogas_compression*t_CS_PV*(1/1000);  %[MJ] Thermal
Energy required from biogas
% Biogas_vol_compressionPV=Energy_biogas_compressionPV/HC_N;                                    %[m3]
Biogas volume required to compress biogas
% ZZZZZ_PV=abs(sum(Positive_volumeBiogasGROSSPV))-abs(sum(Negative_volumeBiogasGROSSPV))-
Biogas_vol_compressionPV; %[m3] Rest biogas after compression, must be equal or greater than zero


ZZZZZ_PV=abs(sum(Positive_volumeBiogasGROSSPV))-abs(sum(Negative_volumeBiogasGROSSPV)); %[m3]
Rest biogas after compression, must be equal or greater than zero


TANK_SIZE_STORAGE_PV=max(Tank_VolumePV)*PER_METHANE; %[m3]


(ZZZZZ_PV/TANK_SIZE_STORAGE_PV)*100

figure
plot(1:n,EelectricalPV)
xlabel('Hour')
ylabel('Electricity generated (kW)')
title('ELECTRICITY GENERATED')
figure
plot(1:365,BIOGAS_balancePV)
xlabel('Day')
ylabel('Energy (kWh)')
title('BIOGAS BALANCE')
figure
```

```
plot(1:365,BIOGAS_balance_VOL_PV)
xlabel('Day')
ylabel('Energy (m3)')
title('BIOGAS BALANCE')
figure
plot(1:366,Accumulative_biogasPV)
xlabel('Day')
ylabel('Volume (m3)')
title('ACUMMULATIVE BIOGAS VOLUME PV')
figure
plot(1:366,Tank_VolumePV)
xlabel('Day')
ylabel('Volume (m3)')
title('BIOGAS TANK VOLUME PV')
```

Appendix E: Matlab sub-functions for solar–bio hybridization for anaerobic digestion and aerobic treatment

FUNCTION AnaerobicDigester( )

```
function [E_thermal,V_biogas] = AnaerobicDigester()
%% ANAEROBIC DIGESTION
global HC_N
V_biogas=2919.96;               %[m3/day] Biogas productivity
E_thermal=V_biogas*HC_N;        %[MJ/day]Thermal energy available
end
```

FUNCTION turbine(Qin,AreaC,Tamb)

```
function [QSolarCollected, Eelectrical, Qstored,E_thermal,QdesignB] =
turbine( Qin,AreaC,Tamb )
%% TURBINE PARAMETERS
global TURBINE_P E_heatexchanger E_condenser E_boiler

MinTurbOp=0.25;                                 %[] Minimum turbine operation
MaxTurbOp=1.20;                                 %[] Maximum turbine operation
F0=-0.0572;                                     %[] Constant
F1=1.0041;                                      %[] Constant
F2=0.1255;                                      %[] Constant
F3=-0.0724;                                     %[] Constant
Ef_Turbine=0.35;                                %[] Turbine thermal
efficiency
Pdesign=TURBINE_P;                              %[kW] Turbine power design
Qdesign=Pdesign/Ef_Turbine;                     %[kW] Turbine heat design
Qheat=0.5*Qdesign;                              %[kW] Heat recovered in the
condenser
Pmin=Pdesign*MinTurbOp;                         %[kW] Minimum turbine power
output
Pmax=Pdesign*MaxTurbOp;                         %[kW] Maximum turbine power
output
Qmin_Th=fzero(@(x)((F0+F1*(x/Qdesign)^1+F2*(x/Qdesign)^2+F3*(x/Qdesign)^3)*Pd
esign)-Pmin,Qdesign*0.5);    %[kW] Min Thermal input including boiler eff
Qmax_Th=fzero(@(x)((F0+F1*(x/Qdesign)^1+F2*(x/Qdesign)^2+F3*(x/Qdesign)^3)*Pd
esign)-Pmax,Qdesign*1.5);    %[kW] Max Thermal inputincluding boiler eff
Eelectrical_par=Pdesign*0.05;                              %[kW] Parasitic
electrical energy
QdesignB=Qdesign/E_boiler;                     %[kW] Turbine heat design with
boiler eff.
%% OPTICAL EFFICIENCY REFRACTORS
Ef_1=0.99;                                          %[] Tracking error and
twist
```

```
Ef_2=0.968;                                      %[] Geometric Accuracy
Ef_3=0.925;                                      %[] surface reflectance
Ef_4=0.97;                                       %[] Concentration factor
Ef_5=1;                                          %[] Cleanliness factor
Ef_7=0.98;                                       %[] Dust
Ef_6=Ef_1*Ef_2*Ef_3*Ef_4*Ef_5*Ef_7;              %[] SCA field error
Ef_8=1;                                          %[] Fraction of field
Ef_9=0.95;                                      %[] Shadow
Ef_10=0.963;                                     %[] Transmisivity
Ef_11=0.96;                                      %[] Absortivity
Ef_12=1;                                         %[] Unaccounted
Ef_13=Ef_6*Ef_8*Ef_9*Ef_10*Ef_11*Ef_12;          %[] Optical efficiency

%% PIPING LOSS
Q_loss_pipe_ref=10;                              %[W/m2] Piping heat loss
at design temp (316.5 °C)
Q_pipe_ref=Q_loss_pipe_ref*AreaC/1000;           %[kW] Piping heat loss at
design temp (316.5 °C)
PHLTC1=0.001693;                                 %[] Constant
PHLTC2=-1.68E-05;                                %[] Constant
PHLTC3=6.78E-08;                                 %[] Constant
Tin_WF=300;                                      %[°C] Working fluid temp
Solar field inlet
Tout_WF=350;                                     %[°C] Working fluid temp
Solar field outlet
Tavg_WF=(Tin_WF+Tout_WF)/2;                      %[°C] Average working
fluid temp
Q_pipe=(PHLTC3*(Tavg_WF-Tamb)^3+PHLTC2*(Tavg_WF-Tamb)^2+PHLTC1*(Tavg_WF-
Tamb))*Q_pipe_ref;        %[kW] Heat loss in the pipe system

%% THERMAL ENERGY FOR TURBINE
Q_rec_loss=6.60896;
%[W/m2] Receiver heat loss
QSolarCollected=(Qin*AreaC*Ef_13)-(Q_rec_loss*AreaC/1000)-(Q_pipe);
%[kW] Heat collected


QSolarCollected=QSolarCollected.*E_heatexchanger;

if QSolarCollected<0
    QSolarCollected=0;
end

if QSolarCollected<Qmin_Th
    QSolarUseful=0;
%[kW] Thermal energy for turbine
    Qstored=QSolarCollected;
%[kW] Thermal energy for storage
else
    if QSolarCollected>Qmax_Th
        QSolarUseful=Qmax_Th;
        Qstored=QSolarCollected-Qmax_Th;
    else
        QSolarUseful=QSolarCollected;
        Qstored=0;
    end
```

```
end

Eelectrical=(F0+F1*(QSolarUseful/Qdesign)^1+F2*(QSolarUseful/Qdesign)^2+F3*(Q
SolarUseful/Qdesign)^3)*Pdesign; %[kW] Electrical power generated
Eelectrical=Eelectrical-Eelectrical_par;


if Eelectrical<0
    Eelectrical=0;
else
    Eelectrical=Eelectrical;
end

E_thermal=(F0+F1*(QSolarUseful/Qdesign)^1+F2*(QSolarUseful/Qdesign)^2+F3*(QSo
larUseful/Qdesign)^3)*Qheat*E_condenser; %[kW] Heat extracted in the
condenser

if E_thermal<0
    E_thermal=0;
else
    E_thermal=E_thermal;
end
end
```

FUNCTION turbine_biogas(Qin,n)

```
function [Eelectrical,E_thermal,Pmin,Pmax] = turbine_biogas(Qin,n) %Qmin_Th <
Qin < Qmax_Th
% if n=1, the input value must be Thermal energy to calculate electrical
power
% If n=2, the input value must be Electrical power to calculate thermal
energy
% Input energy in [kW]

%% TURBINE PARAMETERS
global TURBINE_P E_heatexchanger E_condenser E_boiler
        MinTurbOp=0.25;                                  %[] Minimum turbine
operation
        MaxTurbOp=1.20;                                  %[] Maximum turbine
operation
        F0=-0.0572;                                      %[] Constant
        F1=1.0041;                                       %[] Constant
        F2=0.1255;                                       %[] Constant
        F3=-0.0724;                                      %[] Constant
        Ef_Turbine=0.35;                                  %[] Turbine thermal
efficiency
        Pdesign=TURBINE_P;                               %[kW] Turbine power
design
        Qdesign=Pdesign/Ef_Turbine;                      %[kW] Turbine heat
design
        Qheat=0.5*Qdesign;                               %[kW] Heat recovered
in the condenser
```

```
        QdesignB=Qdesign/E_boiler;                    %[kW] Turbine heat
design with boiler eff.
        Pmin=Pdesign*MinTurbOp;                        %[kW] Minimum turbine
power output
        Pmax=Pdesign*MaxTurbOp;                        %[kW] Maximum turbine
power output

Qmin_Th=fzero(@(x)((F0+F1*(x/QdesignB)^1+F2*(x/QdesignB)^2+F3*(x/QdesignB)^3)
*Pdesign)-Pmin,QdesignB*0.5);    %[kW] Min Thermal input including boiler eff

Qmax_Th=fzero(@(x)((F0+F1*(x/QdesignB)^1+F2*(x/QdesignB)^2+F3*(x/QdesignB)^3)
*Pdesign)-Pmax,QdesignB*1.5);    %[kW] Max Thermal inputincluding boiler eff
        Eelectrical_par=Pdesign*0.05;                            %[kW]
Parasitic electrical energy

        switch n
            case 1      %To calculate power given heat
                if Qin<0
                    Qin=0;
                end

                if Qin<Qmin_Th
                    QSolarUseful=0;
%[kW] Thermal energy for turbine
                    Qstored=0;
%[kW] Thermal energy for storage non use for biogas input
                else
                    if Qin>Qmax_Th
                        QSolarUseful=Qmax_Th;
                        Qstored=Qin-Qmax_Th;
                    else
                        QSolarUseful=Qin;
                        Qstored=0;
                    end
                end

%[kWt] Thermal energy for turbine

Eelectrical=(F0+F1*(QSolarUseful/QdesignB)^1+F2*(QSolarUseful/QdesignB)^2+F3*
(QSolarUseful/QdesignB)^3)*Pdesign-Eelectrical_par;            %[kWe]
Electrical power generated

E_thermal=(F0+F1*(QSolarUseful/QdesignB)^1+F2*(QSolarUseful/QdesignB)^2+F3*(Q
SolarUseful/QdesignB)^3)*Qheat*E_boiler;                    %[kWt] Thermal
energy extracted in the condenser


            case 2      %To calculate thermal energy given electrical power
(Qin is here, the electrical power)
                Eelectrical=Qin+Eelectrical_par;%[kW] Electrical power
desired

                if Eelectrical>Pmin && Eelectrical<Pmax

E_thermal(1)=(fzero(@(x)((F0+F1*(x/QdesignB)^1+F2*(x/QdesignB)^2+F3*(x/Qdesig
nB)^3)*Pdesign)-Eelectrical,QdesignB))/E_boiler;             %[kWth] Thermal
energy required for the specified electrical power with boiler eff.
```

```
E_thermal(2)=(F0+F1*(E_thermal(1)/QdesignB)^1+F2*(E_thermal(1)/QdesignB)^2+F3
*(E_thermal(1)/QdesignB)^3)*Qheat*E_condenser;                    %[kW]
Thermal energy extracted in the condenser
                    Eelectrical=Eelectrical-Eelectrical_par;
%[kW] NET Electrical power generated
                else
                    E_thermal(1)=0;
                    E_thermal(2)=0;
                    Eelectrical=0;
                end
            otherwise
                disp('other value for function MAE')
        end
end
```

FUNCTION daily_monthly(B,z)

```
function [ A,AA ] = daily_monthly( B,z )
% z=1  sum
% z=2  mean
%% function to add daily values into monthly cells
n=size(B);
n=n(1);
 %Accumulative days
D=[31
    59
    90
    120
    151
    181
    212
    243
    273
    304
    334
    365];
switch z
    case 1
        tempo=1;
        for i=1:12
            A(i,1)=sum(B(tempo:D(i,1),1));
            AA=0;
            tempo=1+D(i,1);
        end
    case 2
        tempo=1;
        for i=1:12
            A(i,1)=mean(B(tempo:D(i,1),1));
            AA(i,1)=std(B(tempo:D(i,1),1));
            tempo=1+D(i,1);
        end
    otherwise
        disp('other value for function MAE')
end
```

Appendix F: Additional figures for a two-module Fresnel lens solar thermal collector

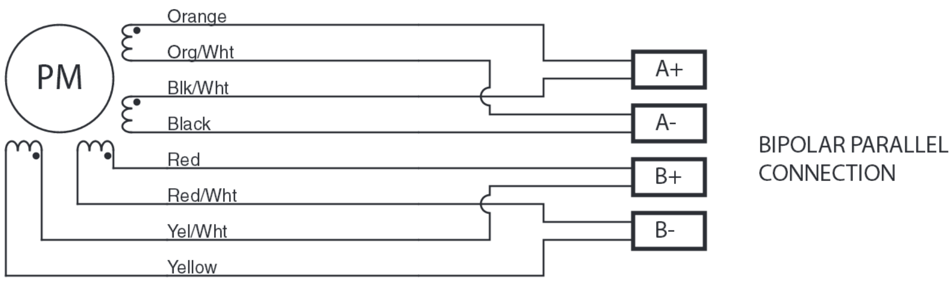

Figure VII-1. Bipolar parallel connection to connect stepper motor to drive

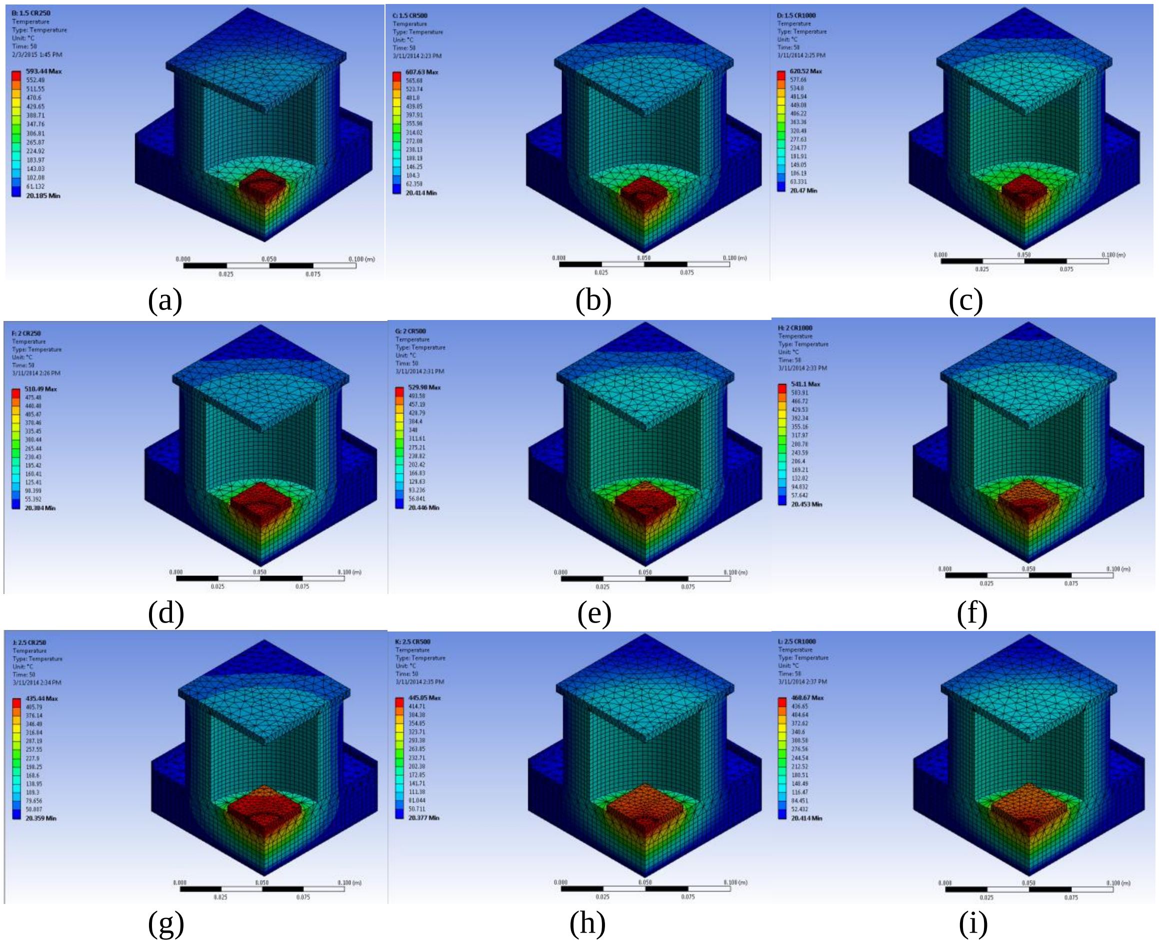

Figure VII-2. Temperature profiles obtained using FEM simulation*

Figure VII-2. (cont'd)

*: (a) 1451 mm^2 absorber area and 256 CR; (b) 1451 mm^2 absorber area and 576 CR; (c) 1451 mm^2 absorber area and 1000 CR; (d) 2580 mm^2 absorber area and 256 CR; (e) 2580 mm^2 absorber area and 576 CR; (f) 2580 mm^2 absorber area and 1000 CR; (g) 4032 mm^2 absorber area and 256 CR; (h) 4032 mm^2 absorber area and 576 CR; (i) 4032 mm^2 absorber area and 1000 CR

Appendix G: Astronomical algorithm for solar tracking system

```
%This script receives minute, second, day, month, year, hour, observer
%time, latitude, longitud and elevation to calculate the topocentric
%position of the sun
P=820; %millibars    annual average local pressure
T=11; %C  annual average local temperature
```

JULIAN CALCULATION

```
if(month == 1 || month == 2)
    Year=year-1;
    Month=month+12;
else
    Year=year;
    Month=month;
end
ut_time = ((hour - UTC)/24) + (minute/(60*24)) + (second/(60*60*24));
D = day + ut_time;
if(year == 1582)
    if(month == 10)
        if(day <= 4) % The Julian calendar ended on October 4, 1582
            Earth_heliocentric_position_latitude = 0;
        elseif(day >= 15) % The Gregorian calendar started on October 15, 1582
            A = floor(Year/100);
            Earth_heliocentric_position_latitude = 2 - A + floor(A/4);
        else
            disp('This date never existed!');
            month = 10;
            day = 4;
            Earth_heliocentric_position_latitude = 0;
        end
    elseif(month<10) % Julian calendar
        Earth_heliocentric_position_latitude = 0;
    else % Gregorian calendar
        A = floor(Year/100);
        Earth_heliocentric_position_latitude = 2 - A + floor(A/4);
    end

elseif(year<1582) % Julian calendar
    Earth_heliocentric_position_latitude = 0;
else
    A = floor(Year/100); % Gregorian calendar
    Earth_heliocentric_position_latitude = 2 - A + floor(A/4);
end
```

POLYNOMIAL EXPRESSION FOR DELTA T (DT)

```
yy=year+(month-0.5)/12;
tt=yy-2000;
DT=62.92+0.32217*tt+0.005589*tt^2;
%the difference between the Earth rotation time and the Terrestrial Time(TT)
```

```
%valid for years between 2005 - 2050
delta_t =DT;

Julian_day = floor(365.25*(Year+4716)) + floor(30.6001*(Month+1)) + D +
Earth_heliocentric_position_latitude - 1524.5;
Julian_ephemeris_day = Julian_day + (delta_t/86400);
Julian_century = (Julian_day - 2451545) / 36525;
Julian_ephemeris_century = (Julian_ephemeris_day - 2451545) / 36525;
Julian_ephemeris_millenium = Julian_ephemeris_century / 10;

L0table = [175347046.0 0 0
 3341656.0 4.6692568 6283.07585
 34894.0 4.6261 12566.1517
 3497.0 2.7441 5753.3849
 3418.0 2.8289 3.5231
 3136.0 3.6277 77713.7715
 2676.0 4.4181 7860.4194
 2343.0 6.1352 3930.2097
 1324.0 0.7425 11506.7698
 1273.0 2.0371 529.691
 1199.0 1.1096 1577.3435
 990 5.233 5884.927
 902 2.045 26.298
 857 3.508 398.149
 780 1.179 5223.694
 753 2.533 5507.553
 505 4.583 18849.228
 492 4.205 775.523
 357 2.92 0.067
 317 5.849 11790.629
 284 1.899 796.298
 271 0.315 10977.079
 243 0.345 5486.778
 206 4.806 2544.314
 205 1.869 5573.143
 202 2.4458 6069.777
 156 0.833 213.299
 132 3.411 2942.463
 126 1.083 20.775
 115 0.645 0.98
 103 0.636 4694.003
 102 0.976 15720.839
 102 4.267 7.114
 99 6.21 2146.17
 98 0.68 155.42
 86 5.98 161000.69
 85 1.3 6275.96
 85 3.67 71430.7
 80 1.81 17260.15
 79 3.04 12036.46
 71 1.76 5088.63
 74 3.5 3154.69
 74 4.68 801.82
 70 0.83 9437.76
```

```
 62 3.98 8827.39
 61 1.82 7084.9
 57 2.78 6286.6
 56 4.39 14143.5
 56 3.47 6279.55
 52 0.19 12139.55
 52 1.33 1748.02
 51 0.28 5856.48
 49 0.49 1194.45
 41 5.37 8429.24
 41 2.4 19651.05
 39 6.17 10447.39
 37 6.04 10213.29
 37 2.57 1059.38
 36 1.71 2352.87
 36 1.78 6812.77
 33 0.59 17789.85
 30 0.44 83996.85
 30 2.74 1349.87
 25 3.16 4690.48];

L1table = [628331966747.0 0 0
 206059.0 2.678235 6283.07585
 4303.0 2.6351 12566.1517
 425.0 1.59 3.523
 119.0 5.796 26.298
 109.0 2.966 1577.344
 93 2.59 18849.23
 72 1.14 529.69
 68 1.87 398.15
 67 4.41 5507.55
 59 2.89 5223.69
 56 2.17 155.42
 45 0.4 796.3
 36 0.47 775.52
 29 2.65 7.11
 21 5.34 0.98
 19 1.85 5486.78
 19 4.97 213.3
 17 2.99 6275.96
 16 0.03 2544.31
 16 1.43 2146.17
 15 1.21 10977.08
 12 2.83 1748.02
 12 3.26 5088.63
 12 5.27 1194.45
 12 2.08 4694
 11 0.77 553.57
 10 1.3 3286.6
 10 4.24 1349.87
 9 2.7 242.73
 9 5.64 951.72
 8 5.3 2352.87
 6 2.65 9437.76
```

```
 6 4.67 4690.48];

L2table = [52919.0 0 0
 8720.0 1.0721 6283.0758
 309.0 0.867 12566.152
 27 0.05 3.52
 16 5.19 26.3
 16 3.68 155.42
 10 0.76 18849.23
 9 2.06 77713.77
 7 0.83 775.52
 5 4.66 1577.34
 4 1.03 7.11
 4 3.44 5573.14
 3 5.14 796.3
 3 6.05 5507.55
 3 1.19 242.73
 3 6.12 529.69
 3 0.31 398.15
 3 2.28 553.57
 2 4.38 5223.69
 2 3.75 0.98];

L3table =[289.0 5.844 6283.076
 35 0 0
 17 5.49 12566.15
 3 5.2 155.42
 1 4.72 3.52
 1 5.3 18849.23
 1 5.97 242.73];

L4table = [114.0 3.142 0
 8 4.13 6283.08
 1 3.84 12566.15];

L5table = [1 3.14 0];


A0=L0table(:,1);
B0=L0table(:,2);
C0=L0table(:,3);
A1=L1table(:,1);
B1=L1table(:,2);
C1=L1table(:,3);
A2=L2table(:,1);
B2=L2table(:,2);
C2=L2table(:,3);
A3=L3table(:,1);
B3=L3table(:,2);
C3=L3table(:,3);
A4=L4table(:,1);
B4=L4table(:,2);
C4=L4table(:,3);
A5=L5table(:,1);
```

```
B5=L5table(:,2);
C5=L5table(:,3);

L0 = sum(A0 .* cos(B0 + (C0 * Julian_ephemeris_millenium)));
L1 = sum(A1 .* cos(B1 + (C1 * Julian_ephemeris_millenium)));
L2 = sum(A2 .* cos(B2 + (C2 * Julian_ephemeris_millenium)));
L3 = sum(A3 .* cos(B3 + (C3 * Julian_ephemeris_millenium)));
L4 = sum(A4 .* cos(B4 + (C4 * Julian_ephemeris_millenium)));
L5 = sum(A5 .* cos(B5 + (C5 * Julian_ephemeris_millenium)));

%Earth heliocentric position longitude L
Earth_heliocentric_position_longitude=(L0+L1*Julian_ephemeris_millenium+L2*Julian_ephemeris_mille
nium^2+L3*Julian_ephemeris_millenium^3+L4*Julian_ephemeris_millenium^4+L5*Julian_ephemeris_millen
ium^5)/1e8; %RADS
Earth_heliocentric_position_longitude=Earth_heliocentric_position_longitude*180/pi;%DEG

%Limiting Earth_heliocentric_position_longitude to 360°interval
Earth_heliocentric_position_longitude = Earth_heliocentric_position_longitude - 360 *
floor(Earth_heliocentric_position_longitude/360);
if(Earth_heliocentric_position_longitude<0)
    Earth_heliocentric_position_longitude = Earth_heliocentric_position_longitude + 360;
end

%^^^^^^^^^^^^^^^^^^^^^^^^^^^^^^^^^^^^^^^^^^^^^^^^^^^^^^^^^^^^^^^^^^^^^^^^^^^^^^^^^^^^^^^^^^^^^^^^
^^^^^^^^^^^^^^^^^^^^^^^^
B0table = [280.0 3.199 84334.662
 102.0 5.422 5507.553
 80 3.88 5223.69
 44 3.7 2352.87
 32 4 1577.34];

B1table = [9 3.9 5507.55
 6 1.73 5223.69];

A0=B0table(:,1);
B0=B0table(:,2);
C0=B0table(:,3);
A1=B1table(:,1);
B1=B1table(:,2);
C1=B1table(:,3);

L0=sum(A0 .* cos(B0 + (C0 * Julian_ephemeris_millenium)));
L1=sum(A1 .* cos(B1 + (C1 * Julian_ephemeris_millenium)));

%Earth heliocentric position latitude B
Earth_heliocentric_position_latitude=(L0+L1*Julian_ephemeris_millenium)/100000000;
Earth_heliocentric_position_latitude=Earth_heliocentric_position_latitude*180/pi; %DEG

%^^^^^^^^^^^^^^^^^^^^^^^^^^^^^^^^^^^^^^^^^^^^^^^^^^^^^^^^^^^^^^^^^^^^^^^^^^^^^^^^^^^^^^^^^^^^^^^^
^^^^^^^^^^^^^^^^^^^^^^^^

% R terms from the original code
R0table = [ 100013989.0 0 0
 1670700.0 3.0984635 6283.07585
```

```
 13956.0 3.05525 12566.1517
 3084.0 5.1985 77713.7715
 1628.0 1.1739 5753.3849
 1576.0 2.8469 7860.4194
 925.0 5.453 11506.77
 542.0 4.564 3930.21
 472.0 3.661 5884.927
 346.0 0.964 5507.553
 329.0 5.9 5223.694
 307.0 0.299 5573.143
 243.0 4.273 11790.629
 212.0 5.847 1577.344
 186.0 5.022 10977.079
 175.0 3.012 18849.228
 110.0 5.055 5486.778
 98 0.89 6069.78
 86 5.69 15720.84
 86 1.27 161000.69
 85 0.27 17260.15
 63 0.92 529.69
 57 2.01 83996.85
 56 5.24 71430.7
 49 3.25 2544.31
 47 2.58 775.52
 45 5.54 9437.76
 43 6.01 6275.96
 39 5.36 4694
 38 2.39 8827.39
 37 0.83 19651.05
 37 4.9 12139.55
 36 1.67 12036.46
 35 1.84 2942.46
 33 0.24 7084.9
 32 0.18 5088.63
 32 1.78 398.15
 28 1.21 6286.6
 28 1.9 6279.55
 26 4.59 10447.39];

R1table = [ 103019.0 1.10749 6283.07585
 1721.0 1.0644 12566.1517
 702.0 3.142 0
 32 1.02 18849.23
 31 2.84 5507.55
 25 1.32 5223.69
 18 1.42 1577.34
 10 5.91 10977.08
 9 1.42 6275.96
 9 0.27 5486.78];

R2table = [4359.0 5.7846 6283.0758
 124.0 5.579 12566.152
 12 3.14 0
 9 3.63 77713.77
```

```
 6 1.87 5573.14
 3 5.47 18849];

R3table = [145.0 4.273 6283.076
 7 3.92 12566.15];

R4table = [4 2.56 6283.08];

A0 = R0table(:,1);
B0 = R0table(:,2);
C0 = R0table(:,3);

A1 = R1table(:,1);
B1 = R1table(:,2);
C1 = R1table(:,3);

A2 = R2table(:,1);
B2 = R2table(:,2);
C2 = R2table(:,3);

A3 = R3table(:,1);
B3 = R3table(:,2);
C3 = R3table(:,3);

A4 = R4table(:,1);
B4 = R4table(:,2);
C4 = R4table(:,3);

% Compute the Earth heliocentric radius vector
L0 = sum(A0 .* cos(B0 + (C0 * Julian_ephemeris_millenium)));
L1 = sum(A1 .* cos(B1 + (C1 * Julian_ephemeris_millenium)));
L2 = sum(A2 .* cos(B2 + (C2 * Julian_ephemeris_millenium)));
L3 = sum(A3 .* cos(B3 + (C3 * Julian_ephemeris_millenium)));
L4 = A4 .* cos(B4 + (C4 * Julian_ephemeris_millenium));

% Units are in AU
earth_heliocentric_position_radius = (L0 + (L1 * Julian_ephemeris_millenium) + (L2 *
Julian_ephemeris_millenium^2) + (L3 * Julian_ephemeris_millenium^3) + (L4 *
Julian_ephemeris_millenium^4)) / 1e8;
```

GEOCENTRIC LONGITUDE AND LATITUDE

```
%Geocentric Longitude
Geocentric_longitude=Earth_heliocentric_position_longitude+180; %deg
%Limiting Geocentric_longitude to 360°interval
Geocentric_longitude = Geocentric_longitude - 360 * floor(Geocentric_longitude/360);
if(Geocentric_longitude<0)
    Geocentric_longitude = Geocentric_longitude + 360;
end
%Geocentric latitude
Geocentric_latitude=-Earth_heliocentric_position_latitude; %deg
```

THE NUTATION IN LONGITUDE AND OBLIQUITY

```
%mean elongation of the moon from the sun
X0=297.85036+445267.11148*Julian_ephemeris_century-
0.0019142*Julian_ephemeris_century^2+(Julian_ephemeris_century^3)/189474;
%the mean anomaly of the sun (Earth)
X1=357.52772+35999.05034*Julian_ephemeris_century-0.0001603*Julian_ephemeris_century^2-
(Julian_ephemeris_century^3)/300000;
%the mean anomaly of the moon
X2=134.96298+477198.867398*Julian_ephemeris_century+0.0086972*Julian_ephemeris_century^2+(Julian_
ephemeris_century^3)/56250;
%the moon's argument of latitude
X3=93.27191+483202.017538*Julian_ephemeris_century-
0.0036825*Julian_ephemeris_century^2+Julian_ephemeris_century^3/327270;
%the longitude of the ascending node of the moon's mean orbit on the ecliptic, measured from the
mean equinox of the date
X4=125.04452-
1934.136261*Julian_ephemeris_century+0.0020708*Julian_ephemeris_century^2+Julian_ephemeris_centur
y^3/450000;

PTFNLO=[0   0   0   0   1   -171996 -174.2  92025   8.9
-2  0   0   2   2   -13187  -1.6    5736    -3.1
0   0   0   2   2   -2274   -0.2    977     -0.5
0   0   0   0   2   2062    0.2     -895    0.5
0   1   0   0   0   1426    -3.4    54      -0.1
0   0   1   0   0   712     0.1     -7      0
-2  1   0   2   2   -517    1.2     224     -0.6
0   0   0   2   1   -386    -0.4    200     0
0   0   1   2   2   -301    0       129     -0.1
-2  -1  0   2   2   217     -0.5    -95     0.3
-2  0   1   0   0   -158    0       0       0
-2  0   0   2   1   129     0.1     -70     0
0   0   -1  2   2   123     0       -53     0
2   0   0   0   0   63      0       0       0
0   0   1   0   1   63      0.1     -33     0
2   0   -1  2   2   -59     0       26      0
0   0   -1  0   1   -58     -0.1    32      0
0   0   1   2   1   -51     0       27      0
-2  0   2   0   0   48      0       0       0
0   0   -2  2   1   46      0       -24     0
2   0   0   2   2   -38     0       16      0
0   0   2   2   2   -31     0       13      0
0   0   2   0   0   29      0       0       0
-2  0   1   2   2   29      0       -12     0
0   0   0   2   0   26      0       0       0
-2  0   0   2   0   -22     0       0       0
0   0   -1  2   1   21      0       -10     0
0   2   0   0   0   17      -0.1    0       0
2   0   -1  0   1   16      0       -8      0
-2  2   0   2   2   -16     0.1     7       0
0   1   0   0   1   -15     0       9       0
-2  0   1   0   1   -13     0       7       0
0   -1  0   0   1   -12     0       6       0
0   0   2   -2  0   11      0       0       0
2   0   -1  2   1   -10     0       5       0
2   0   1   2   2   -8      0       3       0
```

```
0	1	0	2	2	7	0	-3	0
-2	1	1	0	0	-7	0	0	0
0	-1	0	2	2	-7	0	3	0
2	0	0	2	1	-7	0	3	0
2	0	1	0	0	6	0	0	0
-2	0	2	2	2	6	0	-3	0
-2	0	1	2	1	6	0	-3	0
2	0	-2	0	1	-6	0	3	0
2	0	0	0	1	-6	0	3	0
0	-1	1	0	0	5	0	0	0
-2	-1	0	2	1	-5	0	3	0
-2	0	0	0	1	-5	0	3	0
0	0	2	2	1	-5	0	3	0
-2	0	2	0	1	4	0	0	0
-2	1	0	2	1	4	0	0	0
0	0	1	-2	0	4	0	0	0
-1	0	1	0	0	-4	0	0	0
-2	1	0	0	0	-4	0	0	0
1	0	0	0	0	-4	0	0	0
0	0	1	2	0	3	0	0	0
0	0	-2	2	2	-3	0	0	0
-1	-1	1	0	0	-3	0	0	0
0	1	1	0	0	-3	0	0	0
0	-1	1	2	2	-3	0	0	0
2	-1	-1	2	2	-3	0	0	0
0	0	3	2	2	-3	0	0	0
2	-1	0	2	2	-3	0	0	0
];

for i=1:63
PTFNLO(i,10)=PTFNLO(i,1)*X0+PTFNLO(i,2)*X1+PTFNLO(i,3)*X2+PTFNLO(i,4)*X3+PTFNLO(i,5)*X4;
PTFNLO(i,11)=(PTFNLO(i,6)+PTFNLO(i,7)*Julian_ephemeris_century)*sin(PTFNLO(i,10)*pi/180);
PTFNLO(i,12)=(PTFNLO(i,8)+PTFNLO(i,9)*Julian_ephemeris_century)*cos(PTFNLO(i,10)*pi/180);
end

%the nutation in longitude
Nutation_longitude=sum(PTFNLO(:,11))/36000000;%deg
%the nutation in obliquity
Nutation_obliquity=sum(PTFNLO(:,12))/36000000;%deg
```

THE TRUE OBLIQUITY OF THE ECLIPTIC

```
U=Julian_ephemeris_millenium/10;
%the mean obliquity of the ecliptic
mean_obliquity_ecliptic=84381.448-4680.93*U-1.55*U^2+1999.25*U^3-51.38*U^4-249.67*U^5-
39.05*U^6+7.12*U^7+27.87*U^8+5.79*U^9+2.45*U^10; %arc seconds
%the true obliquity of the ecliptic
true_obliquity_ecliptic=mean_obliquity_ecliptic/3600+Nutation_obliquity; %deg
```

THE ABERRATION CORRECTION

```
%Aberration_correction
Aberration_correction=-20.4898/(3600*earth_heliocentric_position_radius); %deg
```

THE APPARENT SUN LONGITUDE

```
Apparent_sun_longitude=Geocentric_longitude+Nutation_longitude+Aberration_correction;%deg
```

THE APPARENT SIDEREAL TIME AT GREENWICH AT ANY GIVEN TIME

```
%Apparent_sidereal_time
Apparent_sidereal0_time=280.46061837+360.98564736629*(Julian_day-
2451545)+0.000387933*Julian_century^2-Julian_century^3/38710000;

%Limiting Apparent_sidereal_time to 360°interval
Apparent_sidereal0_time = Apparent_sidereal0_time - 360 * floor(Apparent_sidereal0_time/360);
if(Apparent_sidereal0_time<0)
    Apparent_sidereal0_time = Apparent_sidereal0_time + 360;
end

%the apparent sidereal time at Greenwich
Apparent_sidereal_time_greenwich=Apparent_sidereal0_time+Nutation_longitude*cos(true_obliquity_ec
liptic*pi/180);%deg
```

THE GEOCENTRIC SUN RIGHT ASCENSION

```
Y = (sin(Apparent_sun_longitude * pi/180) * cos(true_obliquity_ecliptic * pi/180)) -
(tan(Geocentric_latitude * pi/180) * sin(true_obliquity_ecliptic * pi/180));
X = cos(Apparent_sun_longitude * pi/180);

sun_right_ascension = atan2(Y, X);

sun_right_ascension =sun_right_ascension*180/pi; %degrees

%Limiting sun_right_ascension to 360°interval
sun_right_ascension = sun_right_ascension - 360 * floor(sun_right_ascension/360);
if(sun_right_ascension<0)
    sun_right_ascension = sun_right_ascension + 360;
end
```

THE GEOCENTRIC SUN DECLINATION

```
Geocentric_sun_declination=asin(sin(Geocentric_latitude*
pi/180)*cos(true_obliquity_ecliptic*pi/180)+cos(Geocentric_latitude*pi/180)*sin(true_obliquity_ec
liptic*pi/180)*sin(Apparent_sun_longitude*pi/180))*180/pi;
%where it is positive or negative if the sun is north or south of the celestial
equator,respectively
```

THE OBSERVER LOCAL HOUR ANGLE

```
Observer_local_hour_angle=Apparent_sidereal_time_greenwich+longitude-sun_right_ascension;

%Limiting H to 360°interval
Observer_local_hour_angle = Observer_local_hour_angle - 360 *
floor(Observer_local_hour_angle/360);
if(Observer_local_hour_angle<0)
```

```
    Observer_local_hour_angle = Observer_local_hour_angle + 360;
end
```

THE TOPOCENTRIC SUN RIGHT ASCENSION

```
%the equatorial horizontal parallax of the sun
Equatorial_horizontal_parallax=8.794/(3600*earth_heliocentric_position_radius); %deg

%the term u
latitude=latitude*pi/180;
Term_u=atan(0.99664719*tan(latitude));

%the term x
Term_x=cos(Term_u)+(elevation/(6378140))*cos(latitude*pi/180);

%the term y
Term_y=0.99664719*sin(Term_u)+(elevation/6378140)*sin(latitude*pi/180);

%the parallax in the sun right ascension
Parallax_sun_right_ascension=atan2((-
Term_x*sin(Equatorial_horizontal_parallax*pi/180)*sin(Observer_local_hour_angle*pi/180)),(cos(Geo
centric_sun_declination*pi/180)-
Term_x*sin(Equatorial_horizontal_parallax*pi/180)*cos(Observer_local_hour_angle*pi/180)));
Parallax_sun_right_ascension=Parallax_sun_right_ascension*180/pi;


%the topocentric sun right ascension
topocentric_sun_right_ascension=Parallax_sun_right_ascension+sun_right_ascension;

%the topocentric sun declination
topocentric_sun_declination=atan(((sin(Geocentric_sun_declination*pi/180)-
Term_y*sin(Equatorial_horizontal_parallax*pi/180))*cos(Parallax_sun_right_ascension*pi/180))/(cos
(Geocentric_sun_declination*pi/180)-
Term_x*sin(Equatorial_horizontal_parallax*pi/180)*cos(Observer_local_hour_angle*pi/180)));
topocentric_sun_declination=topocentric_sun_declination*180/pi; %degrees
```

THE TOPOCENTRIC LOCAL HOUR ANGLE

```
Topocentric_local_angle=Observer_local_hour_angle-Parallax_sun_right_ascension;%deg
```

THE TOPOCENTRIC ZENITH ANGLE

```
%the topocentric elevationation angle without atmospheric refraction correction
topocentric_elevation_angle_Wo_atm_refract_correct=asin(sin(latitude)*sin(topocentric_sun_declina
tion*pi/180)+cos(latitude)*cos(topocentric_sun_declination*pi/180)*cos(Topocentric_local_angle*pi
/180));
topocentric_elevation_angle_Wo_atm_refract_correct=topocentric_elevation_angle_Wo_atm_refract_cor
rect*180/pi; %degrees

%the atmospheric refraction correction
atmosferic_refraction_correction=(P/1010)*(283/(273+T))*(1.02/(60*tan((topocentric_elevation_angl
e_Wo_atm_refract_correct+10.3/(topocentric_elevation_angle_Wo_atm_refract_correct+5.11))*pi/180))
);
```

```
%the topocentric elevationation angle
topocentric_elevation_angle=topocentric_elevation_angle_Wo_atm_refract_correct+atmosferic_refract
ion_correction;%degrees
Topocentric_zenith_angle=90-topocentric_elevation_angle; %degress
```

THE TOPOCENTRIC AZIMUTH ANGLE

```
%topocentric astronomers azimuth angle
topocentric_astronomers_azimuth_angle=atan2((sin(Topocentric_local_angle*pi/180)),(cos(Topocentri
c_local_angle*pi/180)*sin(latitude)-tan(topocentric_sun_declination*pi/180)*cos(latitude)));%rad
topocentric_astronomers_azimuth_angle=topocentric_astronomers_azimuth_angle*180/pi; %deg

%Limiting to 360°interval
topocentric_astronomers_azimuth_angle = topocentric_astronomers_azimuth_angle - 360 *
floor(topocentric_astronomers_azimuth_angle/360);
if(topocentric_astronomers_azimuth_angle<0)
    topocentric_astronomers_azimuth_angle = topocentric_astronomers_azimuth_angle + 360;
end

%the topocentric azimuth angle
Topocentric_azimuth_angle=topocentric_astronomers_azimuth_angle+180;

%Limiting F to 360°interval
Topocentric_azimuth_angle = Topocentric_azimuth_angle - 360 *
floor(Topocentric_azimuth_angle/360);
if(Topocentric_azimuth_angle<0)
    Topocentric_azimuth_angle = Topocentric_azimuth_angle + 360;
end
```

Script output

```
taa=Topocentric_azimuth_angle;
tza=Topocentric_zenith_angle;
```

Appendix H: LabVIEW screenshots for control in solar tracking system

The user enters the information about location, desired focal length (for concentration ratio). The interface shows the topocentric azimuth and zenith angle, before and after the filter (round up or down), number of steps for motors, and error dialogs (Figure VII-3).

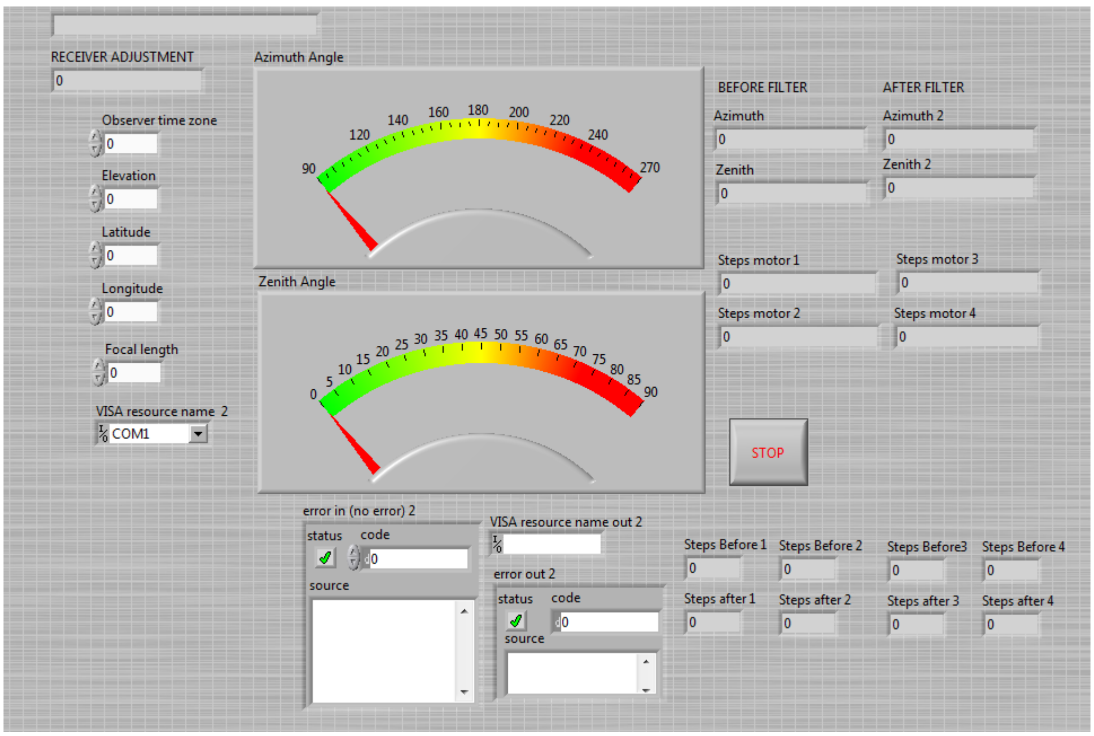

Figure VII-3. User interface for the solar tracking system

The script reads the current time (based on computer's date), and sends the information to the astronomical algorithm sub-VI. After the calculation of the topocentric azimuth and zenith angles, the script compares those values to the permissible range of movement for the unit (Figure VII-4).

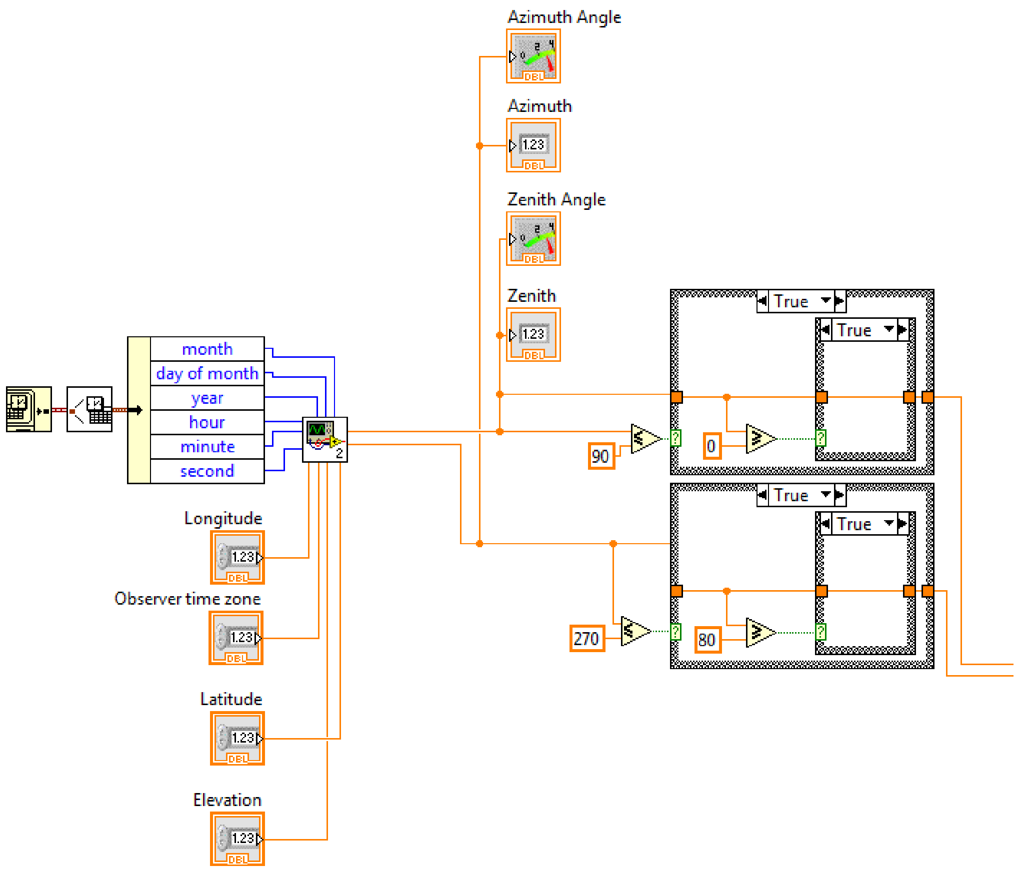

Figure VII-4. Main LabView script. Part 1 (including Sub-VI astronomical algorithm)

The topocentric zenith and azimuth angle values enter in a loop that runs each 30 seconds (Elapsed time), where are converted into number of steps for the motors. Data such as number of steps and position are stored in an Excel file. The number of steps are used for a movement sequence (one for each motor) for the lens adjustment (Figure VII-5).

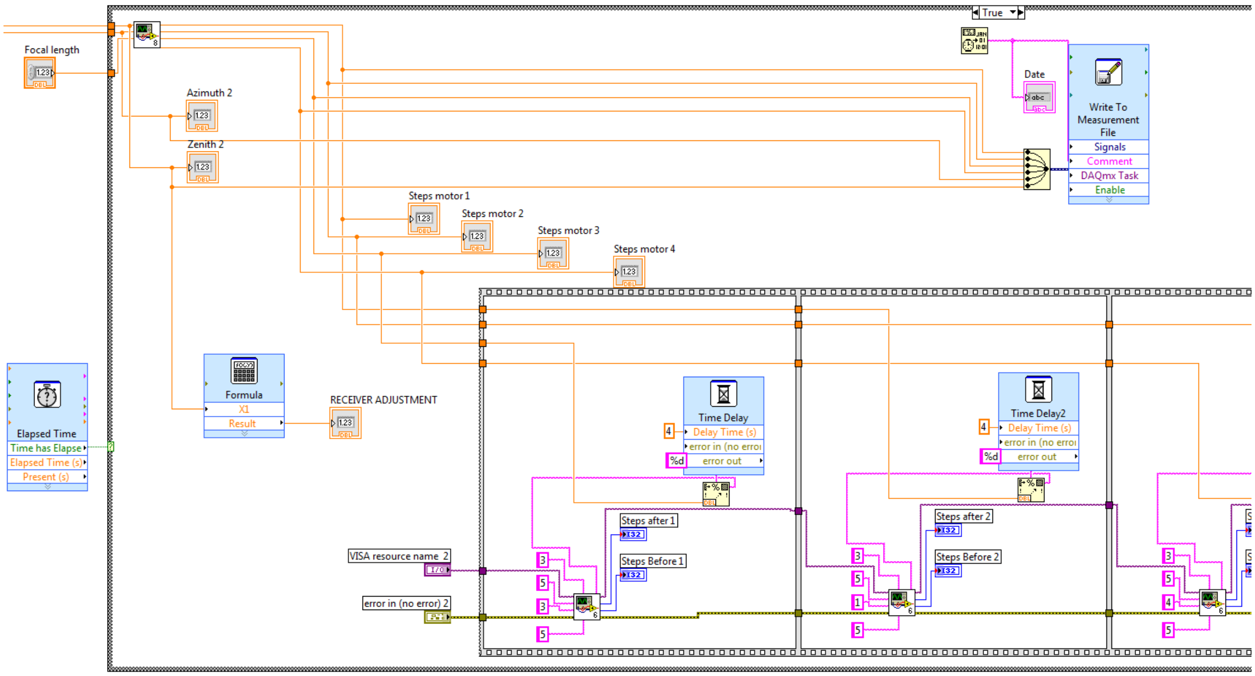

Figure VII-5. Main LabView script. Part 2 (including Sub-VI Motor steps calculations and Motor sequence)

Figure VII-5. (cont'd)

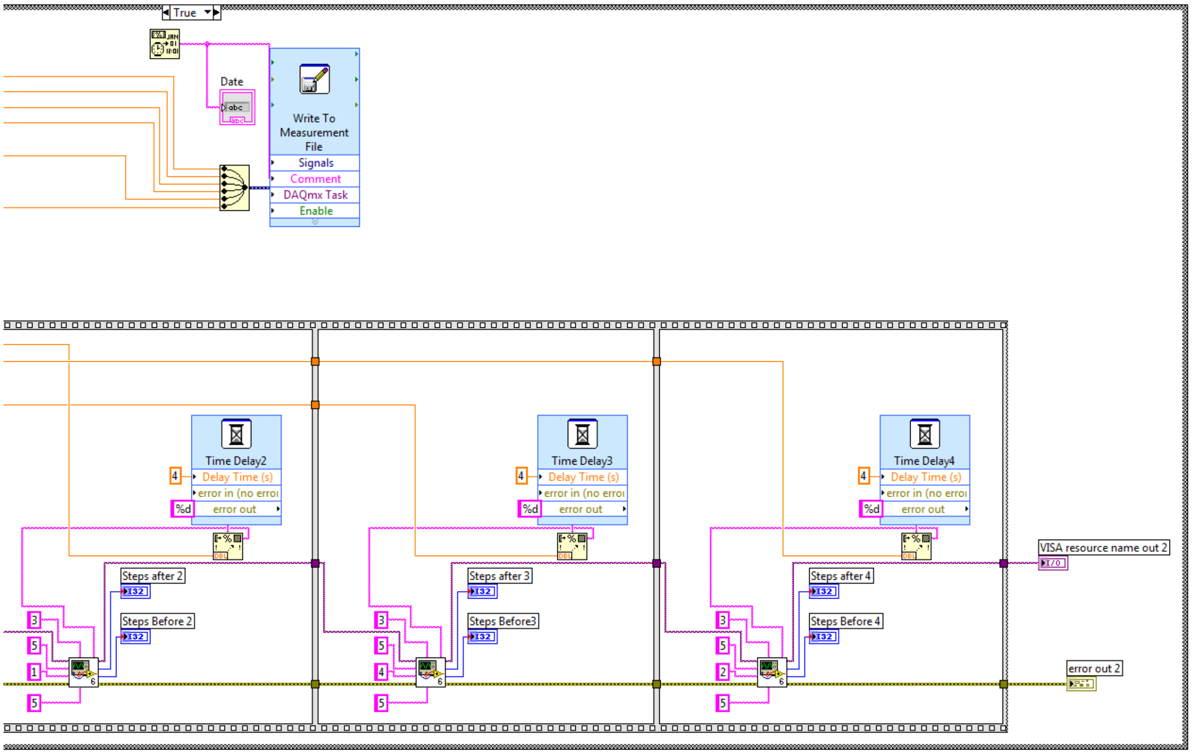

The sub-VI calculates the topocentric zenith and azimuth angles using a Matlab script. The sub-Vi requires location and time values for the calculation (Figure VII-6).

Figure VII-6. Sub-VI astronomical algorithm

The Sub-VI for steps calculations depends on the geometrical characteristics of the bench scale unit. The topocentric angles are converted into steps based on gearbox reduction ratio and linear displacement of the mechanical actuators (Figure VII-7).

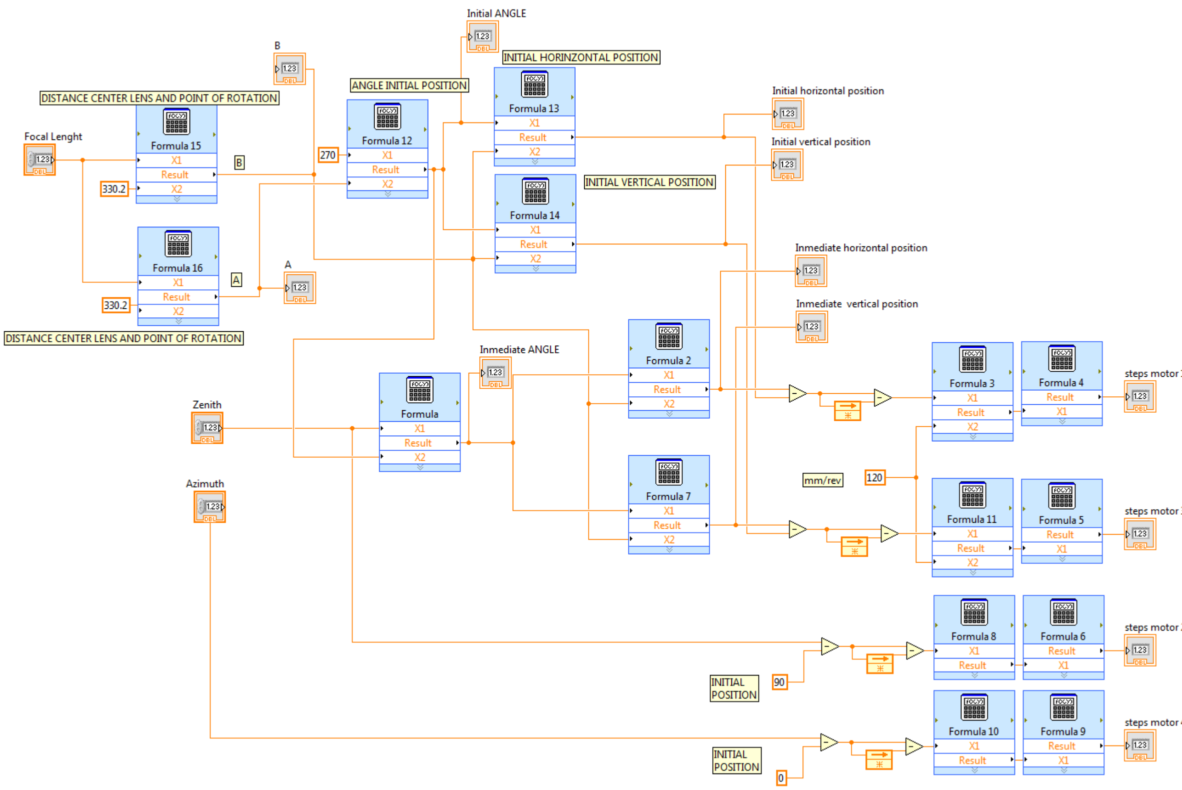

Figure VII-7. Sub-VI Motor steps calculations

The motor sequence include the reading od velocity, acceleration, deceleration, number of steps, and the specific command in SCL language (Figure VII-8).

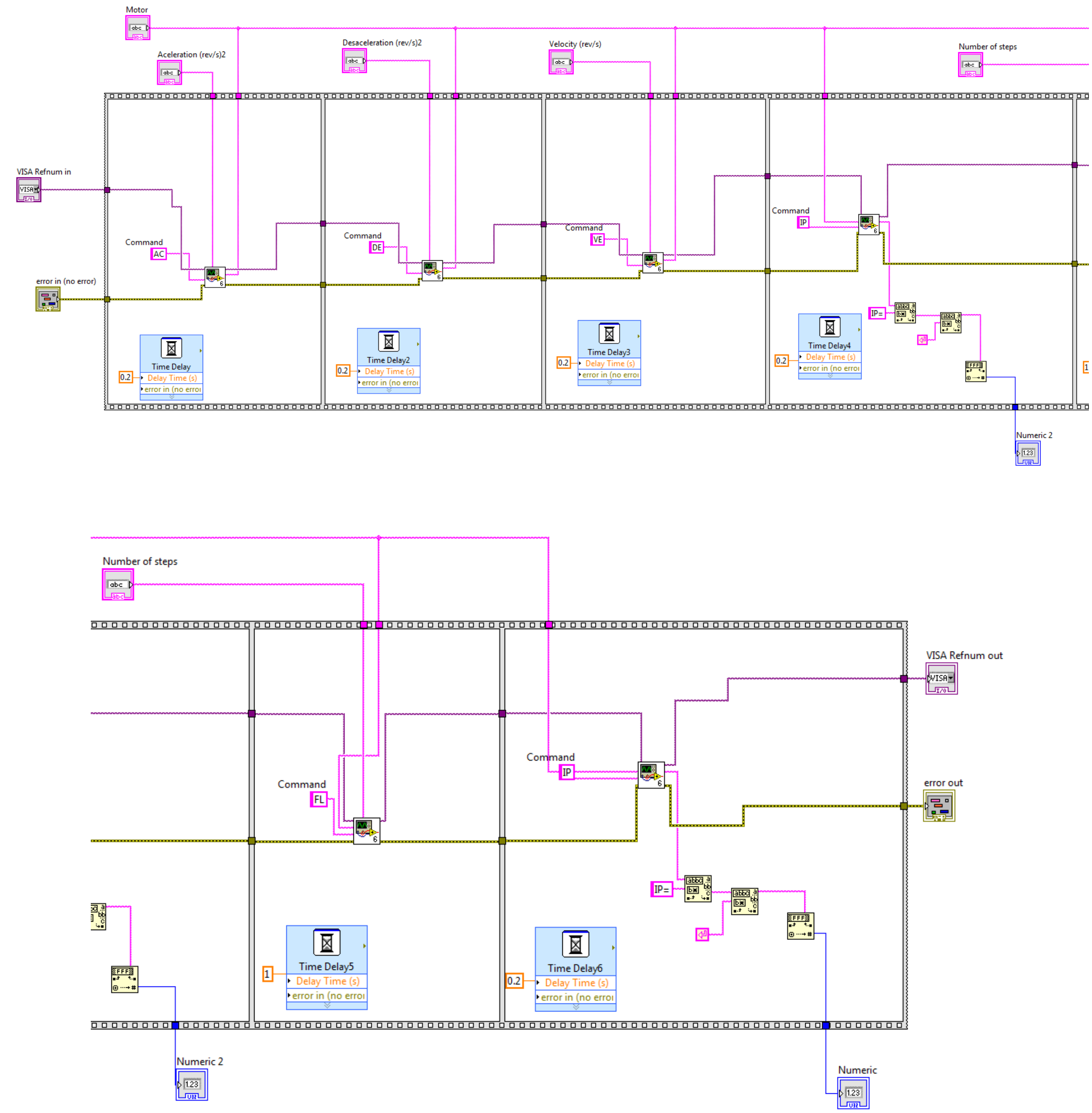

Figure VII-8. Sub-VI Motor sequence. Part 1 (including Sub-VI VISA device)

The sub-VI VISA device send signals to the step motors drives for the movement sequence in the lens adjustment (Figure VII-9).

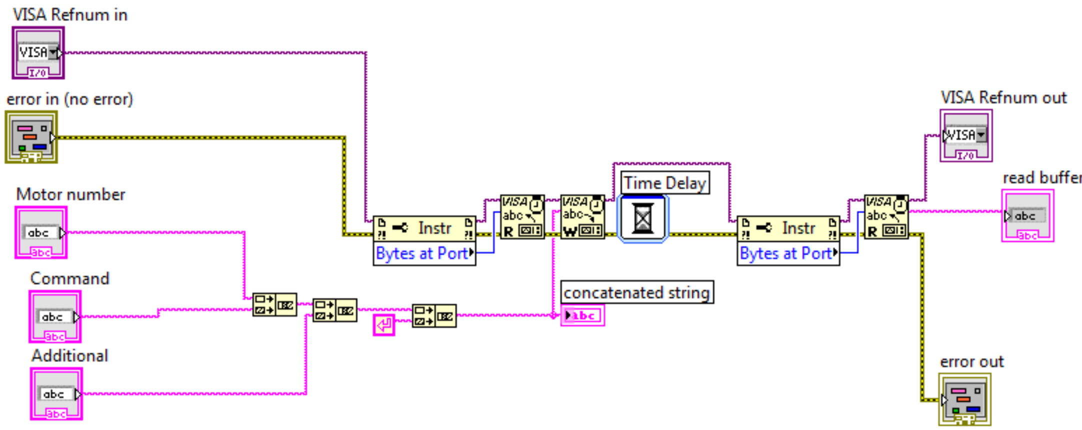

Figure VII-9. Sub-VI VISA device

REFERENCES

REFERENCES

Autodesk. (2015). Simulation CFD.

Baharoon, D. A., Rahman, H. A., Omar, W. Z. W., & Fadhl, S. O. (2015). Historical development of concentrating solar power technologies to generate clean electricity efficiently - A review. *Renewable & Sustainable Energy Reviews, 41*, 996-1027. doi:10.1016/j.rser.2014.09.008

Bao, J. J., Zhao, L., & Zhang, W. Z. (2011). A novel auto-cascade low-temperature solar Rankine cycle system for power generation. *Solar Energy*, *85*(11), 2710-2719. doi:http://dx.doi.org/10.1016/j.solener.2011.08.015

Basu, S., Khan, A. L., Cano-Odena, A., Liu, C., & Vankelecom, I. F. J. (2010). Membrane-based technologies for biogas separations. *Chemical Society reviews, 39*(2), 750. doi:10.1039/b817050a

Behar, O., Khellaf, A., & Mohammedi, K. (2013). A review of studies on central receiver solar thermal power plants. *Renewable and Sustainable Energy Reviews, 23*, 12-39. doi:http://dx.doi.org/10.1016/j.rser.2013.02.017

Bellia, H., Youcef, R., & Fatima, M. (2014). A detailed modeling of photovoltaic module using MATLAB. *NRIAG Journal of Astronomy and Geophysics*, *3*(1), 53-61. doi:http://dx.doi.org/10.1016/j.nrjag.2014.04.001

Bhatti, J., Joshi, P., Tiwari, G. N., & Al-Helal, I. M. (2015). Exergy analysis of photovoltaic thermal integrated biogas system. *JOURNAL OF RENEWABLE AND SUSTAINABLE ENERGY, 7*(6). doi:10.1063/1.4934563

Borges Neto, M. R., Carvalho, P. C. M., Carioca, J. O. B., & Canafístula, F. J. F. (2010). Biogas/photovoltaic hybrid power system for decentralized energy supply of rural areas. *Energy Policy, 38*(8), 4497-4506. doi:http://dx.doi.org/10.1016/j.enpol.2010.04.004

Böer, K. W., & SpringerLink. (1986). Advances in Solar Energy: An Annual Review of Research and Development Volume 3. Boston, MA: Springer US.

Buck, R., & Friedmann, S. (2007). Solar-Assisted Small Solar Tower Trigeneration Systems. *Journal of Solar Energy Engineering, 129*(4), 349. doi:10.1115/1.2769688

Caruana, D. J., & Olsen, A. E. (2012). Anaerobic digestion: processes, products, and applications. New York: Nova Science Publishers.

Casati, E., Galli, A., & Colonna, P. (2013). Thermal energy storage for solar-powered organic Rankine cycle engines. *Solar Energy, 96*, 205-219. doi:10.1016/j.solener.2013.07.013

Chan, Y. J., Chong, M. F., Law, C. L., & Hassell, D. G. (2009). A review on anaerobic–aerobic treatment of industrial and municipal wastewater. *Chemical Engineering Journal, 155*(1–2), 1-18. doi:http://dx.doi.org/10.1016/j.cej.2009.06.041

Chapra, S. C. (1997). *Surface water-quality modeling*. New York: McGraw-Hill.

Chen, G. (2004). Electrochemical technologies in wastewater treatment. *Separation and Purification Technology, 38*(1), 11-41. doi:http://dx.doi.org/10.1016/j.seppur.2003.10.006

Chen, R. (2015). *A closed-loop biorefining system to convert organic residues into fuels*.

Chen, R., Roos, M. M., Zhong, Y., Marsh, T., Roman, M. B., Hernandez Ascencio, W., . . . Liao, W. (2016). Responses of anaerobic microorganisms to different culture conditions and corresponding effects on biogas production and solid digestate quality. *Biomass and Bioenergy, 85*, 84-93. doi:http://dx.doi.org/10.1016/j.biombioe.2015.11.028

Cleaver-Brooks. (2011). Boiler Book 2011.

Colmenar-Santos, A., Bonilla-Gómez, J.-L., Borge-Diez, D., & Castro-Gil, M. (2015). Hybridization of concentrated solar power plants with biogas production systems as an alternative to premiums: The case of Spain. *Renewable and Sustainable Energy Reviews, 47*, 186-197. doi:http://dx.doi.org/10.1016/j.rser.2015.03.061

Corcoran, E., UNEP, & Arendal, G. (2010). *Sick water?: the central role of wastewater management in sustainable development : a rapid response assessment*. Arendal, Norway: United Nations Environment Programme.

Çengel, Y. A. (1998). *Heat transfer: a practical approach*. Boston, Mass: WBC McGraw-Hill.

Deshmukh, M. K., & Deshmukh, S. S. (2008). Modeling of hybrid renewable energy systems. *Renewable and Sustainable Energy Reviews, 12*(1), 235-249. doi:http://dx.doi.org/10.1016/j.rser.2006.07.011

Deshpande, A. M., Satyanarayan, S., & Ramakant. (2012). Kinetic analysis of an anaerobic fixed-film fixed bed-reactor treating wastewater arising from production of a chemically synthesized pharmaceutical. *Environmental Technology, 33*(11), 1261. doi:10.1080/09593330.2011.618952

Duffie, J. A., & Beckman, W. A. (2006). *Solar engineering of thermal processes* (Vol. 3rd). Hoboken, NJ: Wiley.

EdmundOptics. (2016). Advantages of Fresnel lens.

El-Mashad, H. M., van Loon, W. K. P., & Zeeman, G. (2003). A Model of Solar Energy Utilisation in the Anaerobic Digestion of Cattle Manure. *Biosystems Engineering, 84*(2), 231-238. doi:http://dx.doi.org/10.1016/S1537-5110(02)00245-3

El-Mashad, H. M., van Loon, W. K. P., Zeeman, G., Bot, G. P. A., & Lettinga, G. (2004). Design of A Solar Thermophilic Anaerobic Reactor for Small Farms. *Biosystems Engineering, 87*(3), 345-353. doi:10.1016/j.biosystemseng.2003.11.013

Energy. (2007). Summary of results from testing a 30-kW-microturbine and combined heat and power (CHP) system. In E. F. E. M. United States. Dept. of Energy. Office of Energy Efficiency and Renewable, Program (Ed.), *Federal technology alert*: U.S. Dept. of Energy, Office of Energy Efficiency and Renewable Energy.

EPA. (2000). *Decentralized systems technology fact sheet* Retrieved from http://purl.access.gpo.gov/GPO/LPS45110

EPA. (2004). *Primer for municipal wastewater treatment systems* (pp. 29 p.). Retrieved from http://purl.access.gpo.gov/GPO/LPS45629

Federation, W. E. (2009). *Design of Municipal Wastewater Treatment Plants MOP 8, Fifth Edition*: McGraw-Hill Professional.

Fernández, P., & Miller, F. J. (2015). Performance analysis and preliminary design optimization of a Small Particle Heat Exchange Receiver for solar tower power plants. *Solar Energy, 112*, 458-468. doi:10.1016/j.solener.2014.11.012

Franchini, G., Perdichizzi, A., Ravelli, S., & Barigozzi, G. (2013). A comparative study between parabolic trough and solar tower technologies in Solar Rankine Cycle and Integrated Solar Combined Cycle plants. *Solar Energy, 98, Part C*(0), 302-314. doi:http://dx.doi.org/10.1016/j.solener.2013.09.033

Fricke, K., Santen, H., & Wallmann, R. (2005). Comparison of selected aerobic and anaerobic procedures for MSW treatment. *Waste Management, 25*(8), 799-810. doi:http://dx.doi.org/10.1016/j.wasman.2004.12.018

Gazda, W., & Stanek, W. (2016). Energy and environmental assessment of integrated biogas trigeneration and photovoltaic plant as more sustainable industrial system. *Applied Energy, 169*, 138-149. doi:10.1016/j.apenergy.2016.02.037

Giostri, A., Binotti, M., Silva, P., Macchi, E., & Manzolini, G. (2013). Comparison of Two Linear Collectors in Solar Thermal Plants: Parabolic Trough Versus Fresnel. *Journal of Solar Energy Engineering, 135*(1), 011001-011009.

González-González, A., Collares-Pereira, M., Cuadros, F., & Fartaria, T. (2014). Energy self-sufficiency through hybridization of biogas and photovoltaic solar energy: an application for an Iberian pig slaughterhouse. *Journal of Cleaner Production, 65*, 318-323. doi:10.1016/j.jclepro.2013.08.021

Grady, C. P. L., Daigger, G. T., & Lim, H. C. (1999). *Biological wastewater treatment* (Vol. 19.). New York: Marcel Dekker.

Halotechnics. (2013). High temperature thermal fluids. Retrieved from http://www.halotechnics.com/products/

Immanuel Selwynraj, A., Iniyan, S., Polonsky, G., Suganthi, L., & Kribus, A. (2015). An economic analysis of solar hybrid steam injected gas turbine (STIG) plant for Indian conditions. *Applied Thermal Engineering, 75*, 1055-1064. doi:http://dx.doi.org/10.1016/j.applthermaleng.2014.10.055

Jamel, M. S., Abd Rahman, A., & Shamsuddin, A. H. (2013). Advances in the integration of solar thermal energy with conventional and non-conventional power plants. *RENEWABLE & SUSTAINABLE ENERGY REVIEWS, 20*, 71-81. doi:10.1016/j.rser.2012.10.027

Jiang, J.-Q., Graham, N., André, C., Kelsall, G. H., & Brandon, N. (2002). Laboratory study of electro-coagulation–flotation for water treatment. *Water Research, 36*(16), 4064-4078. doi:http://dx.doi.org/10.1016/S0043-1354(02)00118-5

Kakaç, S., & Liu, H. (1998). *Heat exchangers: selection, rating, and thermal design*. Boca Raton, Fla: CRC Press.

Kalogirou, S. (2009). *Solar energy engineering: processes and systems*. Amsterdam; London: Elsevier/Academic Press.

Kapdi, S. S., Vijay, V. K., Rajesh, S. K., & Prasad, R. (2005). Biogas scrubbing, compression and storage: perspective and prospectus in Indian context. *Renewable Energy, 30*(8), 1195-1202. doi:http://dx.doi.org/10.1016/j.renene.2004.09.012

Koai, K., Lior, N., & Yeh, H. (1984). Performance analysis of a solar-powered/fuel-assisted Rankine cycle with a novel 30 hp turbine. *Solar Energy, 32*(6), 753-764. doi:10.1016/0038-092X(84)90249-4

Korres, N., O'Kiely, P., & Benzie, J. (2013). *Bioenergy Production by Anaerobic Digestion Using agricultural biomass and organic wastes*. New York.

Lazarova, V., & Bahri, A. (2005). *Water reuse for irrigation: agriculture, landscapes, and turf grass*. Boca Raton: CRC Press.

Lijó, L., González-García, S., Bacenetti, J., Fiala, M., Feijoo, G., Lema, J. M., & Moreira, M. T. (2014). Life Cycle Assessment of electricity production in Italy from anaerobic co-digestion of pig slurry and energy crops. *Renewable Energy, 68*, 625-635. doi:http://dx.doi.org/10.1016/j.renene.2014.03.005

Liu, A., & Weng, Y. (2009). Effects of Lower Heat Value Fuel on the Operations of Micro-Gas Turbine. *Energy and Power Engineering, 1*(1), 28-37. doi:10.4236/epe.2009.11005

Liu, Z. G., & Liu, Y. (2016). Synergistic integration of electrocoagulation and algal cultivation to treat liquid anaerobic digestion effluent and accumulate algal biomass. *PROCESS BIOCHEMISTRY, 51*(1), 89-94. doi:10.1016/j.progbio.2015.11.003

Livshits, M., & Kribus, A. (2012). Solar hybrid steam injection gas turbine (STIG) cycle. *Solar Energy, 86*(1), 190-199. doi:10.1016/j.solener.2011.09.020

Lovegrove, K., & Stein, W. (2012). *Concentrating solar power technology: principles, developments and applications*. Cambridge, UK: Woodhead Publishing Limited.

Lv, H., Sheng, F., Dai, J., Liu, W., Cheng, C., & Zhang, J. (2015). Temperature-dependent model of concentrator photovoltaic modules combining optical elements and III–V multi-junction solar cells. *Solar Energy, 112*(0), 351-360. doi:http://dx.doi.org/10.1016/j.solener.2014.12.005

Mancini, T., Heller, P., Butler, B., Osborn, B., Schiel, W., Goldberg, V., . . . Moreno, J. (2003). Dish-Stirling systems: An overview of development and status. *Journal of Solar Energy Engineering-Transactions of the Asme, 125*(2), 135-151. doi:10.1115/1.1562634

Martin, I., Pidou, M., Soares, A., Judd, S., & Jefferson, B. (2011). Modelling the energy demands of aerobic and anaerobic membrane bioreactors for wastewater treatment. *Environmental Technology, 32*(9), 921-932. doi:10.1080/09593330.2011.565806

Massoud, M. (2005). *Engineering thermofluids: thermodynamics, fluid mechanics, and heat transfer*. Berlin: Springer.

Mills, D. (2004). Advances in solar thermal electricity technology. *Solar Energy, 76*(1–3), 19-31. doi:10.1016/S0038-092X(03)00102-6

Mizuta, K., & Shimada, M. (2010). Benchmarking energy consumption in municipal wastewater treatment plants in Japan. *WATER SCIENCE AND TECHNOLOGY, 62*(10), 2256-2262. doi:10.2166/wst.2010.510

Modest, M. F. (2013). Chapter 3 - Radiative Properties of Real Surfaces *Radiative Heat Transfer (Third Edition)* (pp. 61-128). Boston: Academic Press.

Modest, M. F. (2013). *Radiative heat transfer* (pp. xxii, 882 pages). Retrieved from http://ezproxy.msu.edu:2047/login?url=http://app.knovel.com/web/toc.v/cid:kpRHTE0003/viewerType:toc/ Retrieved from http://ezproxy.msu.edu:2047/login?url=http://www.sciencedirect.com/science/book/9780123869449

Mollah, M. Y. A., Schennach, R., Parga, J. R., & Cocke, D. L. (2001). Electrocoagulation (EC) — science and applications. *Journal of Hazardous Materials, 84*(1), 29-41. doi:http://dx.doi.org/10.1016/S0304-3894(01)00176-5

NextGrid. (2014). NextGrid CHP Models. Retrieved from http://www.gonextgrid.com/products/nextgrid-chp-models/

Novak, J. T., Banjade, S., & Murthy, S. N. (2011). Combined anaerobic and aerobic digestion for increased solids reduction and nitrogen removal. *Water Research, 45*(2), 618-624. doi:http://dx.doi.org/10.1016/j.watres.2010.08.014

NREL. (2013). Biogas potential in the United States.

NREL. (2015). Solar Prospector.

NREL. (2016a). Solar Photovoltaic Technology Basics. Retrieved from http://www.nrel.gov/workingwithus/re-photovoltaics.html

NREL. (2016b). System Advisor Model (Version 2016.3.14 64 bit): National Renewable Laboratory.

Olivenza-Leon, D., Medina, A., & Hernandez, A. C. (2015). Thermodynamic modeling of a hybrid solar gas-turbine power plant. *ENERGY CONVERSION AND MANAGEMENT, 93*, 435-447. doi:10.1016/j.enconman.2015.01.027

Osorio, F., & Torres, J. C. (2009). Biogas purification from anaerobic digestion in a wastewater treatment plant for biofuel production. *Renewable Energy, 34*(10), 2164-2171. doi:http://dx.doi.org/10.1016/j.renene.2009.02.023

PennState Extention, P. S. C. o. A. S. (2016). Renewable and alternative energy: Types of anaerobic digesters. Retrieved from http://extension.psu.edu/natural-resources/energy/waste-to-energy/resources/biogas/types-of-anaerobic-digesters

Pihl, E., Spelling, J., & Johnsson, F. (2014). Thermo-economic optimization of hybridization options for solar retrofitting of combined-cycle power plants. *Journal of Solar Energy Engineering, 136*(2). doi:10.1115/1.4024922

Popov, D. (2014). Innovative solar augmentation of gas turbine combined cycle plants. *Applied Thermal Engineering, 64*(1–2), 40-50. doi:http://dx.doi.org/10.1016/j.applthermaleng.2013.12.002

Reda, I., & Andreas, A. (2008). Solar Position Algorithm for Solar Radiation Applications. Retrieved from

Ryckebosch, E., Drouillon, M., & Vervaeren, H. (2011). Techniques for transformation of biogas to biomethane. *Biomass and Bioenergy, 35*(5), 1633-1645. doi:10.1016/j.biombioe.2011.02.033

San Miguel, G., Miguel, G. S., & Corona, B. (2014). Hybridizing concentrated solar power with biogas and biomethane as an alternative to natural gas: Analysis of environmental performance using LCA. *Renewable energy, 66*, 580-587.

Schwarzbözl, P., Buck, R., Sugarmen, C., Ring, A., Marcos Crespo, M., Altwegg, P., & Enrile, J. (2006). Solar gas turbine systems: Design, cost and perspectives. *Solar Energy, 80*(10), 1231-1240. doi:10.1016/j.solener.2005.09.007

Siva Reddy, V., Kaushik, S. C., Ranjan, K. R., & Tyagi, S. K. (2013). State-of-the-art of solar thermal power plants—A review. *Renewable and Sustainable Energy Reviews, 27*(0), 258-273. doi:http://dx.doi.org/10.1016/j.rser.2013.06.037

Skoplaki, E., & Palyvos, J. A. (2009). On the temperature dependence of photovoltaic module electrical performance: A review of efficiency/power correlations. *Solar Energy, 83*(5), 614-624. doi:10.1016/j.solener.2008.10.008

Skouri, S., Bouadila, S., Ben Salah, M., & Ben Nasrallah, S. (2013). Comparative study of different means of concentrated solar flux measurement of solar parabolic dish. *Energy Conversion and Management, 76*, 1043-1052. doi:10.1016/j.enconman.2013.08.058

Speece, R. E. (1996). *Anaerobic biotechnology for industrial wastewaters*. Nashville, Tenn: Archae Press.

Sun, Q., Li, H., Yan, J., Liu, L., Yu, Z., & Yu, X. (2015). Selection of appropriate biogas upgrading technology-a review of biogas cleaning, upgrading and utilisation. *Renewable and Sustainable Energy Reviews, 51*, 521-532. doi:10.1016/j.rser.2015.06.029

U.S.ClimateData. (2015). Temperature-Precipitation-Sunchine-Snowfall.

USDA National Agricultural Statistics Service. (2009). Farms, land in farms, and livestock operations.

Wang, L. K., Pereira, N. C., & Hung, Y.-T. (2009). Biological treatment processes (Vol. 8.). New York: Humana Press.

Water Environment, F., & ebrary, I. (2008). Operation of municipal wastewater treatment plants (Vol. no. 11.). Maidenhead: McGraw-Hill Professional.

Wu, Y., Eames, P., Mallick, T., & Sabry, M. (2012). Experimental characterisation of a Fresnel lens photovoltaic concentrating system. *Solar Energy, 86*(1), 430-440. doi:http://dx.doi.org/10.1016/j.solener.2011.10.032

Xie, W. T., Dai, Y. J., & Wang, R. Z. (2013). Thermal performance analysis of a line-focus Fresnel lens solar collector using different cavity receivers. *Solar Energy, 91*(0), 242-255. doi:http://dx.doi.org/10.1016/j.solener.2013.01.029

Xie, W. T., Dai, Y. J., Wang, R. Z., & Sumathy, K. (2011). Concentrated solar energy applications using Fresnel lenses: A review. *Renewable and Sustainable Energy Reviews, 15*(6), 2588-2606. doi:http://dx.doi.org/10.1016/j.rser.2011.03.031

Yiannopoulos, A. C., Manariotis, I. D., & Chrysikopoulos, C. V. (2008). Design and analysis of a solar reactor for anaerobic wastewater treatment. *Bioresource Technology, 99*(16), 7742-7749. doi:http://dx.doi.org/10.1016/j.biortech.2008.01.067

Yue, Z., MacLellan, J., Liu, Y., & Liao, W. (2013). Effects of corn stover as carbon supplement on an integrated anaerobic digestion and ethanol fermentation process. *Journal of Renewable and Sustainable Energy, 5*(6), 063116-063116-063119. doi:10.1063/1.4840095

Zhai, H., Dai, Y. J., Wu, J. Y., Wang, R. Z., & Zhang, L. Y. (2010). Experimental investigation and analysis on a concentrating solar collector using linear Fresnel lens. *Energy Conversion and Management, 51*(1), 48-55. doi:http://dx.doi.org/10.1016/j.enconman.2009.08.018

Zhao, Y., Hong, H., & Jin, H. (2014). Mid and low-temperature solar–coal hybridization mechanism and validation. *Energy, 74*, 78-87. doi:http://dx.doi.org/10.1016/j.energy.2014.03.092

Zhong, Y., Bustamante Roman, M., Zhong, Y., Archer, S., Chen, R., Deitz, L., . . . Liao, W. (2015). Using anaerobic digestion of organic wastes to biochemically store solar thermal energy. *Energy, 83*(0), 638-646. doi:http://dx.doi.org/10.1016/j.energy.2015.02.070

Zhou, Z., Shen, X., Jiang, L.-M., Wu, Z., Wang, Z., Ren, W., & Hu, D. (2015). Modeling of multimode anaerobic/anoxic/aerobic wastewater treatment process at low temperature for process optimization. *Chemical Engineering Journal, 281*, 644-650. doi:10.1016/j.cej.2015.07.017

Zhu, G. D., Wendelin, T., Wagner, M. J., & Kutscher, C. (2014). History, current state, and future of linear Fresnel concentrating solar collectors. *Solar Energy, 103*, 639-652. doi:10.1016/j.solener.2013.05.021

Zhu, J., Wang, K., Wu, H., Wang, D., Du, J., & Olabi, A. G. (2015). Experimental investigation on the energy and exergy performance of a coiled tube solar receiver. *Applied Energy, 156*, 519-527. doi:http://dx.doi.org/10.1016/j.apenergy.2015.07.013

Ávila-Marín, A. L. (2011). Volumetric receivers in Solar Thermal Power Plants with Central Receiver System technology: A review. *Solar Energy, 85*(5), 891-910. doi:http://dx.doi.org/10.1016/j.solener.2011.02.002